Coordination Chemistry Reviews, 108 (1991) 163–311
Elsevier Science Publishers B.V., Amsterdam

THEORETICAL APPROACHES TO THE DESCRIPTION OF THE ELECTRONIC STRUCTURE AND CHEMICAL REACTIVITY OF TRANSITION METAL COMPOUNDS

C.A. TSIPIS

Department of General and Inorganic Chemistry, Faculty of Chemistry, Aristotelian University of Thessaloniki, GR-54006 Thessaloniki (Greece)

(Received 11 July 1990)

CONTENTS

ABBREVIATIONS

A	electron affinity
AO	atomic orbital
Arg-141	arginine-141
BDE	bond dissociation energy

0010-8545/91/$52.15

Bz	benzyl
CAS	complete active space
CASSCF	complete active space self-consistent-field method [61]*
CASSCF-CCI	complete active space self-consistent-field with contracted configuration interaction [223,224]
CCI	contracted configuration interaction
CDD	chemical difference density [182,185]
CET	correlated electron transfer [86]
CI	configuration interaction
CNDO	complete neglect of differential overlap [152]
CNDO/2	CNDO version 2
CNDO/S^2	CNDO version S^2 for interpreting electronic spectra
Cp	cyclopentadienyl
CSOV	constrained space orbital variation [135]
CT	charge transfer
DCCI	dissociation-consistent CI [201,202]
DCD	Dewar–Chatt–Duncanson model [370,371]
DF	Dirac–Fock [57,58]
DFOCE	Dirac–Fock one-centre expansion calculations [211]
DISP	dispersion
DSW-Xα	Dirac-scattered-wave Xα [49,50]
DV-Xα	discrete variational Xα [48]
ECP	effective core potential or pseudopotential [53–56]
EHMO	extended Hückel molecular orbital method [71–78]
EHMO-SCCC	extended Hückel molecular orbital method with self-consistent charge and configuration
2e-2O	two-electron-two-orbital interactions [90]
4e-2O	four-electron-two-orbital interactions [90]
EPM	electrostatic potential map [165]
Es	electrostatic
ESR	electron spin resonance
Et	ethyl
FMO	frontier molecular orbital
FO	frozen orbital
GMO	generalized molecular orbital method
GMO-CI	GMO with CI
GTO	Gaussian-type orbital
GVB	generalized valence bond method [63,64]
GVB-CI	GVB with CI

* The figures in brackets indicate the references in which an introduction to the corresponding technique can be found.

GVB-DCCI	GVB with DCCI [201,202,213]
GVB-RCI	GVB with restricted CI
HF	Hartree–Fock approximation
HF-CI	HF with CI
HF-CI+D	HF-CI plus Davidson correction [452]
HFS	Hartree–Fock–Slater or $X\alpha$ method [43–46]
HOMO	highest occupied molecular orbital
INDO	intermediate neglect of differential overlap [152]
INDO/S-CI	INDO version S for interpreting electronic spectra with CI
IP	ionization potential
IRC	intrinsic reaction coordinate
IR	infrared
LCAO	linear combination of atomic orbital technique
LCAO-SCF-MO	LCAO-self-consistent field molecular orbital
LCGTO-Xα	linear combination of Gaussian-type orbitals Xα [51,52]
LD	local density approximation [37–42]
LDF	local density functional [37–42]
LF	ligand field
LUMO	lowest unoccupied molecular orbital
MCPF	modified coupled pair functional formalism [203]
MCSCF	multiconfiguration self-consistent field technique [27,28]
MCSCF+1+2	MCSCF with singly and doubly excited CI
Me	methyl
MINDO/3	modified intermediate neglect of differential overlap version 3 [152]
MINDO/SR	MINDO version SR for interpreting electronic spectra
MNDO	modified neglect of differential overlap
MO	molecular orbital
MO-CI	molecular orbital calculations with CI
MOVB	molecular orbital–valence bond approximation [86]
MP2	second order Möller–Plesset perturbation theory [290]
MP3	third order Möller–Plesset perturbation theory [290]
MP4(SDTQ)	fourth order Möller–Plesset perturbation theory including singly, doubly, triply and quadruply excited CI [225]
MRD-CI	multireference single and double CI
MS-Xα	multiple-scattering Xα [47]
MSW-Xα	multiple-scattering wave Xα [47]
NDO	neglect of differential overlap [66–70]
NHOMO	next HOMO
NLUMO	next LUMO

NMR	nuclear magnetic resonance
OMO	occupied MO
OV	overlap
PA	proton affinity
Ph	phenyl
PL	polarization
PMO	perturbational molecular orbital analysis [139–144]
PP	perfect pairing
PPP	Pariser–Parr–Pople
PRDDO	projection of diatomic differential overlap
PSHONDO	ab initio SCF program with a very fast integral evaluation
R	alkyl
RCI	restricted CI
RECP	relativistic effective core potential
RHF	restricted HF theory
RHF-CI	RHF with CI
RPM	reaction potential map [167]
SCF	self-consistent field
SCF-MO	self-consistent field molecular orbital
SD-CI	singly and doubly excited CI
SOMO	single occupied MO
SP	square pyramidal
STO	Slater-type orbital
STO-3G	STO expanded to a linear combination of 3 Gaussian type orbitals
TB	trigonal bipyramidal
UMO	unoccupied MO
UV	ultraviolet
VB	valence bond theory

A. INTRODUCTION

Transition metal coordination and organometallic molecules present to the chemist a vast array of structures, along with an overwhelming diversity in properties and reactivity [1–8]. Moreover, their chemistry not only offers rich opportunities for the discovery of new and unusual types of compounds, reactivity patterns and dynamic processes, it also had and continues to have a strong impact upon biology and chemical technology. Certainly, from application-oriented viewpoints, besides the enormously important catalytic activity of transition metals and their compounds [9–15], there is one aspect of organotransition metal chemistry that is revolutionary, namely the treat-

ment of cancer [16]. These features of transition metal compounds have also long been an attractive subject of quantum chemistry [17–20].

The current 'state of the art' of quantum chemistry in the field of transition metal compounds deals mainly with both the 'computational theory' designed for the computer and the 'conceptual theory' designed for the chemist's mind. These two theories encompass many fields, including atoms and small molecules, medium and large molecules, heavy atoms and relativistic effects, biological systems, extended structures, the cluster-surface analogy with its implications for heretogeneous catalysis, molecular structure and reactivity, intermolecular interactions and molecular dynamics, spectroscopy and photophysics. Modern computers and the availability of sophisticated computational routines now allow almost every chemist to perform calculations to his own field of interest with relatively little effort. In this respect, the extremely fruitful synergic relationship between the calculated numbers and experiment is exactly what the experimental chemist needs to understand and predict structural and reactivity trends. This is why quantum chemistry is at its best when it is merged in experiment.

The aim of the present article is to present the actual state of thinking about the electronic structure, bonding and chemical reactivity problems of transition metal compounds. It is not my intention to review all the theoretical work in this area, and there has been a considerable amount done [17–24]. Rather, I will attempt to illustrate how the various methods offered by quantum chemistry can be used in a wide variety of problems encountered in coordination and organometallic chemistry, or at different stages in the same problem. In this respect, comparing the different approaches of interpretations, the reader will be able to judge the merits of the various theories and their applicability to his own field of interest. Moreover, representative examples will also be presented of the most important problems of the molecular and electronic structure, bonding, chemical reactivity, dynamics and related properties of 'chemically interesting' mononuclear transition metal compounds, tackled by quantum chemistry in the last decade.

The format of this presentation will be divided into three major topical sections: (1) computational theory, (2) general theory of chemical reactivity and (3) applications.

B. COMPUTATIONAL THEORY

Computational methods of quantum chemistry have found an increasing number of applications to chemical problems over the last few decades. Thus, quantum chemistry has been very successful as a predictive tool in the study of small or medium size organic molecules and properties such as the ground

state molecular geometries, conformational preferences, transition state geometries and energies, Born–Oppenheimer potential energy surfaces, reaction pathways and the rates of organic reactions could be predicted [25,26]. At the same time, quantum chemistry has also been applied in the field of transition metal compounds and organometallics [17,18]. However, despite the greatly improved computational facilities and the availability of sophisticated quantum chemical calculations, the quantum chemistry of molecular systems containing heavy atoms appears to be less advanced [19,20]. This is largely due to difficulties arising in the treatment of heavy atoms and molecules containing such atoms, related to the quasi-degeneracy of their lowest atomic states, correlation and relativistic effects.

In the study of light atoms and small molecules, the correlation problem, being important for quantitative accuracy, is still dominant. Even in ab initio methods, one has to go beyond the Hartree–Fock (HF) approximation by using either multiconfigurational self-consistent field (MCSCF) techniques or configuration-interaction (CI) methods [27,28]. In transition metal compounds, and especially those involving multiple metal–metal bonds, the correlation effects need to be considered even for a qualitative description of their electronic structures. This is because the energy associated with electron correlation, although being a small fraction of the total energy of an atom or molecule, is comparable in magnitude with energies of chemical significance related to bond dissociation, activation, barriers of rotation, etc. Therefore, in order to obtain meaningful results for transition metal compounds, one has to rely on the highly sophisticated MCSCF or CI methods. Of equal importance is the study of the relativistic effects of the heavy atoms, such as mass-velocity correction (correction to the kinetic energy arising from the variation of mass with speed), and spin–orbit corrections. Several published works [29–35] have been devoted to the evaluation of the influence of relativistic effects on bond lengths, bond strengths and other observables of chemical interest. The relativistic energy has been calculated to be larger than that of electron correlation even for molecular systems of the second row elements, whereas for those systems containing very heavy atoms, relativistic effects dominate many of their chemical properties. In practical applications, one is using generalizations of the Dirac and Breit Hamiltonians [36]. Thanks to many investigators, some simple methods have become feasible. These are lucid, easy to implement in existing non-relativistic computer programs and require a minimal amount of computational effort. An up-to-date summary of contemporary theories, algorithms and computational techniques is provided by the two special volumes edited very recently by Wilson [28,36].

The only general methods available at the present time for performing relativistic electronic calculations on 'chemically interesting' polyatomic molecules containing heavy atoms are of two types: (1) those which use some

local density functional (LDF) expression for the exchange correlation term and (2) those which use ab initio relativistic effective core potentials.

In the density functional approximation [37–42], the many-body effects are expressed in terms of the density distribution, $\rho(\bar{r})$, which is then determined by a one-particle Schrödinger equation with a self-consistent potential, $V(\bar{r})$. In LDF, the exchange-correlation energy and potential at a locality are given by the corresponding quantities for the homogeneous electron gas with the same density. This simple scheme has been applied to a wide range of systems with striking success for ground state properties. The simplest, and certainly the most widely applied, density functional theory is the Hartree–Fock–Slater (HFS), or Xα, method [43,44] as implemented by Baerends et al. [45,46].

Several improved versions of the Xα method such as the multiple-scattering Xα (MS-Xα) [47], the discrete variational Xα (DV-Xα) [48], the Dirac scattered wave Xα (DSW-Xα) [49,50] and the LCGTO-Xα [51,52] have been applied to molecules or molecular clusters in crystals containing more and heavier atoms than can be treated by more conventional methods. The SW-Xα method, in which the potential is spherically averaged within spheres centred around each atom and assumed to be constant in the intersphere regions (muffin-tin potential), is characterized by smaller computational time than the HF method and therefore is the most popular with the chemists. However, its major shortcoming is due to the muffin-tin approximation which neglects the angular dependence of the potential in the vicinities of the atomic centres. The DV-Xα method overcame such problems and found wide application in the study of large metal clusters. The LCGTO-Xα technique, featuring the LD approximation in the form of a computationally simple exchange-correlation potential, uses Gaussian-type instead of STO basis set expansion techniques. In this respect, LCGTO-Xα resembles current HF and CI procedures. All these Xα approximations are admittedly not perfect, but they have found wide application in transition metal compounds because they are very convenient and practical to use, comparable in computer speed with the most simplified of the semiempirical methods, and yet often superior in accuracy to good HF calculations.

In the ECP or pseudopotential approximation [53–56], the chemically uninteresting core electrons are replaced by an effective one-electron potential that is required to produce a nodeless pseudo-orbital φ, which has the same orbital energy, ε_i, as the HF orbital, φ_i, and which has an identical shape to φ_i in the valence region of the atom. The ECP represents the Coulombic, exchange and orthogonality interactions between the valence electrons and the core. They may be derived from atomic HF or Dirac–Fock (DF) wavefunctions by any of several methods, including direct inversion of a HF equation [57], or direct optimization of parameters [58].

All ECP procedures developed so far can be well applied within the framework of both the HF and LD theories [59,60]. Moreover, in the quantum chemical studies of molecular or cluster systems containing heavy atoms, recent developments of the ECP methods led to the formulation of relativistic effective core potential (RECP) methods characterized by an improvement in their predictive capability. These methods are expected to be more widely adopted in the field of coordination chemistry in the near future.

It now becomes clear that accurate ab initio calculations for transition metal compounds are possible today, but the computational effort is very high, even for very simple systems such as free atoms and diatomic molecules. Most of the high quality theoretical calculations on these systems were done by using the complete active space MCSCF followed by multireference single + double relativistic CI (CASSCF/MRD CI/RCI) methods employing valence Gaussian basis sets of higher than double zeta + polarization quality.

The CASSCF method put forward by Roos et al. [61] provides a zero-order starting set of orbitals for inclusion of higher order correlation effects. The orbital space in the CASSCF method is divided into three sub-spaces involving: (i) doubly occupied core or inactive orbitals, (ii) active orbitals and (iii) unoccupied secondary orbitals. In the active orbitals, the electrons important for chemical bonding are distributed in all possible ways. Moreover, within the active subspace, a full CI treatment is performed.

The MRD-CI method considers a few configurations determined by the important configurations in the CASSCF as references. The configurations resulting from single and double (SD) excitations from all these main configurations are included together with the main ones in the final CI problem. Furthermore, correction for the full CI energy, ΔE_Q, may be obtained with the Davidson [62] formula

$$\Delta E_Q = (1 - C_0^2)\Delta E_D$$

where ΔE_D is the correlation energy due to the double excitations and C_0 the coefficient of the main configuration in the SD-CI.

Another important quantum chemical method of high quality, widely applied in the field of transition metal compounds and organometallics, is the generalized valence bond (GVB) method proposed by Goddard [63,64]. GVB is a new, very powerful version of the old well-known valence bond (VB) method which, in contrast to the MO methods, considers two-electron pairing at the outset.

In general, the evolution of 'black-box' quantum chemical programs, coupled with the increasing performance of computer hardware, has resulted in a tremendously expanding role for ab initio techniques in different applications. However, in the investigations of large molecules, the ab initio methods are still too cumbersome to apply [65], especially for the calculation of parts

of hypersurfaces to follow the course of a chemical reaction. The costs are especially high when the desired accuracy can be obtained only with larger than minimal basis sets. So there is still a need for fast and inexpensive, yet reasonably accurate methods. As an alternative to ab initio methods, semiempirical SCF MO procedures can be used.

Many of the semiempirical SCF MO methods are modifications of the Pariser–Parr–Pople (PPP) scheme and contain various degrees of neglect of differential overlap (NDO). Some of the more sophisticated of them, SINDO, MINDO/3 and MNDO, have given quite reliable results, e.g. for binding energies and ground state geometries of first-row molecules [66,67]. Along this line, attempts have recently been made to extend their applicability by including transition metal parametrization and introducing modern algorithms. Some very efficient programs have already been developed [68,69], providing new, inexpensive, rapid and reliable tools for the study of transition metal compounds, though their applicability is not comparable with that of compounds containing first-row elements. Further improvement of their accuracy may also be obtained by inclusion of relativistic effects [70].

During the last 15 years, semiempirical MO calculations, at the extended Hückel molecular orbital (EHMO) level of approximation, have been widely used, particularly by Hoffmann and his coworkers [71], to describe the stereochemical preferences of coordination and organometallic compounds. The EHMO theory, together with orbital interaction rules, frontier orbital theory and symmetry considerations, provided the experimentalists in coordination and organometallic chemistry with a very popular tool for the study of structure, dynamics and reactivity problems concerning 'chemically interesting' molecular systems. Its popularity is mainly due to it being inexpensive and easy to run, even by a non-theoretician on a PC computer, and its transparency, which presents the clearest picture of how the electronic structure of small and large molecules varies with respect to the structure of the molecule. It is curious that the EHMO model has been so successful in accounting for ground state geometries and rotational barriers of compounds [72] despite the approximate nature of the model for the majority of the calculations and the total neglect of electron–electron repulsion, nuclear–nuclear repulsion and electron correlation effects [73,74]. Some improvements of the EHMO model by including relativistic effects for the heavy atoms [70,75,76] and the development of new forms of Coulomb and resonance integrals [77,78] have appeared in the literature very recently. However, being a one-electron MO model, EHMO suffers from the intrinsic problem of MO theory which, although it projects symmetry control, does not make the atom excitation/bond making interplay explicit. Moreover, it fails to produce the correct mechanism of electron delocalization [79–85] and therefore cannot provide an understanding of chemical bonding.

A more recent, equally simple approach, called MOVB theory [86], is claimed to be superior to the simple EHMO model with respect to understanding the mechanism of chemical bonding. MOVB theory, being a fusion of the MO and VB theories, allows one to see explicitly how symmetry dictates atom excitation for optimal electron delocalization mechanisms, that is for optimal bond formation, thus providing a new look at the chemical bonding in transition metal compounds. Nevertheless, both EHMO and MOVB have played their part in shaping our recent picture of bonding in transition metal compounds and providing the basis for understanding and predicting important chemical trends. Actually, this is what experimental chemists need as a frame in which to plan.

The quantum chemical study of 'chemically interesting' large-size molecular systems, at any level of sophistication, is substantially simplified by the introduction of fragments into the theory. Fragments are parts of large molecules that are also parts of smaller molecules and are transferable from molecule to molecule. Such fragments may be very useful as building blocks in large molecules [87]. The well-known fragment molecular orbital formalism [88–90] is so far one of the most popular theories for viewing the geometrical and electronic structures of transition metal compounds and organometallics.

All computational methods of quantum chemistry briefly discussed in this section are now being successfully used to extract the detailed mechanisms of many reactions in transition metal chemistry and particularly in catalysis. However, before proceeding further to illustrate this process with several recent examples, a brief overview of the general theory of chemical reactivity is worth presenting. In this way, I think that the reader will feel comfortable with the terminology and acronyms that will be utilized in the next section.

C. GENERAL THEORY OF CHEMICAL REACTIVITY

The prediction of chemical reactivity presents a constant challenge to the chemist who wants to define optimum conditions for performing specific reactions. In this respect, theory plays a crucial role in providing quantitative data on the structure and energetics of reaction intermediates and transition states and, even more importantly, in providing the qualitative framework in terms of which one can make predictions on new systems.

The quantum theory of chemical reactivity is mainly based on two different approaches [91]: (i) transition state theory and (ii) the collision theory. Whatever procedure is used, knowledge of electronic energy as a function of inter-nuclear distances is needed. The energy associated with the electronic wavefunction of the reacting system is commonly called *the potential*

energy and leads to the concept of *potential energy hypersurfaces*, which are related to the force field applied to any nuclear configuration.

(i) Potential energy hypersurfaces and reaction paths

A satisfactory potential energy can be obtained by means of quantum chemical computational procedures. In principle, there are no restrictions to a theoretical study of the potential energy of a molecular system, which can be evaluated at any point along the reaction path. There are three main procedures for computing potential energy hypersurfaces [92]:

(1) large configuration interaction,

(2) both HF calculation and correlation energy approximated as a sum of Bethe–Goltstone pair energies and

(3) suitably chosen multiconfiguration calculation.

In studying potential energy hypersurfaces, one may follow two general strategies [92–96]: (i) focus the investigation on an accurate, detailed description of local properties of such hypersurfaces and (ii) choose to study the overall, global features of the potential surface. Although the two approaches are necessarily interrelated, they do require somewhat different techniques. A suitable definition of a continuous line connecting reactants and products is still the subject of both extensive investigation and confusion. However, this line should be an important guide ('reaction path', 'reaction coordinate', 'minimum energy path') in locating the transition states and intermediates between reactants and products.

In a potential energy hypersurface, one seeks different points of chemical interest in order to locate the reaction valley on the multiconfigurational potential surface, which corresponds to the minimum energy reaction path. Such points are:

(i) the *stationary points* corresponding to more or less stable molecular structures, for which all first derivatives with respect to the internal coordinates are vanishing. The absolute minimum stationary point corresponds to an equilibrium geometry of the molecule.

(ii) the highest energy point on the minimum energy reaction path connecting two minima, respectively called reactant (R) and product (P) points. This is called the *transition point* or *saddle point* and corresponds to the structure of the transition state. The associated energy ($E^{\neq}$) is then the highest energy on the reaction pathway and $\Delta E^{\neq} = E^{\neq} - E^{R}$ represents the *transition barrier* or *potential barrier*. Potential barriers can be considered to be dynamic indices of chemical reactivity as they are directly related to the dynamics of the reaction [97].

The minimum energy reaction path is nowadays identified [98–102] as that orthogonal trajectory which connects two energy minima via a common

saddle point. The various methods for its calculation are exhaustively discussed in a recent review [95]. Among them, the simplest is based on the selection of the steepest descent pathway, the so-called *intrinsic reaction coordinate* (IRC), starting from the saddle point and going down, respectively, to the reactants (R) and the products (P). The IRC is shown to include conservation of nuclear symmetry [103] and seems to be a concept of high utility [101]. The knowledge of the minimum energy reaction path allows the calculation of the potential barrier and any procedure is convenient which permits the structure of the corresponding state to be obtained. The problem consists, principally, in calculating the energy profile of the reaction, i.e. a large number of possible configurations for the interacting species and determining the easiest reaction path. Along this line, principles such as that of least motion, proposed by Eyrenson [104], can also help to predict the structure of the transition states. According to this principle, a reaction path involves the least change in the nuclear positions and the electronic configurations. Calculation of the energy of various possible models for the transition state can also help to select the most convenient one.

For supermolecules belonging to the arsenal of coordination and organometallic chemistry, an incredibly large number of degrees of freedom is involved, increasing the possible structure arrangements exponentially. Therefore, only approximate potential hypersurfaces may be obtained, using approximate computational methods and techniques [105]. In that case, one calculates only the portion of the surface which is expected to contain the reaction pathway (the bottom of potential valleys). Most of the relevant information is thus gained at the expense of unreliability for the heats of the reactions and potential barriers. Of course, as the complexity of the molecular systems increases, cruder assumptions have to be applied in order to keep computing time and costs low. However, generally, MO theory combined with perturbation techniques has been successful in a large number of reactions in several fields of chemistry.

(ii) Perturbation theory of reactivity

Perturbation theory deals with both the energy changes and electron transfer processes taking place during the formation of a molecular complex AB from the interaction between two molecules A and B. In the general case of the interaction between two molecules A and B by means of orbitals on atom r of A and on atom s of B, it can be shown [106–109] that the interaction energy (or the binding energy), ΔE, is given by the expression

$$\Delta E = -\frac{q_r q_s}{R_{rs}\varepsilon} + 2\sum_{m}^{occ}\sum_{n}^{unocc}\frac{(c_r^m c_s^n \beta_{rs})^2}{E_m - E_n} \qquad (1)$$

The first term in eqn. (1) represents the electrostatic interaction between two atoms carrying formal charges q_r and q_s, whereas the second one introduces the partial electron transfer from ψ_m to ψ_n, responsible for the stabilization of the system owing to covalent bond formation. The contribution of each term to ΔE depends primarily on the magnitude of the $E_m - E_n$ energy gap. When this is large, very little charge transfer occurs and ΔE is determined primarily by the charges on the two reactants, i.e. the electrostatic term is the dominating factor of the reactive interactions. For this reason, we will refer to such a situation as a '*charge controlled*' reaction. Conversely, if q_r and q_s are both small and E_m lies close to E_n, the covalent terms in eqn. (1) predominate and the interaction is referred to as '*orbitally controlled*' or '*frontier controlled*'.

A critical review of the errors introduced by eqn. (1) at short A–B distances has been published by Claverie et al. [110]. Many different methods which also account for the 'short-range' terms of the reactive intermolecular interactions have found application in problems of intermolecular interactions and of chemical reactivity [111]. Among them, the so-called 'supermolecule' method is of special interest [111,112].

In the supermolecule method, the entire complex is considered as a supermolecule and the calculated energy difference between the supermolecule and the monomers is the binding energy, e.g.

$$\Delta E(\mathbf{R}) = E(\mathrm{AB},\mathbf{R}) - E(\mathrm{A}) - E(\mathrm{B}) \tag{2}$$

where $E(\mathrm{A})$ and $E(\mathrm{B})$ are the energies of A and B, respectively in their isolated equilibrium geometries and $E(\mathrm{AB},\mathbf{R})$ is the supermolecule AB energy as a function of its geometry **R**.

In this approach, several methods have been proposed for reducing the interaction energy into various conceptually convenient components [112–119]. In the well-known and widely employed method put forward by Morokuma and Kitaura [112–114], the interaction energy is written as the sum of the electrostatic (E_{ES}), polarization (E_{PL}), exchange repulsion (E_{EX}), charge-transfer (E_{CT}), higher order coupling (E_{MIX}) and dispersion (E_{DISP}) energy terms:

$$\Delta E = E_{ES} + E_{PL} + E_{EX} + E_{CT} + E_{MIX} + E_{DISP} \tag{3}$$

The term E_{MIX} is obtained as a difference between the total SCF value of ΔE and the other components independently calculated, whereas E_{DISP} is not included in the HF supermolecule and had to be calculated from perturbation theory or semiempirically and added to the HF interaction energy.

The basis of the method as well as its practical aspects and limitations have been elegantly discussed by Morokuma and Kitaura [112]. The following decomposition has been applied in the case of metal–ligand interac-

tions [120–125]:

$$\Delta E = E_{ES} + E_{EX} + E_{CTPLX(A\rightarrow B)} + E_{CTPLX(B\rightarrow A)} + E_R \tag{4}$$

In this equation, E_R is the higher order coupling term and the terms $E_{CTPLX(A\rightarrow B)}$ and $E_{CTPLX(B\rightarrow A)}$ account for the donative and back-donative interactions, which can also be divided into σ- and π-type contributions.

Some components of the calculated L_nM–L′ bonding energies were proposed [126–128] as a measure of both the relative donor and acceptor abilities of the ligands L′ and the nucleophilicity of the metal-containing fragments L_nM. In the framework of the HFS transition-state method [129–131], Ziegler and Rauck [132,133] have proposed a decomposition of the calculated L_nM–L′ bonding energies into steric factors (ΔE_0), being purely electrostatic in nature, as well as contributions due to σ-, π-donation and π^*-back donation according to the scheme:

$$D(L_nM\text{–}L') = \Delta E_{prep} + \Delta E_0 + \Delta E_{elec} + \Delta E_R \tag{5}$$

with ΔE_{elec} being a sum of the electronic contributions, ΔE_Γ, from each symmetry representation Γ, e.g. $\Delta E_{elec} = \Sigma_\Gamma \Delta E_\Gamma$. The final term, ΔE_R, corresponds to the contribution from relativistic effects to the bonding energy. ΔE_R has been found to contribute substantially to the bonding energy only for the 5*d* transition metal series [32,134] and therefore could be omitted for their 3*d* and 4*d* counterparts.

The constrained space orbital variation (CSOV) technique introduced by Bauschlicher and coworkers [135] avoids the constraints of population analysis by optimizing the wavefunction in a series of steps. The starting point for the CSOV steps of partial orbital variations is the frozen orbital (FO) wavefunction formed by superimposing the wavefunctions of the free metal and ligand subunits. Within it, the bonding in ML systems is discussed in terms of σ repulsion between the ligand lone pair and the metal, the ligand to metal σ donation when there is an empty or partly occupied d_σ orbital and the metal to ligand π-back donation. Moreover, an unambiguous assignment for the energetic importance of each step can also be obtained by CSOV analysis.

Before ending this section, a brief discussion of the role of the interaction of particular MOs in chemical reactions is worthy of consideration since such interactions provide a substantial insight into the specificity (orientation and stereoselection) of chemical reactions [136]. In the well-known frontier electron approach of chemical reactivity introduced by Fukui et al. [136–138], these particular MOs are the highest occupied MO (HOMO) or sometimes high-lying occupied MOs and the lowest unoccupied MO (LUMO) or sometimes low-lying unoccupied MOs. For open shell systems, the single occupied MOs (SOMOs) play an essential role in orbital interactions between the reactants in a chemical reaction.

Qualitative perturbational molecular orbital (PMO) procedures have also proved to be efficient for analysing the energy effects associated with orbital interactions occurring between the reactants in a chemical reaction [139–144]. This perturbational treatment of chemical reactivity is founded upon one-electron molecular orbital theory and therefore is simpler than the generalized polyelectronic perturbational theory of chemical reactivity already discussed, since it leads to simpler equations for the orbital interaction energy. In closed shell reacting species A and B, the orbital interactions which play a significant role in determining the molecular structure of AB are either stabilizing two-electron-two-orbital (2e-2O) interactions or destabilizing four-electron-two-orbital (4e-2O) interactions [90,144–146]: The theoretical and conceptual aspects of PMO analysis have now become useful guide-lines for analyzing MO wavefunctions of inorganic and organometallic compounds, allowing experimentalists in these fields to use it as a counterpart to their experimental work for understanding structural and reactivity problems.

(iii) Reactivity indices

The reactivity indices are conventional theoretical quantities which can be used as a measure of the relative rates of reaction of similar sorts occurring in different positions in a molecule or in different molecules. In general, they are obtained by the employment of the most simple quantum chemical tool applicable for chemical interactions, namely the MO method. The reactivity indices that have been proposed by the use of MO theory are conveniently divided into two groups: *dynamic indices* and *static indices.*

Dynamic indices are defined on the basis of the so-called *dynamic model* or *localization method* introduced by Wheland [147], which is referred to the region of the potential energy surface involving the transition state. Therefore, any procedure permitting the structure of the transition state to be obtained may be convenient to estimate dynamic indices. In this regard, knowledge of the reaction path is needed, as we must know the energy of the saddle point. Owing to these facts, such molecular indices have not found wide application so far. Nevertheless, the estimation of dynamic indices remains a central problem in the quantum theory of chemical reactivity. The localization energies, L_μ^+, $L_\mu^{\cdot}$ and L_μ^- corresponding to nucleophilic, radical and electrophilic attack on an atom μ of an aromatic system [147,148] as well as the potential barriers belong to the dynamic indices of chemical reactivity. More recently, a molecular dynamic reactivity index called $P_A(r)$, which corresponds to polarization effects in the interaction energy of the reacting system, has been introduced by Tomasi and coworkers [149], and has been used successfully for the study of the chemical reactivity in protonation processes.

TABLE 1

The notation, description and definition of static molecular indices[a]

Notation	Description	Definition[b]	Ref.
ε_{FMO}	The frontier orbital's eigenvalue; usually ε_{HOMO} and ε_{LUMO}	Normal definition	
E_{tot}	The total electronic energy	Normal definition	
$V(\vec{R})$	The electrostatic potential at a point R in the vicinity of an atom or molecule	$V(\vec{R}) = \sum_{\mu} \frac{Z_\mu}{\lvert\vec{R}_\mu - \vec{R}\rvert} - \int \frac{\rho(\vec{r})\mathrm{d}\vec{r}}{\lvert\vec{r} - \vec{R}\rvert}$ $= \sum_{\mu=1}^{v} \frac{Z_\mu - q_\mu}{\lvert\vec{R}_\mu - \vec{R}\rvert}$	111, 153, 164
$E(\vec{R})$	The electric field created by the molecule for a unit positive charge at point R	$E(\vec{R}) = \sum_{\mu} \frac{Z_\mu - q_\mu}{\lvert\vec{R}_\mu - \vec{R}\rvert^3} (\vec{R}_\mu - \vec{R})$	153, 176
q_μ^E, q_μ^N	The electrophilic and nucleophilic charges calculated from the occupied and unoccupied MOs, respectively	Normal definition	
$q_{(i,\mu)}^E$, $q_{(i,\mu)}^N$	The electron charges as before, calculated only for the corresponding ith MO	Normal definition	
Q_μ, $Q_{\mu\nu}$, ...	The net atomic and group charge respectively	Normal definition	
$\Delta\rho_M(r)$	The molecular difference density	$\Delta\rho_M(r) = \rho_M(r) - \sum_{\mu} \rho_\mu(r)$ $\rho_\mu(r) = \sum_{m,n} P_{mn}^{\mu}(r)\varphi_m^*(r)\varphi_n(r)$	179–182
L_μ	The local anisotropy of the electronic charge on atom μ	$L_\mu = \sum_{m\in\mu} \sum_{n\in\mu} P_{mn}^2 - \sum_{l=0}^{k} \left(\sum_{m=l^2+1}^{m=(l+1)^2} P_{mn} \right)^2 \frac{1}{2l+1}$	186

V_μ, V_M, V_i	The atomic, molecular and molecular orbital valency, respectively	$V_\mu = \sum_{m\in\mu} 2P_{mm} - B_{\mu\nu}$ $= \sum_{\mu\neq\nu} B_{\mu\nu} = \sum_{m\in\mu}\sum_{\nu\neq\mu}\sum_{n\in\nu} P_{mn}^2$ $= 2Q_\mu - \sum_{m\in\mu}\sum_{n\in\nu} (\underline{P}\,\underline{S})_{mn}(\underline{P}\,\underline{S})_{nm}$	158, 186–189
		$V_M = \frac{1}{2}\sum_\mu V_\mu = \sum_i V_i$	191
		$V_i = \frac{1}{2}\sum_\mu \sum_{m\in\mu}\sum_{\nu\neq\mu}\sum_{n\in\nu}\sum_j n_i n_j C_{im}C_{in}C_{jm}C_{jn}$	
$B_{\mu\nu}$	Wiberg's bond index	$B_{\mu\nu} = \sum_{m\in\mu}\sum_{n\in\nu} P_{mn}^2$ $= \sum_{m\in\mu}\sum_{n\in\nu} (\underline{P}\,\underline{S})_{mn}(\underline{P}\,\underline{S})_{nm}$ $= \sum_{m\in\mu}\sum_{n\in\nu} (\underline{S}^{1/2}\underline{P}\,\underline{S}^{1/2})_{mn}$	156, 158, 188, 190
ΔV	The valence reduction	$\Delta V = \sum_\mu^{\text{atoms}} (V_\mu^{\text{normal}} - V_\mu^{\text{actual}})$	154
N_μ^α	The free electron index	$N_\mu^\alpha = \frac{1}{2}\left[\sum_{m\in\mu} 2P_{mn} - \sum_{m\in\mu}\sum_{n\in\nu} P_{mn}^2 + B_{\mu\mu}\right] - \sum_{\nu\neq\mu} B_{\mu\nu}$	159
$(1/2)B_{\mu\mu}$	The number of electrons on atom μ		
F_μ	The free valency	$F_\mu = \sum_{m\in\mu} 2P_{mm} - \sum_\nu \sum_{m\in\mu}\sum_{n\in\nu} P_{mn}^2$ $= V_\mu - \sum_{\nu(\nu\neq\mu)} B_{\mu\nu}$ $= V'_\mu - \sum_{\nu\neq\mu} B_{\mu\nu}$	158, 186, 189
S_μ^E, S_μ^N, S_μ^R	The electrophilic, nucleophilic and radical superdelocalizabilities	$S_\mu^E = 2\sum_j^{\text{occ}}\sum_{m=1}^{N_\mu} (c_{jm}^\mu)^2/\varepsilon_j$, $S_\mu^N = 2\sum_j^{\text{unocc}}\sum_{m=1}^{N_\mu} (c_{jm}^\mu)^2/\varepsilon_j$, $S_\mu^R = \frac{1}{2}(S_\mu^E + S_\mu^N)$	136, 153

Notation	Description	Definition[b]	Ref.
$S_{i\mu}^{E}$, $S_{i\mu}^{N}$, $S_{i\mu}^{R}$	The electrophilic, nucleophilic and radical superdelocalizabilities calculated with for the ith MO		
$\pi_{\mu\mu}$, $\pi_{\mu\nu}$	The self-atom and atom–atom polarizabilities	$\pi_{\mu\mu} = 2\sum_{i}^{N}\sum_{j\neq i}^{N} n_i \frac{c_{\mu i}^2 c_{\mu j}^2}{\varepsilon_i^{(0)} - \varepsilon_j^{(0)}}$	153
		$\pi_{\mu\nu} = 2\sum_{i}^{N}\sum_{j\neq i}^{N} n_i \frac{c_{\mu i} c_{\mu j} c_{\nu i} c_{\nu j}}{\varepsilon_i^{(0)} - \varepsilon_j^{(0)}}$	

[a] The subscripts μ and ν denote atoms in the molecule, M, whereas i denotes a particular MO. The superscripts E, N and R denote electrophilic, nucleophilic and radical features of the indices.

[b] Z_μ is the charge on the nucleus μ located at $\vec{R}_\mu$; $\rho(r)$ is the electronic density function; P_{mm} and P_{mn} are density matrix elements for orbitals m and n associated to atoms μ and ν, respectively; l is the angular momentum quantum number; $\underline{S}$ and $\underline{P}$ are the usual overlap and density matrices, respectively.

Static indices are defined on the basis of the so-called *static model* or the *isolated molecule method* [150], which is referred to the region of the potential energy hypersurface involving the isolated reactants. The molecular indices calculated by this model are correlated with the reaction path under the assumption of the non-crossing rule [151], which states that, for similar reactants, the ratio of the energy necessary to reach any particular point on the respective reaction path curves is (approximately) proportional to the ratio of the activation energies.

At first sight, the static model seems to be invalid since, during the collision of two molecules, there is a complete reorganization of the electronic system and it is not obvious that the height of the potential barrier is simply related to the organization of the electrons in the isolated molecules. Since no configuration change of the reactants is taken into account, the use of the static model is limited to the case of weak interactions during the course of the reactions. However, the reactivity of a set of similar molecules $\{A_i\}$ interacting with the same molecule B to give similar reactions can be calculated by means of some molecular indices obtained from the wavefunctions of the isolated A_i molecules. In addition, as extensive experimental results indicated that chemical reactions usually begin at a localized position in the reactants, these molecular indices can also be used to predict this position in a particular reactant.

Several proposed static indices are related to the molecular charge distribution (nuclei and electrons), which plays a fundamental role in chemical reactivity. In other words, the static indices seem to be the best ones for reactions where E_{ES} is the determining term in eqn. (3). The most important static indices proposed so far are collected in Table 1.

All static molecular indices are associated with a particular region of a molecule and are related to the potential barrier of a reaction taking place at that region. Most of them are calculated from the first-order density matrix of the system and their ease of calculation has made them useful for parametrizing bonding effects as well.

Static index definitions at any level of sophistication are already developed [152–159] and can be currently adapted to available computer programs.

(*a*) *Energy indices*

The energy indices are related to various components of the energy characterizing the ground state of an isolated molecule. Accordingly, the eigenvalues of the frontier orbitals, ε_{FMO}, the total electronic energy, E_{tot}, the electrostatic potential, $V(\vec{R})$ and the electric field, $E(\vec{R})$ could be considered as energy indices.

Neither ε_{FMO} nor E_{tot} have been used as static reactivity indices so far. However, very recently [160–162] these quantum chemical MO indices have

been found very effective in parametrizing ligand bonding effects in coordination and organometallic compounds.

Reinhold et al. [160], studying the bonding properties of α-diimine complexes, suggested the use of the LUMO energies of the ligands as a measure of their π-acceptor ability. The LUMO energies, as well as some other parameters calculated from the first-order density matrix, such as the local anisotropies and Wiberg indices, have also been used by Ban et al. [161] to quantify the π-acceptor ability in a series of ten-valence isoelectronic diatomic ligands. More recently, we have investigated [162] the effectiveness of a series of quantum chemical MO indices in parametrizing ligand bonding effects of simple diatomic species being potential ligands in coordination and organometallic compounds. We have found that the bonding effects are, in fact, reflected in the energies and regiospecificities of the most appropriate and chemically relevant donor and acceptor MOs involved in the formation of the synergic bonding (σ-dative and π-back bonding). More importantly, very good linear correlations between ε_{FMO} and an experimentally defined parameter, P_L, called the ligand constant have been established [162]. The ligand constant, P_L, accounting for the overall attracting or releasing quality of a ligand, is defined as the change in oxidation potential measured in volts induced by the replacement of one carbonyl ligand in $Cr(CO)_6$ by the ligand L [163].

More information on the reactivity of a molecule could be obtained by the use of the electrostatic potential $V(\vec{R})$ as a static reactivity index [111,164]. The electrostatic potential, being a real physical property, is exactly equal in magnitude to the electrostatic (Coulombic) interaction energy, E_{ES}, between the unperturbed charge distribution of the system and a positive unit point charge located at $\vec{R}$. Moreover, it gives directly a global picture of the interaction energy of atom or molecule μ with point-charge reactant over the whole space surrounding it. When the reactant is not a point-charge, $V(\vec{R})$ can still be employed to simplify the calculation of E_{ES}, which for two rigid charge distributions $\rho_A(\vec{r},\vec{R}_\alpha)$ and $\rho_B(\vec{r},\vec{R}_\beta)$ is given by the equation:

$$E_{ES}(A,B)=\sum_k q_{Bk} V_A(\vec{k},\vec{R}_\alpha) \tag{6}$$

By computing contour maps of $V_A(\vec{R})$ in various planes throughout a molecule, it is easy to see and compare the special regions in which $V(\vec{R})$ is negative and to which an electrophile would initially be attracted. Moreover, the presence of negative potential wells is associated with possible locations of an approaching electrophile and the method is therefore suitable for evaluating chemical reaction paths.

The calculation of electrostatic potential maps (EPMs) as a guide to the reactive regions of molecules was pioneered by Bonaccorsi et al. [165] and they were quickly adopted [166], along with reaction potential maps (RPMs)

[167], as a major tool for the elucidation of the reactive properties of molecules. The RPMs are created by calculating both the electrostatic and charge transfer interaction terms for the interaction between the molecule and a model reagent successively placed at all points in space. The equipotential energy maps created in this process are evaluated by perturbation theory.

The use of the electrostatic potential as a tool to correlate structure and reactivity in a wide variety of cases is now well-established [167–170]. The concept is especially useful in the field of huge polymers and, in particular, of biopolymers for which understanding of the role of the overall macromolecular structure upon the reactivity of their reaction sites represents one of the fundamental problems that faces both experimentalists and theoreticians [171,172]. Along this line, of particular interest is the use of $V(\vec{R})$ in the study of the binding of metal species to the subset of the nucleic acid bases consisting of cytosine and guanine [173,174]. In these studies, the role that the molecular electrostatic potential plays in determining the site of primary metal coordination and subsidiary metal–ligand and ligand–ligand interactions in the resulting complex have been emphasized.

The interactions of platinum anti-tumour drugs with a variety of nucleic acid bases have also been investigated and the results have recently been reviewed by Bourdeaux [175]. In a very interesting study, Abdul-Ahad and Webb [176] used both $V(\vec{R})$ and $E(\vec{R})$ along with other indices in an effort to correlate electronic structure with antitumour activity and toxicity in a variety of Pt–amine complexes. The regression equations proposed are noteworthy but have only limited applicability.

Finally, it is important to note that both $V(\vec{R})$ and $E(\vec{R})$, along with other quantum chemical indices, have also been used as variables in either single- or multi-variable regressions by Brown and Simas [153] in an attempt to parametrize chemical reactivity with static molecular indices. The appropriate Hammett function, σ, has been used as a measure of the chemical reactivity and some very good correlations have been established, providing thereby the means for predicting the reactivities of aromatic compounds for both cyclic and exocyclic sites of reactivity.

(b) Charge indices

The charge indices are related to the various characteristics of the electron density distribution in the ground state of an isolated molecule. Accordingly, the electrophilic and nucleophilic charges, q_μ^{E} and q_μ^{N}, respectively, their corresponding FMO analogues $q_{i\mu}^{\mathrm{E}}$, $q_{i\mu}^{\mathrm{N}}$ and $q_{i\mu}^{\mathrm{R}}$, the net charges Q_μ and $Q_{\mu\nu}$ . . ., the molecular difference density, $\Delta\rho_{\mathrm{M}}(\mathrm{r})$ and the local anistropy of the electronic charge, L_μ, could be considered as charge indices.

The net atomic charges, the electrophilic and nucleophilic charges as well as the frontier electron densities follow the normal definitions. Although these

static indices have met with criticism, they have been used successfully in many cases [177,178]. The problems with these indices are deeply rooted in the fundamental principles of quantum mechanics, as they are not observables and therefore cannot be uniquely defined.

A more reliable and physically meaningful picture of the electron density distribution in a molecule is given by the molecular difference density, $\Delta\rho_M(r)$. The molecular difference density has been related to chemical bonding in a molecule [179–182]. Thus, a chemical bond is characterized by positive $\Delta\rho_M(r)$ values between the bonding atoms. More recently [183,184], instead of $\Delta\rho_M(r)$ the second derivative of the molecular density $\nabla^2\rho_M(r)$ has been proposed as an index of chemical bonding. In this case, a chemical bond is characterized by large negative $\nabla^2\rho_M(r)$ values between the bonding atoms.

A more chemically useful definition of electron difference densities has been given recently by Schwarz et al. [182,185]. They have proposed a recipe for the unique definition of an 'oriented' ground state density called *chemical difference density* (CDD). Such an analysis of the difference densities allowed the determination of not only the positional parameters of the atoms, but also their respective directional parameters and quadrupole moments. Moreover, the CDD gives insight into the electronic structure of a molecule and, by the orientation parameters involved, provides further information of chemical relevance related to intermolecular interactions. Therefore, additional work is needed to illustrate how effectively CDD may reflect chemical reactivity in a molecule, thus providing a new reactivity index.

The local anisotropy, L_μ, representing the anisotropy of the electronic environment on the atom μ in a molecule, has been proposed as a qualitative measure of the π-acceptor capacity of diatomic ligands [161], although its effectiveness has been questioned recently [162]. However, L_μ associated with the lability of an atom in a particular environment has proved to be a good predictor of the bonding mode of diatomic ligands [162].

(c) *Valency indices*

The first quantum chemical definition of atomic valency, V_μ, in terms of the density matrix elements of the molecules was proposed by Armstrong et al. [186,187] based upon Wiberg's bond index, $B_{\mu\nu}$ [188]. The definition of V_μ was extended by Gopinathan and Jug [189] to include open shell systems and was also generalized to CI calculations [155]. Exactly the same definition of V_μ for closed shell systems has recently been proposed for ab initio (or EHMO) wave-functions based either on the 'standard' density matrix [158] or on the density matrix based on the Löwdin orthogonalized basis [156,158,190]. The two definitions differ with respect to the definition of the Wiberg's bond index.

Both V_μ and $B_{\mu\nu}$ are very useful concepts in understanding chemical bond-

ing but cannot be considered as reactivity indices. In order to have a means of measuring chemical reactivity, the *free valency index*, F_μ, has been defined [154,158,186,187,189]. Furthermore, Jug and Gopinathan [154] have recently presented a method based on the concept of *valence reduction*, ΔV, which provides complementary information on chemical reactions along reaction pathways. The method has been successfully applied to concerted and non-concerted thermal reactions, as well as to photochemical reactions.

Gopinathan et al. [191] have also defined the *molecular orbital valency*, V_i, by decomposing the *total valency* of a molecule M, denoted as V_M, into its MO components. V_i provides a quantitative measure of the bonding nature of the ith MO, having a value close to unity for strongly bonding MOs and being very small for the core, lone pair and non- or anti-bonding MOs. Other applications of V_i have also been presented.

Very recently, Stradella et al. [159] have proposed the *free electron index*, N_μ^a, of atom μ in a molecule, applications of which have shown that values close to the number of electrons in lone pairs or radicals can be derived from Lewis formulae.

All valency indices have found important applications in understanding electronic structure and reactivity problems in simple organic and inorganic molecules. They would therefore be expected to be helpful also in understanding similar problems in more complicated molecules and in particular those belonging to the fields of coordination and organometallic chemistry.

(*d*) *Superdelocalizability and polarizability indices*

The superdelocalizability has been introduced as a static reactivity index by Fukui [136] using the simple Hückel formalism. Recently [153] it has also been defined at the CNDO level of approximation and has proved to be the best index for predicting the reactivity of aromatic compounds for both cyclic and exocyclic sites. Superdelocalizabilities have also been defined for any MO and of particular importance among them are those related to FMOs. They include both electrostatic and perturbational effects and therefore may be more effective in parametrizing chemical reactivity than the simple energy and charge indices. In fact this is the case for the aromatic substitution [153]. Despite their success in predicting chemical reactivity, superdelocalizabilities were also found to be effective MO indices for parametrizing ligand bonding effects of diatomic ligands [162].

Finally, the polarizability indices defined either by the Hückel or the more sophisticated approximations have also been used successfully as predictors of the reactive sites in organic molecules. The effectiveness of the polarizabilities as reactivity indices is based upon the linear effect of the charge and polarizability on the energy of the system and therefore their use is compatible with linear free energy relationships. Polarizabilities have been used success-

fully as variables in multiple regressions correlating chemical reactivity in a series of aromatic compounds [153]. Obvious extensions to reactivity problems of coordination and organometallic compounds would be worthwhile.

D. APPLICATIONS

In this section, attempts will be made to review the recent developments towards understanding chemical reactivity through the quantum chemical methods briefly overviewed in the previous sections. Attention will be paid to the various types of reaction encountered in molecular coordination and organometallic chemistry which are of key importance in understanding the versatile stereochemistry, chemical reactivity, catalytic and biological activity of coordination compounds and organometallics. Moreover, considering that the elementary steps in almost all of the reactions of particular interest in organotransition metal chemistry involve M–L bond cleavage and M–L bond formation, the theoretical aspects of the metal–ligand interactions and their energetics developed in the last decade will be presented. Actually, the last decade has witnessed intensive research activity in the burgeoning field of transition metal thermochemistry, including both experimental and theoretical approaches [192]. High quality ab initio calculations provided reliable thermodynamic quantities, particularly the M–L bond dissociation energies (BDEs) for almost all transition metals, M, and several rudimentary ligands, L, which were classified as:

(i) pure σ-donor ligands, such as H, OH_2, NH_3 and R (R = alkyl),

(ii) σ/π-donor ligands, such as O, OH, OCH_3, SH, NH_2 and PH_2,

(iii) strong π-acceptor ligands, such as CO, CN, C_2H_4 and C_2H_2,

(iv) σ-donor/π-acceptor ligands of intermediate character, such as N_2 and PR_3 and

(v) other ligands of key importance, such as CR (carbynes) and CR_2 (carbenes).

Structure and reactivity problems concerning solid state inorganic chemistry, encompassing clusters, extended structures and surfaces will not be considered, although research activity in this virgin area has grown exponentially in the last decade.

(i) Transition metal hydrides. Dihydrogen activation and reactivity

(a) Bond dissociation energies of MH and MH^+ systems

The simplest of the transition metal compounds are those involving one transition metal atom, M, or ion, M^+, and one simple ligand, L. These monoligated transition metal compounds have been treated both experimentally and theoretically [192–195] in order to understand their chemistry which could provide insights into fundamental aspects of organometallic

chemistry and catalysis. Experimentally these types of compound have been studied either by gas phase spectroscopy or matrix isolation spectroscopy [194–200]. The results obtained so far are used to check quantum chemical calculations, allowing theoreticians to develop more efficient methods capable of achieving very high accuracies in the determination of geometries and electron distributions in such simple systems.

High quality theoretical results on the BDEs of the simplest of the monoligated transition metal compounds, i.e. the metal hydrides, MH, and their

TABLE 2

Theoretical and experimental bond dissociation energies (kcal mol^{-1}) for the cationic transition metal hydrides of the first row transition metals

Compound	Ground state	$D_e(M^+-H)$	$D_0(M^+-H)$	Computational method	Ref.
ScH^+	$^2\Delta$	57.5	55.2 (55.3 ± 2.3)[a]	GVB-DCCI	201,202
			56.0	MCPF	203
		54.8	52.7	MCSCF+1+2CI	204
		55.1		MRD-CI	205
TiH^+	$^3\Phi$	56.4	54.0 (53.3 ± 2.5)	GVB-DCCI	201,202
			53.3	MCPF	203
			46.5	MCSCF+1+2CI	206
		53.3		MRD-CI	205
VH^+	$^4\Delta$	46.1	43.6 (47.3 ± 1.4)	GVB-DCCI	201,202
			48.6	MCPF	203
		49.6		MRD-CI	205
CrH^+	$^5\Sigma^+$	26.9	24.3 (27.7 ± 2.0)	GVB-DCCI	201,202
			27.7	MCPF	203
		25.1		MCSCF+1+2CI	207
MnH^+	$^6\Sigma$	41.8	39.6 (47.5 ± 3.4)	GVB-DCCI	201,202
			43.7	MCPF	203
			46.0	HFS	208
		40.8		HF-SDCI	209
FeH^+	$^5\Delta$	49.4	47.0 (48.9 ± 1.4)	GVB-DCCI	201,202
			52.3	MCPF	203
CoH^+	$^4\Phi$	45.9	43.6 (45.7 ± 1.4)	GVB-DCCI	201,202
			44.5	MCPF	203
NiH^+	$^3\Delta$	38.2	35.7 (38.6 ± 1.8)	GVB-DCCI	201,202
			41.0	MCPF	203
			42.0	CASSCF-CCI	210
CuH^+	$^2\Sigma^+$	23.5	20.9 (21.2 ± 3.0)	GVB-DCCI	201,202
			18.5	MCPF	203
ZnH^+	$^1\Sigma^+$	55.1	52.4 (54.1 ± 3.0)	GVB-DCCI	201,202
		35.1		DFOCE	211
			57.8	HFS	208

[a] Figures in parentheses are experimental data taken from ref. 212.

cationic species, MH^+, for both first and second row transition metals are collected in Tables 2–5, along with experimental results for the sake of comparison.

It is clear from the results shown in the tables that theoretical BDEs are en bloc in excellent agreement with experiment, especially for the cationic species where experimental analysis based on guided ion beam tandem mass spectrometric methods [195,212] is more refined. It is also clear from the tables that all the computational methods used gave the same ground states for all species studied, with only a few exceptions such as those referred to the ZrH^+ and RuH^+ systems.

(b) Electronic structure and bonding of the MH and MH^+ systems

The electronic structure of the MH and MH^+ systems, independently of the computational method, was found to reflect more or less the electronic configuration of the transition metal atom or ion. This was attributed to the fact that H acts just as a weak perturber of the electronic structure of the heavy atom M or ion M^+. Considering that the bonding between M (or M^+)

TABLE 3

Theoretical and experimental bond dissociation energies (kcal mol^{-1}) for the cationic transition metal hydrides of the second row transition metals

Compound	Ground state	$D_e(M^+-H)$	$D_0(M^+-H)$	Computational method	Ref.
YH^+	$^2\Sigma^-$	60.1	57.8 (58 ± 3)[a]	GVB-DCCI	213
			59.4	MCPF	203
ZrH^+	$^3\Phi$	57.0	54.6 (54 ± 3)	GVB-DCCI	213
	$^3\Delta$		56.7	MCPF	203
NbH^+	$^4\Delta$	51.3	48.7 (53 ± 3)	GVB-DCCI	213
			52.5	MCPF	203
MoH^+	$^5\Sigma^+$	33.8	31.2 (41 ± 3)	GVB-DCCI	213
			35.3	MCPF	203
TcH^+	$^6\Sigma^+$	48.8	46.3	GVB-DCCI	213
			50.7	MCPF	203
			56.6	HFS	208
RuH^+	$^2\Sigma^-$	34.5	31.7 (40 ± 3)	GVB-DCCI	213
	$^5\Delta$		37.8	MCPF	203
RhH^+	$^4\Delta$	37.8	34.8 (35 ± 3)	GVB-DCCI	213
			41.5	MCPF	203
PdH^+	$^1\Sigma^+$	43.7	40.6 (46 ± 3)	GVB-DCCI	213
			49.0	MCPF	203
AgH^+	$^2\Sigma^+$	2.6	2.1 (15 ± 3)	GVB-DCCI	213
			10.6	MCPF	203
CdH^+	$^1\Sigma^+$	44.4	42.0 (49.3)	GVB-DCCI	213
			47.6	HFS	208

[a] Figures in parentheses are experimental data taken from ref. 212.

TABLE 4

Theoretical and experimental bond dissociation energies (kcal mol^{-1}) for the first row transition metal hydrides

Compound	Ground state	D_e(M–H)	D_0(M–H)	Computational method	Ref.
ScH	$^1\Sigma^+$	52.2	(47.5±2)[a]	MCPF	214
		56.0		MRD-CI	205
			28.5	MCSCF	215,216
			41.5	HF	217–219
TiH	$^4\Phi$	47.5	(38.0±3)	MCPF	214
		48.9	46.9	CASSCF-CI	220
		46.1		MRD-CI	205
		39.2	37.3	MCSCF	215,216
			36.9	HF	217–219
		45.0		ECP-CI	221
VH	$^5\Delta$	53.7	(37.9±3)	MCPF	214
		53.0	50.8	CASSCF-CI	220
		53.7		MRD-CI	205
		40.8	38.5	MCSCF	215,216
CrH	$^6\Sigma^+$	49.1	(41.2±3)	MCPF	214
		48.4	46.3	CASSCF-CI	220
		45.9		CI (R)	222
		46.1	43.9	MCSCF	215,216
		47.1		HFS	208
MnH	$^7\Sigma^+$	38.5	(<32.0)	MCPF	214
		39.4	37.1	CASSCF-CI	220
		43.8	41.8	MCSCF	215,216
FeH	$^4\Delta$	38.5	(29.6±3)	MCPF	214
			(46.0±3)		
		65.3	48.0	CASSCF-CI	220
			31.1	MCSCF	215,216
			34.0		
CoH	$^3\Phi$	44.7	(42.2±3)	MCPF	214
			(54.0±10)		
			47.9	MCSCF	215,216
NiH	$^2\Delta$	62.0	(60.0±3)	MCPF	214
			(65.0±6)		
		64.3	61.5	CASSCF-CI	220
		63.6	60.9	CASSCF-CCI	223,224
		60.6		ECP-MP4(SDTQ)	225
		57.7	54.9	MCSCF	215,216
CuH	$^1\Sigma^+$	60.6	(60.0±3)	MCPF	214
			59.7	MCSCF	215,216
			60.3	ECP-CI	221
		59.5		HFS	208
		54.2		CI (R)	222
		54.4		RECP-CI	226
ZnH	$^2\Sigma^+$	22.4	(20.5±0.5)	MCPF	214

[a] Figures in parentheses are experimental data taken from refs. 195 and 212.

TABLE 5

Theoretical and experimental bond dissociation energies (kcal mol^{-1}) for the second row transition metal hydrides

Compound	Ground state	D_e(M–H)	D_0(M–H)	Computational method	Ref.
YH	$^1\Sigma^+$	67.3		MCPF	227
ZrH	$^2\Delta$	56.5	(37.3)[a]	MCPF	227
NbH	$^5\Delta$	60.0	(48.1)	MCPF	227
MoH	$^6\Sigma^+$	50.5	(46.0 ± 3)	MCPF	227
			(53.0 ± 5)		
			58.01	HFS	208
TcH	$^5\Sigma^+$	45.0		MCPF	227
RuH	$^4\Phi$	54.0	(56.0 ± 5)	MCPF	227
RhH	$^3\Delta$	64.8	(59.0 ± 5)	MCPF	227
PdH	$^2\Sigma^+$	51.2	(56.0 ± 6)	MCPF	227
		68.9		MP4 (SDTQ)	225
			46.0		228
			32.0		229
			30.0		230
AgH	$^1\Sigma^+$	51.2	(54.0 ± 3)	MCPF RECP	227
			45.1		231
			35.1		232
			48.0	HFS	208

[a] Figures in parentheses are experimental data taken from refs. 195 and 212.

and H takes place exclusively through σ-orbitals, the following five bonding mechanisms could be operative in the transition metal hydrides and their cationic species:

(1) ns–$1s$ bonding,
(2) ns np_σ–$1s$ bonding,
(3) ns $(n-1)d_\sigma$–$1s$ bonding,
(4) $(n-1)d_\sigma$–$1s$ bonding,
(5) overlap induction.

The relative importance of these different mechanisms depends upon several competing factors, the following being the most important [201–203,213,214,220,227]:

(1) the relative separations of the low-lying metal electronic states,
(2) the relative orbital sizes of the transition metal,
(3) the intrinsic bond strength of H to various size, ns, $(n-1)d$ or hybridized metal orbitals and
(4) the loss of high-spin $(n-1)d$–$(n-1)d$ exchange energy on bonding.

The evolution of the energy separations between the low-lying electronic states of the first and second row transition metal atoms and their cationic species is shown in Table 6.

TABLE 6

Evolution of the energy separations, $\Delta E = E(sd^{n+1}) - E(s^2d^n)$, (in eV) between $(n+1)s^2nd^n$ and $(n+1)s^1nd^{n+1}$ electronic configurations of the first and second row transition metal atoms, along with the corresponding energy separations, $\Delta E = E(sd^n) - E(d^{n+1})$, (figures in parentheses), between $(n+1)s^1nd^n$ and nd^{n+1} electronic configurations of their cationic species

M(M^+)	ΔE			M(M^+)	ΔE		
	GVB-DCCI[a]	MCPF[b]	Exptl.		GVB-DCCI	MCPF	Exptl.
Sc(Sc^+)	(0.15)	1.51 (0.89)	1.44 (0.60)	Y(Y^+)	(0.83)	1.40 (0.20)	1.36 (0.88)
Ti(Ti^+)	(−0.04)	0.81 (0.36)	0.81 (0.11)	Zr(Zr^+)	(0.17)	0.53 (0.23)	0.59 (0.31)
V(V^+)	(−0.51)	0.27 (−0.10)	0.26 (−0.34)	Nb(Nb^+)	(−0.30)	0.35 (−0.46)	0.18 (−0.33)
Cr(Cr^+)	(−1.82)	−1.04 (−1.42)	−1.00 (−1.52)	Mo(Mo^+)	(−1.74)	1.88 (−1.91)	1.47 (−1.59)
Mn(Mn^+)	(2.59)	2.64 (2.40)	2.14 (1.81)	Tc(Tc^+)	(1.22)	0.72 (0.89)	0.41 (0.51)
Fe(Fe^+)	(0.89)	1.13 (0.76)	0.88 (0.25)	Ru(Ru^+)	(−0.82)	0.82 (−1.05)	0.87 (−1.09)
Co(Co^+)	(0.53)	(−0.06)	0.42 (−0.43)	Rh(Rh^+)	(−1.83)	0.45 (−2.15)	0.53 (−2.13)
Ni(Ni^+)	(0.05)	0.23 (−0.57)	−0.03 (−1.09)	Pd(Pd^+)	(−2.64)	1.02 (−3.21)	0.95 (−3.19)
Cu(Cu^+)	(−2.60)	−1.33 (−2.57)	−1.49 (−2.81)	Ag(Ag^+)	(−4.90)	(−5.42)	(−5.04)

[a] From ref. 202.

[b] From ref. 203.

The trends observed are similar for every series of the transition metal atoms (or ions). Thus there is a monotonic decrease of ΔE from Sc(Sc^+) to Cr(Cr^+) and from Y(Y^+) to Mo(Mo^+). For Mn(Mn^+) and Tc(Tc^+) there is a discontinuity and again, going to the right in the rows, ΔE decreases monotonically from Mn(Mn^+) to Cu(Cu^+) and from Tc(Tc^+) to Ag(Ag^+). These trends of ΔE could be understood in terms of two competing effects [220]: (i) a general stabilization of $(n-1)d$ with respect to ns with increasing Z, and (ii) a preference for a maximum number of high-spin coupled $(n-1)d$ orbitals.

The bonding mechanism and its energetics in MH and MH^+ systems are affected by the metal orbital size, which determines the overlap binding ability towards a neighbouring H atom. Among the valence AOs of a metal atom (or ion), only the ns are 'overlap active', whereas $(n-1)d$ tend to be 'overlap inert' and np AOs are over-extending [235,236]. Accordingly, transition metals are orbitally inhomogeneous, e.g. their valence $(n-1)d$, ns and np AOs have no comparable radii of maximal electron density, R_{max}, and therefore, are not equally available for overlap with the orbitals of some other atom. For both first and second row transition metals and their cationic species, the radial extent of the ns and $(n-1)d$ orbitals decreases as one moves from the left to the right of the series. Moreover, the $(n-1)d$ orbitals decrease in size much faster than the ns orbitals across the series. Thus, for the first row transition metals, the ratio of $\langle R_s \rangle / \langle R_d \rangle$ increases monotonically from 2.3 to 3.36 Å [227] and for their cationic species from 1.76 to 2.76 Å [202], while for the second row it increases, again monotonically, from 1.61 to 2.67 Å [227] and for their cationic species from 1.46 to 2.18 Å [213]. The larger radial overlap of $(n-1)d$ and ns orbital in the second row atoms results in better sd hybridization and greater d involvement in the bonding of the second row transition metal hydrides. This is also reflected in the calculated intrinsic s and d bond strengths of MH^+ systems determined by Goddard et al. [202,213]. Based upon these values, Goddard and his coworkers indicated that, for the first row MH^+ systems, the optimum size for a 4s orbital bonding to H is smaller than 1.49 Å and for a 3d orbital is at least 1.56 Å. For the second row counterparts, the corresponding values refer to 5s and 4d orbitals and are 1.6 and 1.9 Å, respectively.

Loss of exchange energy plays an important role in moderating the BDEs to high-spin systems. The formation of a 'd bond' results in loss of approximately half of the exchange energy between the bonding and the other non-bonding $(n-1)d$ metal orbitals. Such a loss of exchange energy increases as the number of $(n-1)d$ electrons increases. Moreover, the more equal size of ns and $(n-1)d$ orbitals, the smaller the d–d exchange energy and therefore first row transition metals bond to H predominantly with their 4s orbital rather than the 3d orbitals, while the second row transition metals tend to

bond with 4*d* rather than 5*s* orbitals. The combination of all the aforementioned factors establishes the qualitative picture of the bonding in MH^+ and MH systems [201–203,213,214,220,227].

For the first row MH^+ systems, the bonding arises from the $3d^n4s^1 + H$, $3d^{n+1} + H$ and $3d^{n+1}4s^1 + H^+$ asymptotes. At the GVB level, Goddard and coworkers [201] have found that the bond orbital on M^+ has a significant amount of $3d_\sigma$ character for ScH^+ through CrH^+ (average is 45% 4*s*, 14% 4*p* and 41% $3d_\sigma$). A similar average composition (46% 4*s*, 16% 4*p* and 38% $3d_\sigma$) has also been obtained at the MCPF level [203]. However, for MnH^+–CuH^+, the GVB bond orbital was found to be mostly 4*s*-like (74% 4*s*, 12% 4*p* and 14% $3d_\sigma$), whereas the MCPF natural orbital was found to involve an average $3d_\sigma$ contribution that is as large as for ScH^+–CrH^+ (51% 4*s*, 13% 4*p* and 36% $3d_\sigma$).

The same atomic asymptotes are also important for the second row MH^+ systems, but with larger contribution from the $4d^{n+1}$ atomic asymptote. Thus, at the MCPF level the natural orbitals contain 56% and 78% $4d_\sigma$ character for YH^+–MoH^+ and TcH^+–PdH^+ systems, respectively [203]. At the GVB level, the bond orbitals for the same species contain 60% and 20% $4d_\sigma$ character, respectively [213].

For the first row hydrides, MH, the bonding arises from a mixture of the low-lying atomic asymptotes, $3d^{n+1}4s^1$, $3d^n4s^2$ and $3d^{n+2}$. It is obvious that the first one leads to direct 4*s*–1*s* bonding, the second to 4*s*4*p*–1*s* bonding and the third to direct 3*d*–1*s* bonding. The relative importance of these different mechanisms depends upon the relative atomic separations. At the MCPF level, the natural orbital contains 30% 3*d* character in ScH and only 1% in CuH. For the second row transition metal hydrides, the natural orbital exhibits 49% 4*d* character in YH and 77% in PdH. In general, as the separation between the atomic states decreases, the mixed state character of the ground state electronic structures of the MH systems increases.

The mixed state character of the MH radicals is also reflected in both the dipole moment and the 3*d* population, which have been found to be very sensitive to the mixing of the atomic asymptotes [214]. Moreover, the excellent linear correlation (Fig. 1) of the MH^+ BDEs with the sd^n promotion energy, E_p, necessary to promote a metal atom (or ion) from its ground state to an electron configuration involving one electron in the *ns* orbital, also implies that the dominant binding orbital on the metal is the 4*s* AO, but that there is significant $3d_\sigma$ character, as well [212].

It was also argued [233] that the maximum MH and MH^+ BDE corresponding to $E_p = 0$ represents a good estimate of intrinsic M–H bond energies (57–60 kcal mol^{-1}), even if the metals are ligated, and therefore E_p can be achieved by the ligands. For the second row transition metals, promotion energy is less important and therefore the amount of *d* character in the metal

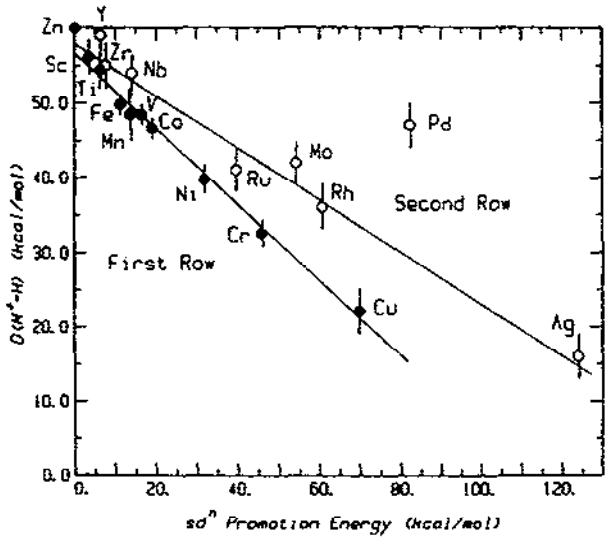

Fig. 1. First row (solid symbols) and second row (open symbols) transition metal ion hydride bond energies vs. the atomic metal ion promotion energy to an sd^n spin-decoupled state. Reproduced with permission from ref. 212.

bonding orbital is much larger than for the first row metals [212,233]. This is reflected in the not so good correlation of the BDE to E_p for the second row MH^+ systems, also shown in Fig. 1.

Finally, in the language of the MOVB theory developed recently by Epiotis [85,86,234–236], the bonding in MH and MH^+ systems could be of a special type called *overlap induction*. In overlap induction, depicted schematically in Fig. 2, an initial electron transfer creates a field which directs the remaining

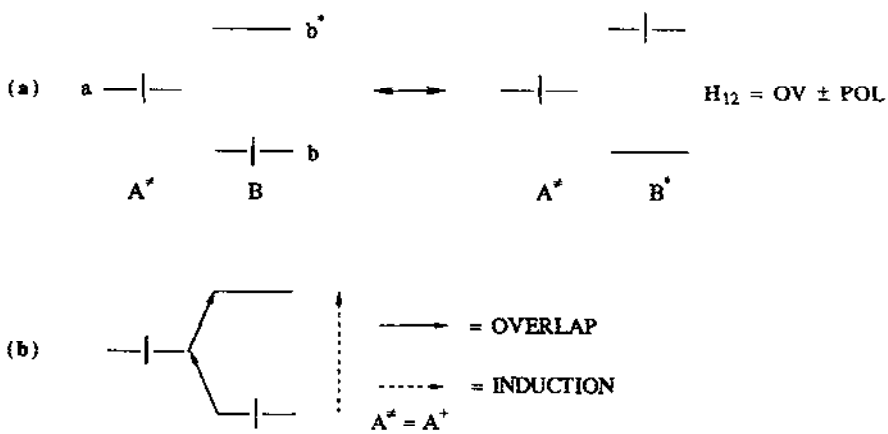

Fig. 2. Definition (a) and pictorial representation (b) of overlap induction. Reproduced with permission from ref. 235.

electrons to interstitial positions from where they can form covalent bonds with local non-metal AOs.

The interaction of the two configurations shown in Fig. 2 is given by

$$H_{12} = m\,OV \pm n\,POL \tag{7}$$

where OV is the overlap term and POL is the induction term given by the matrix element $\langle b|H|b^*\rangle$. Such a new picture of the bonding is consistent with the computational results and shows that transition metals do not have to rely on overlap to make strong bonds with ligands.

A comparison of the equilibrium bond distances between similar states of MH and MH^+ species showed a general contraction upon ionization of the outermost σ-bonding MO of the neutral species. The actual bond lengths of MH^+ are, on average, 0.07 Å shorter than those of the low-lying states of MH [205]. Moreover, the low-lying states of MH^+ lie within a smaller energy region than the similar states of the corresponding MH systems, again suggesting that the two series of compounds are not akin to one another.

(c) M–H bonding in saturated transition metal complexes

Coordinatively saturated L_nMH complexes play a role in many catalytic reactions, but thermochemical data on their M–H bond strengths are not well known. Nevertheless, recent theoretical efforts [208,237,238] have provided such data which have been collected in Table 7, juxtaposed with available experimental data.

Ziegler et al. [208,237] have studied the homolytic M–H bond energies in a number of representative L_nMH complexes, encompassing early as well as middle to late transition metal centres, namely $(CO)_5MH$ (M = Mn, Tc, Re), $(CO)_4MH$ (M = Co, Rh, Ir), $(CO)_4NiH^+$, $(CO)_5FeH^+$, Cp_2MH (M = Sc, Y, La, V, Mn, Tc, Re), Cp(CO)NiH, $Cp(CO)_2FeH$ and $Cp(CO)_3CrH$ complexes (where Cp = the cyclobutadienyl ligand) using MO calculations based upon density functional theory. It was found that the intrinsic M–H bond energies, e.g. the bond energies between H and L_nM fragments (in their ground states) of the same conformations as the L_nM moieties in the combined L_nMH complexes, do not change noticeably (48–55 kcal mol^{-1}) across a transition series, irrespective of the vast differences in electronegativity between the metal centres. Moreover, the M–H bond energies increase on descending a triad due to an increase in bonding overlap. The observed trends in M–H bond energies were explained qualitatively [237] on the basis of the σ-bonding contribution, $-\Delta E_\sigma$, to the total $D(L_nM–H)$ bond energies involving both ionic and covalent terms. It is the relative importance of these two terms which is responsible for the remarkable similarity of bond energies, $D(L_nM–H)$, across a transition series.

TABLE 7

M–H bond energies (in kcal mol^{-1}) in coordinatively saturated L_nMH complexes, $D(L_nM–H)$

Compound	Theor.	Exptl.	Ref.
Cp_2ScH	50.0		237
Cp_2YH	67.0		237
Cp_2VH	48.0		237
$Cp(CO)_3CrH$	54.0		237
$(CO)_6CrH^+$	60.7 ± 2	58.0 ± 3[a]	238
$(CO)_6MoH^+$	67.8 ± 3	65.0 ± 3[a]	238
Cp_2MnH	50.0		237
$(C_5H_4CH_3)(CO)_3MnH^+$	59.5 ± 3.4	71.0 ± 3[a]	238
$(CH_3)(CO)_5MnH$	59.5 ± 3.4	67.0 ± 3[a]	238
$(CO)_5MnH$	54.0		208
Cp_2TcH	59.0		237
$(CO)_5TcH$	60.0		208
Cp_2ReH	60.0		237
$(CO)_5ReH$	67.0		208
$(CH_3)(CO)_5ReH^+$	67.1	73.0 ± 3[a]	238
Cp_2FeH^+	57.0 ± 4	54.0 ± 5[a]	238
$Cp(CO)_2FeH$	54.0		237
$(CO)_5FeH^+$	60.0	74.0 ± 5[a]	208
	57.0 ± 4		238
$Cp(CH_3)(CO)_2FeH$	57.0 ± 4	53.0 ± 3[a]	238
Cp_2RuH^+	55.6 ± 3	79.0 ± 5[a]	238
$Cl(CH_2)RuH$		55.6 ± 3	238
$(CO)_4CoH$	55.0	57.0[b]	208
$Cp(CO)_2CoH^+$	55.5 ± 2.3	73.0 ± 5[a]	238
$(CN)_5CoH^{3-}$	55.5 ± 2.3	58.0[b]	238
$(CO)_4RhH$	61.0		208
$Cp(CO)_2RhH^+$	50.1 ± 3	80.0 ± 5[a]	238
$(CO)_4IrH$	68.0		208
$(CO)_4NiH^-$	62.0	62.0 ± 3[a]	208
	38.5 ± 1.4		238
$Cp(CO)NiH$	50.0		237

[a] From ref. 239.
[b] From ref. 240.

In the case of $(CO)_nMH$, Ziegler et al. [208] have also calculated the heterolytic M–H bond energies corresponding to the protonic (acidic) dissociation

$$(CO)_nM–H \rightarrow (CO)_nM^- + H^+$$

These BDEs are given by the so-called proton affinity of the $(CO)_nM^-$ species denoted as $PA[(CO)_nM^-]$, which can be expressed in terms of the homolytic $D[(CO)_nM–H]$ bond energies, the ionization potential, IP_H, for the hydrogen

atom and the electron affinity, $A[(CO)_nM]$, of the $(CO)_nM$ radical, according to the equation

$$PA[(CO)_nM^-] = IP_H + D[(CO)_nM{-}H] - A[(CO)_nM] \quad (8)$$

The homolytic bond energies of the $(CO)_nM{-}H$ systems along with the electron affinities of $(CO)_nM$ are of crucial importance in determining the trends (increase) in proton affinities down a triad, whereas electron affinity determines the trends (decrease) along a period.

Bursten and Gatter [241] have used non-empirical Fenske–Hall MO calculations to investigate the acidic ($L_nM{-}H \rightarrow L_nM^- + H^+$) vs. the hydridic ($L_nM{-}H \rightarrow L_nM^+ + H^-$) character of several organometallic hydride complexes. The calculations indicated that a large HOMO–NHOMO separation in L_nM^- seems diagnostic of hydridic behaviour. Moreover, the reactivity of the hydrogen is closely related to the orbital energetics of the conjugate base of the metal hydride and in particular to both the HOMO–NHOMO and HOMO–LUMO energy gaps.

Recently, Carter and Goddard [238] have established an important relationship between the gas and condensed phase thermochemistry of transition metal compounds, allowing one to convert $M^+{-}X$ BDEs (from experiment or theory) in unsaturated MX^+ complexes to those appropriate for coordinatively saturated ones, $\underline{M}X$ ($\underline{M} = L_nM$). The analysis was based on the quantitative evaluation of (i) the loss of differential exchange and (ii) the loss of promotional energy which necessarily accompany covalent bond formation, with the assumptions that exchange and promotional energy effects dominate orbital hybridization and overlap contributions and the metal centres in coordinatively saturated complexes possess d^n electronic ground states. Along this line they have found that the intrinsic gas-phase BDEs are useful starting points for comparison, analysis and prediction of condensed phase BDEs, which are obtained as $D(\underline{M}{-}X) = D(M{-}X) + \Delta K$, where $\Delta K = E_{lost}(MX) - E_{lost}(\underline{M}X)$, ($E_{lost}(\underline{M}X) = K_{lost}(\underline{M}X) = 0.0K_{dd}$, $0.5K_{dd}$ and $1.5K_{dd}$ for single, double and triple bond, respectively) and K_{dd} is the dd exchange integral.

The results obtained (Table 7) are generally pursuant to the experimental data available. Moreover, one could see that the BDEs in coordinatively saturated systems decrease going across a row and increase going down a column. For compounds with zero-valent M or with ionic or donor–acceptor character M–X bonds, the method is not appropriate.

(d) Dihydride vs. η^2-H_2 bonding. The concept of overlap dispersion

In recent years, there has been considerable activity in the investigation of the interaction of dihydrogen, H_2, with a metal or metal-containing fragment, L_nM, because of its relevance to homogeneous and heterogeneous catalysis.

In most cases, the H–H bond is cleaved through an oxidative addition process to form the traditional metal dihydrides, **1**.

1 **2**

However, a number of compounds involving the novel η^2-H_2 type of bonding, **2**, wherein the H–H bond remains essentially intact, have been synthesized and well characterized [242–251]. Moreover, in several of these compounds both dihydrogen and hydride ligands are present and there is evidence for exchange among them. In certain cases, the dihydrogen bonding is at a near balance point between dissociative and non-dissociative dihydrogen bonding [244]. In the light of recent advances in the study of dihydrogen complexes, many of the known polyhydride complexes may well be more appropriately described as dihydrogen complexes or may contain equilibrium amounts of dihydrogen complexes. The factors governing the stability of the dihydrogen species, **2**, relative to their more conventional dihydride forms, **1**, have been explored extensively by theoretical methods at various levels of sophistication [252–261].

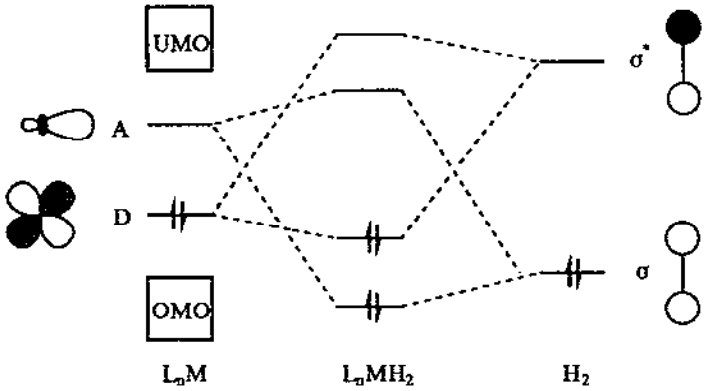

3

The general qualitative features of the interaction of a hydrogen molecule with a transition metal L_nM complex have been pioneered by Saillard and Hoffmann [254]. These features are depicted schematically in **3**. Dihydrogen can act as a σ-donor, through interaction between σ_{H_2} and a vacant σ orbital

on the metal denoted as A (acceptor orbital) and as an acceptor by interaction of $\sigma^*_{H_2}$ with a filled π orbital on the metal denoted as D (donor orbital). Both are stabilizing 2e-2O interactions entailing electron density flow between L_nM and H_2 in opposite directions, e.g. $L_nM \leftarrow H_2$ and $L_nM \rightarrow H_2$, leading to H–H bond weakening and M–H bond formation. The repulsive (destabilizing) 4e-2O interactions between σ_{H_2} and the lower filled MOs of L_nM, representing what chemists normally call 'steric effects', have been found to be small except for short distances of H_2 approach.

Saillard and Hoffmann [254] have analyzed in detail dihydrogen interaction with d^6-ML_5, d^8-ML_4 and CpML complexes. They proposed that coordinative unsaturation is essential as a prerequisite for dihydrogen activation and formation of metal dihydrides, the initial stages dominated by $\sigma_{H_2} \rightarrow M$ electron transfer. The similarities and differences between the dihydrogen activation on a discrete transition metal complex and a metal surface have also been discussed at the level of EHMO theory combined with the tight binding approximation.

EHMO calculations have also been used by Jean et al. [255] to study the interaction of H_2 with d^6-ML_5 fragments (M = W, Cr, Fe and L = H^-, CO) to form either η^2-H_2 coordinated or dihydride complexes. The formation of a dihydrogen complex is shown to be exothermic, irrespective of the nature of the metal and ligands. However, the relative stability of a dihydrogen complex with respect to the corresponding dihydride strongly depends on the electronic properties of the metal and ligands and in particular on the ability of the ML_5 fragment to populate $\sigma^*_{H_2}$ MO. In general, strong π-donor L_nM fragments favour the formation of dihydrides, whereas poor ones stabilize the dihydrogen complex. Obviously any route to diminish the $\sigma^*_{H_2}$ MO population would favour the formation of the dihydrogen complex. The dihydride formation is not favoured in the case of metals with low-lying $(n-1)d$ AOs such as Fe or in the process of substituting pure σ-donor ligands (H^-) by π-acceptor ligands (CO), particularly *trans* to the incoming H_2.

The role of the ligand in the above dilemma for d^6-$ML_5(H_2)$ complexes has been investigated by Hay and Kober [256,257] using ab initio wavefunctions and relativistic effective core potentials. Two model compounds were chosen for this study, namely $W(CO)_3(PH_3)_2(H_2)$ and $W(PH_3)_5(H_2)$, where the effects of replacing the strongly π-acceptor CO ligands by PH_3 of intermediate π-acceptor capacity can be probed. Using optimized geometries from ab initio HF calculations, being in excellent agreement with experimental studies, the six-coordinate η^2-H_2 form was found to be the most stable species for the $W(CO)_3(PH_3)_2(H_2)$ complex, while the seven-coordinate dihydride, $W(PH_3)_5(H_2)$, was found to be most stable. Among the various models of H_2 bonding to the $W(CO)_3(PH_3)_2$ fragment, the η^2-H_2 bonded species **4** and **5** were found to be stable with respect to the d^6-$W(CO)_3(PH_3)_2(C_{4v})$ and H_2

species by 17 kcal mol^{-1} and more stable than the end-on form, **6**, which is bound by only 10 kcal mol^{-1}. Moreover, structure **4** with the H_2 axis parallel to the P–W–P axis is slightly more stable (0.3 kcal mol^{-1}) than structure **5**, where the H_2 axis is parallel to the C–W–C axis.

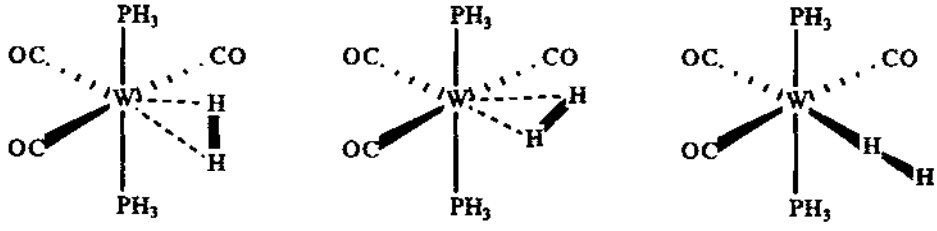

The origin of the stabilization of the dihydrogen complex could easily be drawn from the orbital correlation diagram shown in Fig. 3. It is clear from Fig. 3 that the preference for η^2-H_2 coordination in d^6-$ML_5(H_2)$ complexes

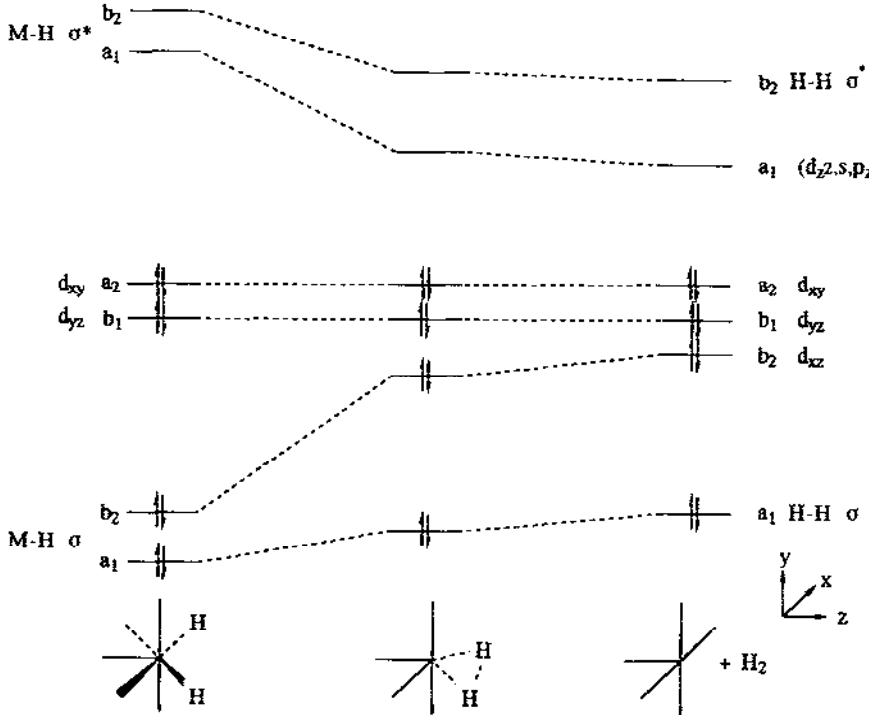

Fig. 3. Orbital correlation diagram for a d^6 ML_5 fragment interacting with H_2. Reproduced with permission from ref. 257.

correlates with the overall stabilization of the d AOs and particularly the d_{xz} (d_π) AOs, since this stabilization makes the $M(d_\pi) \rightarrow H_2(\sigma^*)$ back bonding less favourable. In fact, this is the case for the $W(CO)_3(PH_3)_2(H_2)$ complex where the strong π-acceptor CO ligands enhance the stabilization of the metal's d AOs. In contrast, when CO ligands are replaced by the less stabilizing PH_3 ligands, the dihydride $W(PH_3)_5(H_2)$ complex is the most favoured form (the seven-coordinate dihydride complex was found to be 3 kcal mol^{-1} more stable than the corresponding dihydride complex). These results are also consistent with the calculated values of the $d_\pi \rightarrow d_\sigma$ promotion energies, which were found to be 9–12 kcal mol^{-1} larger in $W(CO)_3(PH_3)_2$ relative to $W(PH_3)_5$ fragments [257].

Burdett et al. [258–260] have investigated the electronic features that stabilize η^2-H_2 complexes relative to their dihydride analogues by use of simple molecular orbital ideas associated with open and closed three-centre bonding. They concluded that all dihydrogen complexes possess a common structural feature corresponding to a three-membered ring, **7**, which involves the two hydrogen atoms of dihydrogen and the metal-containing fragment.

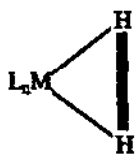

7

Along this line, one basic requirement for a stable dihydrogen species, **7**, is that the set of the three-centre ring orbitals must contain no more than two electrons.

The above requirement is fulfilled for L_nM fragments possessing an empty LUMO directed towards dihydrogen, since dihydrogen itself is a two-electron donor. Accordingly, all stable dihydrogen complexes could be described as containing close three-centre-two-electron bonds. In any other case, the dihydride complexes are favoured, as for the low spin d^8-ML_4 square planar complexes. Actually, these species in which the d_{z^2} AO is occupied, entail an unstable closed three-centre arrangement containing four electrons, eventually favouring formation of a dihydride. Moreover, these complexes could afford a η^1-H_2 bonded species involving a linear M–H–H unit perpendicular to the ML_4 plane. Indeed, Baerends and coworkers [261] infer from their HFS calculations of the η^1- and η^2-bonding of X_2 (X=H or F) to $PtCl_4^{2-}$ that the preference for the former descends from the nodal structure of both the acceptor MO and the metal fragment donor MO, invoking π-bonding in the η^2-coordination. Indeed, the existence of a species involving Pt–I–I has

been verified and both η^1- and η^2-bonding modes were revealed in a matrix study of PdH_2 [262]; ab initio results offer an explanation on the grounds of the small energy difference of the two forms [263,264]. Calculations carried out by Baerends and his coworkers indicated the preference for η^2-coordination of X_2 to $Cr(CO)_5$, since both σ-donative and π-back donative interactions were calculated to be stronger than for η^1-coordination.

Based upon the three-centre picture of the dihydrogen bonding to L_nM fragments, Burdett et al. [259] have also commented on possible rearrangement processes in excited states, e.g. the H_2 loss from $Cr(CO)_5(H_2)$ upon near UV photolysis. Similarly, the low-lying triplet states of L_nM complexes may be thought responsible for the formation of dihydrides, contrary to anticipations based on the nature of their ground states.

It is noticeable that most of the reported $L_nM(H_2)$ complexes involve a d^6-ML_5 fragment. However, theoretical results seem to favour other L_nM fragments as well. Thus, both butterfly d^8-ML_4 and trigonal pyramidal d^{10}-ML_3 fragments may afford stable dihydrogen species provided that they exhibit poor π-donor capacity. This happens when the ligands, L, are strong π-acceptors, such as CO and NO, and in particular in a position *trans* to the incoming dihydrogen. Consequently, the $M(d_\pi) \rightarrow H_2(\sigma^*)$ charge transfer is reduced, hence stabilizing the three-centre orbital set, characteristic of dihydrogen coordination. In fact, dihydrogen complexes of the $Fe(CO)(NO)_2$ and $Co(CO)(NO)_2$ (butterfly d^8-ML_4 fragments) have already been characterized in liquid xenon [265].

Recently, Blomberg et al. [266] have studied ligand effects on the stability of the L_nMH_2 complexes (M = Ni and Pd, L = C_2H_4, C_2F_4, CO, PH_3, N_2, H_2O, Cl^- and $n = 1$ or 2) using high quality calculations including near degeneracy and dynamical correlation effects. The calculations performed were of the CASSCF + CCI with standard basis sets of double ζ quality in the valence regions augmented with a diffuse *d* function on metal. For Pd, Cl, F and P atoms, ECPs for the inner shells have been used. The geometrical parameters for the MH_2 moieties used were those previously calculated [267-269]. It is important that the lowest singlet state ($^1A_1$) of NiH_2 has a bent geometry with a H—Ni—H angle of 49°. This structure, corresponding to a slightly stable complex, bound by 8 kcal mol^{-1} with respect to the singlet asymptote, exhibits the ring-type binding, where the hydrogens bind both to nickel's *sd*-hybridized orbitals and to each other [267,268]. The ground state of NiH_2 is found to be a linear $^3\Delta_g$ state, with the lowest singlet $^1A_1$ state almost 34.6 kcal mol^{-1} higher in energy at this geometry. Therefore, it has been speculated that the $^1A_1$ bent equilibrium configuration state is the ground state of the metal complex when ligands are added. In other words, the $^1A_1$ state of NiH_2 is probably akin to the *cis* conformation of L_nNiH_2 complexes resulting from the interaction of L_nNi species with dihydrogen.

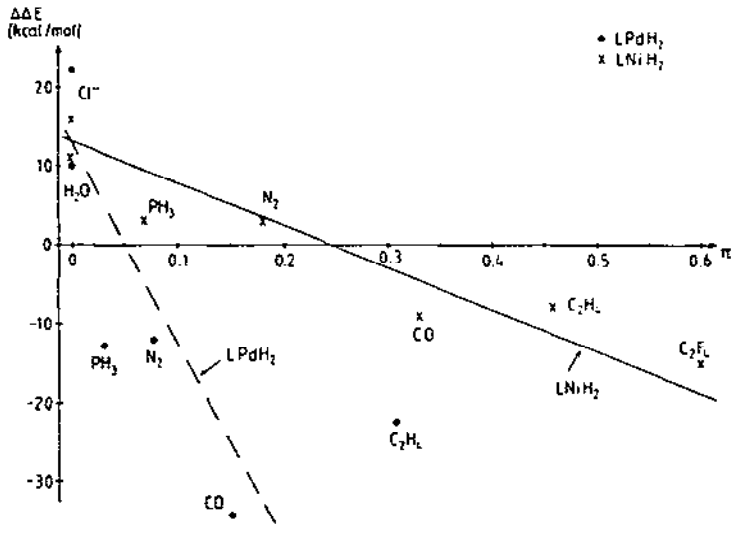

Fig. 4. Changes in $M-H_2$ interaction energy ($\Delta\Delta E$) as a function of the π^*-MO population in the M–L complexes. The crosses and dots represent the nickel and palladium complexes, respectively. Reproduced with permission from ref. 266.

The π^* orbital occupation of ligands L, as given by the Mulliken charge, as well as the singlet–triplet splitting of the LM species have been used [266] as a measure of the covalency of the M–L bond, which correlated well with the destabilizing effect of the ligand on the M–H bond. This is clearly shown in Fig. 4, where changes in $M-H_2$ interaction energy ($\Delta\Delta E$) as a function of the π^* orbital population in the L_nM complexes are depicted schematically.

Finally, Burdett and Pourian [260], using the isolobal connection model [87], have extended the study of stable dihydrogen species to a wide range of systems from main group chemistry involving both $H_3^+(H_2)_n$ and $AH_m(H_2)_n$ species. It is important that the structures of all these species, most of them already known, along with the structures of the $L_nM(H_2)_n$ complexes were brought together by the identification of stable orbital topologies using simple molecular orbital concepts. Positive bond overlap population between two atoms does not guarantee the stability of a particular complex, but is an indication of the electronic factors that are important in its stabilization. This is in line with the suggestion, put forward by Epiotis [85,86,234,235], that metals do not have to rely on overlap to make strong bonds with ligands.

Epiotis, using the MOVB theory, has introduced the concept of *overlap dispersion* as the bonding mechanism in transition metal compounds and organometallics which sustain either modest or weak overlap interaction. For example, in the case of NiH_2 species, overlap dispersion can be expressed

in the VB language as follows:

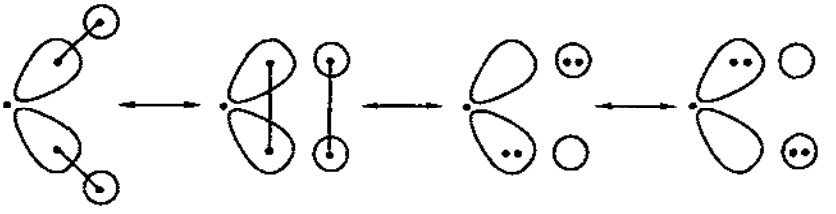

(9)

The critical *correlated electron transfer* (CET) configuration interaction is depicted schematically in Fig. 5. Overlap dispersion bonding is produced by moving electrons two at a time in a correlated sense from a parent principal configuration, being usually the perfect pairing (PP) or a closed shell configuration. Moreover, it is clear from Fig. 5 that the interaction matrix elements between the appropriate configurations, denoted generally as H_{ij}, can be expressed by the general equation:

$$H_{ij} = m\,\mathrm{OV} \pm n\,\mathrm{DISP} \tag{10}$$

where OV is the overlap term and DISP the dispersion term. The negative sign of eqn. (10) corresponds to overlap dispersion, whereas the positive sign corresponds to anti-overlap dispersion. The DISP term is maximized under the following conditions [85,86]: (i) the metal or metal-containing fragment and ligand orbitals involved in the bonding mechanism should extend in the same region of space and (ii) the geometry of the metal or metal-containing fragment and the ligand should be such that the transition dipoles associated with the $M(d) \rightarrow M(s)$ and $L \rightarrow L^*$ excitations interact to a maximum extent.

(e) Second M–H bond strengths. The concept of bond cooperativity

The few available high quality computational results of the second M–H BDEs in transition metal compounds [204,206,271], along with the calculated geometries of the systems studied, have been collected in Table 8.

Knowledge of both the first and second metal–ligand BDEs is of crucial importance in understanding oxidative addition and reductive elimination processes in transition metal chemistry. However, even for simple radical species like hydrogen atoms and alkyls, both theoretical and experimental determination of the second BDE is extremely tricky and laborious. Nevertheless, such information is now available for several simple systems [204,206,212,271].

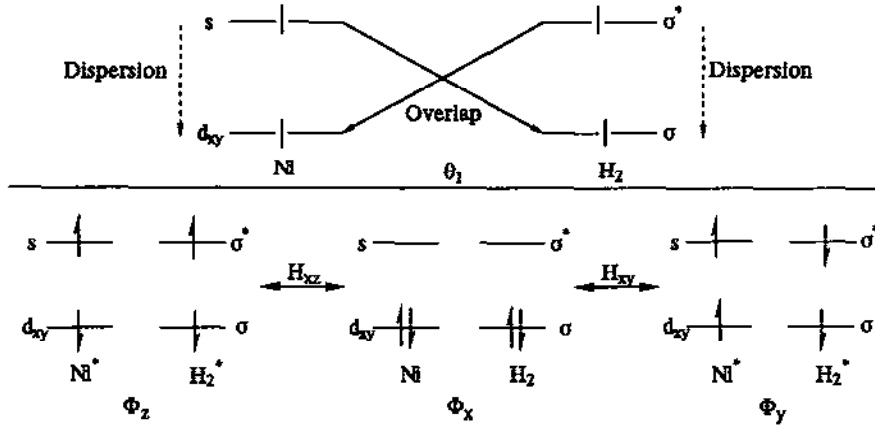

$$\Phi_x = | \, d_{xy} \, \bar{d}_{xy} \, \sigma \, \bar{\sigma} \, |$$

$$\Phi_y = | \, \bar{d}_{xy} \, \sigma \, \bar{\sigma}^* \, s \, | - | \, \bar{d}_{xy} \, \sigma \, \sigma^* \, \bar{s} \, | - | \, d_{xy} \, \bar{\sigma} \, \bar{\sigma}^* \, s \, | + | \, d_{xy} \, \bar{\sigma} \, \sigma^* \, \bar{s} \, |$$

$$\Phi_z = | \, d_{xy} \, \sigma \, \bar{\sigma}^* \, s \, | - | \, \bar{d}_{xy} \, \bar{\sigma} \, \sigma^* \, s \, | - | \, d_{xy} \, \sigma \, \bar{\sigma}^* \, \bar{s} \, | + | \, d_{xy} \, \bar{\sigma} \, \sigma^* \, \bar{s} \, |$$

$$H_{xy} = 2W - Z$$

$$H_{xz} = 2Z - W$$

$$W \propto \underset{\text{I}}{< d_{xy} \, | \, \sigma^* >} \underset{\text{II}}{< \sigma \, | \, \hat{H} \, | \, s >} + \underset{\text{III}}{< \sigma \, | \, s >} \underset{\text{IV}}{< d_{xy} \, | \, \hat{H} \, | \, \sigma^* >} + \underset{\text{V}}{(d_{xy} \, \sigma^* \, | \, \sigma \, s)}$$

= OVERLAP TERM (OV)

$$Z = (d_{xy} \, s \, | \, \sigma \, \sigma^*) = \text{DISPERSION TERM (DISP)}$$

Fig. 5. Principal bond diagram of NiH_2 and the key bielectronic configuration interaction responsible for overlap dispersion. Reproduced with permission from ref. 234.

TABLE 8

Calculated geometries and BDEs for a few MH_2^+ systems studied so far

Molecule	State	$R_e(M^+–H)$ (Å)	(H–M^+–H) (deg)	$D_e(HM^+–H)$ (kcal mol^{-1})	Ref.
ScH_2^+	$^1A_1$	1.745	106.7	51.7	204
	$^1A_1$	1.762	105.8	51.5	271
TiH_2^+	$^2B_1$	1.71	107.0	34.7	206
	$^2A_1$	1.71	61.0	34.7	206
CrH_2^+	$^4B_2$	1.635	107.5	19.4	271
MoH_2^+	$^4B_2$	1.705	64.6	35.1	271
	$^4B_2$	1.722	112.3	34.7	271

Harrison and coworkers [204,206] have investigated the electronic and geometric structures of ScH_2^+ and TiH_2^+ systems by ab initio MCSCF and CI techniques. At the MCSCF+1+2 level, the angular potential energy surface of ScH_2^+ ($^1A_1$) presents one minimum (optimum angle 106.7°) whereas that of TiH_2^+ ($^2A_1$) presents two almost symmetrically located minima (optimum angles 61° and 120°) with an intervening energy barrier of $\sim$1.3 kcal mol^{-1} at $\sim$90°. For TiH_2^+, $^2B_1$ is formally the ground state with two other states, namely $^2A_2$ and $^2A_1$ just $\sim$0.95 and $\sim$1.5 kcal mol^{-1} higher. In both ScH_2^+ and TiH_2^+ species, the bonding character is due to *sd* hybridization and overlap with 1*s* AOs of hydrogen atoms.

Two distinct minima on the angular potential energy surface of MoH_2^+ ($^4B_2$) at optimum angles of 64.6° and 112.3° with a barrier at 88° of less than 1.5 kcal mol^{-1} have been reported by Schilling et al. [271] using GVB-RCI calculations. In contrast, CrH_2^+ ($^4B_2$) although hinting at a second well at small angle, reveals only one optimum geometry, 107.5°. The CrH_2^+ ($^4B_2$) angular potential energy surface is very similar to that of TiH_2^+ ($^2A_1$) with the flat portion of the curve varying from 70 to 120°. Both CrH_2^+ and MoH_2^+ possess similar ground states, $^4B_2$, corresponding to a d^5 electronic configuration of the metal, with the bonding character being dominated by metal *sd* hybridization. However, in MoH_2^+, partition of the metal's *d* AOs ($\sim$80%) in the bonding is higher than that in CrH_2^+ ($\sim$70%), thus leading to strong bonding at both small (65°) and large (112°) angles. The bonding mode of H_2 in the unsaturated CrH_2^+ and MoH_2^+ systems is of the dihydride rather than the η^2-H_2 type found in analogous saturated systems, such as $M(CO)_5(H_2)$ (M = Cr, Mo, W) and $M(CO)_2(PR_3)_2(H_2)$ (M = Mo, W) complexes. This is another indication of the crucial role played by the ligands on the dihydrogen bonding to transition metals.

Based upon the computational results on CrH_2^+ and MoH_2^+ systems, Schilling et al. [271] have also speculated that all metal dihydrides of the first row transition metals will tend to adopt geometries similar to those of MoH_2^+, corresponding to two possible minima with the bond angles depending on the electron configuration of the metal. Moreover, for these dihydrides the second M–H bond is expected to be weaker than the first, though comparable or even stronger for their second row analogues. However, some experimental results concerning ScH_2^+ [212] suggest that the second BDE is greater than the first by 3.1 kcal mol^{-1}. Similarly, Harrison's calculations on ScH_2^+ [204] also suggest that the second bond is almost as strong as the first, providing thermochemical evidence for bond cooperativity in transition metal compounds, which means that every coordinate bond assists every other such bond via CET delocalization.

Bond cooperativity, being the hallmark of overlap dispersion has been introduced by Epiotis [85,86] through MOVB theory. Because of bond

cooperativity, a second bond, let us say $M-L_2$, will be stronger than the first, $M-L_1$, everything else being equal. In other words, in the series of reactions:

$$M + L_1 \rightarrow M-L_1 \tag{11}$$

$$M + L_2 \rightarrow M-L_2 \tag{12}$$

$$L_1-M + L_2 \rightarrow L_1-M-L_2 \tag{13}$$

reaction (13) would be expected to be more exothermic than reaction (12) because in reaction (13) L_1 cooperates with L_2. A number of computational and experimental thermochemical data on oxidative addition reactions of transition metal compounds constitute strong evidence for bond cooperativity [86].

(f) Dihydrogen activation. The nature of the oxidative addition and reductive elimination processes

Since sigma bond activation has been recognized as an indispensable step in catalytic processes, many theoretical studies have been concentrated on the dihydrogen activation by transition metal atoms [253,267–270,272–276], ions [206,277], discrete complexes [254,257,266, 278–290] and models for metal surfaces [254,272,291–297].

The most carefully studied metal reaction system is dihydrogen activation by transition metal atoms and ions, since this is the experimentally and theoretically more manageable reaction system for understanding the details of the electronic interactions and dynamic features. For these reaction systems, two primary processes are possible:

$$M^{n+} + H_2 \rightarrow MH^{n+} + H \tag{14}$$

$$M^{n+} + H_2 \rightarrow MH_2^{n+} \tag{15}$$

where M is a transition metal and $n=0$ or 1.

Both processes have been investigated extensively by high quality computational techniques [206,253,267–270,272–277]. Moreover, reaction (14) has been approached experimentally by Armentrout et al. [194,195,298] who, combining the experimental results with molecular orbital ideas and conservation of spin, suggested that M^{n+}-promoted dihydrogen activation depends on both configuration and spin state of the metal. In other words, there exists a state specific chemistry for transition metal ions which involves three categories of reactivity.

(i) Transition metal ions with unoccupied 4*s* and $3d_\sigma$ AOs react with H_2 efficiently, forming, through insertion into the H–H bond, metal dihydrides

as intermediates. Moreover, these transition metal ions reacting with HD afford MH^+ and MD^+ in the near statistical 1:1 ratio. Examples are the Ti^+ (^4F, $3d^3$) and V^+ (^5D, $3d^4$) states.

(ii) Transition metal ions with either $4s$ or $3d_\sigma$ AOs occupied react with H_2 efficiently via a direct mechanism if they have low spin. These transition metal ions reacting with HD afford MH^+ and MD^+ in a 3:1 ratio. Examples are the Fe^+ (^4F, $3d^7$) low-lying excited state and the Co^+ (^3F, $3d^8$), Ni^+ (^2D, $3d^9$) and Cu^+ (^1S, $3d^{10}$) states.

(iii) Transition metal ions with either $4s$ or $3d_\sigma$ AOs occupied but with the ion in high spin state react with H_2 inefficiently at the thermodynamic threshold. These transition metal ions reacting with HD afford MH^+ and MD^+ in the ratio favouring MD^+ at low energies. Examples are the Mn^+ (^7S, $4s3d^5$) and the Fe^+ (^6D, $4s3d^6$) states.

The above reactivity rules were formulated for the diabatic character of the reaction surfaces and therefore fail when adiabatic interactions become important. Adiabatic surfaces connect ground state $M^+(3d^n)$ reactants with ground state MH^+ products. When mixing of reaction surfaces evolving from ground states with those from more reactive excited states occurs, a change in reactivity is observed. This is the case for Sc^+ (^3D, $4s3d$) and Ti^+ (^4F, $4s3d^2$) ground states which, although belonging to category (iii), react like category (i) ions, Sc^+ (^3F, $3d^2$) and (^4F, $3d^3$), because the repulsive ground state reaction surfaces undergo avoided crossings with the attractive excited state reaction surfaces. It should be noted that the reactivity rules put forward by Armentrout et al. are consistent with high quality theoretical results on the potential energy surfaces of dihydrogen activation by transition metal atoms and ions [206,253,267–270,272–277].

Rappé and Upton [277] presented ab initio potential energy surfaces for the reaction of ^3D, ^1D, ^3F and ^1D states of Sc^+ with H_2 for two different interaction geometries corresponding to the collinear and perpendicular approach of the reactants. Of the 65 possible low-lying space and spin components of the reacting system, only a relatively small fraction are definitely reactive. In general, the ground states of Sc^+ favour hydride formation, whereas excited ones favour dihydride formation (diabatically) in accordance with Armentrout's reactivity rules. Thus, all components of the ground ^3D and lowest ^1D states react, via endothermic but unactivated processes, to afford ScH^+ from a collinear interaction, although interactions at other angles are also likely to proceed to this product. The calculated ΔH_0 value for the lowest product state from Sc^+ (^3D) was found to be 48.6 kcal mol^{-1}. However, a low-lying Sc^+ state with a filled $3d$ orbital (antibonding to H—H) can interact with the singlet (^1D) or triplet (^3D) (when spin-orbit coupling effects are considered) ground state to afford activated ScH_2^+ from a perpendicular interaction geometry. Moreover, some other low-lying $3d^2$ Sc^+ com-

ponents (singlet or triplet) can interact with Sc^+ ground states each spin to activate the H–H bond.

The reductive elimination of H_2 from ScH_2^+ and TiH_2^+ has been investigated by Harrison and coworkers [204,206] using ab initio MCSCF and CI techniques. For ScH_2^+, the reductive elimination reactions

$$ScH_2^+ \ (^1A_1) \rightarrow Sc^+ \ (^3D) + H_2 \ (^1\Sigma_g) \tag{16}$$

and

$$ScH_2^+ \ (^1A_1) \rightarrow Sc^+ \ (^1D) + H_2 \ (^1\Sigma_g^+) \tag{17}$$

corresponding to spin-forbidden and spin-allowed processes, were found to be endothermic by only 2 kcal mol^{-1} for the first and at least 9 kcal mol^{-1} for the second reaction, respectively. On the other hand, the corresponding processes for TiH_2^+, given by the equations

$$TiH_2^+ \ (^2B_1) \rightarrow Ti^+ \ (^4F) + H_2 \ (^1\Sigma_g^+) \tag{18}$$

and

$$TiH_2^+ \ (^2B_1) \rightarrow Ti^+ \ (^2F) + H_2 \ (^1\Sigma_g^+) \tag{19}$$

were found to be exothermic by ~ 20 and ~ 16 kcal mol^{-1}, respectively. It is obvious that TiH_2^+ can easily dissociate on the $Ti^+ \ (^4F) + H_2 \ (^1\Sigma_g^+)$ surface, or on the $Ti^+ \ (^2F) + H_2 \ (^1\Sigma_g^+)$ surface through a spin-orbit coupling mechanism.

Dihydrogen activation by neutral transition metal atoms follows similar reactivity patterns to those of the transition metal ions. Thus, different electronic states exhibit differences in reactivity, as is clearly shown by the calculated ab initio potential energy surfaces for the dissociation of MH_2 systems [267–270,272–276] given in Figs. 6–10.

Looking at the lowest low spin and high spin potential surfaces of MH_2 systems shown in Figs. 6–10, we can see a remarkable similarity between FeH_2, CoH_2, NiH_2 and PtH_2. Both the low and high spin surfaces are almost perfectly parallel. It is important that dihydrogen activation takes place on the low spin surfaces with little or no barrier, through formation of weakly bound bent complexes (H–M–H bond angles being equal to 105°, 95°, 50° and 100°, respectively).

For NiH_2 [267,268] and PtH_2 [275], the electronic state responsible for the capture of H_2 is the lowest closed shell $^1A_1$ excited state, whereas for their triplet ground states, the corresponding potential surfaces have a repulsive nature. At the bent minimum of the potential surface, the H–H bond distance is larger for PtH_2 than NiH_2, suggesting that Pt might be better for hydrogenation catalytic processes in line with experiment.

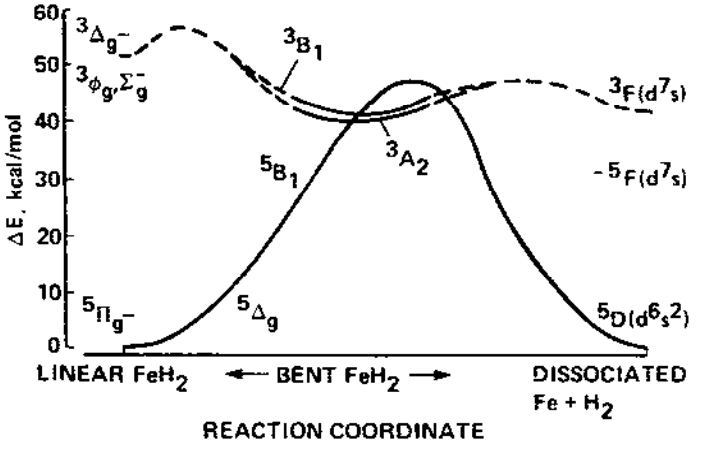

Fig. 6. Dissociation curves for triplet and quintet states of FeH_2. The energies are relative to H_2 and the ^5D (s^2d^6) state of iron. Reproduced with permission from ref. 272.

Though belonging to the same periodic column with Ni and Pt, Pd is unreactive towards H_2. This was attributed by Low and Goddard [269,270] to the unreactive nature of the d^{10} ground state of Pd and the large excitation energy of ~ 22 kcal mol^{-1} needed to promote the Pd atom to the reactive s^1d^9 excited configuration. This excitation proved to be a prerequisite in a series of GVB-CI calculations of MR_2 complexes (M = Pd or Pt and R = H or CH_3). It is obvious then why reductive elimination from PdR_2 complexes is exothermic and from PtR_2 endothermic. Pd prefers the d^{10} configuration whereas Pt prefers the s^1d^9. The close resemblance of the difference in the

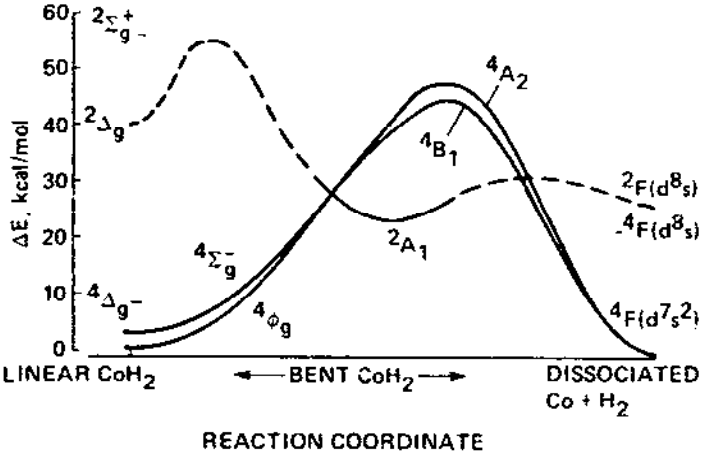

Fig. 7. Dissociation curves for doublet and quartet states of CoH_2. The energies are relative to H_2 and the ^4F (s^2d^7) state of cobalt. Reproduced with permission from ref. 272.

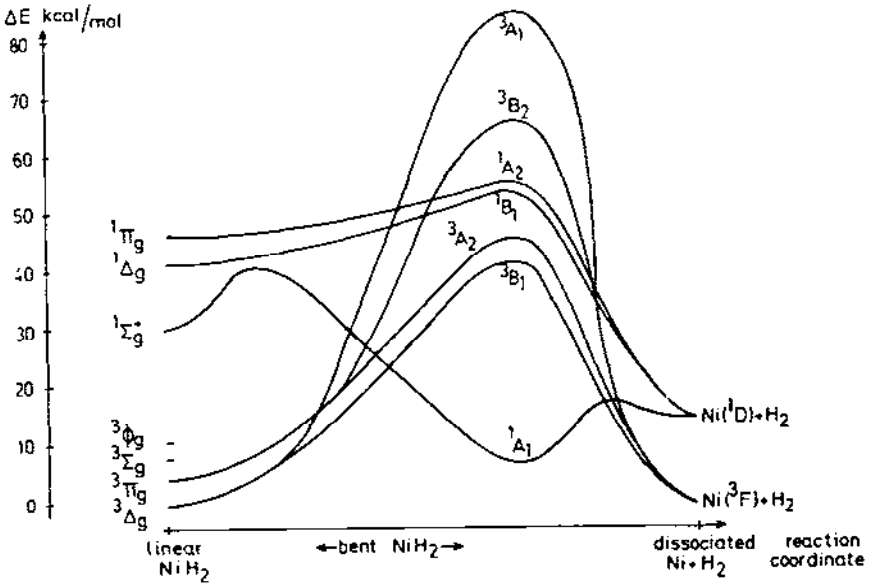

Fig. 8. Dissociation curves for all triplet and singlet states of NiH_2. The energies are relative to H_2 and the ^3F state of nickel. Reproduced with permission from ref. 268.

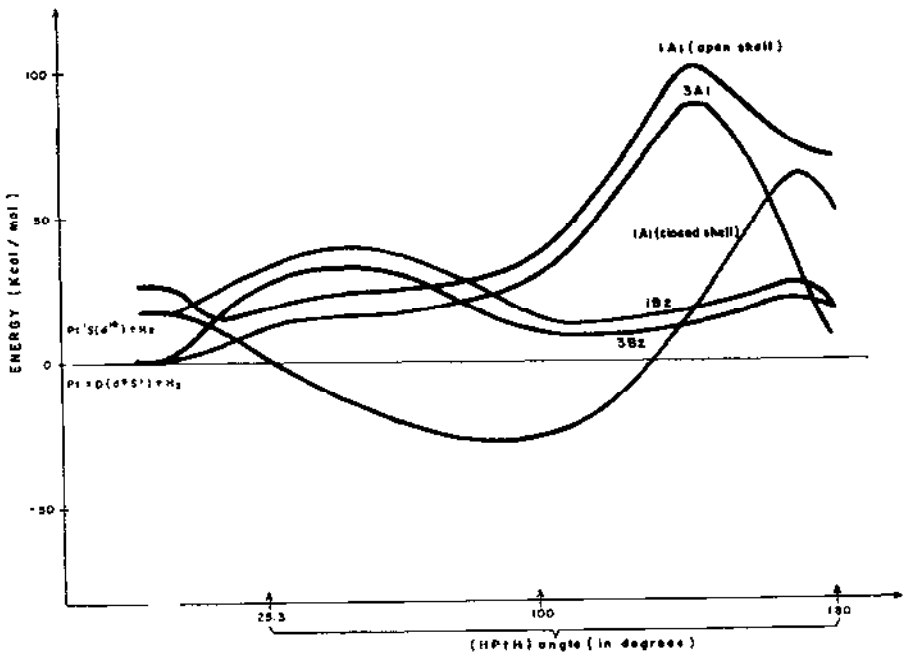

Fig. 9. Dissociation curves for all triplet and singlet states of PtH_2. The energies are relative to H_2 and the 3D (s^1d^9) state of platinum. Reproduced with permission from ref. 275.

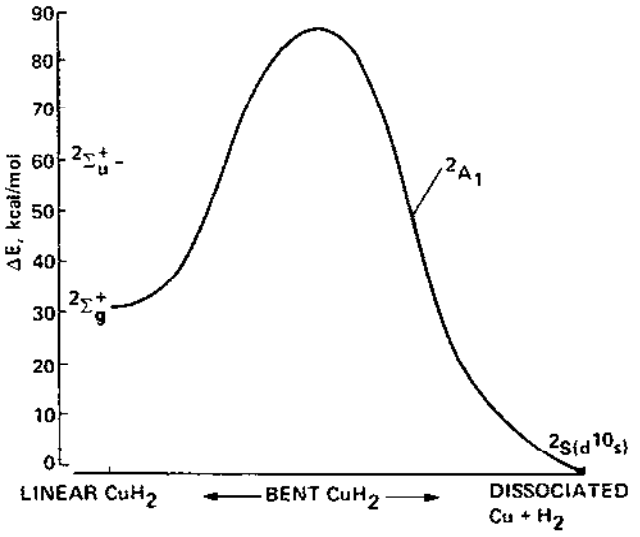

Fig. 10. Dissociation curve for the $^2A_1$ state of CuH_2. The energies are relative to H_2 and the ^2S (s^1d^{10}) state of copper. Reproduced with permission from ref. 272.

s^1d^9–d^{10} state splittings of Pd and Pt and the difference in the driving force for reductive elimination from MR_2 complexes strongly supports the electronic promotion rather than the charge transfer idea for oxidative addition and reductive elimination processes.

Analogous is the situation for dihydrogen activation by Cu atoms which, by adopting an s^2d^9 configuration, can capture H_2. The high barrier for dihydrogen activation by the Cu atom (~ 28 kcal mol^{-1}) calculated by a core potential ab initio variational and perturbational CI study [273,274] indicates that, in the ground state (^2S, s^1d^{10}), Cu is completely inactive in accordance with the matrix isolation experiments [299]. However, the photoactivated Cu atoms possessing the ^2P excited state easily capture and activate dihydrogen.

The lowest low spin potential surfaces are also the chemically most interesting for dihydrogen activation by Fe (^3F, s^1d^7) and Co (^2F, s^1d^8) atoms [272], although some lower-lying high spin states also promote the reaction. This might be the case for the gas phase dihydrogen activation by Ni, Fe and Co atoms where there are no neighbouring atoms to favour the chemically interesting low spin states. In that case, the forbidden dissociation reactions with the lowest barrier could proceed either in gradation or in a concerted way which may also proceed via spin-orbit coupling to the low spin states. Therefore, in the gas phase chemistry of Fe, Co and Ni we would expect different reactivity patterns, owing to the possible occurrence of quite different spin-orbit induced reaction mechanisms.

Finally, the lowest doublets relating to the ground state collision of both collinear and perpendicular interactions of Sc with H_2 have proved very repulsive at the MRD-CI level [276]. In contrast, the lowest quadruplet states correlating to collision between ground state H_2 and (^4F, s^1d^2) Sc are less repulsive, being therefore interesting in reaction dynamics.

All theoretical studies of dihydrogen activation by transition metal atoms and ions reveal the important role of excited states in the M–H_2 interactions. The same excited states also seem to be responsible for reductive elimination and oxidative addition of H_2 in discrete L_nM complexes. Theoretical studies published so far [266,272,274,284,288] strongly support that appropriate electronic structures of L_nM compounds responsible for H_2 capture could be induced by the ligands L. Thus, in $Pd(OH_2)_2$, the s^1d^9 electronic configuration is induced which is able to capture the H_2 molecule. This is supported by the population analysis which shows a tendency to depopulate the *d* AOs in $Pd(OH_2)_2$ [288]. Moreover, the CuH_2 system does not have to resort to photoexcitation of the Cu atom in order to be capable of dihydrogen activation, since the central Cu atom has the appropriate electronic structure [274]. Similarly, the effect of phosphine ligands on the reactivity of $Pt(PH_3)_2$ systems studied by Low and Goddard [284] is to stabilize the d^{10} vs. s^1d^9 states and therefore facilitate reductive elimination.

There are a few theoretical studies concerning the mechanism and energetics of oxidative addition of H_2 and the microscopic reverse reductive elimination taking place on discrete transition metal complexes [254,257,266,278–290]. The oxidative addition of H_2 to the d^8 square-planar $RhCl(PH_3)_3$ complex has been studied by Dedieu and Strich with the EHMO [278] and ab initio methods [279]. Both computational methods indicated that the end-on approach of H_2 is preferred to the side-on at the beginning of the reaction. The bonding interaction between the σ_u^* MO of H_2 and an occupied *d* AO of Rh has been suggested to facilitate dihydrogen bond breaking in this reaction.

Hoffmann and coworkers [286], analyzing the reductive elimination reactions with the EHMO method, concluded that: (1) reductive elimination of R_2 from L_2MR_2 complexes is facilitated, when the b_2 MO of the L_2M fragment is lowered in energy, (2) better σ-donor R groups favour the process, (3) stronger donor ligands L *trans* to R induce a higher barrier for the elimination reaction. Moreover, activation energies were calculated for the reductive elimination of H_2 from PdH_4^{4-} and C_2H_6 from $Pd(CH_3)_2(PH_3)_2$ models; the reductive coupling for H–H bonds (4.6 kcal mol^{-1}) is characterized by a lower barrier than that for C–C bonds (39.1 kcal mol^{-1}).

Balazs et al. [281] have studied reductive elimination ($L_2MXY \rightarrow L_2M + XY$; L=$PH_3$; M=Pt, Pd and Ni; XY=$H_2$, H–$CH_3$ and H_3C–CH_3) using the SCF-Xα-SW approach. They discussed a correlation between the

relative rates of the reductive elimination processes and the molecular orbital character of the starting compounds. A simple model to correlate the occupancy of antibonding M–X(Y) MOs and the rates of reductive elimination with the relative electronegativities of M and XY has been proposed. According to this model, $L_2MX(Y)$ compounds undergoing relatively rapid reductive elimination of XY molecule possess occupied antibonding M–X(Y) MOs, whereas those compounds undergoing slow elimination have only vacant antibonding analogues.

The energetics and mechanism of the model oxidative addition reaction

$$H_2 + Pt(PH_3)_2 \rightarrow cis\text{-}Pt(PH_3)_2(H_2) \qquad (20)$$

have been widely studied [280,282–285,289] using ab initio HF and correlated wavefunctions and employing RECPs for Pt core electrons. The reaction energetics and transition state geometries have been summarized in Table 9.

Noell and Hay [282,283] have examined the addition of H_2 to $Pt(PH_3)_2$ and $Pt[P(CH_3)_3]_2$ in the framework of ab initio HF, MCSCF and CI methods with RECPs for Pt core electrons and a flexible Gaussian basis set for the valence electrons. From charge distribution analysis and geometrical changes detected along the reaction pathway, three phases were identified for the reaction course: (1) an initial repulsive interaction, (2) a partial charge transfer from Pt to H_2 through the delocalization of $5d_{xy}$ (b_2) AO of Pt into the σ_u^* MO of H_2 and (3) the final M–H bond formation. The transition state, still involving a significant H–H interaction (Table 9), was found to be of C_{2v} symmetry with symmetric Pt–H bonds. The reaction energetics were found

TABLE 9

Reaction energies (in kcal mol^{-1}) and transition state geometries (bond distances in Å and bond angles in deg) for the $Pt(PH_3)_2 + H_2$ model oxidative addition reaction

ΔE_r[a]	$\Delta E^{\neq}$[b]	Transition state geometry			Method	Ref.
		R_{Pt-H}	R_{H-H}	θ_{P-Pt-P}		
−7	17.4	1.81	0.90	120.0	HF	283
−5	16.6				SD-CI	283
−5	18.2				GVB-CI	283
−37	5.2	2.07	0.77	147.7	RHF	280,285
−27	8.7				SD-CI	280,285
−16	4.0	2.20	0.75	137.4	HF	284
−16	2.3				GVB-CI	284
8	0.8	1.70			MP2	290
−9	4.0				MP3	290

[a] ΔE_r is the reaction energy (exothermicity).

[b] $\Delta E^{\neq}$ is the activation energy.

to be not significantly altered in MCSCF and CI calculations, as well as in substituting PH_3 by the $P(CH_3)_3$ ligand. However, the *cis* dihydride complex was found to be 7 kcal mol^{-1} more stable than the reactants for PH_3 and essentially thermoneutral for $P(CH_3)_3$ complexes. The *trans* isomers were found to be 4 and 23 kcal mol^{-1} more stable than the *cis* isomers, respectively. It is important that the calculated barrier for the reverse reductive elimination reaction was found to be 24 kcal mol^{-1}, a somewhat unexpected high value considering that *cis* dihydride Pt(II) complexes are very infrequently observed.

Analogous phases depicted in Fig. 11 were also observed in a GVB and CI study of the model $H_2 + Pt(PH_3)_2$ reaction carried out by Low and Goddard [284]. Thus, the first phase corresponds to the formation of a donor/acceptor bonding of H_2 to $Pt(PH_3)_2$, with the H–H bond remaining intact. This is a repulsive interaction with an overall energy increase of 2.3 kcal mol^{-1}. The second phase involves the electronic promotion of the Pt central atom from d^{10} to s^1d^9 and has been verified by analysis of the

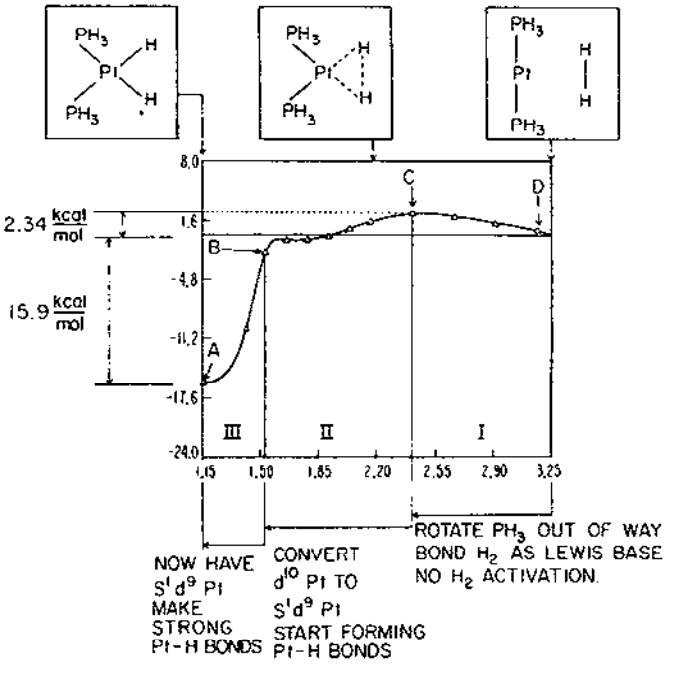

H_3P-Pt-PH_3	100°	111°	153°	176°	180°
H-H	1.93 Å	1.10 Å	0.74 Å	0.73 Å	0.74 Å
Pt-H	1.50 Å	1.66 Å	2.45 Å	3.19 Å	∞

Fig. 11. Potential energy curve along the reaction coordinate of oxidative addition of H_2 to $Pt(PH_3)_2$. Reproduced with permission from ref. 284.

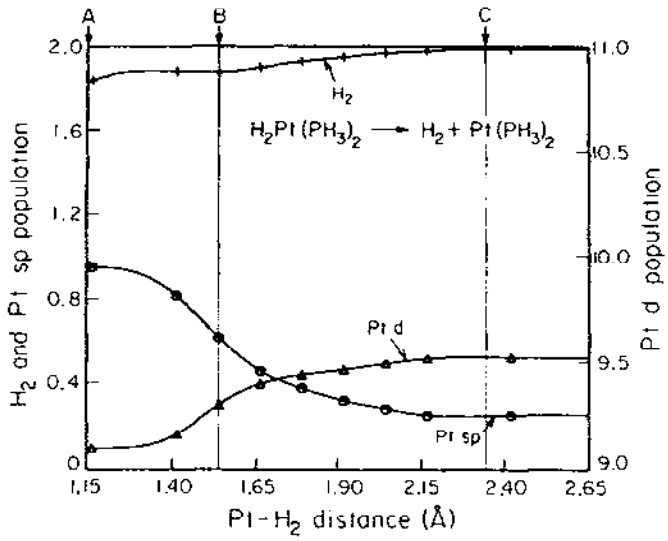

Fig. 12. Mulliken population along the reaction coordinate of oxidative addition of H_2 to $Pt(PH_3)_2$. Reproduced with permission from ref. 284.

Mulliken populations of the *d* and *s* AOs of Pt and σ_g and σ_u^* MOs of H_2 as a function of the reaction coordinate (Fig. 12). The VB and MO pictures of this second phase are practically equivalent. Finally, the third phase corresponds to the formation of the two M–H covalent bonds. The full optimization used in ref. 284, in contrast to the partial optimization used in ref. 283, accounts for the differences in reaction energetics and transition state geometries (see Table 9).

Potential energy hypersurfaces of the model $H_2 + Pt(PH_3)_2$ reaction have also been investigated by Obara and coworkers [280,285] at the ab initio RHF + CI level. Full optimization of the transition state and equilibrium geometries have been carried out by the energy gradient method, using RECPs for Pt core electrons. The authors suggested that the oxidative addition reaction proceeds through an 'early transition state' of C_{2v} symmetry with its geometry resembling that of the reactants. At this transition state, the effect of the steric repulsion between bulky phosphines was found to be negligible, but it destabilizes the *cis* adduct. Noell and Hay [282,283] estimated the steric repulsion of $P(CH_3)_3$ to be 7 kcal mol^{-1} at the P–Pt–P interligand angle of 100°. It is obvious that the $H_2 + Pt(PH_3)_2$ system could easily go through the C_{2v} transition state and then deviate from the sterically undesirable *cis* path to afford the less destabilized *trans* product. An energy decomposition analysis revealed [280,285] that both donation and back donation are important at the transition state. In addition, it has been found that a decrease in the interligand P–Pt–P angle increases the reactivity of

the metal centre with an activation energy of 10 kcal mol^{-1} per 10° change in the range from 100 to 140°. The differences between Obara's transition state geometry and that of Low and Goddard [284] (Table 9) must be due to the different ECPs and basis sets used. This is also the case for the results obtained by Hay and Rohlfing [289] who used 'norm-conserving' ECPs.

Another important class of transition metal compounds provoking H–H and C–H bond activation processes is that of d^8 ML_4 (M = Ru, Os; L = CO or PR_3) and CpML (M = Rh, Ir; L = CO or PR_3; Cp = η^5-C_5H_5 or η^5-C_5Me_5). These coordinatively unsaturated active species could be generated from saturated (18-electron) ML_5, CpML(L') (L' = CO or PR_3) and CpML(R)(H) (R = H or alkyl group) systems by thermal or photolytic expulsion of L, L' and RH, respectively. Dihydrogen activation by these compounds has been investigated by Ziegler et al. [290] using non-local density functional calculations. Complete energy profiles for the $H_2 + ML_4$ and H_2 + CpML reactions (Fig. 13), as well as optimized geometries for the active species, transition states and products of the reactions are reported. Once more three distinct phases characterizing oxidative addition of the H_2 to transition metal compounds [282–284], e.g. adduct formation→transition state formation→dihydride complex formation, are present. The reaction energy profiles clearly indicated that oxidative addition of H_2 is more facile for CpML than for ML_4. Indeed, CpML species have only empty σ-type metal-based MOs, while ML_4 species possess both occupied and empty MOs, the former impeding the addition reaction. The higher HOMO energy in CpML species also helps to reduce the energy barrier for the addition reaction of H_2. Finally, Ziegler et al. [290] have calculated average M–H bond energies for the CpML(H_2) and $L_4M(H_2)$ compounds and found the order of stability for the M–H bonds in the dihydrides to be:

$$\bar{D}_e(\text{Ir–H}) > \bar{D}_e(\text{Rh–H}) > \bar{D}_e(\text{Os–H}) > \bar{D}_e(\text{Ru–H})$$

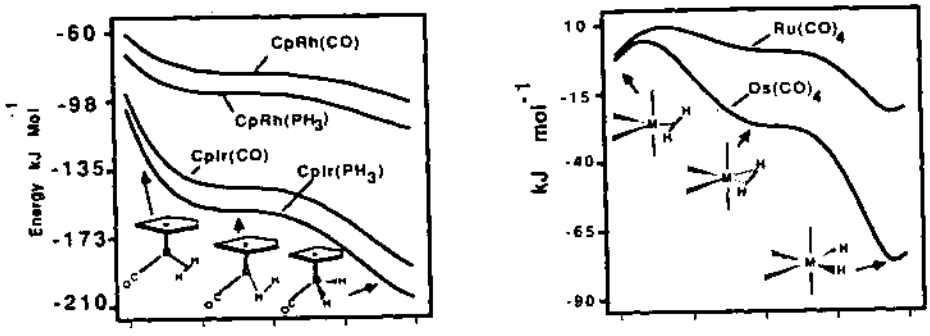

Fig. 13. Energy profiles for the addition of H_2 (a) to CpRhL and CpIrL with L = CO, PH_3 and (b) to $Ru(CO)_4$ and $Os(CO)_4$. Reproduced with permission from ref. 290.

The particularly strong bonds formed by third row metals have been attributed to relativistic effects which may contribute up to 10 kcal mol^{-1} as well as to better bonding overlaps in 5*d* elements with respect to 4*d* elements.

(g) Dihydrogen activation by d^0 metal centres. The mechanism of H/D exchange reactions

Dihydrogen activation by d^0 metal centres is also possible and has been experimentally identified in a number of H/D exchange reactions, formulated generally as

$$L_nM{-}H + D{-}D \rightarrow L_nM{-}D + H{-}D \qquad (21)$$

The mechanism of these H/D exchange reactions has also been investigated theoretically for both early transition [300] and rare earth metal [287] complexes. For H/D exchange reactions of early transition metal compounds, such as Cl_2TiH^+, Cl_2TiH and Cl_2ScH, Steigerwald and Goddard [300] have determined accurate wavefunctions, activation energies and transition state geometries using ab initio GVB calculations. They have found that these reactions proceed through a direct four-centre concerted mechanism with low activation barriers, amounting to 2.0, 21.7 and 17.4 kcal mol^{-1} for Cl_2TiH^+, Cl_2TiH and Cl_2ScH, respectively. These values clearly indicate that activation energies are lower when the M–H bond is non-polar and covalent and involves mostly metal *d* AO character.

The mechanism of dihydrogen activation by rare earth metal compounds, such as Cp_2LuR (R = H or alkyl group), has recently been investigated by Hoffmann and coworkers [287] at the EHMO level of approximation. They have found that the reactive d^0 L_nM species only need to possess an empty MO capable of stabilizing the σ bond electron pair of H_2 in the symmetric four-electron, four-centre transition state shown in **8**. Notice that in this transition state the three hydrogen atoms are in the plane between the Cp rings.

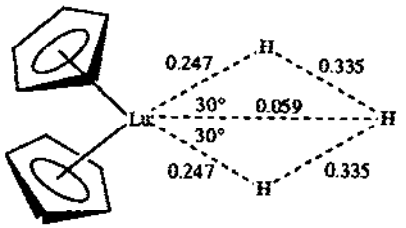

8

The coordination mode in **8** can be formally viewed as an H_3^- ligand coordinated to a Cp_2Lu^+ fragment with the four electrons of H_3^- delocalized

over the four centres. Such a bonding picture of the transition state is consistent with the overlap population analysis data shown in **8**. The possibility for a coordinated H_3 unit as an intermediate in the H/D exchange in $[Ir(H)(H_2)bqL_2]^{2+}$ has recently been suggested by Crabtree and Lavin [246].

Experimental data for H/D exchange reactions [244–246,265] prompted Burdett et al. [259] to investigate several structures geometrically feasible for polyhydrogen species which are possibly formed as intermediates. In particular they investigated the mechanism of the H/D exchange reaction occurring in $Cr(CO)_4(H_2)_2$ dissolved in liquid xenon. It was suggested that the most promising routes for the H/D exchange are: (1) one involving coordinated H_3 and H ligands with both open, **9**, and closed, **10**, geometries for H_3 being of low energy structures and (2) one involving a coordinated open H_4 species, **11**. Moreover, the exchange process proceeding through the topologically simple intermediate containing a square H_4 ligand, **12**, was found to be of high energy because of the direction of charge flow between ligand and metal in the intermediate. Species containing a coordinated tetrahedral H_4 ligand, **13**, have also been studied in both their η^2- and η^3-bonding modes.

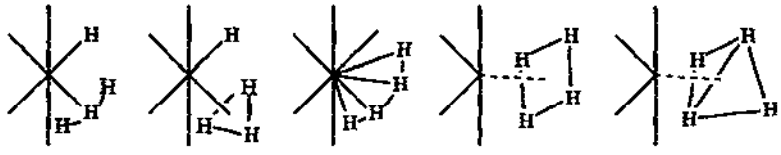

9 **10** **11** **12** **13**

Very recently, Kober and Hay [257] have also investigated the mechanism of scrambling of H_2/D_2 mixtures to HD by $Cr(CO)_4(H_2)_2$ with the aid of ab initio calculations. Contrary to the suggestions of Burdett et al. [259], the polyhydride forms having either a square H_4 or an $H_3^+-H^-$ species coordinated to $Cr(CO)_4$ were found to be very high in energy. The most stable geometrical structure of the *cis*-$Cr(CO)_4(H_2)_2$ complex is that involving the two dihydrogen ligands in an upright position relative to the equatorial plane. The rotational barrier for each ligand about the $Cr-H_2$ bond was calculated to be 1.5 kcal mol^{-1}, whereas the interconversion of the bis-dihydrogen complex to a dihydrogen–dihydride complex was found to be a relatively low-energy pathway for the H_2/D_2 exchange reactions (activation barrier of 24 kcal mol^{-1}).

(ii) Transition metal alkyls. Alkane activation and reactivity

(a) Electronic structure and bonding in transition metal alkyls

Isolobal arguments suggest [254] that an alkyl group and a hydrogen atom should bond to transition metals in a similar fashion. In fact, detailed

TABLE 10

Theoretical and experimental BDEs (in kcal mol^{-1}) for some transition metal methyl systems studied so far

Compound	Ground state	$D_e(M-CH_3)$	$D_0(M-CH_3)$	Computational method	Ref.
$ScCH_3^+$	^2E	54.5	$(59\pm3)^a$	GVB-DCCI	302
Cp_2ScCH_3		52.6		HFS	237
Cp_2VCH_3		38.5			237
$CrCH_3^+$	$^5A_1$	24.1	(30 ± 2)	GVB-DCCI	302
		18.0		MCSCF+1+2	207
$CrCH_3$	$^6A_1$	44.5	(41 ± 7)	HFS	208
$Cp(CO)_3CrCH_3$		29.2		HFS	237
$MnCH_3^+$	$^6A_1$	40.3	(51 ± 5)	GVB-DCCI	302
		55.9		HFS	208
Cp_2MnCH_3		23.4		HFS	237
$(CO)_5MnCH_3$		36.6		HFS	208
$Cp(CO)_2FeCH_3$		43.0		HFS	237
$(CO)_5FeCH_3^+$		57.1		HFS	208
$NiCH_3$	$^2A_1$	54.0	(55 ± 3)	CNDO/S[2]	303
$(CO)_4CoCH_3$		38.2		HFS	208
$Cp(CO)NiCH_3$		41.6		HFS	237
$(CO)_4NiCH_3^+$		60.0		HFS	208
$CuCH_3$	$^1A_1$	56.9	(55 ± 4)	HFS	208
$ZnCH_3^+$	$^1A_1$	60.7	(71 ± 3)	GVB-DCCI	302
		68.8		HFS	208
YCH_3^+	$^2A_1$	58.3	(64 ± 7)	GVB-DCCI	302
Cp_2YCH_3		66.0		HFS	237
$MoCH_3^+$	$^5A_1$	30.2		GVB-DCCI	302
$MoCH_3$	$^6A_1$	48.0	(46 ± 3)	HFS	208
$TcCH_3^+$	$^6A_1$	43.0		GVB-DCCI	302
		62.6		HFS	208
Cp_2TcCH_3		36.3		HFS	237
$(CO)_5TcCH_3$		42.5		HFS	208
$(CO)_4RhCH_3$		45.4		HFS	208
$PdCH_3^+$	$^1A_1$	47.1	(59 ± 5)	GVB-DCCI	302
$AgCH_3$	$^1A_1$	42.3		HFS	208
$CdCH_3^+$	$^1A_1$	48.5		GVB-DCCI	302
		55.2		HFS	208
Cp_2LaCH_3		65.0		HFS	237
Cp_2ReCH_3		37.3		HFS	237
$(CO)_5ReCH_3$		47.8		HFS	208
$(CO)_4IrCH_3$		50.7		HFS	208

[a] Figures in parentheses are experimental data taken from refs. 195 and 212.

calculations [207,208,302] on selected transition metal methyl cations, MCH_3^+, showed that the metal–methyl bonds are very similar to the σ bonds in MH^+ systems. This similarity includes bond orbital overlaps, electron transfer, metal orbital hybridization and bond dissociation energies. The experimental and theoretical values of BDEs of some transition metal methyl systems studied so far are collected in Table 10.

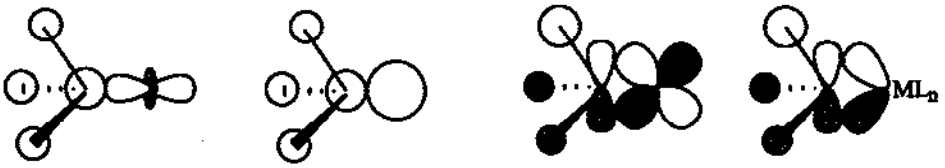

14 **15** **16**

The M–CH_3 bonds in the neutral MCH_3 systems are shown to be weaker than the corresponding M–H bonds in their MH analogues, as a result of exchange repulsions between occupied metal orbitals and the fully occupied σ-orbital on the methyl group, shown in **14** and **15**. However, in the cationic species MCH_3^+, the presence of the positive charge on the metal reduces these repulsions because of the contraction of the metal orbitals and increases the charge transfer from CH_3 to M^+, **16**. Therefore, the M^+–CH_3 bond strength in these systems is increased to the point where the discussed bond becomes stronger than, or as strong as, the corresponding M^+–H bond in MH^+ systems, in accordance with experimental data [195,212]. The same is also true for saturated transition metal methyls investigated by Ziegler et al. [208,237] by density functional theory. Actually, it was found that the M–CH_3 bond is considerably weaker than the M–H bond for the late to middle transition metals as a result of the repulsive 4e-2O interaction between the fully occupied $1\sigma_{Me}$ MO and the σ-bonding L_nMCH_3 orbital φ_σ shown in Fig. 14. These repulsive interactions contribute a destabilization,

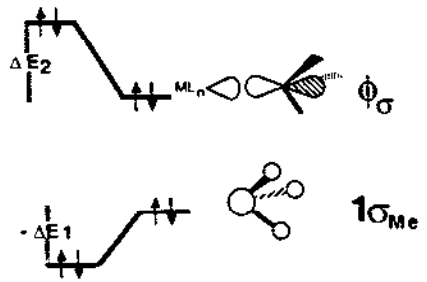

Fig. 14. Destabilization of the M–CH_3 bond from the interaction between $1\sigma_{Me}$ and φ_σ ($\varphi_\sigma = c_1 2\sigma_{Me} + c_2\sigma_{ML}$). Reproduced with permission from ref. 237.

$\Delta E_2 - \Delta E_1$ to the M–CH_3 bond, given quantitatively [237] by the expression, $\Delta E_2 - \Delta E_1 \propto \langle 1\sigma_{Me}|\sigma_{ML}\rangle^2 \; C_1^2$, where C_1 is the coefficient of σ_{ML} in the φ_σ MO.

For the early transition metal methyls, due to the higher polarity of the M–CH_3 bond, the repulsive interaction is smaller and therefore their M–CH_3 and M–H bonds become comparable in strength. Moreover, for the saturated transition metal methyl the M–CH_3 bond strength was found [208,237] to increase on descending a triad (Sc, Y, La; Mn, Tc, Re; Co, Rh, Ir) as a result of an increase in the σ-bonding overlap between $2\sigma_{Me}$ and σ_{ML}.

The ab initio LCAO and one-centre expansion (OCE) calculations of Hotokka and Pyykkö [304] on $Ti(CH_3)_4$ and TiH_4 verified once more the similarity of bonding between H and CH_3 towards transition metals.

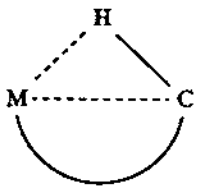

17

The 'agostic' interactions [305] between C–H σ bonds and empty metal *d* AOs (the d_π AOs in the M–C–H plane) more important for the early transition metals are responsible for their stronger M^+–CH_3 bond relative to M^+–H bonds when compared with late transition metal complexes. Obviously, 'agostic' interactions, **17**, are favoured by small M–C–H bond angles which reduce the metal's *ns* and the alkyl's sp^3 radical orbitals [306,307] and therefore weaken the metal -alkyl bond strength. Despite the many experimental and theoretical studies [254,306–310], 'agostic' interactions remain both puzzling and challenging owing to their importance for the problem of C–H bond activation [311]. Both density functional LCGTO-Xα [310] and ab initio GVB and CASSCF [309] calculations were unable to confirm the unusual geometry of the CH_3 group in Cl_3TiCH_3 established experimentally by electron diffraction techniques and attributed to agostic interactions [308]. Thus, no flattening of the methyl ligand can be predicted from the calculations and therefore the key to an agostic interaction seems to be the low-energy methyl rocking distortion due to stabilization of the rocking motion by low-lying *d* orbitals on Ti [309].

(b) Alkane activation. The nature of C–H and C–C activation processes

Recent advances in the field of alkane activation have been the observation that the C–H bond of hydrocarbons can add to appropriate transition metal

centres under mild conditions. Both naked transition metal atoms (or ions) and metal complexes have been found to be reactive towards C–H and C–C bond activation. In the light of the experimental and theoretical data on the C–H bond activation by transition metal complexes available so far, two different activation processes have emerged:

(i) by coordinatively unsaturated electron-rich transition metal centres through an oxidative addition reaction, e.g.

$$L_nM + R{-}H \rightarrow L_nM(R)(H) \tag{22}$$

where R is an alkyl, alkenyl or aryl group and

(ii) by strong Lewis acidic transition or rare earth metal complexes through a 'sigma bond metathesis' reaction, e.g.

$$L_nM{-}R + R'{-}H \rightarrow L_nM{-}R' + R{-}H \tag{23}$$

where R and R′ are hydrogen atoms, alkyl, alkenyl, alkynyl or aryl groups.

The mechanism and reaction energetics of C–H and C–C bond activation processes by transition metal atoms (or ions) and metal complexes have recently been investigated by modern experimental methods [194,195,312,313] and also by high quality computations [254,266,270, 281,285–287,314–316]. Most of the theoretical studies performed so far concern activation process (i) and in particular by the nickel group metals and their complexes [266,270,281,285,286,314–316]. Methane and ethane have been used to model the C–H and C–C bond activation (oxidative cleavage as well as reductive coupling), respectively.

Åkenmark et al. [314] carried out SCF and valence CI calculations on several states of linear and bent $Ni(CH_3)_2$ as well as on its square planar *cis*-$(H_2O)_2Ni(CH_3)_2$. The unsaturated $Ni(CH_3)_2$ exhibit a linear structure with a high spin ($^3B_2$) ground state. However, addition of strongly coordinated ligands to the bent structure produces a singlet state capable of C–C reductive coupling.

EHMO activation energies of 15 and 39.1 kcal mol^{-1} were calculated by Tatsumi et al. [286] for the reductive elimination of C_2H_6 from $M(CH_3)_2(PH_3)_2$ for M = Ni and Pd, respectively. These energies are substantially lower than those reported by Blomberg et al. [315] at the CASSCF-CI level. Similarly, the activation energies for the reverse addition reactions have also been found to be different in the two calculations (55 kcal mol^{-1} for the EHMO and 42 kcal mol^{-1} for the ab initio calculations for which correlation effects were taken into consideration). Ligand effects have also been stated [266] to be substantial. The Ni–C bond in $NiHCH_3$ is stabilized by 7 kcal mol^{-1} or destabilized by as much as 3, 11, 16, 27 kcal mol^{-1} by the addition of Cl, PH_3, N_2, CO or C_2H_4, respectively. Destabilizing ligands are expected to decrease the elimination barrier but to increase the addition

barrier. For the same reason, the stabilizing ligands should have the opposite effect. It should be noted that $NiHCH_3$ is unbound by 9 kcal mol^{-1} relative to Ni ($^1D, s^1d^9$) and there is a barrier of 13 kcal mol^{-1} for the elimination reaction and 22 kcal mol^{-1} for the addition reaction.

The reaction profiles of C–H and C–C reductive coupling from Pd and Pt bis(phosphine) complexes have recently been investigated by ab initio calculations [270,285,316]. The difference in the Pt–H and Pt–C bond strengths being 61–70 and 34–41 kcal mol^{-1}, respectively, is thought to account for the observed differences in the ab initio RHF+CI study of the oxidative addition of H_2 and CH_4 to $Pt(PH_3)_2$. The former is exothermic and the latter almost thermoneutral, exhibiting activation barriers of 8 and 28 kcal mol^{-1}, respectively.

Low and Goddard [270,316], studying analogous reactions by the GVB–CI* RCI method, found an increase in the exothermicity of the reductive elimination from the MR_1R_2 complexes of 20–25 kcal mol^{-1} by the addition of phosphine ligands. The results, depicted schematically in Fig. 15, have been rationalized in terms of the electronic promotion idea for oxidative addition of H_2, CH_4 and C_2H_6 to Pd and Pt compounds [260].

Using non-local density functional calculations of the complete energy profiles for the reactions

$$CpML + CH_4 \rightarrow CpML(H)(CH_3) \qquad (M = Rh, Ir;\ L = CO, PH_3) \qquad (24)$$

and

$$M(CO)_4 + CH_4 \rightarrow M(CO)_4(H)(CH_3) \qquad (M = Ru, Os) \qquad (25)$$

in concurrence with arguments discussed in the H–H bond activation, d^8 CpML complexes are more efficacious in C–H activation than d^8 ML_4 complexes [254,290], which present considerably higher activation barriers. The similarity of arguments in both cases is further supported by the observation of an intermediate σ-type $CpLM{-}HCH_3$ in the course of the reaction.

Naked metal ions, M^+, are also reactive towards alkane activation [194,195,312,313]. However, these reactions are very complicated even for methane. Observed reactions of atomic metal ions and methane are

$$M^+ + CH_4 \begin{cases} \longrightarrow MH^+ + CH_3 & (26) \\ \longrightarrow MCH_3^+ + H & (27) \\ \longrightarrow MCH_2^+ + H_2 & (28) \end{cases}$$

Armentrout and Beauchamp [195] concocted M^+ reactivity series pursuant to those already defined for H_2 activation. One of the basic requirements for the favourable insertion of M^+ into C–H and C–C bonds [195,212] is that the sum of the two M–C bond energies in $M(CH_3)_2^+$ should be comparable

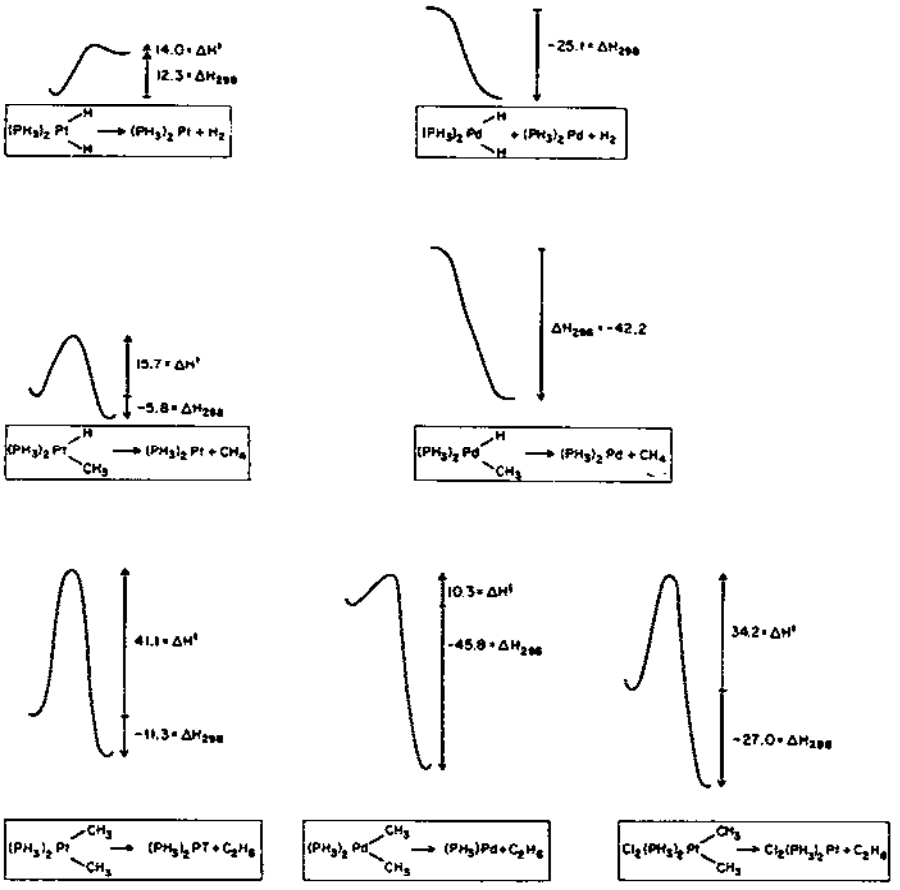

Fig. 15. Estimated energetics for R_1–R_2 reductive coupling of $(PH_3)_2M(R_1)(R_2)$ complexes (M = Pd, Pt). All quantities are enthalpies at 298 K. Reproduced with permission from ref. 316.

with or exceed the C–H and C–C bond energies, which are 96–100 and 85–90 kcal mol^{-1}, respectively. Moreover, Armentrout and Georgiadis [212] verified the concept of bond cooperativity [85,86] in $M(CH_3)_2^+$ systems.

The mechanism of alkane activation through the 'sigma bond metathesis' reactions (activation process (ii)) has been investigated theoretically by Hoffmann and coworkers [287]. Both theory and experiment suggest that alkane activation by d^0 (or d^0f^n) L_nMR compounds involves a direct electrophilic attack at the C–H σ bond of alkane, possibly generating a sigma complex capable of forming a symmetric four-centre transition state, as is shown in **18**. It was found that the greater the *s* character associated with the reacting σ bonds the more bonding is the transition state and therefore its higher stability facilitates the activation process. Considering the poorer overlap of the sp^3 orbital of R compared with that of H, one would expect the transition

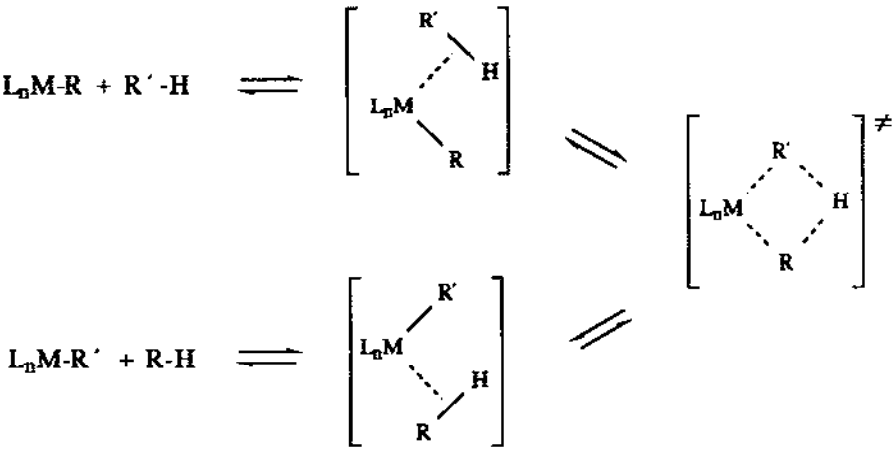

18

state for the C–C bond activation reaction by L_nMR complexes, shown in **19**, to be of higher energy and therefore direct attack of M–R at C–C bonds seems quite unlikely.

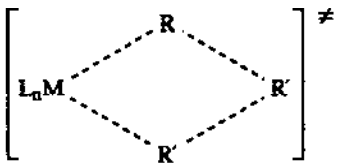

19

The 'sigma bond metathesis' mechanism is similar to that of insertion of ethylene into M–R bonds. Insertion of olefins into M–R bonds was shown to be of key importance in the Cossee mechanism [317], which is widely accepted for Ziegler polymerization of olefins, and has met theoretical consideration [318,319]. An ethylene-coordinated state is predicted to precede the transition state, the latter being a symmetrical four-centre transition state similar to that shown in **19**. Such a transition state is facilitated by d^0 methyltitanium complexes but not for their d^2 counterparts.

(iii) Transition metal oxides. Dioxygen activation and reactivity

Several extensive reviews have appeared in the literature summing up the available information on a variety of dioxygen complexes [6,320–322] often involved in biological and catalytic processes.

(a) Electronic structure and bonding of transition metal oxides

Few high quality theoretical studies address transition metal oxide systems [323–330], most of them applying highly sophisticated techniques on the simplest monoligated transition metal oxide systems, MO and MO^+ [323–327]. The observed trends in BDEs (Table 11) along the transition series are similar to those of metal hydrides and alkyls, though M–O bonding is much more complex owing to the combined σ/π-donor ability of O_2.

The bonding picture of transition metal oxides is characterized by two general features [324,325]: (i) the formation of covalent M(d)–O(p) bond with considerable sd hybridization on the metal and (ii) the ionic contribution from the substantial charge transfer (~0.7e) from metal to the oxide ligand.

Moreover, the short M–O bond distance allows significant M(d_π)–O(p_π) overlap, which purveys partial triple character to the bond. The degree of covalent bonding in MO and MO^+ systems increases with decreasing separation between the s^2d^n and s^1d^{n+1} occupations. Moving to the right-hand side of a transition row, the ionic contribution to M–O bonding increases; CuO and AgO systems are almost purely ionic systems (see Table 11). On the other hand, moving to the left, the decrease of the d electrons increases the ability to form bonds and therefore the M–O bond strength also increases.

The metal–oxo bonding in saturated transition metal compounds strongly depends on the nature of the other ligands involved in the coordination sphere. In fact, fundamental differences in the M–O bonds of high-valent

TABLE 11

Theoretical and experimental bond dissociation energies (in kcal mol^{-1}) for some transition metal MO and MO^+ systems

Compound	Ground state	D_e(M–O)	Computational method	Ref.
TiO	$^3\Delta$	118.5 (158.4)[a]	ECP-CI	221
CrO	$^5\Pi$	71.2 (101.5)	MCSCF-SDCI	324
CrO^+	$^4\Pi$	57.0 (77.0)	MCSCF-CI	323
MoO	$^5\Pi$	84.6 (115.3)	MCSCF-SDCI	324
FeO	$^5\Delta$	81.7 (96.8)	CAS-MCSCF	325
RuO	$^5\Delta$	(122.2)	CAS-MCSCF	325
NiO	$^3\Sigma^-$	(89.2)		
NiO^+		24.0 (45±4)		
PdO	$^3\Sigma^-$			
CuO	$^2\Pi$	43.4 (64.3)	MCSCF-SDCI	326
		61.5	ECP-CI	327
AgO	$^2\Pi$	28.4 (52.8)	MCSCF-SDCI	324
		44.0	ECP-CI	327

[a] Taken from ref. 230.

mono- and dioxo-complexes of Cr, Mo, W and Re, being important species for epoxidation and metathesis of olefins, have been identified by Rappé and Goddard [328–330] with the use of ab initio GVB and CI calculations.

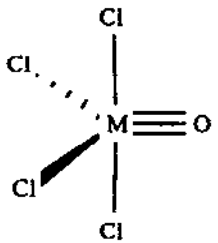

20

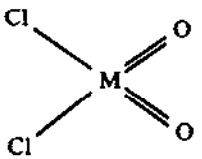

21

Utilization of two d_π bonds to one or two oxygen atoms leads the M–O bond to the propinquity of a triple, **20**, or double, **21**, bond, respectively, the corresponding bond energies being 51 and 82 kcal mol^{-1} for Cr and 79 and 102 kcal mol^{-1} for the Mo complex, respectively. It is important that the M–O bond length is nearly the same for the double and triple bond with differences of the order of 0.01 Å for both Cr and Mo, in accordance with the small shifts in the M–O stretching frequencies observed experimentally.

Rappé and Goddard [329] have also suggested that for the double bond-to-triple bond conversion to occur it is essential for the metal to form two auxiliary, partially ionic bonds to electronegative ligands (such as halides or alkoxides) so that the M–O bonds are covalent. Moreover, the electronic configuration of the metal must allow an empty d_σ orbital in order to form the donor–acceptor bond ($M(z^2) \leftarrow O(z)$) with this effect being favoured only for the left-hand side portion of the transition metals.

Geometrical preferences in transition metal dioxo species have been investigated at the level of the EHMO approximation [331,332]. Tatsumi and Hoffmann [331] have found that d^0 MoO_2^+ is bent, with an optimal angle near 100°, a fact attributed to the d_π orbital utilization in stabilizing the bent MoO_2^+. The d_π orbital utilization rationale for a *cis* preference in d^0 L_4MO_2 octahedra and a *trans* preference in d^2 L_4MO_2 has been discussed by Mingos [332] using $MoO_2(PH_3)_4^{n+}$ ($n=2, 0$). However, more recently, Mingos and coworkers [333] have recognized that metal d_π–ligand π conflicts are responsible for the *cis* geometry of the M(O)(CO) moiety in d^2 $L_4M(CO)(O)$ octahedral complexes. Such π-acid/π-donor d_π conflicts are also exhibited by mixed oxocarbyne complexes and have as a result the accumulation of electron density on the terminal oxo ligand.

Of special importance is the existence of 'distortional isomerism' in octahedral Mo and W oxo complexes shown in **22**–**24**. Such an isomerism, first proposed by Chatt et al. [334] to characterize metallic complexes differing

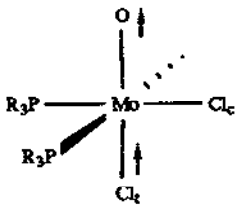

22

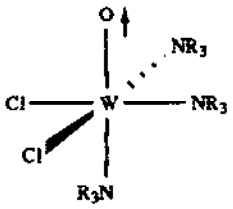

23

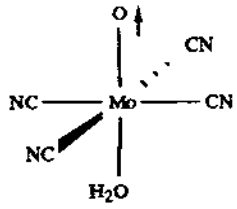

24

only in the length of one or several bonds, has been adopted as 'bond-stretch isomerism' by Hoffmann and coworkers [335] and has been investigated at the EHMO level of approximation. Two electronic mechanisms have been proposed. The first one involves a first-order Jahn–Teller effect favoured either by π-donor ligands *cis* to oxygen or by π-acceptor ligands *trans* to the oxygen. As a matter of fact, all the characterized bond-stretch isomers carry π-acceptor or π-donor ligands. The second mechanism, being typical of three-centre four-electron π-systems, involves a second-order Jahn–Teller effect. In this case, both σ and π effects are of key importance for bond-stretch isomerism.

(b) Mechanism and energetics of hydrocarbon oxidation by transition metal oxides

The mechanism and reaction energetics of hydrocarbon (alkane and alkene) oxidation by high valent dioxo complexes, formulated as $Cl_2M(O)_2$ (M = Cr, Mo, W) have been investigated by Rappé and Goddard [328–330] and Upton and Rappé [336] using ab initio theoretical methods. Their most important conclusion is that the second oxo group is intimately involved in the reaction sequence and plays a central role in stabilizing critical intermediates. Alkane oxidation proceeds through the addition of R–H across one M–O π bond forming an organometallic intermediate that reductively eliminates an alkyl chloride or an alcohol according to the reactions:

$$Cl_2M(O)_2 + R{-}H \rightarrow Cl_2M(O)(OH)(R) \begin{cases} \longrightarrow ClM(O)(OH) + RCl & (29) \\ \longrightarrow Cl_2M(O) + ROH & (30) \end{cases}$$

Both processes (29) and (30) were found to be exothermic, with alcohol formation favoured, whereas R radical formation, being favoured in the gas phase, was found to be approximately thermoneutral for $R = CH_3$, but increasingly exothermic for higher homologues. The reaction energetics and composition of alkane oxidation by $Cl_2M(O)_2$ complexes strongly depend on the M–L bond strength.

The energetics for the oxidation of ethylene by Cl_2CrO_2 and Cl_2MoO_2 [328–330,336], shown in Fig. 16, endorse the mechanism by Sharpless et al.

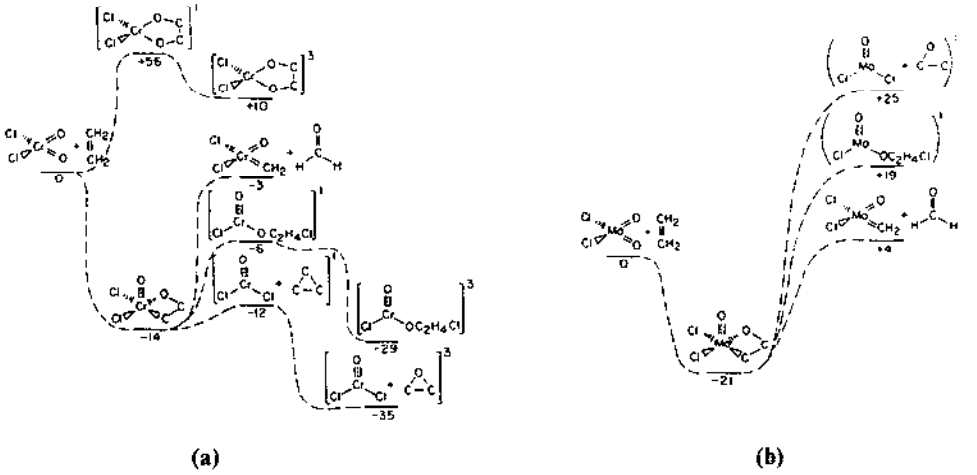

(a) (b)

Fig. 16. Energetics (ΔG_{300}) for the reaction of C_2H_4 with (a) Cl_2CrO_2 and (b) Cl_2MoO_2. Reproduced with permission from ref. 329.

[337], which is initiated by a 2+2 addition of the olefin across one M–O π-bond. It is obvious that the direct ene addition reaction product is not thermally accessible. This explains the observation that olefin oxidation by $Cl_2M(O)_2$ complexes does not produce *cis* diols but forms epoxides and *cis* hydrochlorins.

A radical mechanism has been proposed by Sevin [338] for ethylene epoxidation by Fe(IV)-oxo porphyrins based upon qualitative VB considerations. In particular, he has studied an optimal reaction path for reaction (31) by a complementary use of MO and VB methodologies and found that the reactant's approach in an isosceles geometry (C_{2v} reaction path) is very exothermic. However, this reaction, being spin and symmetry allowed, could proceed by only one carbon atom of C_2H_4 approach to the O atom, leading to an intermediate Fe–O–C–C open species, exhibiting a radical character with the unpaired electron on the terminal carbon atom, Fe(III)–O–C–C':

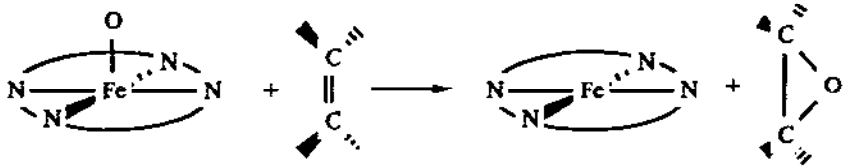

(31)

An alternative mechanism has recently been proposed by Jørgensen [339] on the basis of INDO, CNDO and EHMO calculations. It was found that the structure of oxo-iron porphyrins is one in which the oxygen atom is inserted into the iron–nitrogen bond, as shown in **25**.

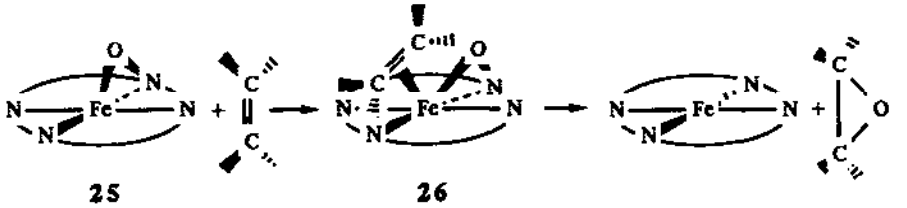

25 26 (32)

Based upon this structure Jørgensen suggested that the first step in the reaction of olefin epoxidation is a binding of the olefin to the iron centre in an orientation perpendicular to the Fe–O bond, **26**, followed by a slipping displacement of the olefin toward the oxygen as the next step. This movement of the alkene moiety leads to favourable interactions between the π^*-MO of the alkene and the lone pair on oxygen which is antisymmetric with respect to the Fe–O–N plane, **27**. The proposed mechanism accounts well for the stereoselectivity of the epoxidation process observed experimentally.

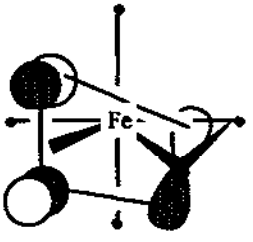

27

(c) Transition metal-dioxygen bonding and reactivity

Mononuclear transition metal complexes containing dioxygen ligands have been of considerable interest because of the desire to understand the chemistry of metalloporphyrins (hemoglobin, myoglobin, chlorophyll, cytochromes, catalase and peroxidase) which relates principally to redox reactions and the transport, storage and activation of molecular oxygen. Items of interest include geometric structure, i.e. side-on (η^2) vs. end-on (η^1) bonding mode of O_2 and the angle of bend if η^1-bound, spin state and charge distribution. Results obtained from theoretical work have been reviewed recently [320,321,340]. Therefore, only some recent advances in the field of dioxygen–metal complexes and dioxygen activation processes will be discussed here.

In an extensive review [341] of dioxygen complexes, it was noted that the Griffith geometries, **28**, are most common, but iron complexes are one of the few cases where Pauling geometries, **29**, are observed. Despite the many advances in the field, controversies still exist regarding the nature of the metal–dioxygen bond as well as the ground state of oxy-metal porphyrins which may correspond either to a M^{2+}–O_2^0 dioxygen or a M^{3+}–O_2^- superoxide formulation of the MO_2 unit.

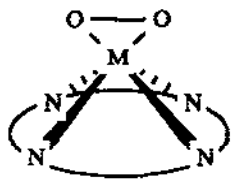

28

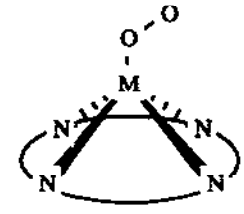

29

Earlier theoretical work based upon PPP and MSW-Xα calculations [342] suggested that the FeO_2 unit in oxy-iron porphyrin formulated as $PFeO_2$ (P = porphyrin dianion) could be viewed as an equal mixture of $Fe^{2+}(S=0)$–$O_2^0(S=0)$ and $Fe^{2+}(S=1)$–$O_2^0(S=1)$. INDO-SCF-CI calculations of Herman and Loew [343] suggested that $PFeO_2$ has a diamagnetic $Fe^{2+}(S=1/2)$–$O_2^0(S=1/2)$ singlet ground state $^1A'$ with considerable Fe^{3+} $(S=1/2)$–$O_2^-(S=1/2)$ character as well. Ab initio LCAO-MO-SCF calculations performed by Dedieu et al. [340] on a number of $(L)PFeO_2$ ($L=NH_3$) systems favoured a closed shell type singlet state, $Fe^{2+}(S=0)$–$O_2^0(S=0)$. Moreover, the most stable conformation corresponds to the staggered structure with the O–O bond projecting along the bisections of the Fe–N bonds [344] in accordance with experimental data. The eclipsed structure was found to be only slightly higher (by 2–3 kcal mol^{-1}) in energy than the staggered structure. Furthermore, Strich and Veillard [345] showed that the most stable geometry of oxy-iron porphyrins places the iron out of the plane by 0.25 Å. More recently, Newton and Hall [346], using generalized molecular orbital (GMO) calculations with CI, concluded that the FeO_2 unit in the model $[(NH_2)_2CH]_2(NH_3)FeO_2$ systems is best described as a singlet dioxygen ($^1\Delta_g$) σ donating to and π accepting from a Fe^{2+}. The calculations also predicted a low-lying triplet state for the FeO_2 unit, but not low enough in energy to explain the paramagnetism of hemoglobin. A singlet ground state of Fe^{2+}–O_2^0 structure having, in addition, some Fe^{3+}–O_2^- character, has been found by Rohmer [347] for oxyferroporphyrin on the basis of ab initio HF-CI calculations. It is important that the lowest SCF energy for $PFeO_2$ corresponds to a triplet $^3A'$ with the formal configuration $(xy)^2(xz)^2(yz)^2(\pi_g^a)^2(\pi_g^b)^1$, whereas the lowest CI energy corresponds to an open shell singlet state b^1A' with the formal configuration $(xy)^2(xz)^2(yz)^1$ $(\pi_g^a)^2(\pi_g^b)^1$. It is obvious, then, how important the CI is for an accurate description of the electronic structure and the relative energies of the ground and low-lying excited states in dioxygen systems [346–348].

RHF-CI and GMO-CI calculations performed on Co and Mn porphyrins have also been reported by Newton and Hall [346,348]. For the CoO_2 system, the ground state is best described as a superoxide complex, Co^{3+} $(S=0)$–$O_2^-(S=1/2)$, with the unpaired electron in a nearly pure π_g O_2 orbital

[346]. For the MnO_2 system, the most likely ground state structure was found to be the side-on Griffith geometry with three unpaired electrons in orbitals that are primarily Mn *3d* in character. However, an end-on Pauling ground state with three unpaired electrons in metal orbitals, consistent with ESR and IR, could not be eliminated as a possibility according to the calculations.

SCF-MS-Xα molecular orbital calculations have been carried out on the $M(PH_3)_4(O_2)^+$ (M = Co, Rh, Ir) systems [349] as well as on the high symmetry (D_{2d}) $Cr(O_2)_4^{3-}$, $Mo(O_2)_4^{2-}$ and $Nb(O_2)_4^{3-}$ systems [350]. The considerable involvement of the peroxide σ_g MOs in the covalent interaction with Mo *4d* AOs results in a lower O_2^- charge, thus providing unique catalytic properties to Mo(IV) dioxygen complexes in olefin epoxidation. For all $M(PH_3)_4(O_2)^+$ systems studied by Norman and Ryan [349], the $\pi_g(\perp)$ MO, being essentially non-bonding, was found to be the HOMO, whereas the π_u MO has a negligible effect on the bonding.

More recently, Ziegler [351], using the HFS method, calculated the electronic structure and bonding energies in the $M(PH_3)_2(O_2)$ (M = Ni, Pd, Pt) and $M(PH_3)_4(O_2)^+$ (M = Co, RH, Ir) systems. The calculations indicated that both systems, in agreement with previous findings, can be formulated as superoxo complexes. Moreover, it was found that the back donation, $M \rightarrow O_2$, is more important for the stability of these complexes than the donation $M \leftarrow O_2$. It has also been demonstrated that the $M(PH_3)_4$ fragments are less prone to form π complexes than the $M(PH_3)_2$ fragments because a substantial energy is required to deform the pseudo-square planar conformation of $M(PH_3)_4$ in the free state to the butterfly geometry adopted in the $M(PH_3)_4(O_2)^+$ complexes. For metals of the same transition series, the bonding energy in $M(PH_3)_2(O_2)$ was calculated to be about 21 kcal mol^{-1} larger than in $M(PH_3)_4(O_2)^+$. In addition, the calculated bonding energies within a triad follow the stability order $3d > 5d > 4d$.

The reaction of $(PH_3)_2PtO_2$ with SO_2 to form a sulphate complex has been studied by structure and energy surface calculations using the atom superposition and electron delocalization MO theory [352]. It was found that sulphate formation proceeds most readily through a five-atom cyclic intermediate, involving the coordination of SO_2 with one O atom of the complex followed by M–O bond breaking and reorientation, which further rearranges to form the bidentate coordinated sulphate (Fig. 17).

The computational simulation of the mechanism of action of superoxide dismutase [353,354] has suggested that the enzyme does not undergo a sequential reduction and oxidation by superoxide, but follows the catalytic pathway:

$$Cu^{2+} + O_2^- \overset{O_2^-}{\rightleftharpoons} Cu^+ - O_2^- \overset{2H^+}{\rightleftharpoons} Cu^{2+} + H_2O_2 \overset{O_2^-}{\rightleftharpoons} Cu^{2+} - O^{2-} \qquad (33)$$

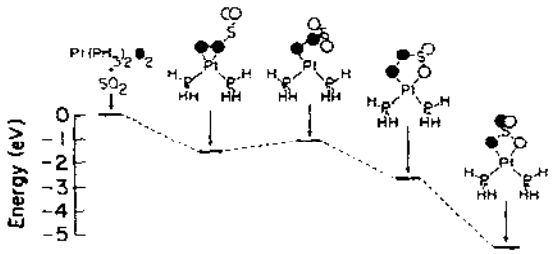

Fig. 17. Relative energies of the various species involved in the ultimate formation of coordinated sulphate. Reproduced with permission from ref. 352.

Osman and Basch [353] have calculated the energetics of the Cu^{2+}—O_2^- interaction and indicated that the presence of Arg-141 is responsible for a change in the redox chemistry of superoxide. Similarly, Rosi et al. [354] performed ab initio calculations on the Cu^{2+}—O_2^- system, considering the effects of an ammonia ligand on Cu^{2+} and of an NH_4^+ interacting with superoxide. They provided increasing evidence that hydrogen bonding between Arg-141 and a coordinated superoxide anion prevents electron transfer to Cu^{2+}, thus altering drastically the commonly accepted picture for the superoxide dismutation mechanism. The calculations show that an intermediate Cu^{2+}—O_2^- is stable as long as superoxide is hydrogen bonded to the ammonium ion.

Finally, Nappa and McKinney [355] have very recently investigated the selectivity control by axial ligands in manganese porphyrin-catalysed hydrocarbon oxidations. They found that varying the axial ligands results in marked changes on product distribution. Thus, reducing the donor ability of the axial ligand reduces the oxy radical character of the oxomanganese intermediate, $[PMn(V)O]^+X$, which results in a shift from stepwise to more concerted processes for O transfer. Moreover, reducing the donor ability of the axial ligand also increases the oxidizing power of the catalyst.

The dioxygen activation processes discussed above are only a few recent representative examples among the many others which have been extensively reviewed by Bŏca [321].

(iv) Transition metal carbonyls. Carbon monoxide activation and reactivity

(a) The nature and energetics of the M−CO bond

The chemical bond between a transition metal atom and a carbonyl ligand plays an important role as a model to study the chemisorption on the metal surface in many heterogeneously catalysed processes. Absorption of C–O on metal surfaces, especially Ni and Cu, has been investigated both experimentally [356,357] and theoretically [266,276,289,358–369]. In particular, nickel

carbonyls have become standard test molecules for theoretical chemists in this area.

The calculated BDEs of various electronic states of some MCO and MCO^+ systems studied so far have been collected in Table 12.

The interaction energy is greatly affected by electron correlation effects, which must be considered even at the zeroth-order level to obtain reasonable bonding and potential energy curves for metal carbonyls. Blomberg et al. [366] showed that correlating the electrons on CO has a large effect on the binding energy of NiCO, which increases from 16 to 33 kcal mol^{-1}. The difference in BDE with and without CO correlation is 17 kcal mol^{-1}, which is about half of the total BDE.

The binding mechanism of CO to transition metals has often been approached within the framework of the traditional Dewar–Chatt–Duncanson (DCD) scheme [370,371], which involves ligand-to-metal σ donation with concomitant metal-to-ligand $d\pi$ back-donation. The coupling of the σ donor/π acceptor character allows a synergism which can increase the M–CO bond strength substantially. Although early ab initio descriptions supported this model [372], more recent calculations suggest a modified version of the traditional view [361,362,365–369].

In a series of ab initio calculations, Bauschlicher and coworkers [360,362,365], using the CSOV method, discussed the bonding in MCO systems in terms of σ repulsion between the metal ns and the CO 5σ CO-to-metal σ donation when there is an empty or partly occupied d_σ orbital and metal-to-CO $2\pi^*$ back donation. In all cases studied, it was found that the metal-to-CO π back donation is more important than the donation of CO σ electron density to the metal when the $3d_\sigma$ and $4s$ shells are filled.

Blomberg et al. [266] applied a VB description of the MCO bonding, involving two configurations which emanate from ground and excited states of CO, the population of the latter being a direct measure of the M–CO covalent character.

The binding mechanism is totally different in MCO^+ and in MCO systems [364,366,369]. In MCO^+ systems, the fundamental binding component is electrostatic in nature with no more than 10% σ L→M donation and practically no M→L d_π back donation. This is consistent with both the M–C bond lengths being large in MCO^+ relative to similar MCO species and BDEs depending only on the bond length and the attractive component of the $M–CO^+$ potential curves.

Harrison and coworkers [364] explained the different bonding mechanism in MCO and MCO^+ systems on the basis of the synergistic view of the σ/d_π bonding. When one of the two components of the bonding cannot take place, the effect of the other is also greatly diminished. For the MCO^+ systems, the d_π metal back donation does not occur, mainly for energetic

TABLE 12

Calculated BDEs (in kcal mol^{-1}) for some transition metal MCO and MCO^+ systems with various electronic states

Compound	State	D_e(M–CO)	Computational method	Ref.
ScCO	$^4\Sigma^-$	26.3	MRD-CI	276
	$^4\Pi$	26.0	MRD-CI	276
$ScCO^+$	$^3\Sigma^-$	13.5	MCSCF + 1 + 2-CI	364
	$^3\Pi$	7.3	MCSCF + 1 + 2-CI	364
	$^3\Delta$	10.2	MCSCF + 1 + 2-CI	364
$TiCO^+$	$^4\Sigma^-$	8.9	MCSCF + 1 + 2-CI	364
VCO^+	$^5\Delta$	11.4	MCSCF + 1 + 2-CI	364
$CrCO^+$	$^6\Sigma^+$	13.9	MCSCF + 1 + 2-CI	364
	$^4\Pi$	21.5	MCSCF + 1 + 2-CI	364
FeCO	$^5\Sigma^-$	22.6	CASSCF	365
	$^3\Sigma^-$	28.6	CASSCF	365
	$^3\Delta$	18.2	CASSCF	365
NiCO	$^1\Sigma^+$	25.6	CASSCF	365
		30.0	SCF	289
		93.4	MP2	289
		33.0	CASSCF-CCI	366
		40.0	CASSCF-CCI	266
		29.9	CASSCF-CCI	361
		34.6	HF	367
		62.3	CI	367
	$^3\Sigma^+$	−5.3	CASSCF	365
	$^3\Delta$	−5.5	CASSCF	365
		−2.1	CASSCF-CCI	361
		−2.3	CI	367
$NiCO^+$	$^2\Sigma^+$	26.0	CASSCF	366
$NiCO^-$		20.0	CASSCF	366
PdCO	$^1\Sigma^+$	13.1	SCF	289
		37.4	MP2	289
PtCO	$^1\Sigma^+$	19.8	SCF	289
		44.5	MP2	289
		45.9	RECP-MCSCF	368
		70.3	RECP-CI	368
	$^3\Sigma^+$	8.8	RECP-MCSCF	368
		19.4	RECP-CI	368
	$^3\Delta$	6.9	RECP	368
		18.2	RECP-CI	368
CuCO	$^2\Sigma^+$	−8.3	CASSCF	365
		Unbound	MO-CI	369
		−12.7		360
$CuCO^+$	$^1\Sigma^+$		MO-CI	369

reasons. The gain in energy due to covalent binding, if charge is transferred from M^+ to CO, cannot compensate for the cost of that transfer and therefore the electrostatic interaction dominates. Moreover, Allison et al. [372], using this information on the MCO^+ systems, evaluated gas phase data of a variety of bare and ligated first row transition metal ions. According to the authors, in MCO^+ systems the CO ligand would not modify the electronic structure of the M^+ ion and therefore, to the extent that the chemistry of the ion is determined by its electronic configuration, one would anticipate similar chemistry for M^+ and MCO^+, consistent with the electrostatic bonding scheme in MCO^+ systems.

Finally, in the MOVB language, the bonding mechanism in MCO and MCO^+ systems is described as overlap dispersion [85,86,235], which can be expressed by the VB structures:

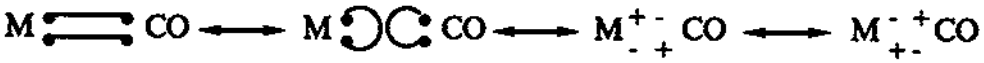

(34)

A plethora of computational results on MCO and MCO^+ systems are in support of the overlap dispersion mechanism of bonding. Moreover, relationships between M–CO bond strengths in $M(CO)_n$ systems [373] and the ground state $s^2d^n \rightarrow$excited d^{n+2} promotion energy have been established. These correlations suggest that the electron pair (or the odd electron) has to be taken off the *ns* AO, which can overlap with a totally symmetric doubly occupied ligand MO, and 'hidden' in an $(n-1)d$ AO which, being contracted relative to *ns* AO, cannot form an antibond with the ligand MO. Accordingly, the $(n-1)d$ AOs are the repository of the original *ns* electron pair at the expense of promotion energy.

(b) Electronic and molecular properties of saturated mononuclear transition metal carbonyls

The electronic structure of coordinatively saturated mononuclear transition metal carbonyls is prominent [46,52,128,290,374–390]. After some controversy [374], it now seems well-established [46,375–377] that π-back donation is more pronounced in the M–CO bond than σ-donation. For example, in $Cr(CO)_6$ it was found that the former is about twice as strong as the latter [46]. In addition, LCAO-Xα computations revealed a synergic effect of 173 kcal mol^{-1}, of the same order of magnitude as the individual σ- and π-bonds in the complex.

Rohlfing and Hay [289,378], found that the π back-bonding portion of the interaction is underestimated at the SCF level. However, second-order Möller-Plesset perturbation theory (MP2), including electron correlation effects, produces geometries and binding energies for MCO and $M(CO)_4$

(M = Ni, Pd, Pt) species which are in agreement with experiment. In general, correlation shortens r(M–C), lengthens r(C–O) and increases D_e(M–CO). The predicted relative stability based on M–CO BDEs obtained by both SCF and MP2 calculations was found to be in the order Ni > Pt > Pd, as observed experimentally.

Near degeneracy correlation effects have also been shown to be mainly responsible for the failure of the HF model to reproduce correctly the M–CO bond lengths in $Fe(CO)_5$ [379]. Previous studies by Demuynck et al. [380] showed that, at the SCF level, the axial Fe–CO distance is overestimated by 0.17 Å, whereas their equatorial bond distance agrees with experiment. Large CCI calculations are needed to reconcile theory and experiment. The difference between the axial and equatorial bond lengths at the SCF level was attributed to the different correlation effects for the axially and equatorially coordinated ligands. One effect is the increase of correlation due to the penetration of the axial carbon σ lone pair into the metal d shell, which results in an increase of the strength of the π bond. The latter is particularly important for the axial ligands, where the lone pair penetrates into a formally empty d AO.

LCGTO-Xα calculations performed on $Ni(CO)_4$ and $Fe(CO)_5$ by Rösch et al. [52,381] indicated the capability of the method to give results better than those of HF calculations, almost reaching the quality of CI studies. This is clearly shown from the comparison of the M–CO bond lengths calculated by different methods: $Ni(CO)_4$ ($d_{Ni-C} = 1.805$, 1.884 and 1.921 Å from LCGTO-Xα, CI and HF calculations, respectively, with the experimental value being 1.825 Å). For $Fe(CO)_5$, these values are $d^{ax}_{Fe-C} = 1.774$, 1.798 and 2.047 Å and $d^{eq}_{Fe-C} = 1.798$, 1.836 and 1.874 Å; the experimental ones are 1.807 and 1.827 Å for axial and equatorial Fe–C bonds, respectively. The deviations are significantly smaller than those encountered in HF calculations. However, the local density approximation overestimates the metal-to-carbon bond strength (D_0(Ni–CO) = 197.6 kcal mol^{-1}; exptl. 141.1 kcal mol^{-1} [382]; D_0(Fe–CO) = 231.5 kcal mol^{-1}; exptl. 140.7 kcal mol^{-1} [382]).

In spite of many investigations of the electronic and molecular structure energies have been reported in the literature [46,52,377–379,381,383–386]. The results have been collected in Table 13. It is clear that the calculated values for the mean bond energy, D(M–CO) of $M(CO)_n$ between M in the d^n valence configuration and n CO ligands, reveal the order $4d < 5d < 3d$ for a series of homologous $M(CO)_n$ systems with metal centres from the same triad. Ziegler et al. [385] have also calculated the first CO ligand dissociation energy, ΔH, of $M(CO)_n$ and found the values: $\Delta H_{Cr} = 35.1$, $\Delta H_{Mo} = 28.4$ and $\Delta H_W = 33.9$, for $M(CO)_6$, $\Delta H_{Fe} = 44.2$, $\Delta H_{Ru} = 22.0$ and $\Delta H_{Os} = 23.7$ for $M(CO)_5$ and $\Delta H_{Ni} = 25.3$, $\Delta H_{Pd} = 6.5$ and $\Delta H_{Pt} = 9.1$ kcal mol^{-1} for $M(CO)_4$.

TABLE 13

Calculated mean bond energies (in kcal mol^{-1}) of $M(CO)_n$ compounds

Compound	D(M–CO)	Computational method	Ref.
$Ni(CO)_4$	17.9 (45.6)[a]	SCF	290,378
	55.6	MP2	290,378
	−11.3	HF	377
	49.4	LCGTO-Xα	52,381
	42.8	HFS	385
$Pd(CO)_4$	9.5	SCF	290,378
	28.7	MP2	290,378
	10.5	HFS	385
$Pt(CO)_4$	12.8	SCF	290,378
	33.5	MP2	290,378
	14.1	HFS	385
$Fe(CO)_5$	−10.9 (41.5; 55.0±12)	HF	377
	46.3	LCGTO-Xα	52
	51.6	HFS	385
	42.8	SCF-CI	384
	47.0	MINDO/SR	386
$Ru(CO)_5$	39.0	HFS	385
$Os(CO)_5$	42.3	HFS	385
$Cr(CO)_6$	34.9 (36.8)	LCAO-Xα	46
	33.5	HF-CI	46
	50.4	HFS	385
$V(CO)_6^-$	71.0	HFS	385
$Mn(CO)_6^+$	32.3	HFS	385
$Mo(CO)_6$	42.5 (40.5)	HFS	385
$W(CO)_6$	50.2 (46.0)	HFS	385

[a] Figures in parentheses are experimental data taken from refs. 387 and 388.

Upon separation of ΔH and D(M–CO) into contributions from steric factors, σ-donation, π-back donation and relativistic effects, it was found that the repulsive (steric) 4e-2O interactions between occupied metal orbitals and the σ lone pair of CO considerably destabilize the M–CO bonds in carbonyls (particularly $M(CO)_4$ and $M(CO)_5$) of $4d$ and $5d$ transition metals. This destabilization, in conjunction with a stronger π-back donation in carbonyls of $3d$ metals, is responsible for the calculated order $3d > 4d > 5d$ for the M–CO bond strength in the non-relativistic limit. However, relativistic effects, through the so-called mass–velocity term, reduce the electronic kinetic energy and therefore stabilize M–CO bonding much more for carbonyls of $5d$ metals than for their $4d$ analogues. This is why the inclusion of relativistic effects changes the order to $3d > 5d > 4d$.

Ziegler [126,128] has also proposed the use of the electronic contributions of particular symmetries to the protonation energy of metal carbonyls as a

good measure of their nucleophilicity. Thus, for the metal carbonyls, $M(CO)_5^-$ (M = Mn, Tc, Re), $M(CO)_5$ (M = Fe, Ru, Os), $Cr(CO)_5^{2-}$, $Co(CO)_5^+$, $M(CO)_4$ (M = Ni, Pd, Pt), $M(CO)_4^-$ (M = Co, Rh, Ir), $Fe(CO)_4^{2-}$, $Cu(CO)_4^+$ and $Co(CO)_3(PH_3)^-$, the ΔE_{A_1} term corresponding to the donor–acceptor interactions between the metal carbonyls and the hydrogen atom quantifies their nucleophilicity. According to the values of the ΔE_{A_1} term, the nucleophilicity decreases along a transition series with increasing nuclear charge on the metal and increases vertically down a triad.

(c) Isomerization processes in metal carbonyls

Very few theoretical studies deal with the relative stability of geometrical isomers in transition metal carbonyls [380,386,389,390]. After the first fastidious work on transition metal pentacoordination and metal carbonyls undertaken by Hoffmann and his collaborators [391,392], LCAO-SCF-MO were used by Demuynck et al. [380] to address the intramolecular rearrangement problem in five-coordinate complexes. Assuming a Berry pseudorotation mechanism for the intramolecular rearrangements in a series of five-coordinate complexes, including the metal carbonyls $M(CO)_5$ (M = V, Cr, Mn and Fe), $Mn(CO)_5^-$, $Co(CO)_5^+$, $Co(CO)_4CH_3$ and $Co(CO)_4C_2H_4$, Demuynck and his collaborators calculated the relative stabilities of the trigonal bipyramidal (TB) and square pyramidal (SP) geometries along the isomerization pathway. For $V(CO)_5$, $Cr(CO)_5$ and $Mn(CO)_5$, the SP structure is predicted to be more stable than the TB structure. In general, the preferred conformation of the metal carbonyls was found to be dependent on the number of *d* electrons of the central atom: it changes from SP for the d^5–d^7 systems (V, Cr, Mn) to TB for the d^8 systems ($Fe(CO)_5$, $Mn(CO)_5^-$ and $Co(CO)_5^+$). These results are in agreement with those of Elian and Hoffmann [392] and experiment. The barrier to intramolecular exchange is predicted to increase when increasing the positive charge on the central metal (0.6 and 3.8 kcal mol^{-1} for $Fe(CO)_5$ and $Co(CO)_5^+$, respectively) and substituting a CO ligand either by CH_3 or C_2H_4. In the latter case, a concerted process involving the coupling of the olefin rotation with Berry pseudorotation provides a satisfactory account of the barriers reported for the $Fe(CO)_4$(olefin) complexes (~11–15 kcal mol^{-1}).

More recently, Blyholder and Springs [386] have carried out MINDO-type MO calculations for $Fe(CO)_5$ in TB and SP configurations as well as at points along the intervening Berry pseudorotation. They found that the corresponding potential energy curve does not contain a barrier (Fig. 18), so the activation energy for ligand exchange between axial and equatorial positions is just the difference in energy between the TB and SP geometries. This difference is calculated to be 2.0 kcal mol^{-1}, in agreement with the estimate of 1 kcal mol^{-1} from NMR data. In addition, they have found that the metal *d* orbitals mix with the lower lying orbitals in $Fe(CO)_5$, thus affecting the

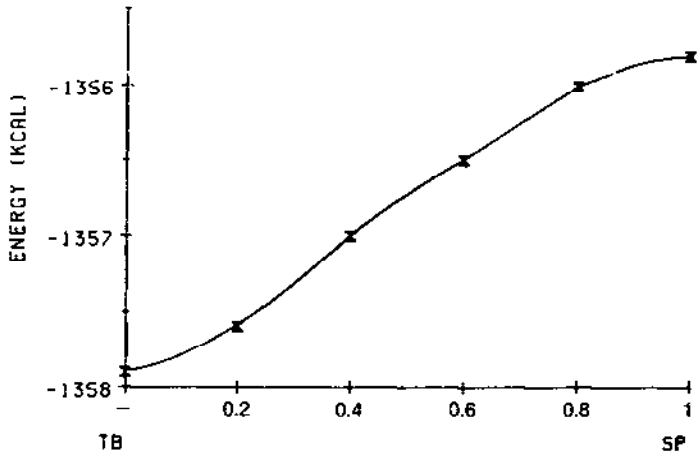

Fig. 18. Potential energy along the Berry pseudorotation path from TB to SP structure. Reproduced with permission from ref. 386.

relative axial vs. equatorial bonding which is critical to obtain axial Fe–CO bond lengths in agreement with experiment.

The only theoretical studies of *cis–trans* isomerization in substituted octahedral transition metal carbonyls are those reported by Marynick et al. [389] and by Daniel and Veillard [390].

Marynick and his collaborators used PRDDO to calculate the relative energies and optimized geometries for a series of complexes of general formulae $M(NH_3)_4(CO)_2$ and $M(NH_3)_2(CO)_4$, $M = Cr^0$, Mn^+, Fe^{2+} and Co^{3+}. The calculated isomerization energies, $\Delta E = E_{cis} - E_{trans}$, have been found to be: -13.4, -6.1, $+1.0$ and $+1.3$ kcal mol^{-1} for Cr^0, Mn^+, Fe^{2+} and Co^{3+} $M(NH_3)_4(CO)_2$ complexes, respectively, and -6.3, -1.5, -0.1 and $+1.0$ kcal mol^{-1} for the corresponding $M(NH_3)_2(CO)_4$ complexes. Similar calculations on $Cr(CO)_2(N_2)_4$ and $Cr(CO)_4(N_2)_2$ also predict the *cis* isomers to be favoured energetically by 2.2 and 1.6 kcal mol^{-1}, respectively, pursuant to available experimental evidence. For $Cr(CO)_4(PH_3)_2$ and $Cr(CO)_2(PH_3)_4$ complexes, the *cis–trans* isomerization energy was found to be close to zero. The dramatic change in isomerization energy upon the substitution of NH_3 with PH_3 was attributed to the π-acceptor capacity of PH_3 with the acceptor orbital being best ascribed as P–H σ^* [393].

Daniel and Veillard [390] have reinvestigated the above problem by carrying out ab initio SCF and CASSCF calculations for the systems $M(CO)_4L_2$ ($M = Cr$, Mo and $L = NH_3$, PH_3, C_2H_4) and $M(CO)_4LL'$ ($M = Mo$, $L = C_2H_4$ and $L' = CH_2$). The results obtained have been summarized as follows: (i) for $M(CO)_4L_2$ with $L = NH_3$, PH_3, the *cis* isomer is more stable than the *trans*; (ii) for $M(CO)_4L_2$ with $L = C_2H_4$ or $M(CO)_4LL'$, the *trans* isomer is the more

stable; (iii) going from Cr to Mo increases the stability of the *cis* isomer for $L = NH_3$, PH_3, but decreases it for $L = C_2H_4$. It should be noted that knowing the relative stabilities of the geometrical isomers is of crucial importance in understanding the high stereospecificity of many photodissociation and photosubstitution reactions of transition metal carbonyls.

(d) Photodissociation and photosubstitution reactions of transition metal carbonyls

Transition metal carbonyls have gained increasing importance in laser chemistry as a source of metal atoms or reactive precursors for chemical vapour deposition of thin films or layers on surfaces [394,395]. The photochemical loss of a carbonyl ligand is a global reaction for metal carbonyls. The reaction is known for the following unsubstituted metal carbonyls:

$$M(CO)_6 \xrightarrow{h\nu} M(CO)_5 + CO \qquad (M = Cr, Mo, W) \tag{35}$$

$$[M(CO)_6]^- \xrightarrow{h\nu} [M(CO)_5]^- + CO \qquad (M = V, Nb, Ta) \tag{36}$$

$$Fe(CO)_5 \xrightarrow{h\nu} Fe(CO)_4 + CO \tag{37}$$

$$Ni(CO)_4 \xrightarrow{h\nu} Ni(CO)_3 + CO \tag{38}$$

The details of the mechanism of reaction (35) have been worked out by Hay [396] and mostly by Burdett et al. [397]. Hay pointed out that photodissociation of $Cr(CO)_6$ should yield $Cr(CO)_5$ initially in an excited state, since the $^1A_{1g}$ ground state of $Cr(CO)_6$ correlates with its $^1A_1$ counterpart of $Cr(CO)_5$. Therefore, the potential energy surface of the electronically excited hexacarbonyl must correlate with electronically excited pentacarbonyl. Hay assumed that photodissociation occurs within the singlet manifold and that the excited pentacarbonyl is in the lowest excited state, ^1E for SP and $^1E'$ for TB configurations. Burdett et al. assumed that the photoactive excited state of $M(CO)_6$ is the $^1T_{2g}$ state and analyzed in detail the pathways interconnecting the $^1A_1$ ground state and the ^1E for the SP as well as the $^1E'$ for the TB configurations of $M(CO)_5$. Daniel et al. [384] have also studied the state correlation diagram connecting $M(CO)_6$ to $M(CO)_5$ in its SP configuration corresponding to the least motion path for the CO ligand dissociation using ab initio CI calculations, reaching the conclusion of Burdett.

The photodissociation of $Fe(CO)_5$ (reaction (37)) has been studied by Daniel et al. [384] by ab initio calculations of the potential energy surfaces for the dissociation of an equatorial ligand under C_{2v} constraint. It was found that a triplet potential energy surface connects, without any barrier, the LF state $^3E'$ of $Fe(CO)_5$ to the ground state $^3B_2$ of the products $Fe(CO)_4 + CO$. It was also proposed that the photodissociation occurs through excitation to a singlet state followed by population of the $^3E'$ state via intersystem

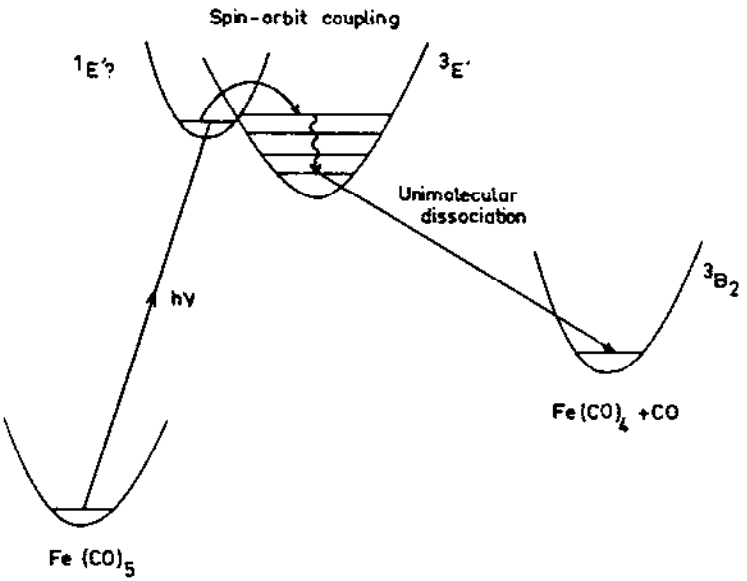

Fig. 19. Proposed mechanism for the photochemical dissociation of $Fe(CO)_5$. Reproduced with permission from ref. 384.

crossing and subsequent dissociation to the products of the reaction along the $^3B_2$ potential energy surface. This mechanism for the photodissociation of $Fe(CO)_5$ is depicted schematically in Fig. 19. The photodissociation process was found to be endothermic (43 kcal mol^{-1}), whereas the reverse reaction was found to be spin-forbidden in the absence of spin-orbit coupling, but becomes allowed with a very low barrier when spin-orbit coupling is introduced. It should be noted that the lowest LF excited state $^3E'$ correlating with the ground state of the products, appears independently of the assumption on the nature of the dissociating ligand (axial or equatorial) and on the symmetry retained along the reaction path (C_{2v} or C_s for an equatorial departure, C_{3v} or C_s for an axial one).

The photodissociation of $Ni(CO)_4$ represents another case where the products should be initially in an excited state and the following mechanism has been proposed [381,398]:

$$Ni(CO)_4 \xrightarrow{h\nu} Ni(CO)_4^* \xrightarrow{-CO} Ni(CO)_3^* \rightarrow Ni(CO)_3 + h\tilde{\nu} \qquad (39)$$

LCGTO-Xα calculations performed by Rösch et al. [381] on $Ni(CO)_4$ and its photofragments indicated that the LUMO ($13a_1$ MO) of $Ni(CO)_3$ plays the key role in photodissociation process. Moreover, the origin of the observed luminescence was assigned to emission from the charge transfer excited fragment $Ni(CO)_3^*$. Actually, more recently, Rösch and coworkers [399] analyzing the near-UV gas phase spectra of $Cr(CO)_6$, $Fe(CO)_5$ and $Ni(CO)_4$

by INDO/S CI have found that the optical spectra are determined exclusively by M-to-L charge transfer transitions, whereas $d \rightarrow p$ and $d \rightarrow s$ excitations do not contribute significantly, above 200 nm. Moreover, the lowest lying excitations in $Cr(CO)_6$ and $Fe(CO)_5$ are predicted to be of the $d \rightarrow d$ type, while such excitations are not available for $Ni(CO)_4$. Therefore, this might be the reason for the luminescence accompanying the photodissociation of $Ni(CO)_4$, being absent in the analogous processes in $Cr(CO)_6$ and $Fe(CO)_5$.

The mechanism of the photosubstitution of d^6 metal carbonyls

$$M(CO)_5L + L' \xrightarrow{h\nu} M(CO)_4LL' + CO \tag{40}$$

has been investigated by Daniel and Veillard [400] through ab initio CI calculations, correlation diagrams and potential energy curves. For the substitution of the axial carbonyl in $M(CO)_5L$ by an incident nucleophile L', the proposed mechanism involves: (i) excitation of $M(CO)_5L$ into the ^1E LF state followed by elimination of a carbonyl to form the $M(CO)_4L$ species of SP configuration with L apical in the ^1E state; (ii) a Berry pseudorotation path of SP $M(CO)_4L$ first to a TB in the $^1B_2$ state and then to a SP with L basal in the $^1A'$ excited state; (iii) an internal conversion of the $^1A'$ excited state of the SP configuration with L basal to its $^1A'$ ground state, which will react with the incident nucleophile L' to afford *cis*-$M(CO)_4LL'$. For an equatorial CO ligand substitution, the mechanism is similar to that of the axial CO elimination but without any rearrangement of the $M(CO)_4L$ species. Despite its simplicity, the proposed mechanism accounts for the high stereospecificity of the photosubstitution reactions of d^6 metal carbonyls with a variety of ligands.

(e) Nucleophilic substitution and addition reactions of transition metal carbonyls

Transition metal carbonyls reacting with nucleophiles, Nu, could afford either substitution of CO by the nucleophile, or addition of the nucleophile to CO, according to the chemical equations:

$$L_nM(CO) + Nu \rightarrow L_nMNu + CO \tag{41}$$

$$L_nM(CO) + Nu \rightarrow L_nM(CNu{=}O) \tag{42}$$

The reactivity of transition metal carbonyls in nucleophilic substitution reactions (eqn. (41)) has been investigated by Brown et al. [401] within the framework of perturbation theory. They have calculated the interaction energy, ΔE, for a series of metal carbonyls formulated as $\underline{M}(CO)_3$ ($\underline{M} = C_6H_6Cr$, C_5H_5Mn, C_4H_4Fe or C_3H_3Co) and $[LFe(CO)_3]^+$ ($L = C_5H_5$, C_6H_7 or C_7H_9) with a wide range of nucleophiles (both hard and soft) in polar and non-polar solvents. The ΔE values have been used to compare the ease of attack at (a) the central metal atom, (b) a carbonyl carbon atom and (c) an averaged

ring carbon atom. For polar solvents, the predicted site of attack by a hard nucleophile on $C_6H_6Cr(CO)_3$ and $C_5H_5Mn(CO)_3$, as indicated by the magnitude of ΔE, is metal > carbonyl > ring and the reverse for attack by a soft nucleophile. The order changes as we move from the Cr to Co complex to carbonyl > metal > ring with, again, the reverse for attack by a soft nucleophile. In the cationic species, attack by a hard nucleophile may occur at either metal or carbonyl, while for a soft nucleophile, initial metal attack is predicted with a crossover to ring attack as solvent polarity increases.

The nucleophilic addition to the carbonyl ligand (eqn. (42)) has been thoroughly investigated through ab initio LCAO-SCF-MO calculations by Dedieu and Nakamura [402,403]. The reaction

$$H^- + Fe(CO)_5 \rightarrow Fe(CO)_4(CHO)^-$$

has been used as a prototype, but comparative calculations on the reactions

$$H^- + M(CO)_4 \rightarrow M(CO)_3(CHO)^- \qquad (M = Fe \text{ or } Ni)$$

have also been carried out. The most important conclusions are: (i) in the early stages of the reaction, the direction of attack, being electrostatically controlled, is almost equidistant from the axial and equatorial ligands, (ii) the last stage is characterized by a bending of the attacked carbonyl ligand and is orbitally controlled. Of key importance for the energetics and the stereochemical course of the reaction is the existence of a low-lying empty metal orbital (here d_{z^2}) pointing towards the attacked carbonyl ligand (the axial ligand is slightly preferred). The mixing of this orbital with the π^* MO of CO and the s AO of H^- stabilizes the bonding combination $\pi^*_{CO} + s_{H^-}$ and (iii) the reactions have been found to be highly exothermic. Thus, for the nucleophiles, H^-, OH^- and CH_3^- the exothermicities are 69.2, 71.3 and 78.3 kcal mol^{-1}, respectively. On the other hand, the nucleophilic addition to $Ru(CO)_5$ is found to be more exothermic by about 7 kcal mol^{-1}, in line with the lower energy of the empty d_{z^2} orbital in $Ru(CO)_5$ than in $Fe(CO)_5$.

(f) The nature of carbonyl insertion reaction of transition metal compounds

Carbonyl insertion processes into M–R bonds (M = H, alkyl) are key steps in many homogeneous catalytic transformations, such as the oxo reaction, Reppe reaction and various related reactions. Therefore, many experimental studies have been carried out for the better understanding of this important reaction [405].

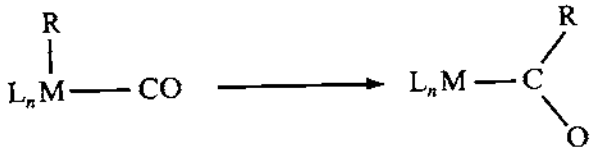

(43)

One of the most interesting points concerning the course of this crucial process is whether R migrates to the CO ligand or the CO ligand migrates to insert into the M–R bond. Besides the many elegant experimental studies on this problem, a few theoretical studies based on semiempirical and ab initio methods have also been reported in the last few years [128,403,406–416].

The first theoretical investigation of organometallic migration reactions was undertaken by Berke and Hoffmann [406] within the framework of EHMO theory. They studied the reaction path for the methyl migration reaction in $CH_3Mn(CO)_5$ and extended the analysis to the more general case of organometallic migration reactions. The reaction path involves a five-coordinate intermediate and a transition state close in energy to the intermediate. The calculated energy barrier for the H^- shift is relatively low, actually smaller than that for the CH_3^- migration. In general, a poorer σ donor migrating group raises the activation energy, while a better σ donor lowers it (compare the activation barriers for Cl, CH_3, C_2H_5 and n-C_3H_7, being equal to 66, 19.6, 15.2 and 14.8 kcal mol^{-1}, respectively). Substitution of the carbonyl by NO^+ and PH_3 ligands has no significant effect on the migration reaction. Substitution of the Mn metal centre by Re changes the activation energies from 19.6 to 32.7 kcal mol^{-1}, indicating that the migration reaction should be more difficult as one proceeds down a group.

The apparent poor migratory aptitude of H^- towards CO compared with CH_3^- has been investigated by Ziegler et al. [128] using HFS calculations. They found that the intramolecular migration of R in $RMn(CO)_5$ is more endothermic for $R=H^-$ ($\Delta H=38$ kcal mol^{-1}) than for $R=CH_3^-$ (17.9 kcal mol^{-1}) owing to the different strength of the Mn–R bonds. Moreover, Ziegler et al. also found that analogous migrations to a metal-linked CS group are easier than to CO because of the lower energy of the π^* MO in CS than in CO ligand ($\Delta H=4.8$ and 16.7 kcal mol^{-1} for CH_3^- and H^- shifts in $RMn(CO)_4CS$, respectively). All migration reactions studied revealed activation barriers of less than 2 kcal mol^{-1}.

Dedieu and Nakamura [403,407] have studied the stereochemistry and the energy profile of the insertion step in $HMn(CO)_5$ with the use of ab initio SCF-CI calculations. It was shown that the insertion process is best described as a hydride migration toward the CO ligand and is characterized by a high energy barrier ($\sim$15 kcal mol^{-1} at the SCF level). The energy profile of the reaction was found to be strongly dependent upon the degree of electron correlation, especially of the non-dynamical type, included in the calculation. The stereochemical course of the hydride migration is governed by the orbital interactions occurring in the HOMO, which correspond to the bonding combination of the s AO of H^- and the π^* MO of CO somewhat destabilized by the 5σ MO of CO. The geometry of the transition state, being a late

transition state, is close to a five-coordinate formyl intermediate, but without adopting an η^2-coordination mode for the formyl group. Ziegler et al. [128] have found that the η^1-structure of the product formed in migration reactions, namely $RMn(CO)_4CX$, could be rearranged to the η^2-structure which was found to be more stable than the η^1-structure (~17 and 32 kcal mol^{-1} more stable for $RMn(CO)_5$ and $RMn(CO)_4CS$, respectively).

Besides the intramolecular migration reactions of octahedral d^6 metal complexes discussed so far, migrations are also known for complexes with other coordination geometries and electronic configurations. Among them, the migrations in square planar d^6 systems have been analyzed theoretically. Thus, Sakaki et al. [408] used an ab initio MO method to study the model reaction $Pt(CH_3)(F)(CO)(PH_3) \rightarrow Pt(COCH_3)(F)(PH_3)$. Three possible reaction paths were stimulated, namely one for methyl migration, one for carbonyl migration and one for the concerted migration of CO and CH_3 with simultaneous opening of the FPtP angle. From the energy change along the assumed paths, CH_3 migration proved the easiest and CO the most unfavourable. The factors determining the courses of reaction have also been explained. Of key importance was found to be the orbital mixing between Pt d_{xy}, $d_{x^2-y^2}$ and the lone-pair orbital of $COCH_3$ group. Assuming a 'transition state' located at the midpoint between the unoptimized transition states for CH_3 and CO migrations and using the orbital mixing concept to look for the favourable direction of F and PH_3 motion, Sakaki et al. found that F and PH_3 should move toward the direction where the Pt vacant d AOs point toward the CO lone pair, which led to CH_3 migration. Similar conclusions have also been found by Koga and Morokuma [409,410] who investigated the model carbonyl insertion reactions $M(CH_3)(H)(CO)(PH_3) \rightarrow M(H)(COCH_3)(PH_3)$, (where M = Pd and Pt), by means of the ab initio MO method with energy gradient. The transition state structures, **30** and **31**, obtained for both complexes indicated that the reaction path is methyl group migration through a three-centre transition state. Although the structural behaviour of the reactions of Pd and Pt complexes is almost identical, their energetics are quite different. The reaction is more endothermic and the activation barrier higher for the Pt complex. The calculated activation barriers were found to be 13.5 and 21.8 kcal mol^{-1} at the MP2 level for Pd and Pt complexes, respectively, whereas the endothermicities of the reactions were found to be 8.8 and 17.6 kcal mol^{-1}, respectively. These differences have been ascribed to the difference of M–CH_3, M–CO and M–$COCH_3$ bond strengths between Pd and Pt complexes. These bonds of the Pt complex are stronger by 7, 11 and 9 kcal mol^{-1}, respectively, than the corresponding ones in the Pd complex. Substitution in the methyl group influences its migration reaction energy profile. An electron-withdrawing fluorine atom makes the reaction unfavourable, whereas an electron-releasing methyl substitution gives the reverse effect.

Moreover, a stronger *trans* effect on the M–CH_3 bond makes it weaker, to give a lower activation barrier.

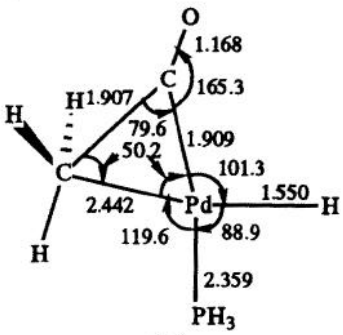

30

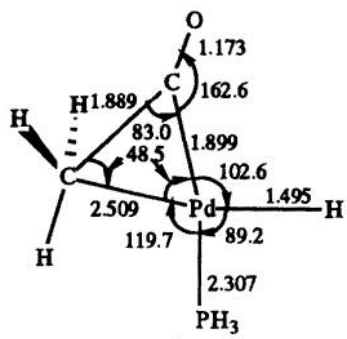

31

Very recently, Ziegler and coworkers [411] have studied by means of density functional theory the migratory insertion reaction $RCo(CO)_4 \rightarrow RC(O)Co(CO)_3$ for R = H and CH_3 as well as the CO dissociation of $HCo(CO)_4$, which are important steps in the cobalt-based catalytic cycle of the hydroformylation process. They have calculated structural and energetic parameters for reactants and intermediates of the catalytic cycle. Thus, both $RCo(CO)_4$ (R = H and CH_3) complexes were found to form two stable isomers of TB geometry. The C_{3v} structures with R in the axial position were found to be 15 and 10 kcal mol^{-1} lower in energy than the C_{2v} isomers with R in the basal position. The coordinatively unsaturated catalyst $HCo(CO)_3$ resulting from CO dissociation has as its most stable conformation a butterfly-shaped geometry with the hydride in an apical position. This configuration, being ideally suited for π-interactions with incoming olefins, can be reached directly by a dissociation of an equatorial CO ligand of $HCo(CO)_4$, with the Co–CO dissociation energy calculated to be 44.5 kcal mol^{-1}.

The migratory insertion of CO into the Co–CH_3 bond affording a coordinatively unsaturated acyl intermediate $CH_3C(O)Co(CO)_3$ has been investigated by a linear transit procedure [411]. Among the several stable isomers of the acyl intermediate, those with the acyl oxygen facing the vacant site are lowest in energy due to the formation of η^2 interactions. The migration of the CH_3 group to a *cis* carbonyl ligand of $CH_3Co(CO)_4$ was found to have a low activation barrier of only 2 kcal mol^{-1} and an endothermicity of no more than 17 kcal mol^{-1}. In contrast, the direct insertion of a CO ligand into the Co–CH_3 bond was disfavoured by a high activation barrier of 48 kcal mol^{-1}. The corresponding hydride migration process was found to be considerably more endothermic, an observation ascribed to the higher bond strength of Co–H compared with Co–CH_3, as well as to the absence of an η^2 interaction in the formyl intermediate. Moreover, an examination of the coordinatively saturated complex $RC(O)Co(CO)_4$ (R = H, CH_3) re-

vealed that the neutral formyl compound is thermodynamically unstable with respect to decarbonylation to the parent hydrido complex. The reaction was found to have an exothermicity of -16.5 kcal mol^{-1}, whereas the acyl complex was found to be stable with an endothermicity of 5 kcal mol^{-1} for the corresponding decarbonylation process from $CH_3(CO)Co(CO)_4$ to $CH_3Co(CO)_4$.

Antolovic and Davidson [412–414] have also studied the molecular geometry and electronic structure of several species of the hydroformylation reaction catalysed by cobalt complexes using ab initio HF and CI calculations. For all species investigated, several stable conformations were found, and the geometry, FMOs and the character of chemical bonds of these conformations were examined. For $(CO)_4CoH$ and $(CO)_3CoH$, all of the sterically plausible TB conformations of the closed-shell form correspond to distinct energy minima on the potential energy surfaces. The hydroformylation reaction energetics were found to depend considerably on the choice of the initial and terminal sites of the migrating hydrogen. Intermolecular electron correlations analogous to London dispersion forces were found to dominate the stabilization of the complexes. For example, at the experimental bond lengths of the $(CO)_4CoH$ they contribute approximately half of the total bond energy to each M–CO bond.

Carbonyl insertion processes into M–R bonds of biscyclopentadienyl complexes of Group 4 metals and actinides have been investigated theoretically by Hofmann and coworkers [415–417] within the framework of EHMO theory. These processes, being extremely facile, sometimes lead to isolable monoacyl complexes exhibiting some unusual structural features. They contain an η^2-bonded acyl group RCO with both carbon and oxygen bound to the metal centre, a fact which is in contrast to the η^1 coordination of RCO in octahedral d^6 metal alkyls discussed previously. Moreover, these alkyl complexes could exist in two different conformers, one with the C–O vector pointing away from the additional ligand X, the η^2-acyl O-outside conformer, **32**, and the other one with the opposite C–O orientation, the η^2-acyl O-inside conformer, **33**.

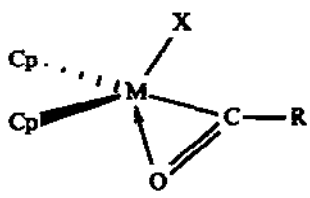

η^2 acyl O-outside

32

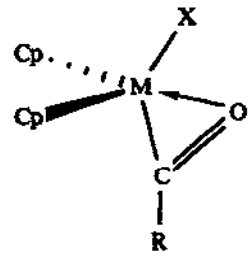

η^2 acyl O-inside

33

Hoffmann and coworkers addressed the basic question of central versus lateral attack of CO to Cp_2MR_2 complexes. To this end, they analyzed the initial stages of the CO insertion processes on two model molecules $Cp_2Zr(CH_3)_2$ and $Cp_2V(CH_3)_2^{2+}$ using EHMO calculations, from which the following message becomes evident: (i) the directionality of the LUMO of d^0 Cp_2MR_2 systems, shown in **34**, favours a lateral or outside approach of a CO over a central one. Such a regiospecific attack accounts well for the initial formation of conformers **32** with O-outside orientation of the acyl group in the course of CO insertion; (ii) conformers **32** cannot be isolated but rearrange spontaneously and irreversibly to the thermodynamically more stable conformers **33**. This preference for conformers **33** is clearly shown in the calculated potential energy surfaces for both O-inside and O-outside conformers and can be explained by considering the better overlap situation between the LUMO of the d^0-Cp_2MR fragment and the HOMO of the acyl ligand shown in **35**; (iii) there is an easy pathway for the interconversion of the η^2 O-outside structure which is the kinetic product of the CO insertion reaction to the thermodynamically more stable η^2 O-inside structure involving an η^1-acyl coordination and M–C single bond rotation. Such an η^1-acyl coordination is also evident as a minimum in the O-outside potential energy surfaces. The calculated activation energy for the isomerization process in $Cp_2Zn(COR)(R)$ compounds, found to be 13.5 kcal mol^{-1}, is in good agreement with experimental data, ranging from 11.4 to 15.6 kcal mol^{-1}.

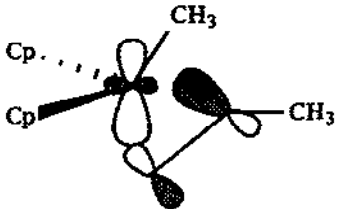

η^2 acyl O-outside

34

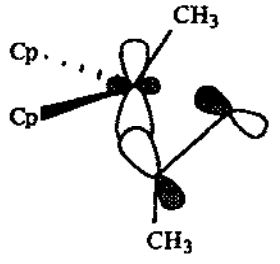

η^2 acyl O-inside

35

Finally, the stereoselectivity and the energy profile of the carbonylation reactions of $Ir[N(SiH_3)_2](PH_3)_2(H_2)$ and Cp_2ZrR_2 ($R=CH_3$, H and Cl), along with the electronic structure and bonding of reactants and products, have recently been studied by Zhu and Kostic [418] through the non-parametrized Fenske–Hall method. It was found that the stereoselectivity of the carbonylation processes is controlled by the composition and localization of the FMOs, which are markedly dependent upon the RZrR angle. Thus, the LUMO is localized laterally, **36**, when the angle is acute ($R=CH_3$) and

centrally, **37**, when it is obtuse (R = H). Therefore, the lateral attack at $Cp_2Zr(CH_3)_2$, experimentally verified, could be easily understood. The unreactivity of Cp_2ZrCl_2 has been attributed to the repulsion between the lone pairs of the Cl and CO ligands (steric effects). The lateral attack is also very favourable for the Ir complex, in line with the nature of its LUMO, shown in **38**.

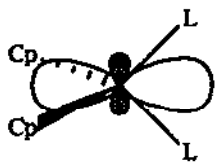

36

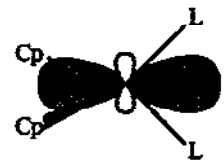

37

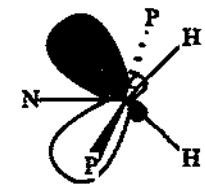

38

(v) Transition metal olefin complexes. Olefin activation and reactivity

(a) The nature and energetics of the M–C_2H_4 bond

Besides being starting reagents in many types of reactions in organometallic chemistry, transition metal–olefin complexes offer convenient means by which to study olefin chemisorption on metal surfaces [419–422]. However, high level ab initio calculations on naked transition metal–olefin complexes are limited to nickel [419,420,423] and copper [226] complexes.

A pioneer GVB-CI study of NiC_2H_4 [419,420] proved an eddy against the standard DCD model. In particular, the bonding involves mainly $L(\pi) \rightarrow Ni$ charge transfer with only minor $Ni \rightarrow L(\pi^*)$ back donation, resulting in a negligible charge migration. The experimental and theoretical results of Ozin et al. [419,422] led to the prediction of a triplet ground state ($^3A_1$) for NiC_2H_4 with a binding of 14.2 kcal mol^{-1}. More recent calculations applying MCSCF and CI techniques [423] showed that Ozin et al. had incorrectly assigned the ground state as a triplet and the correct ground state is a singlet ($^1A_1$) where a σ donation of 0.42e and a π-back donation of 0.67e have been computed. The triplet state was found to be essentially unbound, whereas the binding energy of the singlet state ($^1A_1$) was computed to be 14 kcal mol^{-1} relative to Ni (sd^9, ^1D) and increased to 20 kcal mol^{-1} with the addition of Davidson's corrections. The $^1A_1$ ground state can be reached from the asymptotic $^3A_1$ state only via an energy barrier of about 10 kcal mol^{-1}. However, both states seem to play a fundamental role in the chemisorption of ethylene on nickel surfaces.

For the CuC_2H_4 complex, non-empirical pseudopotential calculations [226] showed that the ground state appears to be the $^2A_1$ (s^1) state and the other three low lying states $^2B_2$ (p_x^1), $^2B_1$ (p_y^1) and $^2A_1$ (p_z^1) are present about 4.6 kcal mol^{-1} above it. According to these calculations, the $^2A_1$ (s^1) state

appears as a weakly bonded Van der Waals complex ($D_e = 8.3$ kcal mol^{-1}), whereas the $^2B_2$ and $^2B_1$ states induce stronger bonding involving Cu⇌C_2H_4 electronic delocalization and/or charge transfer.

An ethylene $\pi \rightarrow \pi^*$ excitation accompanied by an electron transfer from d_σ to d_π metal AOs is essential in the VB description [266] of the bonding in analogy with the MCO systems. This is identical to the conventional $L(\pi) \rightarrow M(d_\sigma)$ and $M(d_\pi) \rightarrow L(\pi^*)$ transfer representation and with overlap dispersion [85,86] in the MOVB reasoning.

A similar bonding mechanism also occurs in the cationic $MC_2H_4^+$ species. Ziegler et al. [424] analyzing the bonding in $MC_2H_4^+$ ($M^+ = Cu^+, Ag^+, Au^+$) by the transition state method at the HFS level, found that it corresponds to a synergic donor–acceptor process. The calculated bonding energies for the Cu^+, Ag^+ and Au^+ ethylene complexes were found to be -79.7, -50.2 and -50.2 kcal mol^{-1}, respectively, whereas the π-acceptor/σ-donor ratio (expressed by the ratio of the corresponding energy contributions) was found to be 1.69, 0.22 and 0.27, respectively.

Allison et al. [372] envisaged that, for an electrostatically bonded $MC_2H_4^+$ system, the geometry of the complex might correspond to the end-on bonding mode of ethylene due to the fact that the C=C double bond appears more polarizable along the bond axis than perpendicular to it, though no verification is available to date. Certainly, such a bonding mode of ethylene to transition metals has not yet been observed. However, M^+–olefin reactions frequently proceed via a M^+ insertion into the allyl C–H bond [425] and a structure of M^+–(1-butene) complexes placing the M^+ in close proximity to this bond could easily explain such a chemical behaviour. This structure corresponds to the electrostatic bonding model.

Saturated transition metal–olefin complexes have been the goal of several semiempirical [426–428] and ab initio [429–432] studies. An excellent review by Albright [23] dealing mainly with the application of fragment molecular orbital concepts has appeared. Therefore, we will concentrate our discussion on the more recent advances in the field and in particular on the results obtained through high quality ab initio calculations available to date.

A number of nickel–ethylene complexes formulated as $Ni(C_2H_4)X_2^{n+}$ ($n = 0$, $X = F^-, Cl^-, CH_3^-, CN^-, NH_2^-$; $n = 2$, $X = H_2O$, NH_3, PH_3 and $n = 0$, $X = H_2O$, NH_3, PH_3) have been studied by Åkermark et al. [429] using ab initio SCF-MO calculations. The calculated bond energies of the nickel–ethylene bond for $Ni(C_2H_4)$ and $Ni(C_2H_4)^{2+}$ were 27.2 and 80.5 kcal mol^{-1}, respectively. The presence of additional ligands in the complexes elevates the binding energies in Ni(0) and lowers them in Ni(II) species. All these trends have been attributed to the electrostatic and charge transfer interactions and are also nicely reflected in the gross charges of the olefin and in the equilibrium C–C bond distances of the ethylene ligand.

The first ab initio calculations on Zeise's salt, $PtCl_3(C_2H_4)^-$ and the related $PdCl_3(C_2H_4)^-$ complex have been carried out by Hay [431] using an extended basis set and RECPs for Pd and Pt. The calculated geometrical parameters and rotational barriers were found to be in good agreement with experimental data. Moreover, the rotational barriers and binding energies were found to decrease in the order Pt > Pd. The more stable geometries are those with the upright conformation of the ethylene ligand, whereas the planar conformation corresponds to less stable geometries.

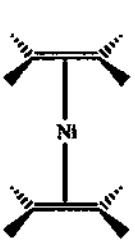

39

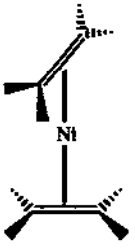

40

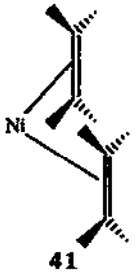

41

Orientational preferences and electronic structures of $Ni(C_2H_4)_2$ and $Ni(C_2H_4)_3$ compounds have been investigated at both the EHMO level by Rösch and Hoffmann [426] and the ab initio level by Pitzer and Schaefer [430] and Siegbahn and Brandemark [432]. For the $Ni(C_2H_4)_2$ complex both EHMO [426] and large basis set HF calculations [430] have been performed on the 'planar' D_{2h} and 'twisted' D_{2d} conformations, shown in **39** and **40**, respectively. A C_{2v} conformation, shown in **41**, has also been considered in the CASSCF-CCI calculations performed by Siegbahn and Brandemark. The first two studies agree almost perfectly with each other and place the two structures very close in energy, within 1.5 kcal mol^{-1} in ref. 426 and within 0.1 kcal mol^{-1} in ref. 430, whereas the third study [432] showed that the twisted D_{2d} structure is the energetically most favourable one, being 10.3 and 32 kcal mol^{-1} more stable than its D_{2d} and C_{2v} counterparts. The preference for the D_{2d} structure has been attributed to the VB configuration $\pi^1\pi^{*1}(A) + d_\sigma^2 d_{\pi d}^1 d_{\pi y}^1 + \pi^1\pi^{*1}(B)$, which has the possibility of forming two simultaneous π bonds. An indication of the importance of this d^8 configuration for the D_{2d} form is the lower d population found for D_{2d} compared with D_{2h}. For the C_{2v} structure, although there is the possibility of forming two simultaneous π bonds, its low binding energy is due to a poor σ interaction with inefficient *sd* hybridization. Another quite different explanation for the preference for the D_{2d} structure was based on perturbation theory arguments [426]. Thus, if the non-degenerate perturbation theory is used for the orbital interactions between d_π and π^*, the two structures are expected to be energetically equivalent. On the other hand, if the perturbation theory is used, the D_{2d} structure should be preferred.

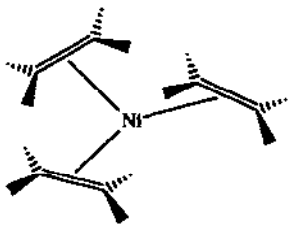

42

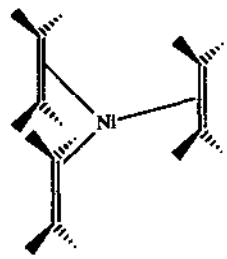

43

For the $Ni(C_2H_4)_3$ complex, the planar D_{3h} structure, **42**, was predicted to be more stable by ~ 17 kcal mol^{-1} at the EHMO level and ~ 24 kcal mol^{-1} at the HF level than the upright form **43**. This has been attributed by Rösch and Hoffmann [426] to the rising of the e' orbital, **44**, as the ethylenes rotate, which diminishes the stabilizing $M(d) \rightarrow L(\pi^*)$ donation. Pitzer and Schaefer [430] extended these arguments to explain the reversal on the stability of the ionized $Ni(C_2H_4)_3^+$ species, with its upright form being 2 kcal mol^{-1} more stable than the planar form.

44

Conformational preferences and electronic structures of iron–olefin complexes of the general formula $Fe(CO)_4(C_2X_4)$, where X = H, F, Cl and CN, have been investigated by the PRDDO approximation [428]. All the compounds studied were found to prefer a TB structure, **45**, with the ethylene ligand occupying an equatorial position. The next lowest energy structure is that of the eclipsed SP, **46**.

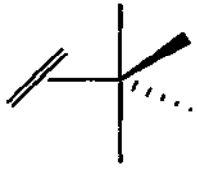

45

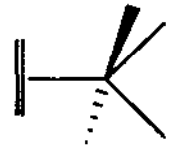

46

In agreement with Hoffmann and coworkers [427], π-accepting substituents were found to raise the isomerization energies. For tetrachloro- and tetracyanoethylene, this effect is so pronounced that the complexes may well be stereochemically rigid at room temperature. The isomerization process in $Fe(CO)_4(C_2H_4)$ has previously been investigated theoretically by Demuynck

et al. [380] by LCAO-MO-SCF ab initio calculations. A concerted mechanism involving the coupling of the olefin rotation with Berry pseudorotation about iron has been proposed.

To make quantitative estimates of the effect of various substituents on the iron–olefin bond strength, Axe and Marynick [428] have calculated ligand exchange energies, ΔE, for the reactions

$$Fe(CO)_4(C_2H_4)+C_2X_4 \rightarrow Fe(CO)_4(C_2X_4)+C_2H_4$$

They found that ΔE values vary in the order $\Delta E_H \approx \Delta E_F \gg \Delta E_{CN} > \Delta E_{Cl}$, in accordance with available experimental data on related systems. Population analyses, difference density plots and correlations with the energy of the free ligand π^* MOs strongly suggested that π-back bonding effects dominate the trends found. Moreover, calculated localized molecular orbitals indicated that the iron–olefin interaction is essentially that of a three-member metallacyclopropane ring.

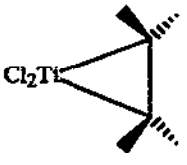

47

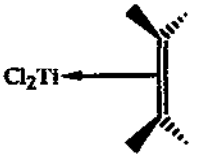

48

GVB calculations on $Cl_2Ti(C_2H_4)$ carried out by Steigerwald and Goddard [433] also lead to a metallacyclopropane resonance structure **47**, that predominates over the π-complex resonance structure, **48**. At the GVB-CI level, structure **47** was found to be 14.8 kcal mol^{-1} more stable than structure **48**. However, this is not the case for $Cl_2Ti(C_2H_4)$ alone. In general, some metal–olefin complexes should be viewed as metallacyclopropanes and others as π-complexes, according to the rules proposed by Steigerwald and Goddard. Thus, high-spin metal containing fragments, weak C–C π bonds in the free olefins and strong M–C σ bonds favour the metallacycle form. The two resonance structures are not truly separated and distinct; they exhibit, however, different chemical reactivity. The chemistry of the metallacycle form is dominated by cycloadditions and cycloreversions of olefins, while that of the π-complex form is dominated by acid–base reactions resulting from enhancement of the electrophilicity of the olefin. These two types of reactivity as well as the olefin insertion reactions will be briefly discussed below.

(b) Metal-promoted cycloadditions and cycloreversions of olefins

Although many experimental results have accumulated, there has been little theoretical analysis of cycloaddition and cycloreversion reactions [433–441].

EHMO calculations were applied by Stockis and Hoffmann [434] on the reaction path of bis(olefin)tricarbonyliron to ferracyclopentane interconversion. They concluded that, in the coupling reaction of bis(olefin) or bis(acetylene) complexes, the controlling factor is the HOMO of the complex, possessing substantial ligand π^*-MO character. Therefore, regioselectivity originates from polarity in the π^* orbital of an unsymmetrical olefin or acetylene. In contrast, regioselectivity of the bis(acetylene) cobalt to cobaltacyclopentadiene cyclization process studied by Wakatsuki et al. [435] with the use of ab initio SCF-MO calculations was found to be controlled by steric factors. Moreover, a transition state of low symmetry, C_s, which accounts well for the observed regioselectivity has been determined.

Steigerwald and Goddard [433], examining the GVB wavefunction of the metallacyclopropane, $Cl_2Ti(C_2H_4)$, showed that the three-membered ring is strained and that simple $2s+2s$ reactions of the Ti–C bonds can relieve this strain. It is the presence of the metal at the apical site and in particular the use of the metal d AOs in the covalent M–C bond which allows the intrinsic strain of the three-membered ring to be relieved by a simple suprafacial $2+2$ reaction. In cyclopropane itself, this reaction is forbidden.

Cycloreversion reactions have also been investigated theoretically [436,437]. Thus, Braterman [436] showed that the thermolysis of metallacycles is explained in terms of frontier orbital symmetry. The degradation of nickelacyclopentane to Ni^0 and cyclobutane is symmetry allowed for $L_2Ni(CH_2)_4$ metallacycles, whereas for $L_3Ni(CH_2)_4$, degradation to Ni^0 and the olefin is symmetry allowed, in agreement with available experimental data. These symmetry restrictions depend on whether $d_{x^2-y^2}$ or d_{z^2} AO is occupied.

EHMO calculations employed by Hoffmann and coworkers [437] resulted in similar conclusions. Thus, generally, if metallacycle degradation to form cyclobutane is symmetry allowed, the formation of ethylene will usually be symmetry forbidden, and vice versa. For the degradation of five-coordinate $L_3Ni(CH_2)_4$ metallacycles to ethylene, an unexpected four-coordinate *trans* complex of C_{2v} symmetry has been proposed to be an important intermediate.

Very recently, Goursot and coworkers [438] have presented a local spin density calculation of the electronic structure of the four-coordinated bis(phosphine)nickelacyclopentane complex, along with the energetics of its degradation pattern. The orbital diagrams and the energetics were found to be largely consistent with EHMO results [437]. Three low-lying electronic configurations were found to be of crucial importance in determining the degradation process. Besides two ^1A singlets with square-planar and tetrahedral structures, a tetrahedral ^3B state is possibly responsible for a low-spin↔high-spin equilibrium. Moreover, the possibility of a facile square-planar↔tetrahedral interconversion suggests an alternative for the ethylene formation in addition

to cyclobutane, without necessitating the decomposition of a tris(triphenylphosphine) complex.

For the several stable metallacyclobutanes and in particular those of the platinacyclobutanes, Wilker and Hoffmann [439] investigated theoretically their highly stereospecific skeletal rearrangement where a substituent at the carbon α to the metal appears to migrate to a β position according to the equation:

(44)

The proposed mechanism for this rearrangement in the case of $L_2Cl_2Pt(C_3H_6)$ was based upon the isolobal analogy which suggested that, after initial loss of a ligand, the LCl_2Pt fragment rearranges to a pyramidal geometry in which it is isolobal to CH^+. Therefore, $LCl_2Pt(C_3H_6)$ is like a non-classical carbonium ion, $C_4H_7^+$, exhibiting a Jahn–Teller hill for C_{3v} geometry and more stable T- and Y-shaped intermediates or waypoints. The stability of various intermediates in the general case of the $L_3M(C_3H_6)$ system is also discussed in terms of electron count and ligand electronegativity concepts.

CASSCF and contracted CI calculations have been performed on the ring opening of cyclopropane by palladium and several palladium(II) compounds, such as $PdCl_2$, $PdCl_4^{2-}$ and $PdCl^+$ [440,441]. Two reaction pathways for the ring opening of cyclopropane were studied, corner activation and edge activation:

Corner activation

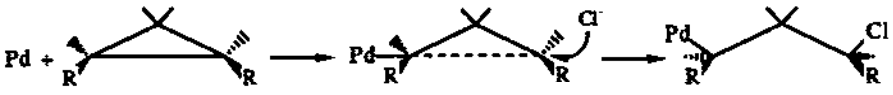

(45)

Edge activation

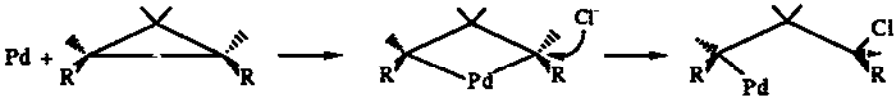

(46)

For Pd(0), only edge activation is predicted to be favourable in these calculations with a low activation barrier of 17 kcal mol^{-1}; the barrier for

corner palladation was estimated to be 30–35 kcal mol^{-1}. The calculations further showed that the energy for the metallacyclobutane is slightly higher (6 kcal mol^{-1}) than that for Pd and cyclopropane, whereas the biradical intermediate formed through a corner attack is 18 kcal mol^{-1} less stable than metallacyclobutane. The edge activation mechanism of ring opening of cyclopropane is in agreement with experimental results concerning platinacyclobutane formation which occurs with retention of configuration at both carbon atoms attacked by the metal.

For the Pd(II) complexes, only corner activation by $PdCl^+$ was found to proceed with a low activation barrier estimated to be ~5 kcal mol^{-1}. For $PdCl_2$ and $PdCl_4^{2-}$, both corner and edge activations are characterized by very high activation barriers of ~24–25 kcal mol^{-1}. To interpret these results, the important role of the excitation energies of the different atomic states on the relative thermodynamic stability of complexes with different numbers of covalent bonds must be understood. In this respect, the sum of the actual number of covalent bonds and the actual charge on the metal were found to be of special importance in determining the atomic state of a metal involved in a complex.

Finally, the C–C bond breaking in cyclopropenium cations and cyclopropenones by various mononuclear and dinuclear transition metal fragments has been investigated theoretically by Jemmis and Hoffmann [442]. Correlation diagrams connecting the extremes of the reaction path showed that the process involves an η^2-bonded cyclopropenium complex which is easily converted to a metallacycle. For the d^8-ML_4 or their isolobal d^{10}-ML_2 species, the reaction path is similar in detail to the disrotatory opening of a bicyclobutyl cation to cyclobutenyl cation.

(c) Nucleophilic attack on a coordinated olefin

Metal-assisted nucleophilic addition to olefins is an important process in organic synthesis via transition metals, allowing one to create new C–C, C–N and C–O bonds. Therefore, it is interesting to know why the reactivity of olefins towards nucleophiles is increased by coordination to metals, as well as which factors affect the activation of olefins and the regio- and stereoselectivity of the nucleophilic addition. These aspects, along with the energetics and reaction profiles of metal-assisted nucleophilic attack of olefins, have been investigated in several theoretical works over the last few years [429,433,443–451]. Before presenting the main conclusions of these studies, it is important to note that the legion of experimental data available suggest that two types of nucleophilic attack on coordinated olefins can be distinguished:

(1) the *trans* nucleophilic addition to olefins upon their interaction with an

external nucleophile Nu, according to the equation

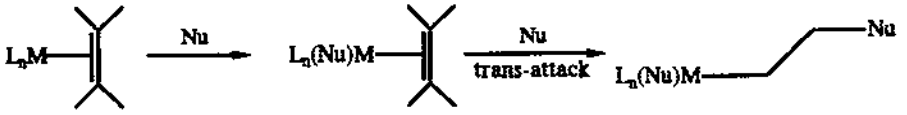

(47)

(2) the *cis* migration of nucleophiles involving the intramolecular migration of a nucleophile to the coordinated olefin molecule according to the equation

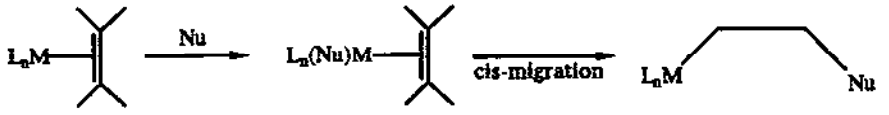

(48)

The first type of nucleophilic attack will be discussed presently, whereas the following section will be devoted to the second.

Earlier, ab initio MO-SCF studies carried out by Åkermark et al. [429] indicated that the induction of a positive charge on the coordinated olefin is more important than the weakening of the C=C double bond in determining its reactivity towards nucleophiles. Thus, in the series of nickel–ethylene complexes $X_2Ni(C_2H_4)^{n+}$, those with $n=0$ and $X=F^-$, Cl^-, CH_3^-, CN^- and NH_2^- undergo nucleophilic attack on the central metal atom because the positive charge induced on the olefin (+0.1) is low relative to that on the metal (ca. +0.9). On the other hand, cationic species ($n=2$; $X=H_2O$, NH_3 and PH_3) exhibiting more favourable metal-to-olefin charge ratio are the main candidates for promoting the nucleophilic addition on the olefin.

A pellucid explanation of the metal-promoted olefin activation was proposed by Eisenstein and Hoffmann [443] using the EHMO approach. Their EHMO calculations indicate that, apart from charge, frontier orbital interactions are important for the activation. In particular, a symmetrically η^2-coordinated olefin is deactivated toward attack by an external nucleophile, since the LUMO of the complex, being mostly olefin π^* in character, was found to be both at higher energy and less localized on the olefin in the complex than in the free olefin. However, an unsymmetrical η^1-coordination of the olefin, resulting by slipping on the L_nM fragment, plays a crucial role in its activation. In the 'slipped' form, the LUMO involves a mixing of olefin π-MO into the LUMO of the symmetrical form, its extent being determined by the LUMO energy of the L_nM fragment. Therefore, similarities and differences of the activation process by various L_nM fragments, such as d^2 Cp_2WR^+, d^6 $Fe(CO)_5^{2+}$ and $CpFe(CO)_2^+$, d^8 PtL_3 and $Fe(CO)_4$ and d^{10} $Ni(PR_3)_2$ olefin complexes can be easily understood.

GVB-CI calculations by Steigerwald and Goddard [433] showed that only those metal–olefin complexes corresponding to π-type (acid–base type) com-

plexes could undergo nucleophilic attack on the coordinated olefin. This is the case for L_nM fragments with the central metal being an oxidized late transition metal such as Pd(II), Pt(II) and Fe(II). However, when the acid–base nature of bonding is reversed, the complexes undergo olefin dissociation or sometimes react at the olefin with electrophiles. This is the case for L_nM fragments with the central atom being a highly reduced late transition metal, such as Ni(0), Fe(0) and Pt(0).

The factors governing the ease of external addition of nucleophiles to (π-olefin)palladium complexes have been discussed in terms of the FMO theory by Bäckvall et al. [444]. They concluded that the *trans*-addition reaction of nucleophiles is accelerated by nucleophiles possessing low lying HOMOs, a fact which suggests that this reaction is a charge controlled process.

The addition of nucleophiles to a C=C double bond in the presence of Pd complexes has been used as a model to exemplify the catalytic roles by paired interacting orbitals introduced by Fujimoto and Yamasaki [445]. The calculations indicated that the activation of ethylene is ascribed mainly to two terms, the reduction of overlap repulsion, and the enhancement of the ability to create the localized bonding orbital on the reaction centre.

Analogous investigations by energy decomposition analysis at the ab initio level were undertaken by Sakaki et al. A series of palladium complexes [446] such as $[PdF_3(C_2H_4)]^-$, $PdF_2(NH_3)(C_2H_4)$, $[PdF(NH_3)_2(C_2H_4)]^+$ and $[PdF(PH_3)_2(C_2H_4)]^+$ as well as $[HgH(C_2H_4)]^+$ [447] have been examined. The calculations showed that the *trans* attack of a nucleophile, NH_3, on the coordinated olefin causes significant destabilization in $[PdF_3(C_2H_4)]^-$ and $PdF_2(NH_3)(C_2H_4)$, but proceeds easily with a rather small activation barrier ($\sim$6–8 kcal mol^{-1} at the HF level) in $[PdF(NH_3)_2(C_2H_4)]^+$ and $[PdF(PH_3)_2(C_2H_4)]^+$. These results suggest that the active species is a cationic palladium(II)–olefin complex in accordance with experimental evidence. The nucleophilic attack was found to include characteristics of both frontier and charge control and therefore neutral and soft ligands favour it. In general, a low lying acceptor orbital of L_nM decreases the exchange repulsion between the nucleophile and the olefin and increases the bonding interaction. Moreover, orbital mixing for FMOs which arise from a second-order perturbation among the lone pair of nucleophile and the two pairs of bonding and antibonding MOs in the palladium–ethylene complex explains why the cationic complex accelerates nucleophilic attack but the neutral and anionic complexes do not.

(d) Olefin insertion reactions

Olefin insertion reactions are key steps in many catalytic cycles; therefore olefin insertion into M–H and M–R (R = alkyl) bonds has been extensively studied theoretically in the last few years [410,429,444,445,448,449]. The first

such study concerning the insertion of ethylene into a Pt–H bond was carried out by Thorn and Hoffmann [448]. Using the EHMO approach, they analyzed the crucial orbitals along a simplified reaction coordinate for platinum hydride complexes with one to three other ligands attached to it. The calculations showed that neither an easy insertion pathway from a five-coordinate intermediate nor a facile reaction by a direct route from a four-coordinate complex with olefin and hydride *trans* to each other is possible. Moreover, the necessary final waypoint of olefin and hydride *cis* was found to be best achieved by a sequence of associative and preferably dissociative steps. The polytopal rearrangements of the five- and three-coordinate intermediates have also been explored in detail.

Åkermark et al. [429], investigating the chemical reactivity of nickel–ethylene complexes through ab initio SCF-MO calculations, showed that intramolecular migration of a nucleophile (e.g. CH_3^- and H^-) to the coordinated ethylene molecule is favoured for the charged complexes, such as $[CH_3Ni(C_2H_4)]^+$, in agreement with experimental data.

The intramolecular migration of a nucleophile to the coordinated olefin is regarded as a [2+2] cycloaddition. Therefore, the reactivity of the π-olefin complexes towards a *cis* migration would be expected to be mainly determined by the frontier orbitals. Along this line, Bäckvall et al. [444], using ab initio calculations with ECPs on (π-ethylene)Pd complexes with different coordinated nucleophiles, H^-, CH_3^-, OH^- and F^-, showed that the necessary condition for an intramolecular *cis* addition to occur is that the orbital describing the metal–nucleophile bond be high enough in energy. This would in turn require that the free nucleophile has a high energy HOMO, i.e. to be a soft nucleophile, such as H^- and CH_3^-. The other nucleophiles studied, being hard, would be unreactive towards the frontier controlled *cis* migration but react very efficiently in the charge controlled *trans* addition processes.

Fujimoto et al. [449] have recently applied the interacting orbital concept to cyclic interactions between ethylene and $RTiCl_2^+$ species (R = CH_3 or H) in an attempt to understand the reactivities of M–C and M–H bonds. Two sets of paired localized orbitals dominate these interactions, the low lying unoccupied orbital having a large amplitude on the *d* AOs of metal and the high lying occupied orbital having a large amplitude on R, suggesting a four-centred transition state. In a more recent paper concerning Pd(II)-catalysed nucleophilic additions to C=C bonds, Fujimoto and Yamasaki [445] showed that Pd is involved more directly in the *cis* than in the *trans* addition processes. The two dominant pairs of interacting orbitals for OH^- and H^- migration in C_2H_4–$Pd(L)Cl_2$ systems (L = OH^- or H^-) shown in **49** and **50**, respectively, clearly indicate that the *cis* migration of the hydride is more plausible than hydroxide migration. This is mainly due to the neighbouring *d* orbital participation in the second pair of orbitals in **50**. Moreover, the

difference between Ti(IV) and Pd(II) systems has been ascribed to the difference in the number of electrons populated in the four-membered ring, being larger than 2 for Pd(II) and closer to 2 for Ti(IV) systems. Accordingly, the Pd(II)-catalysed migratory addition of hydride will occur, if at all, via a loosely bound four-membered cyclic transition state.

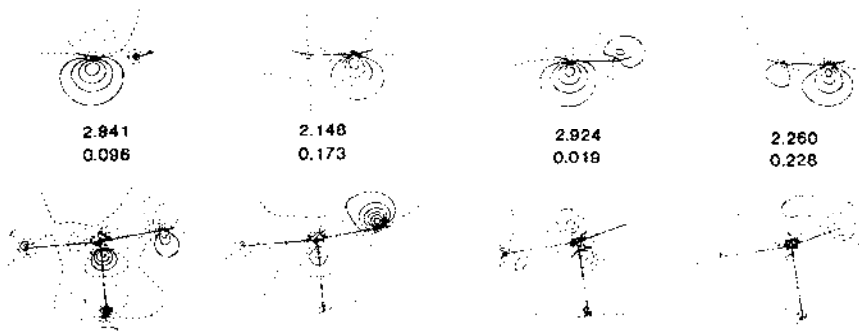

49 **50**

Olefin insertion and β-elimination processes for a series of model reactions, *cis*-$(PH_3)(H)_2M(C_2H_4) \rightleftharpoons (PH_3)(H)M(C_2H_5)$, where M = Ni, Pd, Pt, have recently been investigated by Koga and Morokuma [410] using ab initio RHF calculations with the energy gradient technique for geometry optimization. It was shown that the hydride transfers between the β-carbon atom and the transition metal via a four-centre transition state. The low energy barriers for both directions (0.6–12.5 kcal mol^{-1} at the HF level) strongly support the reversibility of insertion/β-elimination reactions.

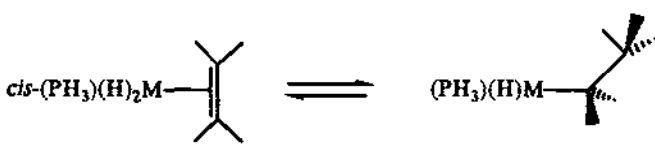

(49)

(e) Olefin hydrogenation by Wilkinson catalyst

The homogeneous hydrogenation of olefins catalyzed by the Wilkinson catalyst, $RhCl(PPh_3)_3$, has been investigated by Dedieu et al. [450] using ab initio LCAO-MO-SCF calculations. They have calculated the relative stabilities of the most probable stereoisomers of various model rhodium complexes, such as $RhClL_2$, H_2RhClL_3, H_2RhClL_2, $H_2RhClL_2(C_2H_4)$ and $HRhClL_2(C_2H_5)$, ($L = PH_3$). Dedieu et al. concluded that the transfer of the first hydrogen to the coordinated olefin in $H_2RhClL_2(C_2H_4)$ is not a simple H-migration but rather an olefin insertion into the Rh–H bond, which

probably involves some rearrangement of the non-reacting ligands in the insertion plane.

Very recently, Morokuma and his coworkers [451], using ab initio MO and energy gradient methods, have studied the potential energy profile for a full catalytic cycle of ethylene hydrogeneration by the Wilkinson catalyst. They have concentrated on the dominant catalytic cycle of the Halpern mechanism, consisting of oxidative addition of H_2, ethylene coordination, intramolecular migratory olefin insertion, isomerization of the ethyl–hydride complex and the reductive elimination of C_2H_6 to regenerate $RhCl(PPh_3)_2$. The first two reactions were found to be exothermic with little or no activation barrier. Olefin insertion followed by isomerization of the *trans*-ethyl–hydride complex to a *cis* complex was found to be the rate-determining step with a barrier height of ~ 20 kcal mol^{-1}. The final step of reductive elimination of C_2H_6 from the *cis* complex is nearly thermoneutral with a modest activation barrier of ~ 15 kcal mol^{-1}. Generally, the potential energy profile, found to be smooth without excessive barriers and stable intermediates, indicates that the Halpern mechanism is favourable.

(vi) Transition metal carbenes. Ligand coupling and cleavage processes

(a) Metal–carbene bonding and energetics

The electronic structure of a few naked transition metal–methylene, MCH_2^+, complexes has been studied by high quality ab initio techniques in the last decade [207,452–457]. The theoretical and experimental values of BDEs of the MCH_2^+ systems studied so far have been collected in Table 14.

To understand the periodic trends of M^+–CH_2 BDEs for the entire first row of the transition metals, Armentrout et al. [458] correlated the BDEs with the metal ion promotion energy, $E_p(sd^{n-1})$. From the excellent linear regression fit obtained, the maximum or intrinsic M^+=CH_2 bond strength was calculated to be equal to 101 kcal mol^{-1}, so that the intrinsic M^+–C π-bond strength is ~ 45 kcal mol^{-1}. Note that the intrinsic M^+–C σ-bond strength was calculated to be ~ 57 kcal mol^{-1} [195,212].

Transition metal carbenes form two distinct classes, exhibiting electrophilic and nucleophilic behaviour, respectively [459,460], owing to the dramatic difference in the M–C bonding between them [454,455]. Thus, in metal 'carbene' complexes, the M–C bond is described in terms of σ-donor/π-acceptor concepts, while in metal 'alkylidene' complexes it corresponds to an olefinic type covalent bond. Electrophilic 'carbene' complexes include the so-called 'Fischer' type carbenes, such as **51**, which undergo stoichiometric cyclopropanation of olefins and Lewis base adduct formation. On the other hand, nucleophilic 'alkylidene' complexes include the so-called 'Schrock' type

TABLE 14

Theoretical and experimental bond dissociation energies (in kcal mol^{-1}) for some naked transition metal MCH_2^+ systems

Compound	State	$D_e(M^+-CH_2)$	Computational method	Ref.
$CrCH_2^+$	$^6B_1$	18.3 (53.8 ± 1.9)[a]	HF-CI	452
		22.3	HF-CI + D	452
		25.0	GVB-RCI	453
		21.0	MCSCF + 1 + 2	207
	$^4B_1$	38.7	MCSCF + 1 + 2	207
		44.0	GVB-RCI	453
	$^6A_1$	35.8	HF	454
		38.7	GVB-RCI	454
$MnCH_2^+$	$^7B_1$	36.0 (70.6 ± 3.0)	HF-CI	452
		40.8	HF-CI + D	452
		58.4	GVB-RCI	456,238
$FeCH_2^+$		69.2 (83 ± 4.0)	GVB-RCI	456,238
$CuCH_2^+$		57.0 (63.9 ± 1.6)		457
$RuCH_2^+$	$^2A_2$	68.0	GVB-RCI	455
	$^4A_2$	65.8	GVB-RCI	455

[a] Figures in parentheses are the experimental $D_0(M^+-CH_2)$ values taken from ref. 458.

complexes, such as **52**, which undergo olefin metathesis, Wittig type alkylations and Lewis acid adduct formation.

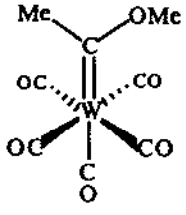

51

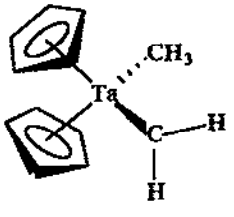

52

Carter and Goddard [454,455], based upon a series of GVB studies on metal carbene (alkylidene) complexes, suggested the following VB view of metal–carbene (alkylidene) bonds.

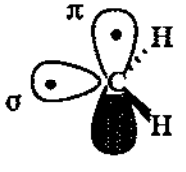

53

54

The ground and low lying excited states of $M(CXY)^+$ systems are formed by combining low lying metal atomic configurations with the triplet $\sigma\pi$, **53**, or the singlet σ^2, **54**, states of the neutral CXY ligand. Obviously, metal carbenes are formed by the interaction of 'low-valent' metal fragments (e.g. $W(CO)_5$) with CXY ligand involving electronegative substituents X and Y (e.g. OR, NR_2, F, Cl) which stabilize the singlet carbene state. On the other hand, metal alkylidenes involve 'high valent' metal fragments (e.g. Cp_2TiR) with CXY ligands involving electron-donating substituents X and Y (e.g. H, R, Ar) which stabilize the triplet alkylidene state.

The above conclusions were drawn by Carter and Goddard on the basis of all electron ab initio calculations of the electronic structure and related properties of representative early and late transition metal MCH_2^+ systems, namely $CrCH_2^+$ and $RuCH_2^+$. The results obtained can be summarized as follows.

(i) The ground state of both $CrCH_2^+$ ($^4B_1$) and $RuCH_2^+$ ($^2A_2$) involve covalent metal–carbon double bonds corresponding to methylidene bonding. They result from CH_2 ($^3B_1$) and Cr^+ (^6S) and Ru^+ (^4F) states, respectively.

(ii) There are low-lying excited states for both $CrCH_2^+$ and $RuCH_2^+$ systems which are metal carbenes. Their BDEs are comparable with the ground state BDE.

(iii) The properties of the lowest carbene state of $CrCH_2^+$ ($^6A_1$) reveal a complex with a single σ donor bond and no π back bond, resulting in a low bond energy (38.7 kcal mol^{-1}) and a large carbene–alkylidene energy gap (18.8 kcal mol^{-1}).

(iv) The lowest carbene state of $RuCH_2^+$ is triply degenerate ($^4A_2$, $^4B_1$, $^4B_2$), resulting from ground state high spin d^7 Ru^+ and $^1A_1$ CH_2. The three states differ only in the occupation of the non-bonding d AOs and contrast with the carbene state of $CrCH_2^+$, possessing both σ-donor and π-acceptor bonds, which results in a high bond energy (65.8 kcal mol^{-1}) and a smaller carbene–alkylidene separation (12.9 kcal mol^{-1}).

(v) From comparison of the carbene states of $CrCH_2^+$ and $RuCH_2^+$, the M^+–CH_2 σ-donor bond strengths are calculated to be worth 35–40 kcal mol^{-1}, while the π-back bond strengths are found to be $\sim$30 kcal mol^{-1}. Moreover, the calculations indicated that the σ-bond becomes stronger and the π-bond weaker as the metal becomes more electrophilic.

(vi) The characteristic geometrical features of the carbene states with respect to the alkylidene states are the longer M–C bond lengths and the smaller HCH bond angles.

The VB ideas of the M^+–CXY systems have also been used by Carter and Goddard [454] to formulate a general design prescription for carbenes and alkylidenes. Such a prescription provides means for controlling the chemical reactivity of carbene complexes. Generally, a desired bonding/reactivity

pattern, be it carbene, alkylidene or an intermediate case, can be designed by appropriate choice of both metal and ligand. In particular:

(i) alkylidene states are lowest for the early and carbene states for the late transition metals, differences being more pronounced for the first row transition metals;

(ii) for the second and third row metals, both types of complexes may be competitive and the ground state may be determined by several factors (e.g. nature of the CXY and/or ancillary ligands;

(iii) when the X and Y substituents of CXY are σ-donative and bulky, alkylidenes are favoured, while electronegative X and Y lead to carbene formation.

The design prescription for carbenes and alkylidenes can also be applied to the synthesis of $L_nM(CXY)$ complexes provided that the quantitative electronic properties of the desired complex are known. Moreover, Carter and Goddard [238,455] have also tried to find correlations between the BDEs of coordinatively unsaturated (naked) MCH_2 and saturated ($ClRuH(CH_2)$) systems, performing equivalent calculations on the latter. They have found that the $Ru{=}CH_2$ BDE of the model complex is 88.2 kcal mol^{-1}, being very close to the theoretically calculated [461] value of 90.3 kcal mol^{-1}. Predicted coordinatively saturated $M^+{-}CH_2$ BDEs from coordinatively unsaturated $M^+{-}CH_2$ BDEs for the first row transition metals are also given by Carter and Goddard [238] and compared with available experimental data. The observed stronger $M{=}CH_2$ bonds in the saturated complexes relative to the unsaturated were attributed to the differential loss of exchange coupling on the metal.

The first accurate MO calculations on a realistic carbene complex, namely $(CO)_3NiCH_2$, were reported by Spangler et al. [462]. They calculated the geometrical parameters of this complex and obtained the Ni=C bond length of 1.83 Å, a little shorter than the experimental value of 1.9 Å and a negligible (0.2 kcal mol^{-1}) rotational barrier around this bond. A comparison between the structures of $(CO)_3NiCH_2$ and $NiCH_2$ shows that they are very similar. The slightly shorter Ni=C bond in the naked species suggests a stronger bond whose dissociation energy has been calculated to be 65 kcal mol^{-1} at the GVB-CI level [463].

Previous theoretical calculations for transition metal carbenes have been limited to low level calculations (HF) using minimal basis sets. Fenske and his coworkers [464] have reported approximate Fenske–Hall calculations on the 'Fischer' type carbene $(CO)_5CrC(OCH_3)CH_3$. They concluded that the reactions of this complex with nucleophiles are frontier rather than charge controlled. Moreover, they have shown that the site of the nucleophilic attack is dependent upon the location of the LUMO, which is well separated from all other MOs, possessing 60% $2p_x$ carbene atom character. Block and

Fenske [465,466] have also reported comparative Fenske–Hall calculations on the corresponding amino and thiomethyl carbenes. More recently, Kostic and Fenske [467,468] have investigated conformations and reactivities of coordinated unsaturated ligands, such as carbene, carbyne, acetylide, vinylidene and vinyl ligands. They suggested that optimal conformations of carbene ligands are those that minimize orbital energies and not necessarily maximize overlaps in the dominant metal–carbon π interactions [467]. A striking example is $BzCr(CO)_2C(OMe)Ph$, which adopts a conformation with smaller Cr=C(OMe)Ph π overlap because it leaves the more stable of the two π-type metal orbitals as the non-bonding HOMO for the complex. The $CpMn(CO)_2CMe_2$ and $CpMn(CO)_2C(OMe)Ph$ complexes are its true epigones. However, the preferred position of the π-accepting carbene ligand in $CpFe(PH_3)_2CH_2^+$ maximizes the attractive π overlap with the calculated rotational barrier [468] being very close to the experimental value.

Nakatsuji et al. [469,470] have studied the electronic structures and chemical reactivities of both 'Fischer' type carbenes such as $(CO)_5Cr{=}CH(OH)$ and $(CO)_4Fe{=}CH(OH)$ and 'Schrock' type carbenes such as $(CH_3)(H)_2Nb{=}CH_2$, adopting a minimal basis set. The M=C bond in the 'Schrock' type complexes was found to be stronger than that of the 'Fischer' type (M=C bond energy 44.4 kcal mol^{-1} for the Cr, 33.6 kcal mol^{-1} for the Fe carbene and 112 kcal mol^{-1} for the Nb alkylidene complex, with respect to the singlet ground states of the fragments). The rotational barrier around the M=C bond was calculated to be larger for the 'Schrock' type than for the 'Fischer' type carbenes (0.41 kcal mol^{-1} for Cr=C, 2.9 kcal mol^{-1} for Fe=C and 11.3 kcal mol^{-1} for Nb=C). The larger rotational barrier in the 'Schrock' type complex was attributed to the absence of the degenerate d_π and p_π type lone pair MOs for the $(CH_3)(H)_2Nb$ fragment. For both classes of compound, the reactivity was shown to be frontier controlled as Fenske and coworkers [464,468] had pointed out previously.

Taylor and Hall [471] have discussed the major differences between 'Fischer' and 'Schrock' type carbenes within the framework of the generalized molecular orbital (GMO) method. Ab initio calculations with a better than minimal basis set were carried out on five model carbenes, namely $[(CO)_5Mo{=}C(OH)H]$, **55**, $[CpCl_2Nb{=}C(OH)H]$, **56**, $[(CO)_5Mo{=}CH_2]$, **57**, $[CpCl_2Nb{=}CH_2]$, **58**, and $[H_2C{=}CH_2]$, **59**. The electronic differences which occur were illustrated by molecular orbital diagrams, fragment analysis of MOs, VB density plots and deformation densities, and dissociation energies. The similar views of the differences between low and high valent metal complexes suggested more recently by Carter and Goddard [454,455] should be noted. The M=C BDE for the electrophilic $(CO)_5Mo{=}CH(OH)$ was calculated to be 60 kcal mol^{-1}, while that of the nucleophilic $CpCl_2Nb{=}CH_2$ is 74 kcal mol^{-1}. Taylor and Hall, interchanging singlet and triplet carbene

fragments with the metal fragments to produce $CpCl_2Nb{=}CH(OH)$ and $(CO)_5Mo{=}CH_2$, showed that the chemical nature of the carbene is controlled by the metal fragment to which it is attached.

Many of the electron-deficient 'Schrock' type carbenes display an interesting structural deformation in which the alkylidene has pivoted about the C, so that remarkably small M–C–H angles down to 78° and correspondingly large M–C–R angles up to 170° are seen [472]. Hoffmann and coworkers [473] suggested that this deformation arises because the metal has several empty unused δ orbitals that can be used to bond with the σ orbital of the carbene.

Hehre and coworkers [474] have studied the equilibrium structures and conformational preferences of Ti and Zr methylidene complexes using HF calculations with STO-3G. They found that the driving force for the bend involves the formation of a three-centre M–H–C bond. Thus, as the CH_2 pivots, the Nb *d* AO also pivots and the Nb–C bond remains intact as it becomes a bent Nb–C bond. At the smallest angle there is significant positive Nb–H overlap population. Therefore, the pivoting of the methylidene involves both a rotation of the Nb–C bond and a direct Nb–H interaction.

The conformation of several *cis* carbene–olefin transition metal complexes (d^6 octahedral, d^4 pseudotetrahedral and d^8 trigonal bipyramidal) have been studied by Volatron and Eisenstein [475] using EHMO calculations. It has been shown that the conformational preference for carbene–olefin complexes results from a subtle balance between metal-to-ligand back donation and direct ligand–ligand interaction. These two factors favour different conformations, the relative importance of each depending on the nature of ligands at the metal, of the substituents at the carbene and the ligand field at the metal. Generally, in the octahedral complexes, if the metal has high lying *d* AOs, back donation determines the preferential conformation. On the other hand, if the metal has low lying *d* AOs, the ligand field interaction determines the most stable conformation. In contrast, for an ae-substituted trigonal bipyramid, the back donation factor remains dominant whatever the ligand type at the metal and substituent at the carbene.

(b) 1,2-Shift and cycloaddition reactions of transition metal carbenes

The 1,2-shift of a hydride or alkyl group

$$L_nRM{=}CH_2 \rightleftharpoons L_nMCH_2R \tag{50}$$

its microscopic reverse, the so-called α-elimination reaction as well as the cycloaddition reaction

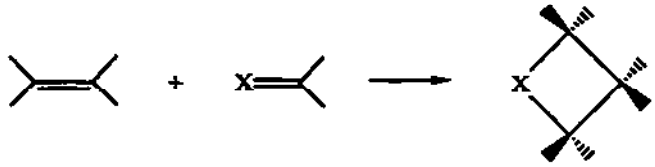

(51)

have been implied as key steps in several catalytic processes, such as the Ziegler–Natta polymerization and olefin metathesis.

An HFS study was carried out by Ziegler et al. [476] on the intramolecular migration of hydride and methyl toward CH_2 in $RMn(CO)_4CH_2$. Both migrations were found to be exothermic processes, by 27 and 17 kcal mol^{-1}, respectively. Moreover, the kinetic products, **60** and **61**, were found to be more stable than the parent hydride and methyl complexes.

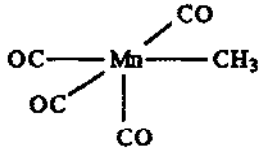

60

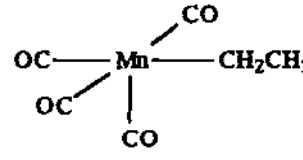

61

Carter and Goddard [477] have used ab initio calculations to investigate the migratory insertion of CH_2 into an adjacent Ru–H bond. Such migratory insertions have long been proposed as chain initiation and propagation steps in the Fischer–Tropsch synthesis of hydrocarbons [478]. They found that the reaction pathway depicted schematically as

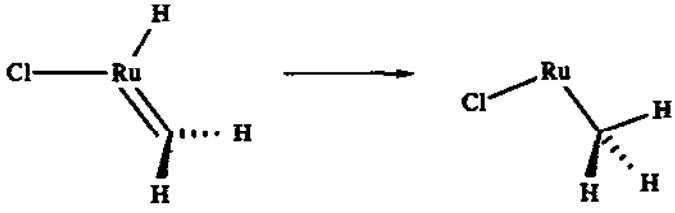

62 **63**

is characterized by a low activation barrier (11.5 kcal mol^{-1}) and is thermodynamically favourable with an exothermicity of 7.1 kcal mol^{-1}. The exothermicity, activation barrier and transition state geometry were calculated at five levels of theory as shown in Fig. 20. The results obtained also suggested that for Ru the reverse reaction of α-hydrogen elimination is subject to a barrier of 18.6 kcal mol^{-1}, which is consistent with the fact that α-H elimination most often occurs for the early transition metals. The related reaction of CH_2 insertion into a Ru–R bond suggests an exothermicity of

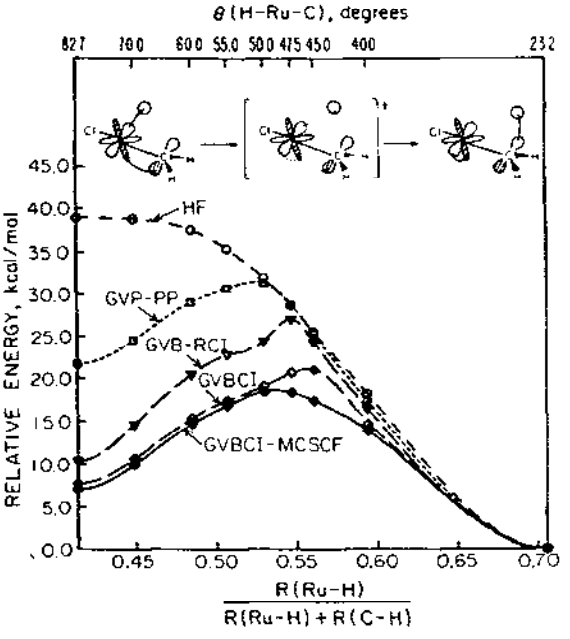

Fig. 20. Reaction coordinate for the insertion of CH_2 into Ru–H in $Cl(H)RuCH_2$ to form $ClRuCH_3$ at five different computational levels. Reproduced with permission from ref. 477.

4.9 kcal mol^{-1} and probably a higher activation barrier than for H, due to the necessary reorientation of the R upon migration from Ru to CH_2 [479]. In addition, the calculations suggest that late transition metals undergo CH_2 insertion relatively easier, while metal alkylidenes of the early transition metals do not insert into M–R bonds, probably due to the much greater strength of the M–C π bond.

Rappé and Goddard [480] have also provided energetics for the cycloaddition reaction (51) through high quality ab initio calculations. They have found that ΔH_{300} is -34.5, 17 and 8 kcal mol^{-1} for $X=Cl_2Ti$, Cl_4Cr and Cl_4Mo, respectively. Moreover, they reported the structures of metallacyclobutanes, which, in contrast to the common assumption of being strongly puckered, were found to be planar. The calculated geometrical parameters

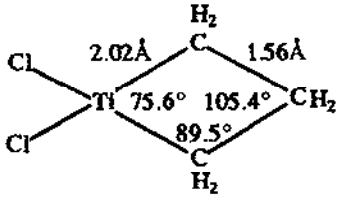

64

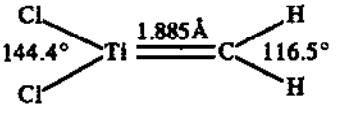

65

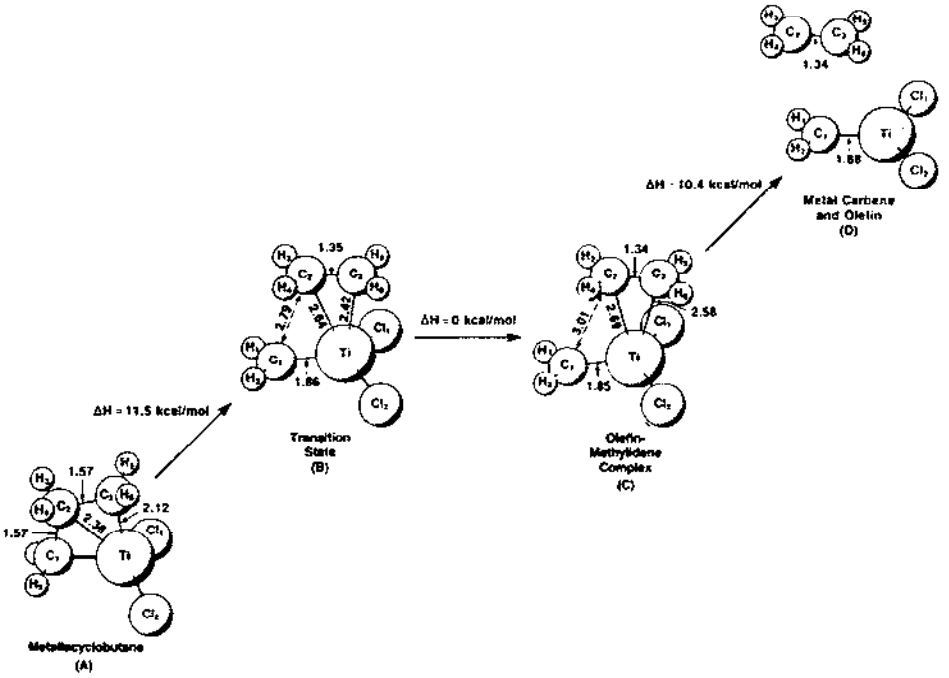

Fig. 21. Calculated geometries and enthalpy changes (at 298 K) for metallacyclobutane degradation to metal carbene and olefin. Reproduced with permission from ref. 336.

for both the metallacyclobutane and the metal alkylidene complex (for X = Cl_2Ti) are shown in **64** and **65**.

The isomerization of dichlorotitanacyclobutane, **64**, to its corresponding olefin–titanium methylidene complex, has been investigated by Upton and Rappé [336] using GVB-CI calculations. The calculated geometries and enthalpy changes (ΔH_{298}) for all species involved in the reaction path are shown in Fig. 21. It is clear that the transition state is essentially degenerate with the product state, there is no activation barrier for the isomerization process and the metallacycle is more stable than the olefin–alkylidene complex.

(c) Carbene coupling and decoupling processes on metal centres

An elegant analysis of the coupling of two methylene groups bound to a 'naked' transition metal centre, such as in $W(CH_2)_2$, has been reported by Hoffmann et al. [481,482]. From this basic picture, the restoration of the ligands leads to an understanding of the effects that a change of metal, electron count, metal framework, ligand, ligand geometry, or organic framework has upon the overall reaction. Thus, the coupling/decoupling processes

(52)

were found to be controlled by the relative location of the carbene $2b_2$ MO and the metal a_2, b_1 and/or $3a_1$ orbitals, as seen in the orbital correlation diagram in Fig. 22. The reaction becomes allowed for d^4 and d^6 electron counts, with small barrier for biscarbene–olefin interconversion, independently of which side of the reaction is thermodynamically more stable.

In a similar manner, Hofmann [417] studied the octahedral d^6 bis-carbene $(CO)_4Cr(CH_2)_2$ complex. The calculated potential energy surface for the least motion (C_{2v}) coupling/decoupling process, shown in Fig. 23, indicates the olefin complex with 16 valence electrons to be more stable.

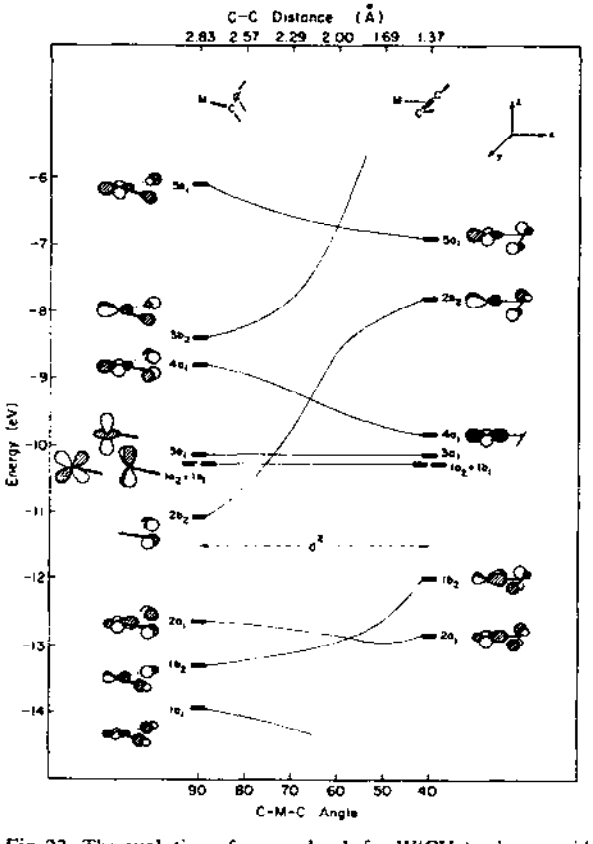

Fig. 22. The evolution of energy levels for $W(CH_2)_2$ along an idealized coupling coordinate. Reproduced with permission from ref. 482.

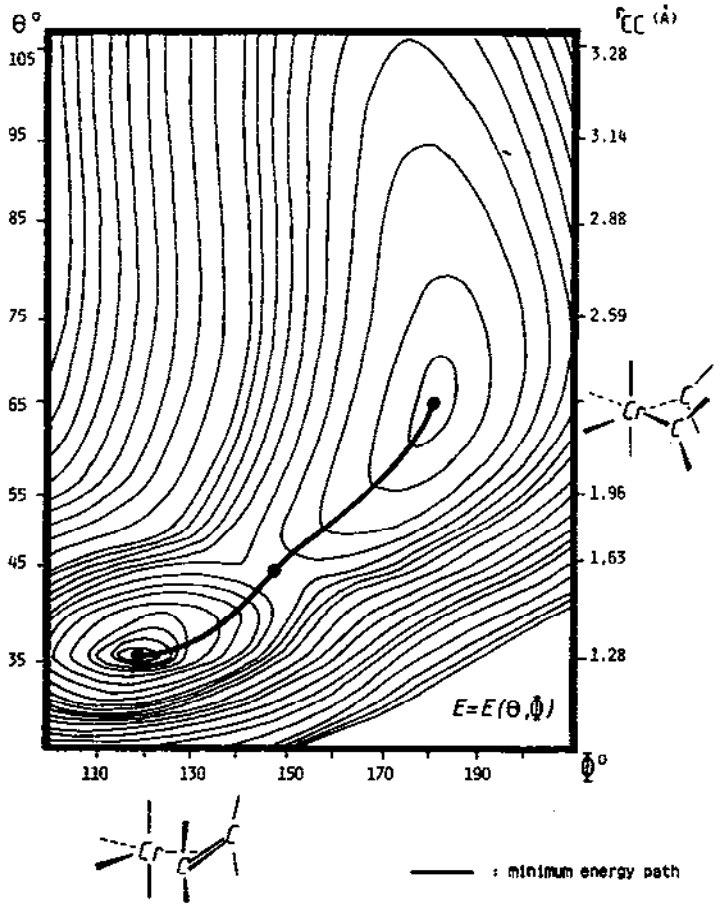

Fig. 23. Potential energy surface for the least motion (C_{2v}) interconversion between $(CO)_4Cr(CH_2)_2$ and $(CO)_4Cr(C_2H_4)$. Reproduced with permission from ref. 417.

The low energy barrier between the two structures **66** and **67** (~10 kcal mol^{-1} even for the least motion path) suggests that carbene–carbene coupling in systems electronically comparable with **66** should occur readily, leading to 16 electron olefin complexes and finally to the corre-

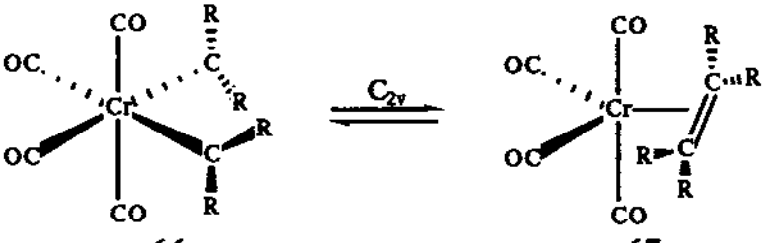

sponding 18 electron species after binding an additional ligand. Although a d^6 electron count makes the least motion process symmetry forbidden, the presence of π-donor substituents on the carbenes or the olefin invokes symmetry restriction even in C_{2v}. This is evident from the potential energy surface, where only one minimum is found corresponding to the bis-carbene system.

(d) Olefin metathesis

The olefin metathesis reaction, formally involving a simultaneous cleavage of two olefin double bonds followed by the formation of the alternate double bonds, in the presence of the appropriate metal complex, is one of the most intriguing and best studied catalytic reactions in organometallic chemistry [483–485]. The currently accepted mechanism involves a metal–alkylidene (carbene) complex as the active chain-carrying catalyst that reacts with an olefin to form the product olefin as shown in the scheme:

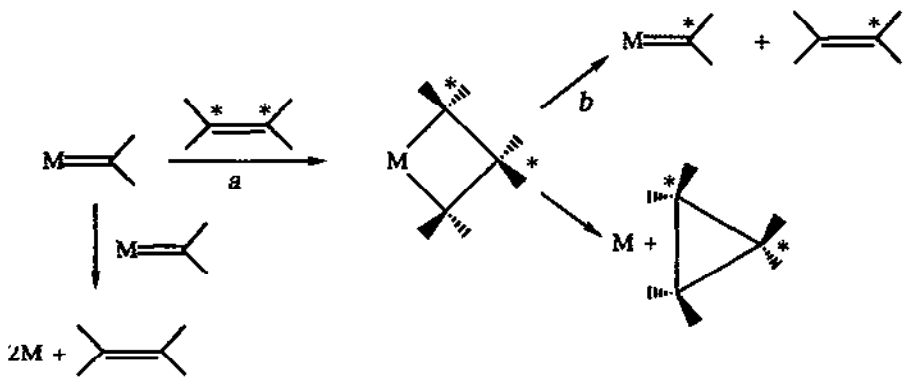

(53)

Until a few years ago, the mode of generation of the active chain carriers was generally obscure, and even metal–carbene complexes when used, e.g. $Ph_2C{=}W(CO)_5$, required activation by heat, light or a cocatalyst. In the last few years, several groups have been able to prepare well-defined metal–carbene and metallacyclobutane complexes capable of inducing metathesis reaction either by themselves or in the presence of a Lewis acid.

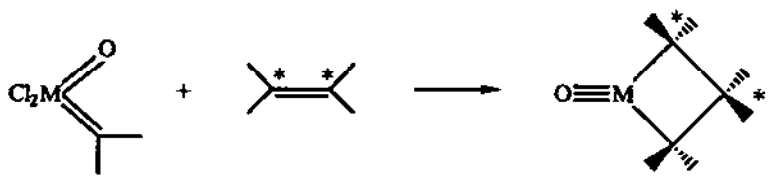

68 **69**

Using accurate ab initio methods, Rappé and Goddard [328,329] have calculated bond energetics and reaction enthalpies for several possible pro-

cesses involved in olefin metathesis reactions. The results of the calculations suggest that oxo-alkylidene complexes formulated as **68** are the active chain carrying metathesis catalysts for the high valent Mo, W and Re complexes, and that the oxygen ligand is intimately involved in the catalytic process. Such an oxo-alkylidene complex favours formation of metallacycles because of conversion of the double bond spectator oxo group in **68** to a triple bond in **69** (which is stronger by 31 kcal mol^{-1} for Cr and 23 kcal mol^{-1} for Mo). Indeed, the calculations lead to just this result with $\Delta G_{300} = -20$, -24 and -18 kcal mol^{-1} for M = Cr, Mo and W, respectively. On the other hand, the potential side reaction

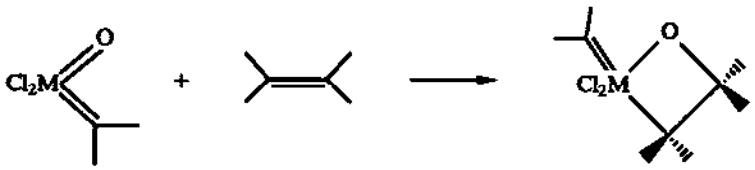

70

is much less favourable ($\Delta G_{300} = +12$, $+2$ and $+0$ kcal mol^{-1} for M = Cr, Mo and W, respectively) because here the spectator group is an alkylidene that provides only a double bond in both **68** and **70**. Moreover, the cycloaddition step postulated in the Herisson–Chauvin mechanism [486] was found to be unfavourable with $\Delta G_{300} = +25$, $+15$ and $+10$ kcal mol^{-1} for M = Cr, Mo and W, respectively.

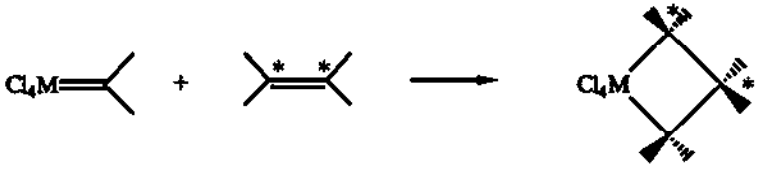

71 **72**

Considering that experimental metathesis solutions generally contain either Lewis bases (e.g. Cl^-, amines, phosphines) or Lewis acids (e.g. aluminium alkylchlorides), Rappé and Goddard have also studied the solution effects on the reaction energetics and profiles. Combining the estimated solvation effects with the calculated gas phase energetics, they proposed the full catalytic cycle for olefin metathesis in the presence of either Lewis bases or Lewis acids illustrated for W oxo-alkylidene complex in Fig. 24. Finally, they suggested that oxo-alkylidene complexes are formed on supported molybdate and tungstate catalysts, and that dioxo precursors can provide a convenient route to formation of well-defined surface catalysts for olefin metathesis and oxidation reactions.

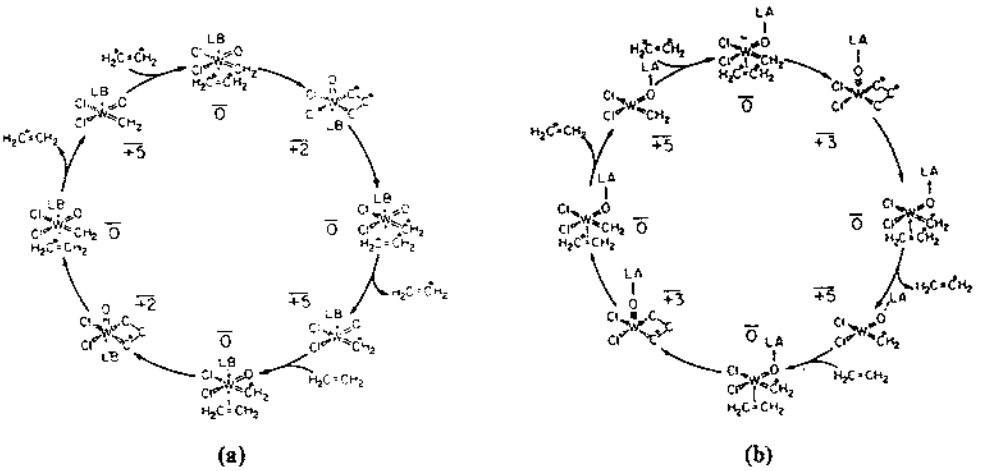

Fig. 24. The full catalytic cycle for olefin metathesis by W oxo-alkylidene with (a) Lewis base and (b) Lewis acid present (energies are ΔG_{300} in kcal mol^{-1}). Reproduced with permission from ref. 329.

The geometric and electronic structures of $MoOCl(CH_3)_3 \cdot AlH_3$ and $MoOCl(CH_3)(CH_2) \cdot AlH_3$, presenting reactive intermediates in the metathesis of olefins catalysed by oxo-alkyl complexes, have been investigated through ab initio LCAO-SCF-MO calculations carried out by Nakamura and Dedieu [487]. The binding of the Lewis acid, AlH_3, to various ligands (O, Cl, CH_2) has been examined and oxo ligand–Lewis acid binding is preferred. Moreover, the influence of Lewis acid binding on reactivity is also discussed on the basis of the corresponding geometric and electronic structure modifications.

Eisenstein and Hoffmann [488] also studied the olefin metathesis reaction pathway using the EHMO method. The set of complexes they examined included $L_4M(CH_2)(C_2H_4)$ (M = Fe, Mo, W; L = Cl, CO, H) and $Cp_2Ti(CH_2)(C_2H_4)$. Analyzing the electronic and geometrical features of the metallacyclobutane formation they showed that: (i) in a metal–carbene–olefin complex there should be a strong electron count and transition series dependence of the relative orientation of the carbene and ethylene ligands, with some of them being active in metathesis; (ii) for many electron counts, the metallacyclobutane form is substantially less stable than the olefin–carbene. However, this result for $Cp_2Ti(CH_2)(C_2H_4)$ is diametrically opposed to the results of other theoretical work [336,474,480].

The electronic structure and chemical reactivity of a number of cyclic carbenes, corresponding either to metallacyclopropene, **73**, or dimetallacyclopropane, **74** complexes have been investigated recently [489,490].

Metallacyclopropene complexes are formed by nucleophilic attack at a coordinated alkyne carbon leading to the conversion of the alkyne to η^2-vinyl ligand. Templeton and coworkers [489] showed, by EHMO calcula-

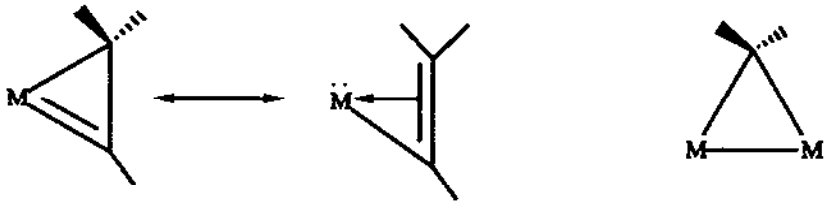

73 **74**

tions, that η^2-vinyl ligands resemble alkynes in their interactions with a single metal centre.

The interconversion of a 1-alkyne complex into a vinylidene via a 1,2 hydrogen shift has been examined by Silvestre and Hoffmann [491] with the use of the EHMO method. The process is represented as:

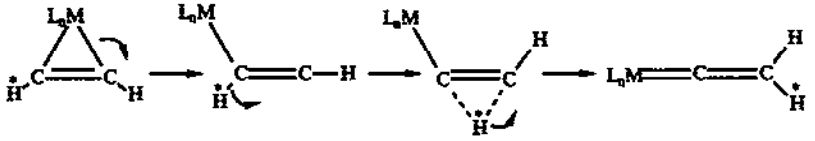

75 **76**

An alternative pathway involving oxidative addition leading to a hydrido-acetylide species followed by hydride migration to the far carbon atom was found to be of much higher energy.

Finally, an important class of dimetallacyclopropane complexes are those based upon the piano-stool dimer frameworks, formulated as $[CpM]_2L_n$, exhibiting a rich and diverse chemistry. It is important that a series of closely related methylene-bridged piano-stool dimers reacting with strong acids yields a variety of results. Thus, $[CpMn(CO)_2]_2(\mu\text{-}CH_2)$, **77**, does not react, $[CpFe(CO)]_2(\mu\text{-}CO)(\mu\text{-}CH_2)$, **78**, affords a compound with an agostic methyl-bridged cation, **79**, and $[CpRh(CO)]_2(\mu\text{-}CH_2)$, **80**, results in the formation of a hydride-bridged cation, **81**, according to the equations:

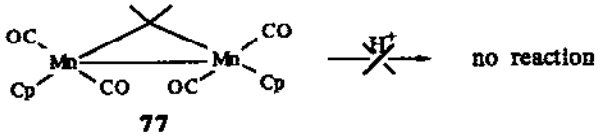

77

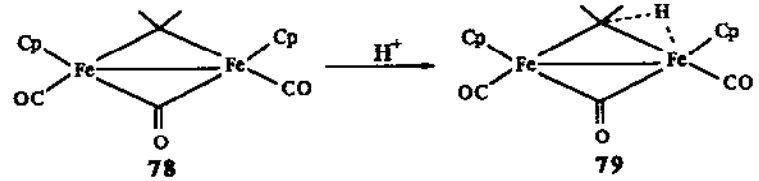

78 **79**

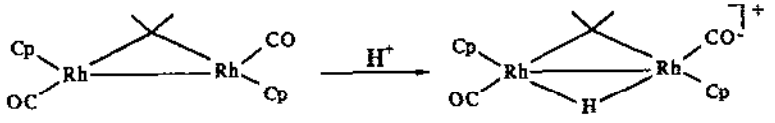

80 **81**

In order to understand such a diverse reactivity, Bursten and Clayton [490] have calculated the electronic structures of **77**, **78** and the cobalt analogue of **80** using the non-empirical Fenske–Hall MO method. The results obtained in conjunction with the FMO theory of chemical reactivity showed that the FMOs as well as the Mulliken atomic charges are critical in determining the kinetic pathway (charge or orbital controlled) of the electrophilic attack by the proton electrophile on the hydrocarbyl-bridged dimers. The HOMOs of **77** and **78** are similar, corresponding to M–M π^* MOs, **82**, inaccessible to incoming electrophiles, suggesting a charge controlled interaction. In contrast, for the cobalt compound the HOMO, **83**, being sterically accessible with an orientation toward the open bridging position, facilitates the formation of the observed thermodynamic product through a frontier rather than a charge controlled electrophilic attack.

82 **83**

(e) The carbenoid character and chemical reactivity of coordinated acyl ligands

Transition metal coordinated acyl ligands exhibit a unique reactivity pattern, which has often been rationalized in terms of carbenoid character of the M–C bond [492,493]. Thus, they react with nucleophiles and undergo deprotonation of the acyl ligands, ketone ligand formation, reductive CO coupling and acyl to ketene or ketenimine transformations. The origin of the reactivity pattern of metal acyl complexes has been traced theoretically by Dedieu and Morokuma [402], Tatsumi et al. [415] and Block et al. [464]. Moreover, the mechanism of acyl ligand coupling to form enediolate ligands in the case of the carbonylation process of $CpZr(CH_3)_2$ has been thoroughly analyzed by Hoffmann [417].

Fenske–Hall calculations carried out by Block et al. [464] on the carbene $(CO)_5Cr(OCH_3)CH_3$ and the acyl $(CO)_5MnCOCH_3$ complexes indicated that the LUMOs of the two compounds differ both in energies and localization. The spatial localization of the LUMO in the carbon atom of the carbene complex explains its electrophilic character, whereas for the acyl complex the

LUMO lies in a band of closely spaced unoccupied levels associated with both the acyl carbon and coordinated CO, inhibiting any prediction of the site of nucleophilic attack in the complex.

The reactivity pattern of $(CO)_4Fe(CHO)^-$ towards electrophiles and nucleophiles has been investigated by Dedieu and Morokuma [402] using ab initio SCF-LCAO-MO calculations. In particular, they compared the electronic structures of the formyl complex, its protonated form $(CO)_4$ Fe(CHOH) and the hydroxycarbonyl system $(CO)_4Fe(COOH)^-$. Using fragment deformation density maps in the plane of the Fe—C π bond, they found that the formyl ligand acts mainly as a σ donor, introducing a negative charge on Fe and the formyl oxygen atom.

Tatsumi et al. [415] showed that the reactivity of the η^2-acyls does not depend on reaching the oxycarbene isomers, but may be traced to a low lying carbenium-ion-like acceptor orbital in the undistorted η^2-acyl structure. Indeed, there is a similarity between an η^2-coordinated acyl and a carbene in that both contain a low lying LUMO, **84** vs. **85**, the large component of which is a carbon p_π AO.

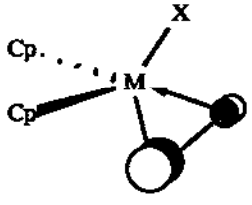

84

85

Obviously, all theoretical results are in support of the carbenoid character of the coordinated acyl ligands.

(vii) Transition metal carbynes. α-Nucleophilic and β-electrophilic additions

Metal carbyne (alkylidyne) complexes have been prepared for a variety of metals and *d* electron configurations [494,495], as typified by the Fischer and Schrock examples, $(CO)_4BrCr{\equiv}CPh$ [496] and $(\eta^5\text{-}C_5Me_5)(Me_3P)_2Cl$-Ta≡CPh [497], respectively. The carbyne moiety (CR) has been considered a strong π-acceptor when counted as a cationic analogue of CO, $[:CR]^+$, or as a π-donor when counted as a trianion analogue to O^{2-}, $[:\dot{\dot{C}}R]^{3-}$. Hoffmann et al. [481,482] have circumvented the dilemma by considering the neutral carbyne as a building block, :ĊR, with two electrons arbitrarily assigned to the σ-donor orbital and the remaining electron assigned to the two orthogonal carbon $p\pi$ AOs. Other formalisms are also available which stress yet other aspects of M≡CR binding: ·ĊR is primed for formation of

three covalent bonds and $[:\ddot{C}R]^-$ can be considered to be crudely isolobal with RC≡CR, η^2-CH=CH_2^- and η^2-C=C=O^- [489].

Few theoretical studies address the electronic structure of metal–carbyne complexes. Excellent papers by Kostic and Fenske [498,499] have established the binding modes of carbynes in many coordination environments. They concluded that CR^+ is a stronger π-acceptor than CO, and that the frontier orbitals dictate reactions of transition metal carbyne complexes. Along this line, experiments have been proposed by which new frontier controlled reactions of carbyne complexes may be discovered. Nakatsuji and coworkers [470], using ab initio SCF-MO calculations, investigated the electronic structure and chemical reactivity of $(CO)_5Cr{\equiv}CH^+$ and $Cl(CO)_4Cr{\equiv}CH$. In both carbynes, the linear geometry was found to be more stable than the bent one. The Cr≡C bond was found to be a triple bond with a bond length of 1.62–1.65 Å. The atomic charges of the carbyne carbons were calculated to be negative (−0.42 and −0.31 for the neutral and the cationic species, respectively), whereas those of the Cr central atom were positive (+0.90 and +1.06, respectively). The charge distribution could not explain the different chemical reactivity reported for the cationic and neutral complexes, since it has been pointed out [470,499] that carbyne complex reactions are frontier controlled. For $(CO)_5Cr{\equiv}CH^+$, the LUMO has the maximum coefficient at the carbyne carbon atom, which is the electrophilic centre. On the other hand, for $Cl(CO)_4Cr{\equiv}CH$, both the LUMO and NLUMO being very close energetically, could be involved in the nucleophilic attack of the complex. Since the LUMO has its maximum coefficient at Cr and NLUMO at both the carbyne carbon atom and Cr, the electrophilic behaviour of the neutral species is evident.

Harrison and coworkers [207,500] have studied the electronic and geometric structure of several 'naked' transition metal carbyne cations by high quality ab initio methods. They concluded that all species studied are characterized by an M≡C triple bond of remarkably similar length (1.772, 1.745 and 1.758 Å for $CrCH^+$ ($^3\Sigma^-$), VCH^+ ($^2\Delta$) and $TiCH^+$ ($^1\Sigma^+$), respectively), except ScH^+ ($^2\Pi$) which exhibits a double bond with a bond length of 1.940 Å and D_e of 79.2 kcal mol^{-1} relative to the $^2\Pi$ state of CH. The calculated D_e values for the other species were 95.9, 90.9 and 53.7 kcal mol^{-1} for $TiCH^+$, VCH^+ and $CrCH^+$, respectively. The high covalent bonding of $TiCH^+$, VCH^+ and $CrCH^+$ is analogous to that of the 'Schrock' type alkylidyne complexes and therefore these species may be considered as methylidyne cations. Moreover, by comparing their BDEs, an intrinsic $M^+{\equiv}CH$ bond of about 146 kcal mol^{-1} has been suggested. In addition, the electron distribution in all three species was found to be remarkably similar with the $3d_\sigma$ orbital on the metal containing ~0.5e, while each d_π orbital hosts ~1.10e with the $4s$,$4p_\sigma$ occupancy varying from 0.1 to 0.2e.

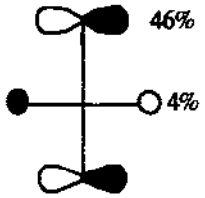

86

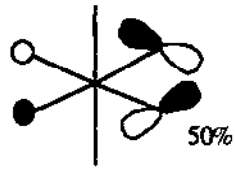

87

The metal–ligand π interactions in Group VI model compounds have been investigated by Templeton et al. [333] using the EHMO method. Calculations on both *cis*- and *trans*-$[W(CH)_2H_4]^{4-}$ confirm the qualitative expectation that the HOMO consists of a non-bonding carbon 2*p* combination for both isomers. These HOMOs shown in **86** and **87** dictate the chemical reactivity of biscarbynes towards nucleophiles and electrophiles. Thus, even though they are not at particularly high energies for filled FMOs, it is anticipated that the carbyne carbons will be very nucleophilic if these orbitals are filled, or very electrophilic if vacant. Calculations on the mixed *cis*- and *trans*-$[W(CH)(O)H_4]^{3-}$ indicated that these oxo-carbyne complexes will exhibit a d_π conflict with the covalency requirements of the carbyne causing electron density to build up on the terminal oxygen. For the *trans* isomer, the degenerate HOMO pair, **88**, at -11.81 eV results from competition between the oxo ligand and the carbyne for π bonding. For the *cis* isomer, the HOMO, **89**, being O and C 2*p* combinations, lies near -12 eV and ligand distortion could further stabilize them. The calculations suggest that *cis*-(oxo-carbyne) complexes may be preparable.

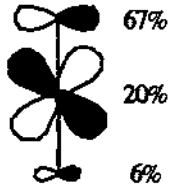

88

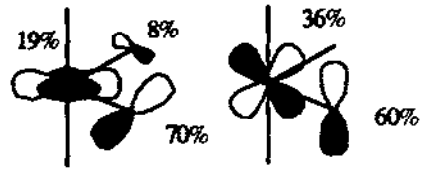

89

Biscarbyne model complexes have also been examined by Hoffmann et al. [481,482] as part of a ligand coupling study. Employing the neutral CR formalism, they found that melding adjacent carbyne ligands into an alkyne was forbidden at d^6 metal centres, allowed but energetically unfavourable in d^4 complexes and both allowed and favourable in d^2 monomers. These theoretical conclusions were verified experimentally by McDermott and Mayr [501] who in attempting to prepare a W biscarbyne system by transforming a CO ligand of the $(CO)_3(Ph_3P)BrW{\equiv}CPh$ complex into carbyne, obtained the expected complex involving a coordinated methylphenylacetylene as a

result of the carbyne–carbyne coupling reaction. It should be noted that, although numerous octahedral d^4 and several d^2 alkyne complexes are known experimentally, stable mononuclear octahedral bisalkynes of any electron count are rare [502].

Despite the great number of available pathways, electrophilic β-addition to convenient unsaturated ligands, such as isocyanides or alkynyl ligands, constitutes an increasingly important route for carbyne complexes [503–505], and has therefore also attracted the interest of theoretical studies [468,506,507].

The bonding, structure, properties and reactivity patterns of isocyanide and aminocarbyne type complexes involved in the synthetic pathways

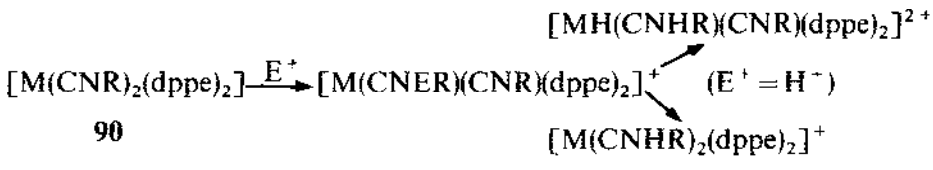

90

(M = Mo or W, R = alkyl or aryl and dppe = $Ph_2PCH_2CH_2PPh_2$)

and

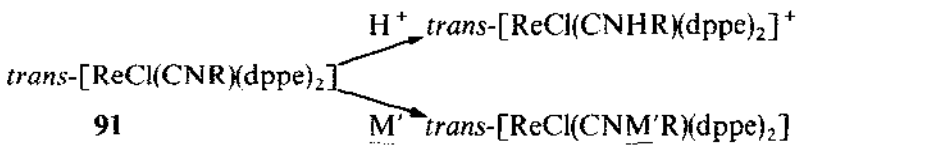

91

(M′ = $CoCl_2(THF)$, $ReOCl_3(PPh_3)$ or WCl_4L_2; L = PPh_3 or $PEtPh_2$)

were investigated with the aid of the EHMO-SCCC method in relation to frontier orbitals theory [507,508]. It is important that the conformation of the ligand might play a crucial role in determining the final products of reactions between Re or Mo isocyanide complexes and electrophiles. For the Re complex, **91**, both the nature of its FMOs and the charge distribution suggest the existence of two competing nucleophilic centres in the complex, those of the Cl and N atoms. However, when the isocyanide ligand bends, the nucleophilicity of the N atom increases while that of Cl decreases. The situation for the Mo bis(isocyanide) complexes, **90**, is analogous. According to the nature of the FMOs and the charge distribution, these also exhibit two competing nucleophilic centres located on Mo and N atoms. Again, when the isocyanide ligand bends, the nucleophilicity of N increases while that of Mo decreases. The opposite is true for linear isocyanide ligands. Summarizing, it could be suggested that bending an isocyanide ligand increases its nucleophilicity at the β-position, except upon ligation to electron

poor metal sites. These compounds are susceptible to nucleophilic attack at the α-position (the ligating atom).

The aminocarbyne complexes, being the products of β-electrophilic addition to isocyanide complexes, were found to possess electrophilic character, easily undergoing α-nucleophilic attack at the ligating atom. In contrast to β-electrophilic addition, α-nucleophilic addition was found to be frontier controlled as is known for other α-additions to carbene [464,470] or cationic carbyne [470,498] complexes.

(viii) Transition metal nitrenes, phosphinidenes and phosphirenes. Ligand stabilization processes

Nitrenes, RN, and phosphinidenes, RP, usually being transient species, could be considered isoelectronic to the carbynes if the latter, for electron count purposes, are considered in their anionic form R–C:$^{(-)}$. Introduction of π-donor substituents (e.g. NH_2, PH_2, OR, etc.) in the α-position stabilizes the nitrene or phosphinidene ligands, though their isomeric forms with multiple bonds, i.e. HN=NH, HN=PH and HP=PH in both their *cis* and *trans* conformations are always energetically preferred [509]. However, these ligands could be even further stabilized through transition metal complexation. These particular stabilization processes have been thoroughly studied with the aid of orbital correlation diagrams obtained through EHMO and ab initio calculations [510–512].

Trinquier and Bertrand [510] have presented a detailed analysis of orbital interactions occurring when phosphinidene and nitrene ligands are bound in an end-on fashion (η^1) to various d^n L_mM fragments. The most favourable fragments are those allowing both the ligand's NHOMO and HOMO to interact with their appropriate orbitals (σ- and π-dative bonding) and the back donation of a metal d pair into the ligand's LUMO. This is accomplished with d^4 ML_5 (C_{4v}), d^6 ML_4 (C_{2v}) and d^8 ML_3 (C_{3v}) fragments and to a lesser extent with d^6 ML_4 (C_{3v}), d^6 ML_3 (C_{2v}) and d^8 ML_2 (C_{2v}) fragments.

Considering the interaction diagram of H_2P–P with a d^n ($n=4$ or 6) ML_5 (C_{4v}) fragment shown in Fig. 25, it is easy to understand why a d^4 ML_5 fragment is more favourable than a d^6. In the former, despite the stabilizing 2e-2O interactions of the a_1–a_1 and b_1–b_1 type, the b_2–b_2 interaction is also a stabilizing 2e-2O interaction. The latter is a destabilizing 4e-2O interaction for d^6 ML_5 complexes, resulting in less favourable orbital interactions. However, upon bending the ligand, $\langle b_2|b_2\rangle$ overlap is minimized and therefore more stable d^6 $(H_2P–P)ML_5$ complexes are obtained due to the cancelling of the repulsive b_2–b_2 interactions. Analogous results have also been obtained by Pfister-Guillouzo and coworkers [511,512] who investigated the electronic structure and chemical reactivity of $HPCr(CO)_5$ and $HPFe(CO)_4$ complexes

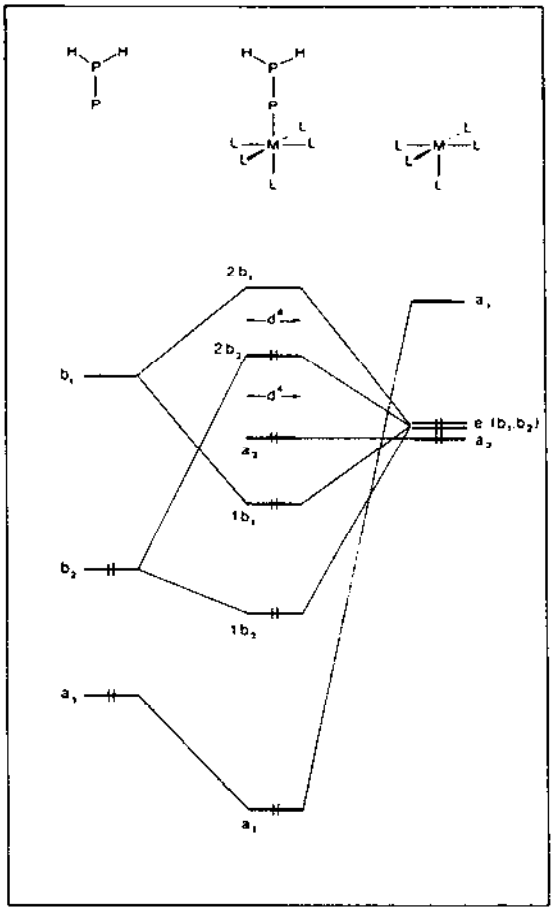

Fig. 25. Interaction diagram for d^6 $H_2PP{-}ML_5$. Reproduced with permission from ref. 510.

using both EHMO and ab initio calculations. For $HPCr(CO)_5$, the preferential structure is that exhibiting a bending phosphinidene ligand with $H\hat{P}Cr = 125°$ and $d(Cr{-}P) = 1.9$ Å. Moreover, the stabilization of the phosphinidene ligand stems from orbital interaction diagrams, in fact, from both the decreasing of destabilizing interactions and the participation of secondary stabilizing interactions. Ab initio calculations (at the PSHONDO level) showed that, although the phosphinidene ligand, HP, has a triplet ground state (singlet–triplet separation of about 26.5 kcal mol^{-1}), the singlet state is more stabilized (energetically favoured by 12.5 kcal mol^{-1}) upon its complexation. This agrees with the singlet phosphinidene hypothesis previously postulated for interpreting its chemical behaviour during trapping reactions [513].

Bending of the phosphinidene ligand is also favoured in the case of the

$HPFe(CO)_4$ complex. For the trigonal bipyramidal complex the calculations showed that the geometry with the HP ligand in the equatorial position is more stable ($\sim$17 kcal mol^{-1}) owing to the stronger π back L$\leftarrow$M charge transfer.

In general, alkyl- and aryl-phosphinidene ligands produce strong bonding interactions to metal-containing fragments, with the strongest ones towards d^8 ML_3 (C_{3v}) fragments resulting in the formation of tetrahedral complexes. In contrast, nitrenes are less bound, because of the much weaker overlaps all bonding interactions become weaker [510].

Bridging phosphinophosphinidene to d^6 ML_5 fragments to form dinuclear complexes has been calculated to be a favourable process, mainly due to strong three-centre orbital interactions. The μ_2 dinuclear compounds with d^6 ML_5 metal-containing fragments were found [510] to have about the same stabilities as the terminally bound mononuclear compounds involving d^4 ML_5 fragments. It is obvious then that d^6 ML_5 fragments would prefer the bridging mode of binding to phosphinidenes, while d^4 ML_5 fragments would prefer to form mononuclear complexes with terminally bound phosphinidenes. This should also hold true for all other favourable fragments.

Pfister-Guillouzo and coworkers [511,512] have also studied the chemical reactivity of $HPCr(CO)_5$, analyzing the FMOs of the complex. Their observations, compared with those of the corresponding carbene complexes, indicate that the chemical reactivity of the more electropositive phosphinidenes could be explained as charge controlled rather than frontier orbital controlled.

Finally, Pfister-Guillouzo and coworkers [511,512] have investigated the factors responsible for the stabilization of phosphirene ligands upon their complexation. The formation of a stable phosphirene complex has been observed during the trapping of the $HPCr(CO)_5$ complex with acetylene [513]. The stabilizing interaction involves the p^* orbital of the phosphorus atom, the π_2^*-MO of acetylene and the d_{xz} AO of Cr. This π metal–phosphorus transfer causes a greater σ delocalization on the phosphirene ring. Photoelectron spectra of stable phosphirene complexes have also been analyzed, further supporting the origin of the stabilization processes occurring upon complexation of the ligands.

(ix) Transition metal complexes of inert ligands. Dinitrogen and carbon dioxide activation and reactivity

(a) Dinitrogen fixation and activation

Dinitrogen fixation and activation, being a reductive process of both biological importance [514] and large scale industrial interest [515,516], has been actively investigated theoretically at various levels of sophistication.

Since coordination to transition metal ions is one of the most powerful ways of activating inert molecules [517,518], several MO studies of transition metal dinitrogen complexes have been carried out [124,125,519–527] to understand the coordination modes and bonding nature, stereochemistry and reactivity, in particular its reduction to N_2H_4 (or further to NH_3) under mild conditions. Theoretical studies performed prior to 1981 have been exhaustively reviewed by Pelikan and Bŏca [519]. The authors have also presented their own results on the geometric and electronic factors of dinitrogen activation by transition metal complexes, using CNDO/2 calculations over an extensive series of dinitrogen-containing complexes. Based upon the calculated values of several quantum chemical indices, such as the Wiberg index, W_{N-N}, the bicentric part of the total molecular energy, E_{N-N}, the π-acceptor index, $X(\pi_A)$, representing the electron density on the N_2 π^*-MO, the total dinitrogen charge, $Q(N_2)$, the $3d$ electron population, d^x, the atomic spin densities, $\rho(A)$, the strength of the N–N bond and the spatial distribution of the electrostatic potential around the complex, the most important factors influencing dinitrogen activation were found. These are (i) the proton numbers, Δn, of the central atom: elements with low electronegativity will support N_2 activation. (ii) the oxidation state of the central atom: low oxidation states will support N_2 activation. (iii) the spin state: low spin or medium spin states will support 1e- and 2e-N_2 activation. (iv) the nature of the equatorial ligands, L_e: the first row donor atoms (O,N) of L_e increase the degree of N_2 activation relative to the second row atoms (S,P). Moreover, anionic L_e support a degree of activation over the neutral ligands.

Hori et al. [520], using ab initio SCF-LCAO-MO calculations, reported that the η^1-end-on N_2 coordination in the $Ni(O_2)(N_2)$ complex was more stable than the η^2-side-on. They have also analyzed the mechanism of N_2 rotation and the nature of bonding between Ni and N_2 using the energy decomposition technique of Kitaura and Morokuma. Also, Hori and coworkers [521,522] have discussed the N_2 reduction on transition metal complexes. In particular they have investigated the effect of protonation to dinitrogen complexes of Cr formulated as $Cr(PH_3)_4(N_2)$ using ab initio calculations. It was ascertained that protonation causes a remarkable rearrangement of the electron distribution in the N_2 moiety. The electron density in d_{xz} AO is mainly transferred to hydrogen s AO, leading to a strengthening of the N–N bond. On the other hand, π_x and d_{π_x}-π^* type polarizations are involved in the weakening of the N–N bond. The large protonation energy (351.3 kcal mol^{-1} for the N_2 complex compared with 115.9 kcal mol^{-1} for the free N_2 ligand) results from the existence of $d\pi$ as HOMO, which has the ability to transfer electrons to the hydrogen $1s$ AO. Hori and coworkers [522] also investigated the successive protonation steps, attempting to reveal the routes for NH_3 and NH_2NH_2 formation.

Blomberg and Siegbahn illustrated through CASSCF and CCI calculations on NiN_2 [523] that for the linear η^1-end-on structure, the DCD model is preferable, since only minor perturbation of Ni and N_2 occurs upon bonding (0.14e are transferred from d_π to π^* MO of N_2 and only 0.07e are involved in the σ donation). For the η^2-side-on structure, the bonding may be described by one covalent VB structure, since both large π transfer of nearly one electron and σ donation occur, resulting in the formation of a clear covalent bond between a Ni d_π AO and a N_2 π^* MO.

More recently, Sakaki et al. [124,125] reported an ab initio MO study of $RhCl(PH_3)_2L$ ($L = \eta^1$-end-on, η^2-side-on N_2, CO, HCN, HNC, NH_3 and C_2H_4), hoping to present a convincing discussion of the N_2 coordination modes and to characterize the N_2 and the Rh(I) coordinate bonds in comparison with Ni(0) with similar ligands. The calculations showed that the η^1-end-on N_2 complex is more stable than the η^2-side-on mode by ca. 16 kcal mol^{-1}. This stability results from the much larger electrostatic stabilization and slightly larger donor $N_2 \rightarrow Rh$ stabilization compared with the η^2-bonded complex; though both modes possess a similar degree of back donation. Moreover, it was found that the π back bonding interaction contributes to the dinitrogen coordination more strongly than the σ donor interaction and the relative importance of the π back donation to the σ donation is larger in N_2 than in other similar ligands such as CO, HCN and HNC.

Finally, a few theoretical efforts [524–527] have been directed towards understanding the bridging bonding mode of N_2 (μ-N_2) in binuclear complexes, being of crucial importance as key steps in catalytic dinitrogen activation. Thus, Kostic and Fenske [524] carried out non-empirical Fenske–Hall calculations on a series of dinuclear cyclopentadienyldicarbonyl complexes of Mn and Cr containing Ge, S, N_2 and PPh bridges. They suggested that the dinitrogen complexes are not centrosymmetric in solution and contain an N_2 ligand rather than two N atoms, with the π^* MO of N_2 being of crucial importance for its bonding to metals. The π-MO of N_2 does not seem to donate electrons to the metal atoms.

$L_4Mo{\equiv}N{-}N{\equiv}MoL_4$ **92** $L_4Mo{-}N{\equiv}N{-}MoL_4$ **93**

Correlated ab initio calculations have been used by Rappé [525,526] to study the effect of metal (Mo and W) and ligand (F, Cl, Br) on the relative stability of the two bridging dinitrogen isomers, **92** and **93** for $[L_4MoN]_2$ species. Valence bond structure **92** is expected to be more reactive than **93** since M–N π bonds should be more reactive than N–N π bonds. It was found that, although structure **92** is not the most stable isomer (the classical structure **93** being more stable by 21 kcal mol^{-1}), it is accessible kinetically (low activation energy) and thermodynamically. There is a pronounced

(26 kcal mol^{-1}) effect of hydrogen substitution for the molybdenum complexes, but even with halogen variation the inactive form is more stable than the activated (azine) form. For the tungsten analogues there is only a minor variation (9 kcal mol^{-1}) with halogen substitution, but for all these complexes the activated form is substantially more stable. Obviously, modification of Mo complexes is probably the more viable approach to obtain active dinitrogen catalysts.

In a recent report, Hoffmann and coworkers [527] observe an activated form of N_2 using EHMO theory. Based upon the energy variation as a function of nitrogen separation for the dinitrogen coupling reaction

$$Cl_4Mo{\equiv}N + N{\equiv}MoCl_4 \rightarrow Cl_4Mo{-}N{\equiv}N{-}MoCl_4 \qquad (54)$$

they found that a synthetic strategy to make a dinitrogen complex should be most favourable if the metal is a late transition metal. The calculated N–N distance is 1.35 Å in the bound minimum for both neutral $[Cl_4MoN]_2$ and anionic $[Cl_4MoN]_2^{2-}$ species.

(b) Carbon dioxide fixation and activation

Only a few molecular orbital studies have been devoted to carbon dioxide complexes of transition metals in the last decade [125,530,531], despite their potential interest for practical application in CO_2 fixation in organic substrates. In this light, the factors which control the formation and the structure of transition metal CO_2 complexes have been elucidated. One of the characteristic features of these complexes is the presence of several coordination modes, i.e. the η^2-side-on, **94**, the η^1-C mode, **95**, and the η^1-O end-on mode, **96**. All these bonding modes have been discussed in both an EHMO study of $[Co(NH_3)_4(CO_2)]^+$ [528] and ab initio MO studies of $Ni(PH_3)_2(CO_2)$, $Cu(PH_3)_2(CO_2)$ [122,125] and $[Co(alcn)_2CO_2]^-$ (alcn = $HNCHCHCHO^-$) [527,534,535] systems.

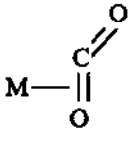

94

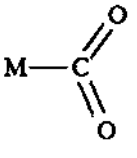

95

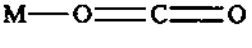

96

Sakaki et al. [122,125], using an energy decomposition analysis, showed that the coordinate MCO_2 bond in $Ni(PH_3)_2(CO_2)$ and $Cu(PH_3)_2(CO_2)$ is mainly stabilized by electrostatic and/or back bonding interactions. The back bonding stabilizes the side-on mode, whereas the electrostatic interactions favour the end-on mode. Therefore, when the metal ion has a sufficient Lewis

basicity such as in the $Ni(PH_3)_2$ fragment back bonding interactions become large to favour the side-on coordination. On the other hand, when the metal ion has a considerable positive charge as in the $Cu(PH_3)_2^+$ fragment, the end-on mode is preferred by the electrostatic interaction of Cu(I) with the negatively charged O atom of the CO_2 ligand. The η^1-C coordination mode is less stable for both complexes. However, this bonding mode of CO_2 was found to be favoured in $[Co(alcn)_2CO_2]^-$, due to the strong back bonding interactions [125,529,530], resulting from its HOMO which is mainly composed of the Co d_{z^2} orbital. Moreover, Sakaki and Dedieu [530] indicated that the driving forces for the bending of CO_2 upon its complexation to Co are the strengthening of the π back bonding interactions between the Co d_{z^2} orbital and the CO_2 π^* MO, the weakening of the 4e-2O $Co(d_{z^2})$–$CO_2(\pi)$ and $Co(d\pi)$–$CO_2(n\pi)$ destabilizing interactions, the presence of an alkali metal counter-cation between M^+ and CO_2 and the polarization of CO_2 by M^+ (M^+ = alkali metal cation). Finally, in a very recent communication, Sakaki and Ohkubo [531] reported on an ab initio MO study of CO_2 insertion into a Cu–H bond. Three complexes, namely $Cu(PH_3)_2(COOH)$, **97**, $Cu(PH_3)_2$-(OCOH), **98**, and $Cu(PH_3)_2(O_2CH)$, **99**, have been examined as possible products.

The compound **99** was calculated to be the most stable of all in accordance with experimental evidence and therefore it is the final product of the exothermic CO_2 insertion reaction into $CuH(PH_3)_2$. The results of the calculations also suggested a rather early transition state with four-centre-like character, and that CO_2 insertion into an M–X bond proceeds easily when X is electron-rich and the metal part can increase polarization, in agreement with experimental results.

(x) Transition metal complexes of other ligands. A few more bonding and reactivity problems

(a) Bonding and energetics of monoligated transition metal species with OH_2, NH_2, NH_3 and PH_3 ligands

Besides hydride and alkyl ligands, water (OH_2) and ammonia (NH_3), being also pure σ donor ligands, have been widely used as ligands in coordination chemistry. However, OH_2 and NH_3 differ from the hydride and alkyl ligands in that they are closed shell lone pair ligands and not open shell radicals. Monoligated transition metal species of both ML and ML^+ types (M = Cu, Ni, Fe, Sc, L = OH_2 or NH_3) have been thoroughly investigated by high quality ab initio calculations [266,360–363,532]. The calculated BDEs of the systems studied at the CASSCF and CCI level are summarized in Table 15. The range of BDEs (each relative to its own asymptote) for both $M(OH_2)$ and $M(NH_3)$ is only 2.8–11.3 kcal mol^{-1} for all the transition metals and states considered.

TABLE 15

Bond dissociation energies (in kcal mol^{-1}) for some $M(OH_2)$ and $M(NH_3)$ systems calculated at the CASSCF and CCI level

Compound	State	D_e(M–L)	Ref.
$Fe(OH_2)$	$^3A_2$	6.0	362
	$^5A_2$	2.8	362
$Ni(OH_2)$	$^1A_1$	8.8	362
		23.8	361
		5.0	363
$Ni(NH_3)$	$^3A_1$	10.8	362
	$^3A_2$	4.8	362
$Ni(OH_2)^+$	$^2A_1$	40.1	362
$Cu(OH_2)$	$^2A_1$	4.6	362
		0.8	210
$Cu(NH_3)$	$^2A_1$	6.7	360
$Sc(NH_3)^+$		36.8	537

The bonding nature of OH_2 and NH_3 to transition metal atoms has been analyzed by the CSOV technique [135]. In the light of the CSOV analysis, the bonding can be viewed as electrostatic and arising from the penetration of the ligand dipole into the metal charge cloud. This is also reflected on the calculated BDEs of model ML systems, where the ligands have been replaced by dipoles having the magnitude of the calculated OH_2 dipole moment [362]. For the positive ions $Ni(OH_2)^+$ and $Sc(NH_3)^+$, the electrostatic character of bonding arises from the attraction of the ligand lone pair by the positive charge and the charge–dipole electrostatic interaction.

Blomberg et al. [361] have also studied the bonding mode of the phosphine ligand, PH_3, a ligand with bonding characteristics intermediate between those of OH_2 and CO, in nickel complexes. They found that the bonding in $Ni(PH_3)$ has contributions from effects found in both $Ni(OH_2)$ and NiCO species. This is clearly shown in **100–102**, where the bonding characteristics of the three species can be compared:

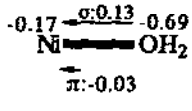

$^1A_1$: D_e = 23.8 kcal·mol^{-1}

100

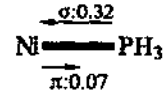

$^1A'$: D_e = 13.7. kcal·mol^{-1}

101

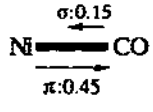

$^1\Sigma^+$: D_e = 29.9 kcal·mol^{-1}

102

It is clear that the σ interaction in $Ni(PH_3)$ dominates over the π interaction and $Ni(PH_3)$ has by far the largest σ transfer of the three species.

Very recently, Mavridis et al. [532,533] investigated the bonding and energetics of monoligated $M(NH_2)^+$ systems of first row transition metals using ab initio CASSCF+1+2 calculations. Both the ground states and several excited states of these systems (M = Sc, Ti, V, Cr and Mn) have been considered. The bond dissociation energies $D_e(M^+-NH_2)$ have been calculated and for the ground states [533] were found to be 79.0, 69.2, 65.5, 40.1 and 42.6 kcal mol^{-1} for $Sc(NH_2)^+$ ($^2A_2$), $Ti(NH_2)^+$ ($^3B_2$), $V(NH_2)^+$ ($^4B_1$), $Cr(NH_2)^+$ ($^5B_1$) and $Mn(NH_2)^+$ ($^6A_1$), respectively. Moreover, the M–N bond lengths were found to be practically constant along the series; the same is also true for the geometry of the NH_2 ligand. The bonding in the ground state of these systems results from the interaction of the M^+ ground states with the $^2B_1$ ground state of NH_2, shown in **103** and is represented in **104**. In all species the metal is losing electrons to the nitrogen atom and the bonding has considerable ionic character.

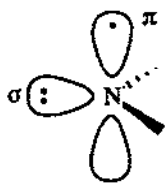

103

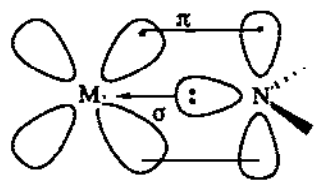

104

(b) Electronic structure and reactivity of transition metal complexes of NO, NS, N_2O, NCO^- and other ligands

There have been only a few theoretical studies of the electronic structure and reactivity of transition metal complexes of NO [534–536], NS [536], N_2O and NCO^- [537] ligands in the last decade. In addition to the earliest qualitative interpretations of the bimodality of the nitrosyl ligand acting as three (NO^+) in linear complexes or one (NO^-) electron donor in bent complexes, Noell and Morokuma [534] investigated the question of the binding of NO to a metal complex within the ab initio SCF framework. They studied the stability of $[Co(NH_3)_5NO]^{2+}$ as a function of the bending angle, φ, of NO and found the most stable conformer at 119°. The stability of the bent complex was attributed to both the charge transfer and electrostatic interactions. The interactions stabilizing the bent complex depend on the occupancy of the π^* MO of NO, therefore in complexes with few electrons, the bent structures appear destabilized and the linear geometry is the equilibrium conformer, in agreement with experimental evidence.

Ground state SCF-DV-Xα calculations have been performed by Basolo and coworkers [535] for $V(CO)_5NO$ and compared with those for $V(CO)_6$

in an attempt to understand the origin of its exceptional reactivity. The π-acceptor ability of the CO ligands seems to be responsible for the facile substitution of $V(CO)_5NO$ by both dissociative and associative mechanisms. The LUMO of the nitrosyl complex consisting of NO π^* (44%) and CO π^* (36%) character becomes more localized on NO upon CO dissociation and is raised in energy. Moreover, NO predominates over the axial CO ligand in both the σ- and π-bonding MOs of the complex.

Very recently, Kersting and Hoffmann [536] have studied the reaction path and the electronic requirements for the possible coupling of two thionitrosyl ligands on Re fragments, using EHMO calculations. To this end, the electronic structure and bonding in complexes of the $[ReCl_4(N_2S_2)]^-$ type have been investigated. From a Walsh diagram analysis and calculations of the total energy, it appears that S–S coupling is more probable than N–N coupling. For the coupling of two nitrosyl ligands in $[ReCl_4(NO)_2]^-$, Kersting and Hoffmann showed that it is disfavoured in general, but might occur via N–N bonding. This observation is due to the reversal of electronegativity for N/O vs. N/S.

The coordination of N_2O and NCO^- ligands to ML_5 metal-containing fragments has been investigated by Tuan and Hoffmann [537] with the aid of EHMO theory. The message from this study is: (i) N-linkage complexes are more stable than their O-linkage counterparts, (ii) the bonding is accomplished mainly through σ bonding with very little or no π-back bonding, (iii) complexes of N_2O and third row transition metals, such as $[Os(NH_3)_5N_2O]^{2+}$ should be stable.

Finally, Ziegler et al. [134] have recently presented non-local density functional calculations on the D(M–L) bond strength in the Cl_3ML model systems of the early transition metals M = Ti, Zr and Hf, as well as the $LM(CO)_4$ model system with the late transition metal M = Co for a series of ligands L = H, CH_3, SiH_3, OH, SH, OCH_3, NH_2, PH_2 and CN. It was found that the M–L bond is more polar for the early than for the late transition metal systems. Moreover, for all ligands, L, except hydrogen, the D(M–L) bond strength is higher for the early than for the late transition metal systems. These results were attributed to the fact that early transition metal fragments possess several vacant d-orbitals available for donation from occupied ligand orbitals, whereas late transition metal fragments have most d-orbitals occupied and thus involved in repulsive interactions with the occupied ligand orbitals. The calculated trends of the D(M–L) bond strengths for the ligands investigated being $OH > OCH_3 > CN > NH_2 > SH > CH_3 > H > SiH_3 > PH_2$ and $CN > OH > H > SiH_3 > SH > CH_3 > NH_2 > PH_2$ for the Cl_3ML and $LCo(CO)_4$ systems, respectively, have been analyzed within the framework of the bond energy decomposition scheme involving both electronic (π- or σ-bonding interactions) and steric terms.

(c) Electronic structure and reactivity of transition metal allyl and hetero-allyl complexes

The reaction between OH^- and a Pd(II)-linked π-allyl ligand, has been investigated as a model reaction for various nucleophilic attacks on the π-allyl ligand by Sakaki et al. [538] using CNDO-type SCF-MO calculations. It was found that, when a nucleophile Y attacks the π-allyl ligand, Pd(II) is reduced to Pd(0) and the allyl derivative $CH_2{=}CHCH_2Y$ leaves the Pd(0) via an intermediate π-olefin-Pd(0) complex according to the scheme:

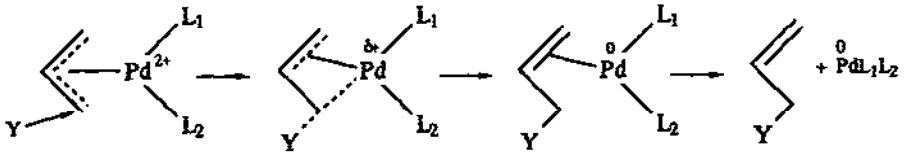

It is suggested that $Pd(PH_3)_2(\pi\text{-}C_3H_5)^+$ is extremely reactive whereas $PdCl_2(\pi\text{-}C_3H_5)^-$ is inert. Such a ligand effect on the reactivity is attributed to orbital mixing and changes in the Pd–Cl and Pd–L (L = PH_3 or CO) bond strengths. Along this line, the neutral π-acceptor ligand is most favourable for the reaction, while the anionic ligand is most unfavourable.

EHMO calculations on $Pd(\eta^3\text{-}CH_2CHCH_2)(CH_3)L$ (L = PH_3, $CH_2{=}CH_2$) and related species have been carried out by Kurosawa et al. [539] as part of a study of spontaneous and olefin-promoted reductive elimination of η^3-allyl(organo)palladium(II) complexes. The following three reaction pathways have been investigated:

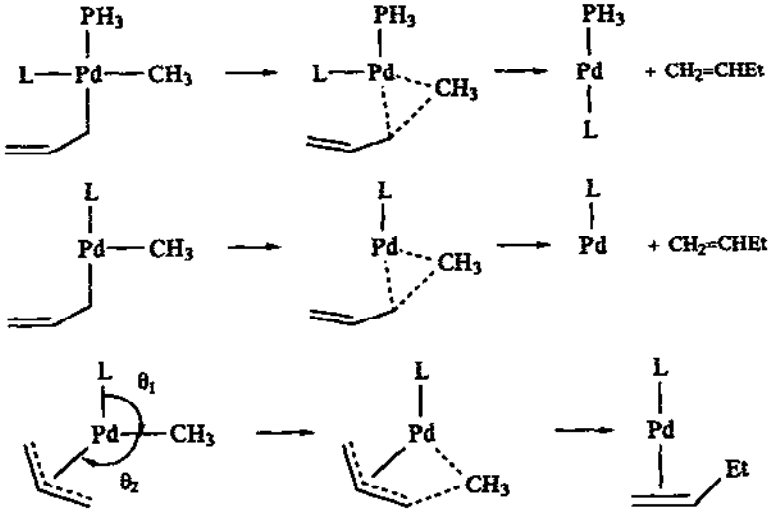

It was found that during the reductive elimination of $Pd(\eta^3\text{-allyl})(CH_3)L$ (L = PH_3, $CH_2{=}CH_2$) in the presence of PH_3, C–C bond formation proceeds

without participation of the η^3- to η^1-allyl conversion. Dissociation of L is also not significant during the C–C bond formation. When L is replaced by an olefin, it plays a role apparently specific to the η^3-allyl system in lowering the barrier to the C–C bond formation.

Dithiocarboxylato, RCS_2^-, and dithiocarbamato, $R_2NCS_2^-$, ligands could be considered as heteroallyl ligands with respect to their bonding mode to transition metals. Thus, they can act either as unidentate ligands through one of the two sulphur atoms, **105**, or as a bidentate ligand through both sulphur donor atoms, **106**. Obviously the coordination mode **105** is similar to that of η^1-allyl ligand, whereas the coordination mode **106** is similar to that of η^3-allyl ligand. Moreover, the calculated FMOs of the dithio ligands are qualitatively similar to those of the allyl ligand. This similarity between the dithio and allyl ligands manifests itself in the fluxionality of the two classes of compounds. One such example is the observed methyl group exchange in $(\eta^5\text{-}C_5H_5)ZrCl[S_2CN(CH_3)_2]$, which has been investigated experimentally and theoretically by Fay and coworkers [540]. Using EHMO calculations Fay and his coworkers analyzed possible mechanisms for the exchange process and found that a mechanism involving C–N bond rotation is preferred.

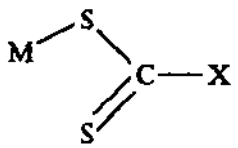

105

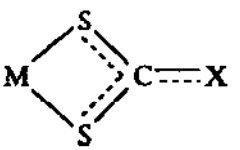

106

The electronic ground states and chemical reactivity of square planar Ni(II) [541] and Pt(II) [542] dithio complexes have been investigated by Tsipis and his coworkers with the aid of EHMO-SCCC calculations. The trimeric nature of the square planar nickel(II) complexes of aromatic dithiocarboxylato ligands in the solid state in a "skewed sandwich" form, their ability to form adducts with Lewis bases as well as their sulphur addition reactions affording perthio complexes by chelate ring expansion have been explained in terms of the energies and character of the FMOs. Schematic pictures of the orbital interactions accounting for the σ- and π-bond formation of pyridine adducts and the chelate ring expansion of the complexes upon reaction with elemental sulphur are shown in **107**, **108** and **109**, respectively.

For the square planar platinum(II) dithio complexes, Tsipis and his coworkers investigated their chemical reactivity towards phosphine bases as well as their fluxional behaviour within the framework of the EHMO theory. Based upon the interactions of the FMOs, being characteristic for nucleophi-

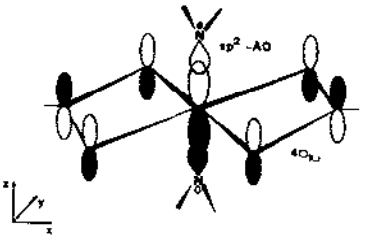

107

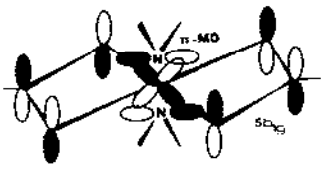

108

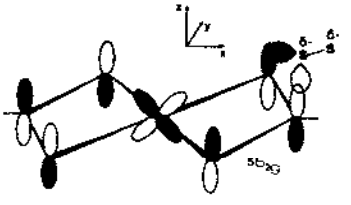

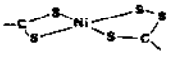

109

lic substitution reactions, the mechanism shown in Fig. 26 has been proposed for the formation of PtS_3P coordination geometries and their fluxional behaviour. According to this mechanism, a frontier controlled non-rigid quasi-five-coordinated four-centre transition state, **110**, is formed via a direct nucleophilic attack of the coordinated bidentate dithio ligand by the phosphine nucleo-

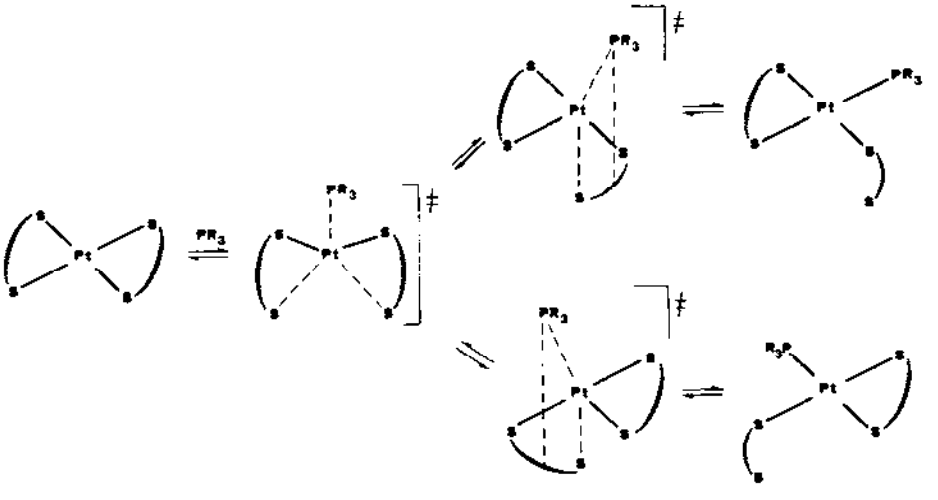

110

Fig. 26. Proposed mechanism for the formation of PtS_3P coordination geometries and their fluxional behaviour.

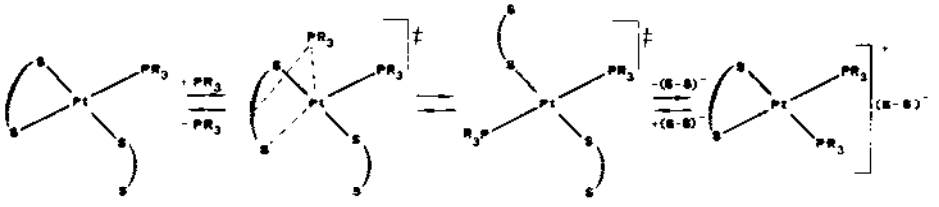

111

Fig. 27. Proposed mechanism for the formation of the $[PtS_2P_2]^+$ coordination geometry.

phile. Further reaction of the PtS_3P compounds with the phosphine nucleophile affords the dithiocarbimato complexes, **111**, as final products, according to the mechanism shown in Fig. 27.

The localization of the LUMO, **112**, of the dithiocarbimato complex on the phosphine ligands accounts well for phosphine exchange processes observed experimentally, whereas its HOMO, **113**, being mainly localized on the nitrogen atom of the dithiocarbimato ligand, is responsible for the electrophilic attack at nitrogen by several electrophiles.

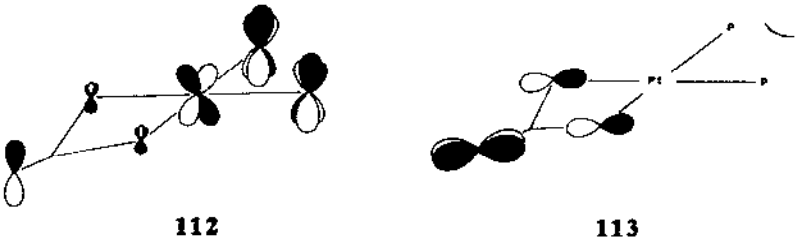

112 **113**

The mechanism of the reactions of square planar nickel(II) *N*-alkyldithiocarbamate complexes with RCO^+ electrophiles affording an important class of Ni(II) amide *N*-carbodithioates has recently been investigated [543] within the framework of the EHMO theory. From the molecular orbital point of view, it seems that the acylation reaction of the bis(*N*-alkyldithiocarbamato)-nickel(II) complexes in the presence of Et_3N proceeds via an S_{E1} rather than an S_{E2} mechanism, involving the deprotonated $[Ni(S_2{=}NR)_2]^{2-}$ complexes as transition states (Fig. 28). Both frontier orbital and electrostatic interactions are in favour of the S_{E1} mechanism.

Anderson and Baird [544] have also carried out INDO/S calculations on the free diethyldithiocarbamate and pyrrole-*N*-carbodithioate ligands and their Ni(II) complexes. According to the eigenvalues of the HOMOs and LUMOs of the complexes, $Ni(Et_2dtc)_2$ is predicted to be more readily oxidized and $Ni(pdtc)_2$ more readily reduced. Moreover, the calculations suggested that attack of a nucleophile should weaken the C—N bond of $Ni(Et_2dtc)_2$ but not affect the C—N bond of $Ni(pdtc)_2$.

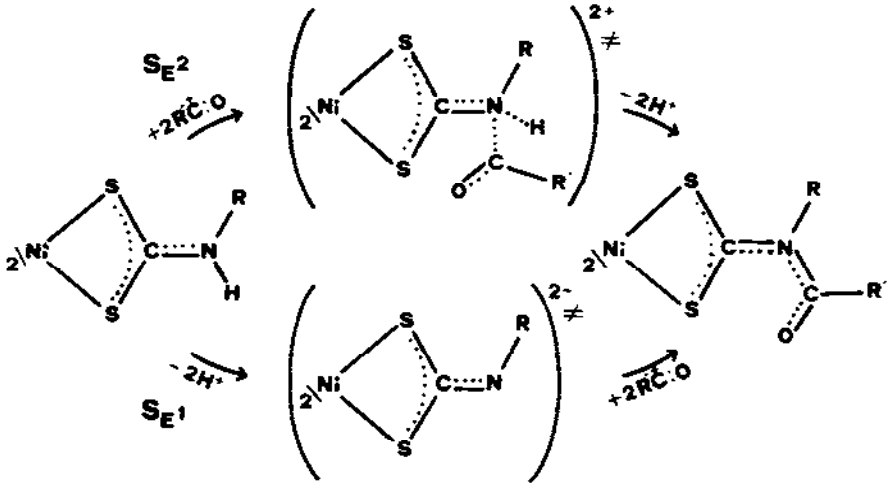

Fig. 28. Possible reaction mechanisms for the acylation of the nickel(II) dithiocarbamates.

More recently, we have investigated [545] the stability and reactivity of the 1:1 and 2:1 halobis(*N*,*N*-dialkyldithiocarbamato)iron(III) towards molecular halogen association by means of EHMO-SCCC calculations following the methodology successfully applied in the case of $\pi-\pi$, $\pi-\sigma$, and $n-\sigma$ CT complexes [546]. We have found that in these systems, treated as supermolecules, the stabilizing forces are of the charge transfer and van der Waals type, since both the σ- and/or π-type orbital interactions have a destabilizing effect. Calculated quantum chemical indices, such as atomic charges, orbital populations and two-centre energy terms, indicated that the charge transfer mechanism in the 2:1 supermolecules, shown in **114**, corresponds to a cyclic charge transfer located mainly on the FeXI nuclear framework.

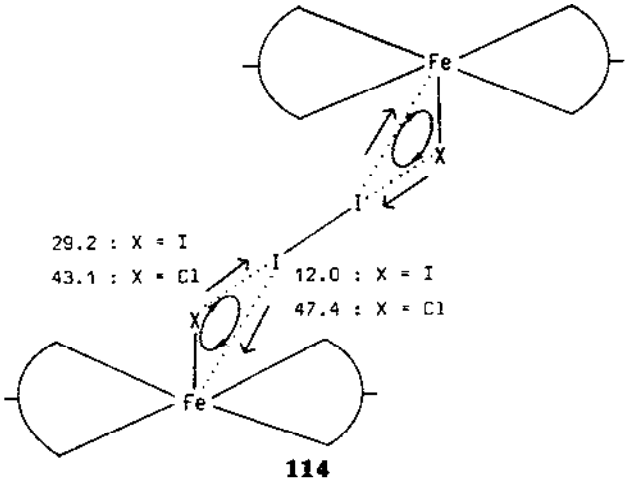

114

The charge transfer occurs mostly through the interactions between the d_{z^2}, d_{xy} and d_{yz} AOs of Fe and the MOs of the tetratomic $X\cdots X'_2\cdots X$ moieties of appropriate symmetry. More important is the finding that weak bonding interactions between the constituent molecules do exist, but surprisingly directly between X'_2 and the Fe(III) atom and not via the apical halogeno (X) ligands. Such interactions have important consequences on magnetic behaviour and chemical reactivity with respect to intramolecular electron transfer processes in these supermolecules.

E. CONCLUDING REMARKS

In view of the facts and data discussed, it may be true that theoretical investigations are not adscititious in the effort to achieve elucidation of the M–L bond nature and behaviour. There certainly exists no general canon for the efficacious selection and application of the most eligible computational method for the study of a certain compound or series of compounds. Nevertheless, fastidious ab initio computations provide the means to understand the energetics, reaction pathways, etc. in simple M–L systems. Attempts to reconcile theory and experiment have resulted in a variety of programs available to the non-theoretical chemists. These programs have produced a vast number of results on practically every class of coordination and organometallic compound. Therefore, extensive reviews of these results purvey the points which will help the experimentalist apply the appropriate computational method for the problem in view. The aim of the application of theory to coordination and organometallic chemistry is that its predictions help the experimentalist to concoct new experiments and anticipate the results.

REFERENCES

1 M.H. Chisholm, Angew. Chem. Int. Ed. Engl., 25 (1986) 21.
2 W.H. Herrmann, Angew. Chem. Int. Ed. Engl., 25 (1986) 56.
3 T.P. Martin, Angew. Chem. Int. Ed. Engl., 25 (1986) 197.
4 A. Yamamoto, Organotransition Metal Chemistry, Fundamental Concepts and Applications, Wiley, New York, 1986.
5 J.P. Collman, L.S. Hegedus, J.R. Norton and R.G. Finke, Principles and Applications of Organotransition Metal Chemistry, University Science Books, Mill Valley, CA, 2nd edn., 1987.
6 W.H. Herrmann, Angew. Chem. Int. Ed. Engl., 27 (1988) 1297.
7 J.S. Thayer, Organometallic Chemistry, VCH Publishers, New York, 1988.
8 R.H. Crabtree, The Organometallic Chemistry of the Transition Metals, Wiley, Chichester, 1988.
9 D.A. King and D.P. Woodruff, Chemical Physics of Solid Surfaces and Heterogeneous Catalysis, Vol. 9, Elsevier, Amsterdam, 1978.
10 E.L. Muetterties and J. Stein, Chem. Rev., 79 (1979) 479.
11 E.L. Muetterties, T.N. Rhobin, E. Band, C.F. Brucker and W.R. Pretzer, Chem. Rev., 79 (1979) 91.
12 G.W. Parshall, Homogeneous Catalysis, Wiley, New York, 1980.

13 E.L. Muetterties and M.J. Krause, Angew. Chem. Int. Ed. Engl., 22 (1983) 135.
14 G.W. Parshall and R.E. Putscher, J. Chem. Educ., 63 (1986) 189.
15 J.M. Basset and B.C. Gates (Eds.), Surface Organometallic Chemistry: Molecular Approaches to Surface Catalysis, NATO Science Committee, Brussels, 1987.
16 M.F. Gielen (Ed.), Metal-based Anti-tumour Drugs, Freund, London, 1988, and references cited therein.
17 C.J. Ballhausen, in G.A. Segal (Ed.), Modern Theoretical Chemistry, Vol. 7, Plenum Press, New York, 1977, p. 105.
18 A. Veillard and J. Demuynck, in H.F. Schaeffer, III (Ed.), Modern Theoretical Chemistry, Vol. 4, Plenum Press, New York, 1977, p. 187.
19 A. Veillard (Ed.), Quantum Chemistry: The Challenge of Transition Metals and Coordination Chemistry, NATO ASI Series, Reidel, Dordrecht, 1986.
20 D.R. Salahub and M.C. Zerner (Eds.), The Challenge of *d* and *f* Electrons, Theory and Computation, ACS Symp. Ser., 394 (1989).
21 D.M.P. Mingos, Adv. Organomet. Chem., 15 (1977) 1.
22 J.K. Burdett, Molecular Shapes, Wiley, New York, 1980.
23 T.A. Albright, Tetrahedron, 38 (1982) 1339.
24 R. Hoffmann, Angew. Chem. Int. Ed. Engl., 26 (1987) 846.
25 M. Simonetta, Top. Curr. Chem., 42 (1973) 1.
26 J.A. Pople, in H.F. Schaeffer, III (Ed.), Modern Theoretical Chemistry, Vol. 4, Plenum Press, New York, 1977, p. 1.
27 P.O. Löwdin, Int. J. Quantum Chem., 29 (1986) 1651.
28 S. Wilson (Ed.), Methods in Computational Chemistry, Vol. 1, Plenum Press, New York, 1987.
29 E.R. Davidson, D. Feller and P. Phillips, Chem. Phys. Lett., 76 (1980) 416.
30 J.G. Snijders and P. Pyykkö, Chem. Phys. Lett., 75 (1980) 5.
31 T. Ziegler, J.G. Snijders and E.J. Baerends, Chem. Phys. Lett., 75 (1980) 1.
32 T. Ziegler, J.G. Snijders and E.J. Baerends, J. Chem. Phys., 74 (1981) 1271.
33 R.L. Martin and P.J. Hay, J. Chem. Phys., 75 (1981) 4539.
34 R.L. Martin, J. Phys. Chem., 87 (1983) 750.
35 K. Faegri, Jr. and J. Almlöf, Chem. Phys. Lett., 107 (1984) 121.
36 S. Wilson (Ed.), Methods in Computational Chemistry, Vol. 2, Plenum Press, New York, 1988.
37 M. Schluter and L.J. Sham, Phys. Today, 35 (1982) 36.
38 S. Lundqvist and N.H. March (Eds.), Theory of Inhomogeneous Electron-Gas, Plenum Press, New York, 1983.
39 M.L. Cohen, Int. J. Quantum Chem., 24 (1983) 243.
40 J.P. Dahl and J. Avery (Eds.), Local Density Approximations in Quantum Chemistry and Solid State Physics, Plenum Press, New York, 1984.
41 L.J. Sham, Int. J. Quantum Chem., 19 (1986) 491.
42 J.P. Perdew, Int. J. Quantum Chem., 19 (1986) 497.
43 J.C. Slater, Adv. Quantum Chem., 6 (1972) 1.
44 J.W.D. Connolly, in A. Segal (Ed.), Semiempirical Methods of Electronic Structure Calculation, Plenum Press, New York, 1977, p. 105.
45 E.J. Baerends, D.E. Ellis and P. Ros, Chem. Phys., 2 (1973) 41.
46 E.J. Baerends and A. Rozendaal, in A. Veillard (Ed.), Quantum Chemistry: The Challenge of Transition Metals and Coordination Chemistry, NATO ASI Series, Reidel, Dordrecht, 1986, p. 159.
47 J.B. Johnson and W.G. Klemperer, J. Am. Chem. Soc., 99 (1977) 7132.
48 B. Ruscic, G.L. Goodman and J. Berkowitz, J. Chem. Phys., 78 (1983) 5443.
49 K.H. Johnson, Ann. Rev. Phys. Chem., 26 (1975) 39.
50 D.D. Koelling, Phys. Rev., 188 (1969) 188.

51 B.I. Dunlap, J.W.D. Connolly and J.R. Sabin, J. Chem. Phys., 71 (1979) 3396, 4993.
52 N. Rösch and H. Jörg, in A. Veillard (Ed.), Quantum Chemistry: The Challenge of Transition Metals and Coordination Chemistry, NATO ASI Series, Reidel, Dordrecht, 1986, p. 179.
53 R.N. Dixon and I.L. Robertson, Theoretical Chemistry, Vol. 3, The Chemical Society, London, 1978, p. 100.
54 Y. Ishikawa and G.L. Malli, in G.L. Milli (Ed.), Fully Relativistic Effective Core Potentials, NATO ASI Series, Plenum Press, New York, 1983.
55 R. McWeeny, Int. J. Quantum Chem., 26 (1984) 693.
56 W.J. Stevens and M. Krauss, Annu. Rev. Phys. Chem., 35 (1984) 357.
57 L.R. Kahn, P. Baybutt and D.G. Truhlar, J. Chem. Phys., 65 (1976) 3826.
58 W.J. Stevens, H. Basch and M. Krauss, J. Chem. Phys., 81 (1984) 6027.
59 J. Andzelm, E. Radzio, Z. Barandiadran and L. Seijo, J. Chem. Phys., 83 (1985) 4565.
60 J. Andzelm, E. Radzio, Z. Barandiadran and D.R. Salahub, J. Chem. Phys., 83 (1985) 4573.
61 B.O. Roos, P.R. Taylor and P.E.M. Siegbahn, Chem. Phys., 48 (1980) 157.
62 S.R. Langhoff and E.R. Davidson, Int. J. Quantum Chem., 8 (1974) 61.
63 W.A. Goddard, III, Phys. Chem., 157 (1967) 81.
64 F.W. Brobrowicz and W.A. Goddard, III, in H.F. Schaeffer, III (Ed.), Methods of Electronic Structure Theory, Plenum Press, New York, 1977, p. 79.
65 R. Gaspar, Int. J. Quantum Chem., 29 (1986) 1043.
66 K. Jug and D.N. Nanda, Theor. Chim. Acta, 57 (1980) 95, 107.
67 M.J.S. Dewar and W. Thiel, J. Am. Chem. Soc., 99 (1977) 5231.
68 C. Nieke and J. Reinhold, Theor. Chim. Acta, 65 (1984) 99 and references cited therein.
69 K. Jug, R. Iffert and J. Schulz, Int. J. Quantum Chem., 32 (1987) 265.
70 P. Pyykkö, in S. Wilson (Ed.), Methods in Computational Chemistry, Vol. 2, Plenum Press, New York, 1988, p. 137.
71 R. Hoffmann, Science, 211 (1981) 995.
72 D.M.P. Mingos, Compr. Organomet. Chem., 3 (1982) 1.
73 M.B. Hall, J. Am. Chem. Soc., 100 (1978) 6333.
74 M.B. Hall, Inorg. Chem., 17 (1978) 2261.
75 S. Larsson and P. Pyykkö, Chem. Phys., 101 (1986) 355.
76 R. Jostes, Theor. Chim. Acta, 74 (1988) 229.
77 R. Irie, Theor. Chim. Acta, 70 (1986) 239.
78 R. Jostes, Theor. Chim. Acta, 74 (1988) 229.
79 N.D. Epiotis, Lect. Notes Chem., 29 (1982) 1.
80 N.D. Epiotis, Lect. Notes Chem., 34 (1983) 1.
81 N.D. Epiotis, Pure Appl. Chem., 55 (1983) 229.
82 N.D. Epiotis, Nouv. J. Chim., 8 (1984) 11.
83 N.D. Epiotis, in D.J. Klein and N. Trinajstic (Eds.), Valence Bond Theory and Chemical Structure, Elsevier, Amsterdam, 1988.
84 N.D. Epiotis, Pure Appl. Chem., 60 (1988) 157.
85 N.D. Epiotis, New J. Chem., 12 (1988) 231.
86 N.D. Epiotis, Top. Curr. Chem., 150 (1989) 47 and references cited therein.
87 R. Hoffmann, Angew. Chem. Int. Ed. Engl., 21 (1982) 711.
88 H. Fujimoto and R. Hoffmann, J. Phys. Chem., 78 (1974) 1167.
89 R. Hoffmann, H. Fujimoto, J.R. Swenson and C.C. Wan, J. Am. Chem. Soc., 95 (1973) 7644.
90 T.A. Albright, J.K. Burdett and M.-H. Whangbo, Orbital Interactions in Chemistry, Wiley, New York, 1985.
91 R. Daudel, G. Leroy, D. Peeters and M. Sana, Quantum Chemistry, Wiley, New York, 1983.
92 D.G. Truhlar, B.C. Garret and R.S. Grev, in D.G. Truhlar (Ed.), Potential Energy Surfaces and Dynamics Calculations, Plenum Press, New York, 1981.

93 P. Pulay, in H.F. Schaeffer, III (Ed.), Applications of Electronic Structure Theory, Plenum Press, New York, 1977.
94 G. Leroy, M. Sana, L.A. Burke and M.-T. Nguyen, in R. Daudel, A. Pullman, L. Salem and A. Veillard (Eds.), Quantum Theory of Chemical Reactivity, Reidel, Dordrecht, 1979.
95 K. Muller, Angew. Chem. Int. Ed. Engl., 19 (1980) 1.
96 K. Fukui, Acc. Chem. Res., 14 (1981) 363.
97 R. Daudel, in R. Daudel and B. Pullman (Eds.), The World of Quantum Chemistry, Reidel, Dordrecht, 1974, p. 93.
98 K. Fukui, J. Phys. Chem., 74 (1970) 4161.
99 K. Fukui, S. Kato and H. Fujimoto, J. Am. Chem. Soc., 97 (1975) 1.
100 A. Tachibana and K. Fukui, Theor. Chim. Acta, 49 (1978) 321.
101 K. Fukui, Angew. Chem. Int. Ed. Engl., 94 (1982) 852.
102 W. Quapp and D. Heidrich, Theor. Chim. Acta, 66 (1984) 245.
103 P. Pechucas, J. Chem. Phys., 64 (1976) 1516.
104 S. Eyrenson, in Sixth Jerusalem Symposium on Chemical and Biochemical Reactivity, 1973.
105 A. Komornicki, K. Ishida, K. Morokuma, R. Ditchfield and M. Conrad, Chem. Phys. Lett., 45 (1977) 595.
106 G. Klopman, J. Am. Chem. Soc., 90 (1968) 223.
107 R.F. Hudson and G. Klopman, Tetrahedron Lett., 12 (1967) 1103.
108 R.G. Pearson, J. Am. Chem. Soc., 85 (1963) 3533.
109 G. Klopman (Ed.), Chemical Reactivity and Reaction Paths, Wiley, New York, 1974.
110 P. Claverie, J.P. Daudey, J. Langlet, B. Pullman, D. Piazola and M.J. Huron, J. Phys. Chem., 82 (1978) 405.
111 J. Tonasi, in H. Ratajczak and W.J. Orville-Thomas (Eds.), Molecular Interactions, Vol. 3, Wiley, New York, 1982, p. 119.
112 K. Morokuma and K. Kitaura, in P. Politzer and D.G. Truhlar (Eds.), Chemical Applications of Atomic and Molecular Electrostatic Potentials, Plenum Press, New York, 1981, p. 215.
113 K. Morokuma, J. Chem. Phys., 55 (1971) 1236.
114 K. Kitaura and K. Morokuma, Int. J. Quantum Chem., 10 (1976) 325.
115 P.A. Kollman and L.C. Allen, J. Chem. Phys., 52 (1970) 5085.
116 M. Dreyfus, B. Maigret and A. Pullman, Theor. Chim. Acta, 17 (1970) 109.
117 J.P. Daudey, P. Claverie and J.P. Malrieu, Int. J. Quantum Chem., 8 (1974) 1.
118 K. Hori, Y. Asai and T. Yamabe, Theor. Chim. Acta, 66 (1984) 77.
119 G. Alagona, C. Ghio, R. Cammi and J. Tomasi, Int. J. Quantum Chem., 32 (1987) 227.
120 J.O. Noell and K. Morokuma, Inorg. Chem., 18 (1979) 2774.
121 K. Kitaura, S. Sakaki and K. Morokuma, Inorg. Chem., 18 (1979) 1558.
122 S. Sakaki, K. Kitaura and K. Morokuma, Inorg. Chem., 21 (1982) 760.
123 S. Sakaki, K. Kitaura, K. Morokuma and K. Ohkubo, Inorg. Chem., 22 (1983) 104.
124 S. Sakaki, K. Morokuma and K. Ohkubo, J. Am. Chem. Soc., 107 (1985) 2686.
125 S. Sakaki, in A. Veillard (Ed.), Quantum Chemistry: The Challenge of Transition Metals and Coordination Chemistry, NATO ASI Series, Reidel, Dordrecht, 1986, p. 319.
126 T. Ziegler, Organometallics, 4 (1985) 675.
127 T. Ziegler, Inorg. Chem., 25 (1986) 2721.
128 T. Ziegler, in A. Veillard (Ed.), Quantum Chemistry: The Challenge of Transition Metals and Coordination Chemistry, NATO ASI Series, Reidel, Dordrecht, 1986, p. 189.
129 R.L. Dekock, E.J. Baerends, P.M. Boerrigter and R.J. Hengelmolen, J. Am. Chem. Soc., 106 (1984) 3387.
130 T. Ziegler, J. Am. Chem. Soc., 107 (1985) 4453.
131 T. Ziegler and A. Rauk, Theor. Chim. Acta, 46 (1977) 1.
132 T. Ziegler and A. Rauk, Inorg. Chem., 18 (1979) 1558.

133 T. Ziegler and A. Rauk, Inorg. Chem., 18 (1979) 1755.
134 T. Ziegler, V. Tschinke, L. Versluis, E.J. Baerends and W. Ravenek, Polyhedron, 7 (1988) 1625.
135 P.S. Bagus, K. Hermann and C.W. Bauschlicher, J. Chem. Phys., 80 (1984) 4378.
136 K. Fukui (Ed.), Theory of Orientation and Stereoselection, Springer Verlag, New York, 1975.
137 K. Fukui, T. Yonezawa and H. Shingu, J. Chem. Phys., 20 (1952) 722.
138 K. Fukui, T. Yonezawa, C. Nagata and H. Shingu, J. Chem. Phys., 22 (1954) 1433.
139 R. Hoffmann, Acc. Chem. Res., 4 (1971) 1.
140 N.D. Epiotis, J. Am. Chem. Soc., 95 (1973) 3087.
141 R. Hoffmann, C.C. Levin and R.A. Moss, J. Am. Chem. Soc., 95 (1973) 629.
142 J.P. Lowe, Science, 179 (1973) 527.
143 O. Eisenstein, N.T. Anh, Y. Jean, A. Devaquet, J. Cantacuzene and L. Salem, Tetrahedron, 30 (1974) 1717.
144 N.D. Epiotis, W.R. Cherry, S. Shaik, R.L. Yates and F. Bernardi, Top. Curr. Chem., 70 (1977).
145 F. Bernardi and A. Bottoni, in I.G. Csizmadia and R. Daudel (Eds.), Computational Theoretical Organic Chemistry, NATO ASI Series, Reidel, Dordrecht, 1981, p. 197.
146 M.-H. Whangbo, in I.G. Csizmadia and R. Daudel (Eds.), Computational Theoretical Organic Chemistry, NATO ASI Series, Reidel, Dordrecht, 1981, p. 233.
147 G.W. Wheland, J. Am. Chem. Soc., 64 (1942) 900.
148 M.J.S. Dewar, J. Am. Chem. Soc., 74 (1952) 3357.
149 R. Bonacorsi, E. Scrocco and J. Tomasi, Theor. Chim. Acta, 43 (1976) 63.
150 H. Fujimoto and K. Fukui, in G. Klopmann (Ed.), Chemical Reactivity and Reaction Paths, Wiley, New York, 1974, p. 23.
151 G. Klopmann, in G. Klopmann (Ed.), Chemical Reactivity and Reaction Paths, Wiley, New York, 1974, p. 1.
152 See, for example, J.N. Murrell and A.J. Harget (Eds.), Semi-empirical Self-consistent-field Molecular Orbital Theory of Molecules, Wiley, New York, 1972, Chap. 1.
153 R.E. Brown and A.M. Simas, Theor. Chim. Acta, 62 (1982) 62.
154 K. Jug and M.S. Gopinathan, Theor. Chim. Acta, 68 (1985) 343.
155 K. Jug, J. Comput. Chem., 5 (1984) 555.
156 J. Baker, Theor. Chim. Acta, 68 (1985) 221.
157 I. Mayer, Theor. Chim. Acta, 67 (1985) 315.
158 I. Mayer, Int. J. Quantum Chem., 29 (1986) 477.
159 O.G. Stradella, H.O. Villar and E.A. Castro, Theor. Chim. Acta, 70 (1986) 67.
160 J. Reinhold, R. Benedix, P. Birmer and H. Henning, Inorg. Chim. Acta, 33 (1979) 309.
161 M. Ban, I. Balint, M. Revész and M. Beck, Inorg. Chim. Acta, 57 (1982) 119.
162 G.A. Katsoulos, M.P. Sigalas and C.A. Tsipis, Inorg. Chim. Acta, 158 (1989) 255.
163 J. Chatt, Coord. Chem. Rev., 43 (1982) 337.
164 J. Tomasi, in P. Politzer and D.G. Truhler (Eds.), Chemical Applications of Atomic and Molecular Electrostatic Potentials, Plenum Press, New York, 1981, p. 257.
165 R. Bonaccorsi, E. Scrocco and J. Tomasi, J. Chem. Phys., 52 (1970) 5270.
166 J. Tomasi, in R. Daudel, A. Pullman, L. Salem and A. Veillard (Eds.), Quantum Theory of Chemical Reactions, Reidel, Dordrecht, 1980, p. 191.
167 H. Moriishi, O. Kikuchi, K. Suzuki and G. Klopman, Theor. Chim. Acta, 64 (1984) 319.
168 E. Scrocco and J. Tomasi, Adv. Quantum Chem., 11 (1978) 116.
169 P. Politzer and K.C. Daiker, in B.M. Deb (Ed.), The Force Concept in Chemistry, Van Nostrand, Reinhold, New York, 1981.
170 R. Cammi, H.-J. Hofmann and J. Tonasi, Theor. Chim. Acta, 76 (1989) 297.
171 A. Pullman and B. Pullman, in P. Politzer and D.G. Truhler (Eds.), Chemical Applications of Atomic and Molecular Electrostatic Potentials, Plenum Press, New York, 1981, p. 381.
172 C. Petrongolo, Gazz. Chim. Ital., 108 (1978) 445.

173 T.J. Kistenmacher, in P. Politzer and D.G. Truhler (Eds.), Chemical Applications of Atomic and Molecular Electrostatic Potentials, Plenum Press, New York, 1981, p. 445.
174 A. Pullman, T. Ebbesen and M. Rholan, Theor. Chim. Acta, 51 (1979) 247.
175 E.A. Bourdreaux, in M.F. Gielen (Ed.), Metal-based Anti-tumour Drugs, Freund, London, 1988, p. 175.
176 P.G. Abdul-Ahad and G.A. Webb, Int. J. Quantum Chem., 11 (1982) 1105.
177 S. Kang and D.L. Beveridge, Theor. Chim. Acta, 22 (1971) 312.
178 S. Kang and M.-H. Cho, Int. J. Quantum Chem., 7 (1973) 319.
179 R.F.W. Bader, in B.M. Deb (Ed.), The Force Concept in Chemistry, Van Nostrand, Reinhold, New York, 1981, p. 39.
180 P. Coppens and M.B. Hall (Eds.), Electron Distributions and the Chemical Bond, Plenum, New York, 1982.
181 D. Cremer and E. Kraka, Angew. Chem. Int. Ed. Engl., 23 (1984) 627.
182 W.H.E. Schwarz, L. Mensching, P. Valtazanos and W. von Niessen, Int. J. Quantum Chem., 29 (1986) 909.
183 R.F.W. Bader and T.T. Nguyen-Dong, Adv. Quantum Chem., 14 (1981) 63.
184 D. Cremer and E. Kraka, Croat. Chem. Acta, 57 (1984) 1259.
185 W.H.E. Schwarz, K. Ruedenberg, L. Mensching, L.L. Miller, P. Valtazanos and W. von Niessen, Angew. Chem. Int. Ed. Engl., 28 (1989) 597.
186 D. Armstrong, P. Perkins and J. Stewart, J. Chem. Soc. Dalton Trans., (1973) 838.
187 D. Armstrong, P. Perkins and J. Stewart, J. Chem. Soc. Dalton Trans., (1973) 2273.
188 K.A. Wiberg, Tetrahedron, 24 (1968) 1083.
189 M.S. Gopinathan and K. Jug, Theor. Chim. Acta, 63 (1983) 511, 527.
190 M.A. Natiello and J.A. Medrano, Chem. Phys. Lett., 105 (1984) 341.
191 M.S. Gopinathan, P. Siddarth and C. Ravimohan, Theor. Chim. Acta, 70 (1986) 303.
192 See articles in the Symposium-in-Print, number 6, Polyhedron, 7 (1988) and references cited therein.
193 W. Weltner Jr. and R.J. Van Zee, Annu. Rev. Phys. Chem., 35 (1984) 291.
194 P.B. Armentrout, in D.H. Russell (Ed.), Gas Phase Inorganic Chemistry, Plenum Press, New York, 1989, p. 1.
195 P.B. Armentrout and J.L. Beauchamp, Acc. Chem. Res., 22 (1989) 315.
196 E.L. Muetterties and M.J. Krauze, Angew. Chem. Int. Ed. Engl., 22 (1983) 135.
197 B.S. Freizer, Talanta, 32 (1985) 697.
198 J. Allison, Prog. Inorg. Chem., 34 (1986) 627.
199 R.R. Squires, Chem. Rev., 87 (1987) 623.
200 H. Schwartz, Acc. Chem. Res., 22 (1989) 282.
201 J.B. Schilling, W.A. Goddard, III and J.L. Beauchamp, J. Am. Chem. Soc., 108 (1986) 582.
202 J.B. Schilling, W.A. Goddard, III and J.L. Beauchamp, J. Phys. Chem., 91 (1987) 5616.
203 L.G.M. Petterson, C.W. Bauschlicher, Jr., S.R. Langhoff and H. Partridge, J. Chem. Phys., 87 (1987) 481.
204 A.E. Alvarado-Swaisgood and J.F. Harrison, J. Phys. Chem., 89 (1985) 5198.
205 P.J. Bruma and J. Anglada, in A. Veillard (Ed.), Quantum Chemistry: The Challenge of Transition Metals and Coordination Chemistry, NATO ASI Series, Reidel, Dordrecht, 1986, p. 67.
206 A. Mavridis and J.F. Harrison, J. Chem. Soc. Faraday Trans. 2, 85 (1989) 1391.
207 A.E. Alvarado-Swaisgood, J. Allison and J.F. Harrison, J. Phys. Chem., 89 (1985) 2517.
208 T. Ziegler, V. Tschinke and A. Becke, J. Am. Chem. Soc., 109 (1987) 1351.
209 M.A. Vincent, Y. Yoshioka and H.F. Schaeffer, III, J. Phys. Chem., 86 (1982) 3905.
210 M. Blomberg, U. Brandemark, I. Panas, P. Siegbahn and U. Wahlgren, in A. Veillard (Ed.), Quantum Chemistry: The Challenge of Transition Metals and Coordination Chemistry, NATO ASI Series, Reidel, Dordrecht, 1986, p. 1.
211 P. Pyykkö, J. Chem. Soc. Faraday Trans., 75 (1979) 1256.

212 P.B. Armentrout and R. Georgiadis, Polyhedron, 7 (1988) 1573 and references cited therein.
213 J.B. Schilling, W.A. Goddard, III and J.L. Beauchamp, J. Am. Chem. Soc., 109 (1987) 5565.
214 D.P. Chong, S.R. Langhoff, C.W. Bauschlicher, Jr., S.P. Walch and H. Partridge, J. Chem. Phys., 85 (1986) 2850.
215 A. Henderson, G. Das and A.C. Wahl, J. Chem. Phys., 83 (1980) 2805.
216 G. Das, J. Chem. Phys., 74 (1981) 5766.
217 P.R. Scott and W.G. Richards, J. Phys. B, 7 (1974) 500, L347, 1679.
218 P.R. Scott and W.G. Richards, J. Chem. Phys., 63 (1975) 1690.
219 P.S. Bagus and H.F. Schaeffer, III, J. Chem. Phys., 58 (1973) 1844.
220 S.P. Walch and C.W. Bauschlicher, Jr., J. Chem. Phys., 78 (1983) 4597.
221 U. Wedig, M. Dolg and H. Stoll, in A. Veillard (Ed.), Quantum Chemistry: The Challenge of Transition Metals and Coordination Chemistry, NATO ASI Series, Reidel, Dordrecht, 1986, p. 79.
222 M. Pelissier, J.P. Daudey, J.P. Malrieu and G.H. Jeng, in A. Veillard (Ed.), Quantum Chemistry: The Challenge of Transition Metals and Coordination Chemistry, NATO ASI Series, Reidel, Dordrecht, 1986, p. 37.
223 M.R.A. Blomberg, P.E.M. Siegbahn and B.O. Roos, Mol. Phys., 47 (1982) 127.
224 W.A. Goddard, III, S.P. Walch, A.K. Rappé and T.H. Upton, J. Vac. Sci. Technol., 14 (1977) 416.
225 C.M. Rohlfing, P.J. Hay and R.L. Martin, J. Chem. Phys., 85 (1986) 1447.
226 J.C. Barthelat, M. Hliwa, G. Nicolas, M. Pelissier and F. Spiegelmann, in A. Veillard (Ed.), Quantum Chemistry: The Challenge of Transition Metals and Coordination Chemistry, NATO ASI Series, Reidel, Dordrecht, 1986, p. 91.
227 S.R. Langhoff, L.G.M. Petterson, C.W. Bauschlicher, Jr. and H. Partridge, J. Chem. Phys., 86 (1987) 268.
228 H. Basch, D. Cohen and S. Topiol, Isr. J. Chem., 19 (1980) 233.
229 P.S. Bagus and C. Bjorkman, Phys. Rev. A, 23 (1981) 461.
230 G. Pacchioni, J. Koutecky and P. Fantucci, Chem. Phys. Lett., 92 (1982) 486.
231 H. Stöll, P. Fuentealba, M. Dolg, J. Flad, L.V. Szentpaly and H. Preuss, J. Chem. Phys., 79 (1983) 5532.
232 J.C.A. Boeyens and R.H. Lemmer, J. Chem. Soc. Faraday Trans., 73 (1977) 321.
233 J.L. Elkind and P.B. Armentrout, Inorg. Chem., 25 (1986) 1078.
234 N.D. Epiotis, J. Mol. Struct. (Theochem) 183 (1989) 45.
235 N.D. Epiotis, J. Mol. Struct. (Theochem) 185 (1989) 83.
236 N.D. Epiotis, New J. Chem., 12 (1988) 257.
237 T. Ziegler, W. Cheng, E.J. Baerends and W. Ravenek, Inorg. Chem., 27 (1988) 3458.
238 E.A. Carter and W.A. Goddard, III, J. Phys. Chem., 92 (1988) 5679.
239 A.E. Stevens and J.L. Beauchamp, J. Am. Chem. Soc., 103 (1981) 190.
240 M.A. Tolbert and J.L. Beauchamp, J. Phys. Chem., 90 (1986) 5015.
241 B.E. Bursten and M.G. Gatter, J. Am. Chem. Soc., 106 (1984) 2554.
242 G.J. Kubas, R.R. Ryak, B.I. Swanson, P.J. Vergammi and H.J. Wasserman, J. Am. Chem. Soc., 106 (1984) 451.
243 G.J. Kubas, Acc. Chem. Res., 21 (1988) 120.
244 G.J. Kubas, R.R. Ryan and D.A. Wrobleski, J. Am. Chem. Soc., 108 (1986) 1339.
245 G.J. Kubas, G.J. Unkefer, B.I. Swanson and E. Fukishima, J. Am. Chem. Soc., 108 (1986) 7000.
246 R.H. Crabtree and M.J. Lavin, J. Chem. Soc. Chem. Commun., (1985) 794, 1661.
247 R.H. Crabtree, M.J. Lavin and L. Bonneviot, J. Am. Chem. Soc., 108 (1986) 4032.
248 R.H. Morris, J.F. Sawyer, M. Shirahian and J.D. Zubkowski, J. Am. Chem. Soc., 107 (1985) 5581.
249 R.L. Sweany, Organometallics, 5 (1986) 387.
250 R.H. Crabtree and D.G. Hamilton, J. Am. Chem. Soc., 108 (1986) 3124.
251 F.M. Conroy-Lewis and S.J. Simpson, J. Chem. Soc. Chem. Commun., (1986) 506.
252 A. Sevin, Nouv. J. Chim., 5 (1981) 233.

253 A. Sevin and P. Chaquin, Nouv. J. Chim., 7 (1983) 353.
254 J.-Y. Saillard and R. Hoffmann, J. Am. Chem. Soc., 106 (1984) 2006.
255 Y. Jean, O. Eisenstein, F. Volatron, B. Maouche and F. Sefta, J. Am. Chem. Soc., 108 (1986) 6587.
256 P.J. Hay, J. Am. Chem. Soc., 109 (1987) 705.
257 E.M. Kober and P.J. Hay, in D.R. Salahub and M.C. Zerner (Eds.), The Challenge of *d* and *f* Electrons, Theory and Computation, ACS Symp. Ser., 394 (1989).
258 J.K. Burdett and S.J. Lee, J. Solid State Chem., 56 (1985) 211.
259 J.K. Burdett, J.R. Phillips, M.R. Pourian, M. Poliakoff, J.J. Turner and R. Upmacis, Inorg. Chem., 26 (1987) 3054.
260 J.K. Burdett and M.R. Pourian, Inorg. Chem., 27 (1988) 4445.
261 F.M. Bickelhaupt, E.J. Baerends and W. Ravenek, Inorg. Chem., 29 (1990) 350.
262 G.A. Ozin and J. Garcia-Prieto, J. Am. Chem. Soc., 108 (1986) 3099.
263 O. Novaro, J. Garcia-Prieto, E. Poulain and M.E. Ruiz, J. Mol. Struct. (Theochem), 135 (1986) 79.
264 M.E. Ruiz, J. Garcia-Pietro, C. Jarque and O. Novaro, J. Am. Chem. Soc., 108 (1986) 3507.
265 G.L. Gadd, R.K. Upmacis, M. Poliakoff and J.J. Turner, J. Am. Chem. Soc., 108 (1986) 2457.
266 M.R.A. Blomberg, J. Schüle and P.E.M. Siegbahn, J. Am. Chem. Soc., 111 (1989) 6156.
267 M.R.A. Blomberg and P.E.M. Siegbahn, J. Chem. Phys., 78 (1983) 986.
268 M.R.A. Blomberg and P.E.M. Siegbahn, J. Chem. Phys., 78 (1983) 5682.
269 J.J. Low and W.A. Goddard, III, J. Am. Chem. Soc., 106 (1984) 8321.
270 J.J. Low and W.A. Goddard, III, Organometallics, 5 (1986) 609.
271 J.B. Schilling, W.A. Goddard, III and J.L. Beauchamp, J. Phys. Chem., 91 (1987) 4470.
272 P.E.M. Siegbahn, M.R.A. Blomberg and C.W. Bauschlicher, Jr., J. Chem. Phys., 81 (1984) 1373.
273 M.E. Ruiz, J. Garcia-Prieto and O. Novaro, J. Chem. Phys., 80 (1984) 1529.
274 J. Garcia-Prieto, M.E. Ruiz and O. Novaro, J. Am. Chem. Soc., 107 (1985) 5635.
275 E. Poulain, J. Garcia-Prieto, M.E. Ruiz and O. Novaro, Int. J. Quantum Chem., 29 (1986) 1181.
276 G.H. Jeung, in A. Veillard (Ed.), Quantum Chemistry: The Challenge of Transition Metals and Coordination Chemistry, NATO ASI Series, Reidel, Dordrecht, 1986, p. 101.
277 A.K. Rappé and T.H. Upton, J. Chem. Phys., 85 (1986) 4400.
278 A. Dedieu and A. Strich, Inorg. Chem., 18 (1979) 2940.
279 A. Dedieu, Inorg. Chem., 19 (1980) 375.
280 K. Kitaura, S. Obara and K. Morokuma, J. Am. Chem. Soc., 103 (1981) 2891.
281 A.C. Balazs, K.H. Johnson and G.M. Whitesides, Inorg. Chem., 21 (1982) 2162.
282 J. Noell and P. Hay, Inorg. Chem., 21 (1982) 14.
283 J. Noell and P. Hay, J. Am. Chem. Soc., 104 (1982) 4578.
284 J.J. Low and W.A. Goddard, III, J. Am. Chem. Soc., 106 (1984) 6928.
285 S. Obara, K. Kitaura and K. Morokuma, J. Am. Chem. Soc., 106 (1984) 7482.
286 K. Tatsumi, R. Hoffmann, A. Yamamoto and J.K. Stille, Bull. Chem. Soc. Jpn., 54 (1981) 1857.
287 H. Rabaâ, J.-Y. Saillard and R. Hoffmann, J. Am. Chem. Soc., 108 (1986) 4327.
288 M.R.A. Blomberg, U. Brandemark, L. Petterson and P.E.M. Siegbahn, Int. J. Quantum Chem., 23 (1983) 855.
289 P.J. Hay and C.M. Rohlfing, in A. Veillard (Ed.), Quantum Chemistry: The Challenge of Transition Metals and Coordination Chemistry, NATO ASI Series, Reidel, Dordrecht, 1986, p. 135.
290 T. Ziegler, V. Tschinke, L. Fan and A.D. Becke, J. Am. Chem. Soc., 111 (1989) 9177.
291 T. Upton, J. Am. Chem. Soc., 106 (1984) 1561.
292 P.E.M. Siegbahn, M.R.A. Blomberg and C.W. Bauschlicher, Jr., J. Chem. Phys., 81 (1984) 2103.
293 E. Shustotovich, R.C. Baetzold and E.L. Muetterties, J. Phys. Chem., 87 (1983) 1100.
294 F. Ruette and G. Blyholder, Theor. Chim. Acta, 74 (1988) 137.
295 P.E.M. Siegbahn, M.A.R. Blomberg, I. Panas and U. Wahlgren, Theor. Chim. Acta, 75 (1989) 143.
296 G. Pacchioni and J. Koutecky, in A. Veillard (Ed.), Quantum Chemistry: The Challenge of Transition Metals and Coordination Chemistry, NATO ASI Series, Reidel, Dordrecht, 1986, p. 465.

297 B. Bigot and C. Minot, in A. Veillard (Ed.), Quantum Chemistry: The Challenge of Transition Metals and Coordination Chemistry, NATO ASI Series, Reidel, Dordrecht, 1986, p. 489.
298 J.L. Elkind and P.B. Armentrout, J. Phys. Chem., 91 (1987) 2037.
299 G.A. Ozin, S.A. Mitchell and J. Garcia-Prieto, Angew. Chem. Int. Ed. Engl., 21 (1982) 380.
300 M.L. Steigerwald and W.A. Goddard, III, J. Am. Chem. Soc., 106 (1984) 308.
301 R.K. Upmacis, M. Poliakoff and J.J. Turner, J. Am. Chem. Soc., 108 (1986) 3645.
302 J.B. Schilling, W.A. Goddard, III and J.L. Beauchamp, J. Am. Chem. Soc., 109 (1987) 5573.
303 M.J. Filatov, O.V. Gritsenko and G.M. Zhidomirov, Theor. Chim. Acta. 72 (1987) 211.
304 M. Hotokka and P. Pyykkö, J. Organometal. Chem., 174 (1979) 289.
305 M. Brookhart and M.L.H. Green, J. Organometal. Chem., 250 (1983) 395.
306 A. Demolliens, Y. Jean and O. Eisenstein, in A. Veillard (Ed.), Quantum Chemistry: The Challenge of Transition Metals and Coordination Chemistry, NATO ASI Series, Reidel, Dordrecht, 1986, p. 301.
307 M.J. Calhorda and J.A. Simoes, Organometallics, 6 (1987) 1188.
308 A. Berry, Z. Dawoodi, A.E. Derome, J.M. Dickinson, A.J. Dowens, J.C. Green, M.L.H. Green, P.M. Hare, P.M. Payne, D.W.H. Raukin and H.E. Robertson, J. Chem. Soc. Chem. Commun., (1986) 520.
309 R.L. Williamson and M.B. Hall, J. Am. Chem. Soc., 110 (1988) 4428.
310 P. Knappe and N. Rösch, J. Organometal. Chem., 359 (1989) C5.
311 R.H. Crabtree, Chem. Rev., 85 (1985) 245.
312 J.L. Beauchamp, in K.S. Suslick (Ed.), High Energy Processes in Organometallic Chemistry, ACS Symp. Ser., 333 (1987) 11.
313 S.W. Buckner and B.S. Freiser, Polyhedron, 7 (1988) 1583.
314 B. Åkermark, H. Johansen, B. Roos and U. Wahlgren, J. Am. Chem. Soc., 101 (1979) 5876.
315 M.R.A. Blomberg, U. Brandemark and P.E.M. Siegbahn, J. Am. Chem. Soc., 105 (1983) 5557.
316 J.J. Low and W.A. Goddard, III, J. Am. Chem. Soc., 108 (1986) 6115.
317 P. Cossee, J. Catal., 3 (1964) 80.
318 P. Novaro, E. Blaisten-Barojas, E. Clementi, G. Giunchi and M.E. Ruiz-Vizcaya, J. Chem. Phys., 68 (1978) 2337.
319 A. Shiga, H. Kawamura, T. Ebara, T. Sasaki and Y. Kikuzono, J. Organometal. Chem., 366 (1989) 95.
320 M.H. Gubelmann and A.F. Williams, Struct. Bonding (Berlin), 55 (1983) 1.
321 R. Böca, Coord. Chem. Rev., 50 (1983) 1 and references cited therein.
322 J.T. Richardson (Ed.), Principles of Catalyst Development, Plenum Press, New York, 1989.
323 J.F. Harrison, J. Phys. Chem., 90 (1986) 3313.
324 C.W. Bauschlicher, Jr., C.J. Nelin and P.S. Bagus, J. Chem. Phys., 82 (1985) 3265.
325 M. Krauss and W.J. Stevens, J. Chem. Phys., 82 (1985) 5584.
326 P.S. Bagus, C.J. Nelin and C.W. Bauschlicher, Jr., J. Chem. Phys., 79 (1983) 2975.
327 G. Igel, U. Wedig, M. Dolg, P. Fuentealba, H. Preuss, H. Stoll and R. Frey, J. Chem. Phys., 81 (1984) 2737.
328 A.K. Rappé and W.A. Goddard, III, J. Am. Chem. Soc., 102 (1980) 5114.
329 A.K. Rappé and W.A. Goddard, III, J. Am. Chem. Soc., 104 (1982) 448.
330 A.K. Rappé and W.A. Goddard, III, J. Am. Chem. Soc., 104 (1982) 3287.
331 K. Tatsumi and R. Hoffmann, Inorg. Chem., 19 (1980), 2656.
332 D.M.P. Mingos, J. Organometal. Chem., 179 (1979) C29.
333 D.C. Brower, J.L. Templeton and D.M.P. Mingos, J. Am. Chem. Soc., 109 (1987) 5203.
334 J. Chatt, L. Manojlovic-Muir and K.W. Muir, J. Chem. Soc. Chem. Commun., (1971) 655.
335 Y. Jean, A. Lledos, J.K. Burdett and R. Hoffmann, J. Am. Chem. Soc., 110 (1988) 4506.
336 T.H. Upton and A.K. Rappé, J. Am. Chem. Soc., 107 (1985) 1206.
337 K.B. Sharpless, A.Y. Teranishi and J.E. Bäckvall, J. Am. Chem. Soc., 99 (1977) 3120.
338 A. Sevin, in A. Veillard (Ed.), Quantum Chemistry: The Challenge of Transition Metals and Coordination Chemistry, NATO ASI Series, Reidel, Dordrecht, 1986, p. 235.

K.A. Jørgensen, J. Am. Chem. Soc., 109 (1987) 698.
A. Dedieu, M.-M. Rohmer and A. Veillard, Adv. Quantum Chem., 16 (1982) 43.
L. Vaska, Acc. Chem. Res., 9 (1976) 175.
D.A. Case, B.H. Huynh and M. Karplus, J. Am. Chem. Soc., 101 (1979) 4433.
Z.S. Herman and G.H. Loew, J. Am. Chem. Soc., 102 (1980) 1815.
M.-M. Rohmer, A. Strich and A. Veillard, Theor. Chim. Acta, 65 (1984) 219.
A. Strich and A. Veillard, Nouv. J. Chim., 7 (1983) 347.
J.E. Newton and M.B. Hall, Inorg. Chem., 23 (1984) 4627.
M.-M. Rohmer, in A. Veillard (Ed.), Quantum Chemistry: The Challenge of Transition Metals and Coordination Chemistry, NATO ASI Series, Reidel, Dordrecht, 1986, p. 377.
J.E. Newton and M.B. Hall, Inorg. Chem., 24 (1985) 2573.
J.G. Norman, Jr. and P.B. Ryan, Inorg. Chem., 21 (1982) 3555.
M. Roch, J. Weber and A.F. Williams, Inorg. Chem., 23 (1984) 4571.
T. Ziegler, Inorg. Chem., 24 (1985) 1547.
S.P. Mehandru and A.B. Anderson, Inorg. Chem., 24 (1985) 2570.
R. Osman and H. Basch, J. Am. Chem. Soc., 106 (1984) 5710.
M. Rosi, A. Sgamellotti, F. Tarantelli, I. Bertini and C. Luchinat, Inorg. Chem., 25 (1986) 1005.
M.J. Nappa and R.J. McKinney, Inorg. Chem., 27 (1988) 3740.
P.S. Bagus, K. Hermann and M. Seel, J. Vac. Sci. Technol., 18 (1981) 435 and references cited therein.
H.H. Lamb, B.C. Gates and H. Knözinger, Angew. Chem. Int. Ed. Engl., 27 (1988) 1127.
P.S. Bagus and B.O. Roos, J. Chem. Phys., 75 (1981) 5961.
T.-K. Ha and N.T. Nguyen, J. Mol. Struct. (Theochem), 109 (1984) 331.
P.S. Bagus, K. Hermann and C.W. Bauschlicher, Jr., J. Chem. Phys., 81 (1984) 1966.
M.R.A. Blomberg, U.B. Brandemark, P.E.M. Siegbahn, K.B. Mathisen and G. Karlström, J. Phys. Chem., 89 (1985) 2171.
C.W. Bauschlicher, Jr., J. Chem. Phys., 84 (1986) 260.
M.R.A. Blomberg, U.B. Brandemark and P.E.M. Siegbahn, Chem. Phys. Lett., 126 (1986) 317.
A. Mavridis, J.F. Harrison and J. Allison, J. Am. Chem. Soc., 111 (1989) 2482.
C.W. Bauschlicher, Jr., P.S. Bagus, C.J. Nelin and B.O. Roos, J. Chem. Phys., 85 (1986) 354.
M.R.A. Blomberg, U. Brandemark, J. Johanson, P.E.M. Siegbahn and J. Wennerberg, J. Chem. Phys., 88 (1988) 4324.
A.B. Rives and R.F. Fenske, J. Chem. Phys., 75 (1981) 1293.
H. Basch and D. Cohen, J. Am. Chem. Soc., 105 (1983) 3856.
M. Merchan, I. Nebot-Gil, R. Gonzalez-Luque and E. Orti, J. Chem. Phys., 87 (1987) 1690.
M.J.S. Dewar, Bull. Soc. Chim. Fr., C18 (1951) 71.
J. Chatt and L.A. Duncanson, J. Chem. Soc., (1953) 2939.
J. Allison, A. Mavridis and J.F. Harrison, Polyhedron, 7 (1988) 1559.
S.B.H. Bach, C. A. Taylor, R.J. Van Zee, M.T. Vala and W. Weltner, Jr., J. Am. Chem. Soc., 108 (1986) 7104.
J.B. Johnson and W.G. Klemperer, J. Am. Chem. Soc., 99 (1977) 7132.
B.E. Bursten, D.G. Freir and R.F. Fenske, Inorg. Chem., 19 (1980) 1804.
J.L. Hubbard and J. Lichtenberger, J. Am. Chem. Soc., 104 (1982) 2132.
C.W. Bauschlicher, Jr. and P.S. Bagus, J. Chem. Phys., 81 (1984) 5889.
C.M. Rohlfing and P.J. Hay, J. Chem. Phys., 83 (1985) 4641.
H.P. Lüthi, P.E.M. Siegbahn and J. Almlöf, J. Phys. Chem., 89 (1985) 2156.
J. Demuynck, A. Strich and A. Veillard, Nouv. J. Chim., 1 (1977) 217.
N. Rösch, H. Jörg and M. Kotzian, J. Chem. Phys., 86 (1987) 4038.
W.E. Dasent, Inorganic Energetics, Cambridge University Press, Cambridge, 1982.
D.E. Shelwood and M.B. Hall, Inorg. Chem., 22 (1983) 93.
C. Daniel, M. Benard, A. Dedieu, R. Wiest and A. Veillard, J. Phys. Chem., 88 (1984) 4805.

385 T. Ziegler, V. Tschinke and C. Ursenbach, J. Am. Chem. Soc., 109 (1987) 4825.
386 G. Blyholder and J. Springs, Inorg. Chem., 24 (1985) 224.
387 K.E. Lewis, D.M. Golden and G.P. Smith, J. Am. Chem. Soc., 106 (1984) 3905.
388 G.P. Smith, Polyhedron, 7 (1988) 1605.
389 D.S. Marynick, S. Askari and D.F. Nickerson, Inorg. Chem., 24 (1985) 868.
390 C. Daniel and A. Veillard, Inorg. Chem., 28 (1989) 1170.
391 A.R. Rossi and R. Hoffmann, Inorg. Chem., 14 (1975) 365.
392 M. Elian and R. Hoffmann, Inorg. Chem., 14 (1975) 1058.
393 D.S. Marynick, J. Am. Chem. Soc., 106 (1984) 4064.
394 H. Schröder, B. Rager, S. Matev, N. Rösch and H. Jörg, in L. Laude, D. Bäuerle and M. Wautelet (Eds.), Interfaces Under Laser Irradiation, Martinus Nijhoff, Dordrecht, 1987, p. 255.
395 K.L. Kompa, Angew. Chem. Int. Ed. Engl., 100 (1988) 1287.
396 P. Hay, J. Am. Chem. Soc., 100 (1978) 2411.
397 J.K. Burdett, J.M. Crzybowski, R.N. Perutz, M. Poliakoff, J.J. Turner and R.F. Turner, Inorg. Chem., 17 (1978) 147.
398 N. Rösch, M. Kotzian, H. Jörg, H. Schröder, B. Rager and S. Matev, J. Am. Chem. Soc., 108 (1986) 4238.
399 M. Kotzian, N. Rösch, H. Schröder and M.C. Zerner, J. Am. Chem. Soc., 111 (1989) 7687.
400 C. Daniel and A. Veillard, in A. Veillard (Ed.), Quantum Chemistry: The Challenge of Transition Metals and Coordination Chemistry, NATO ASI Series, Reidel, Dordrecht, 1986, p. 363.
401 D.A. Brown, J.P. Chester and N.J. Fitzpatrick, Inorg. Chem., 21 (1982) 2723.
402 A. Dedieu and S. Nakamura, Nouv. J. Chim., 8 (1984) 317.
403 A. Dedieu and S. Nakamura, in A. Veillard (Ed.), Quantum Chemistry: The Challenge of Transition Metals and Coordination Chemistry, NATO ASI Series, Reidel, Dordrecht, 1986, p. 277.
404 K.R. Lane and R.R. Squires, Polyhedron, 7 (1988) 1609.
405 G.K. Anderson and R.J. Cross, Acc. Chem. Res., 17 (1984) 67.
406 H. Berke and R. Hoffmann, J. Am. Chem. Soc., 100 (1978) 7224.
407 S. Nakamura and A. Dedieu, Chem. Phys. Lett., 111 (1984) 243.
408 S. Sakaki, K. Kitaura, K. Morokuma and K. Ohkubo, J. Am. Chem. Soc., 105 (1983) 2280.
409 N. Koga and K. Morokuma, J. Am. Chem. Soc., 108 (1986) 6136.
410 N. Koga and K. Morokuma, in A. Veillard (Ed.), Quantum Chemistry: The Challenge of Transition Metals and Coordination Chemistry, NATO ASI Series, Reidel, Dordrecht, 1986, p. 351.
411 L. Versluis, T. Ziegler, E.J. Baerends and W. Ravenek, J. Am. Chem. Soc., 111 (1989) 2018.
412 D. Antolovic and E.R. Davidson, J. Am. Chem. Soc., 109 (1987) 977.
413 D. Antolovic and E.R. Davidson, J. Am. Chem. Soc., 109 (1987) 5828.
414 D. Antolovic and E.R. Davidson, J. Chem. Phys., 88 (1988) 4967.
415 K. Tatsumi, A. Nakamura, P. Hofmann, P. Stauffert and R. Hoffmann, J. Am. Chem. Soc., 107 (1985) 4440.
416 P. Hofmann, P. Stauffert, K. Tatsumi, A. Nakamura and R. Hoffmann, Organometallics, 4 (1985) 404.
417 P. Hofmann, in A. Veillard (Ed.), Quantum Chemistry: The Challenge of Transition Metals and Coordination Chemistry, NATO ASI Series, Reidel, Dordrecht, 1986, p. 253 and references cited therein.
418 L. Zhu and N.M. Kostic, J. Organometal. Chem., 335 (1987) 395.
419 G.A. Ozin, W.J. Power, T.H. Upton and W.A. Goddard, III, J. Am. Chem. Soc., 100 (1978) 4750.
420 T.H. Upton and W.A. Goddard, III, J. Am. Chem. Soc., 100 (1978) 321.
421 H. Basch, M.D. Newton and J.W. Moskowitz, J. Chem. Phys., 69 (1978) 584.
422 G.A. Ozin, Coord. Chem. Rev., 28 (1979) 117.
423 P.-O. Widmark, B.O. Roos and P.E.M. Siegbahn, J. Phys. Chem., 89 (1985) 2180.

424 T. Ziegler and A. Rauk, Inorg. Chem., 18 (1979) 1558.
425 P.B. Armentrout, L.F. Halle and J.L. Beauchamp, J. Am. Chem. Soc., 103 (1981) 6624.
426 N. Rösch and R. Hoffmann, Inorg. Chem., 13 (1974) 2656.
427 T.A. Albright, R. Hoffmann, J.C. Thibeault and D.L. Thorn, J. Am. Chem. Soc., 101 (1979) 3801 and references cited therein.
428 F.U. Axe and D.S. Marynick, J. Am. Chem. Soc., 106 (1984) 6230.
429 B. Åkermark, M. Almemark, J. Almlöf, J.-E. Bäckvall, B. Roos and Å. Støgard, J. Am. Chem. Soc., 99 (1977) 4617.
430 R.M. Pitzer and H.F. Schaeffer, III, J. Am. Chem. Soc., 101 (1979) 7176.
431 P.J. Hay, J. Am. Chem. Soc., 103 (1981) 1390.
432 P.E.M. Siegbahn and V.B. Brandemark, Theor. Chim. Acta, 69 (1986) 119.
433 M.L. Steigerwald and W.A. Goddard, J. Am. Chem. Soc., 107 (1985) 5027.
434 A. Stockis and R. Hoffmann, J. Am. Chem. Soc., 102 (1980) 2952.
435 Y. Wakatsuki, O. Nomura, K. Kitaura, K. Morokuma and H. Yamazaki, J. Am. Chem. Soc., 105 (1983) 1907.
436 P.S. Braterman, J. Chem. Soc., Chem. Commun., (1979) 70.
437 R.J. McKinney, D.L. Thorn, R. Hoffmann and A. Stockis, J. Am. Chem. Soc., 103 (1981) 2595.
438 A. Peluso, D.R. Salahub and A. Goursot, Inorg. Chem., 29 (1990) 1544.
439 C.N. Wilker and R. Hoffmann, J. Am. Chem. Soc., 105 (1983) 5285.
440 J.-E. Bäckvall, E.E. Björkman, L. Pettersson, P. Siegbahn and A. Strich, J. Am. Chem. Soc., 107 (1985) 7408.
441 M.R.A. Blomberg, P.E.M. Siegbahn and J.-E. Bäckvall, J. Am. Chem. Soc., 109 (1987) 4450.
442 E.D. Jemmis and R. Hoffmann, J. Am. Chem. Soc., 102 (1980) 2570.
443 O. Eisenstein and R. Hoffmann, J. Am. Chem. Soc., 102 (1980) 6148; 103 (1981) 4308.
444 J.-E. Bäckvall, E.E. Björkman, L. Pettersson and P.E.M. Siegbahn, J. Am. Chem. Soc., 106 (1984) 4369.
445 H. Fujimoto and T. Yamasaki, J. Am. Chem. Soc., 108 (1986) 578.
446 S. Sakaki, K. Maruta and K. Ohkubo, Inorg. Chem., 26 (1987) 2499.
447 S. Sakaki, K. Maruta and K. Ohkubo, J. Chem. Soc. Dalton Trans., (1987) 361.
448 D.L. Thorn and R. Hoffmann, J. Am. Chem. Soc., 100 (1978) 2079.
449 H. Fujimoto, T. Yamasaki, H. Mizutani and N. Koga, J. Am. Chem. Soc., 107 (1985) 6157.
450 A. Dedieu, Inorg. Chem., 19 (1980) 375. A. Dedieu, A. Strich and A. Rossi, in R. Daudel, A. Pullman, L. Salem and A. Veillard (Eds.), Quantum Theory of Chemical Reactivity, Vol. 2, Reidel, Dordrecht, 1981, p. 193.
451 N. Koga, C. Daniel, J. Han, X.Y. Fu and K. Morokuma, J. Am. Chem. Soc., 109 (1987) 3455. C. Daniel, N. Koga, J. Han, X.Y. Fu and K. Morokuma, J. Am. Chem. Soc., 110 (1988) 3773. N. Koga and K. Morokuma, in D.R. Salahub and M.C. Zerner (Eds.), The Challenge of *d* and *f* Electrons, Theory and Computation, ACS Symp. Ser., 394 (1989).
452 M.A. Vincent, Y. Yoshioka and H.F. Schaeffer, III, J. Phys. Chem., 86 (1982) 3905.
453 E.A. Carter and W.A. Goddard, III, J. Phys. Chem., 88 (1984) 1485.
454 E.A. Carter and W.A. Goddard, III, J. Am. Chem. Soc., 108 (1986) 4746.
455 E.A. Carter and W.A. Goddard, III, J. Am. Chem. Soc., 108 (1986) 2180.
456 M.J. Brusich and W.A. Goddard, III, unpublished results.
457 J. Planelles, M. Merchan, I. Nebot-Gil and F. Tomas, J. Phys. Chem., 93 (1989) 6596.
458 P.B. Armentrout, L.S. Sunderlin and E.R. Fisher, Inorg. Chem., 28 (1989) 4437.
459 K.H. Dötz, H. Fisher, P. Hofmann, F.R. Kreissl, U. Schubert and K. Weiss (Eds.), Transition Metal Carbene Complexes, Verlag Chemie, Deerfield Beach, FL, 1984.
460 J.P. Collman and L.S. Hegedus (Eds.), Principles and Applications of Organotransition Metal Chemistry, University Science Books, Mill Valley, 1980, Chap. 3.

461 E.A. Carter and W.A. Goddard, III, Organometallics, 7 (1988) 675.
462 D. Spangler, J.J. Wendoloski, M. Dupuis, M.M.L. Chen and H.F. Schaeffer, III, J. Am. Chem. Soc., 103 (1981) 3985.
463 A.K. Rappé and W.A. Goddard, III, J. Am. Chem. Soc., 99 (1977) 3966.
464 T.F. Block, R.F. Fenske and C.P. Casey, J. Am. Chem. Soc., 98 (1976) 441.
465 T.F. Block and R.F. Fenske, J. Organomet. Chem., 139 (1977) 235.
466 T.F. Block and R.F. Fenske, J. Am. Chem. Soc., 99 (1977) 4321.
467 N.M. Kostic and R.F. Fenske, J. Am. Chem. Soc., 104 (1982) 3879.
468 N.M. Kostic and R.F. Fenske, Organometallics, 1 (1982) 974.
469 H. Nakatsuji, J. Ushio, S. Han and T. Yonezawa, J. Am. Chem. Soc., 105 (1983) 426.
470 J. Ushio, H. Nakatsuji and T. Yonezawa, J. Am. Chem. Soc., 106 (1984) 5892.
471 T.E. Taylor and M.B. Hall, J. Am. Chem. Soc., 106 (1984) 1576.
472 M.B. Hall, in A. Veillard (Ed.), Quantum Chemistry: The Challenge of Transition Metals and Coordination Chemistry, NATO ASI Series, Reidel, Dordrecht, 1986, p. 391.
473 R.J. Goddard, R. Hoffmann and E.D. Jemmis, J. Am. Chem. Soc., 102 (1980) 7667.
474 M.M. Francl, W.J. Pietro, R.F. Hout, Jr. and W.J. Hehre, Organometallics, 2 (1983) 281.
475 F. Volatron and O. Eisenstein, J. Am. Chem. Soc., 108 (1986) 2173.
476 T. Ziegler, L. Versluis and V. Tschinke, J. Am. Chem. Soc., 108 (1986) 612.
477 E.A. Carter and W.A. Goddard, III, J. Am. Chem. Soc., 109 (1987) 579.
478 P. Biloen and W.M.H. Sachtler, Adv. Catal., 30 (1981) 165.
479 J.J. Low and W.A. Goddard, III, Organometallics, 5 (1986) 609.
480 A.K. Rappé and W.A. Goddard, III, J. Am. Chem. Soc., 104 (1982) 297.
481 R. Hoffmann, C.N. Wilker and O. Eisenstein, J. Am. Chem. Soc., 104 (1982) 632.
482 C.N. Wilker, R. Hoffmann and O. Eisenstein, Nouv. J. Chim., 7 (1983) 535.
483 R.H. Grubbs, Prog. Inorg. Chem., 24 (1978) 1.
484 N. Calderton, J.P. Lawrence and E.A. Ofstead, Adv. Organomet. Chem., 17 (1979) 449.
485 K.J. Ivin, Olefin Metathesis, Academic Press, London, 1983.
486 S. Nakamura and A. Dedieu, Nouv. J. Chim., 6 (1982) 23.
487 J.L. Herisson and Y. Chauvin, Makromol. Chem., 141 (1970) 161.
488 O. Eisenstein and R. Hoffmann, J. Am. Chem. Soc., 103 (1981) 5582.
489 D.C. Brower, K.R. Birdwhistell and J. Templeton, Organometallics, 5 (1986) 94.
490 B.E. Bursten and R.H. Clayton, Polyhedron, 7 (1988) 943.
491 J. Silvestre and R. Hoffmann, Helv. Chim. Acta, 68 (1985) 1461.
492 C.P. Casey, M.A. Andrews, D. McAlister and J.E. Rinz, J. Am. Chem. Soc., 102 (1980) 1927.
493 J.A. Gladysz, Adv. Organomet. Chem., 20 (1982) 1.
494 U. Schubert, in F.R. Hartley and S. Patai (Eds.), Chemistry of the Metal–Carbon Bond, Vol. 1, Wiley, New York, 1982, Chap. 5.
495 F.J. Brown, Prog. Inorg. Chem., 27 (1980) 1.
496 E.O. Fischer and U. Schubert, J. Organomet. Chem., 100 (1975) 59.
497 S.J. McLain, C.D. Wood, L.W. Messerle, R.R. Schrock, F.J. Holander, W.J. Youngs and M.R. Churchill, J. Am. Chem. Soc., 100 (1978) 5962.
498 N.M. Kostic and R.F. Fenske, Organometallics, 1 (1982) 489.
499 N.M. Kostic and R.F. Fenske, J. Am. Chem. Soc., 103 (1981) 4677.
500 A. Mavridis, A.E. Alvarado-Swaisgood and J.F. Harrison, J. Phys. Chem., 90 (1986) 2584.
501 G.A. McDermott and A. Mayr, J. Am. Chem. Soc., 109 (1987) 580.
502 A.J.L. Pombeiro, Polyhedron, 8 (1989) 1595 and references cited therein.
503 H.P. Kim and R.J. Angelici, Adv. Organomet. Chem., 27 (1987) 51.
504 A.J.L. Pombeiro, in J.J. Ziolkowski (Ed.), Coordination Chemistry and Catalysis, World Scientific Publishing Co., Singapore, 1988, p. 100 and references cited therein.
505 A.J.L. Pombeiro, J. Organomet. Chem., 358 (1988) 273.

506 A.J.L. Pombeiro, D.L. Hughes, R.L. Richards, J. Silvestre and R. Hoffmann, J. Chem. Soc. Chem. Commun., (1986) 1125.
507 M.F.N.N. Carvalho, A.J.L. Pombeiro, E.G. Bakalbassis and C.A. Tsipis, J. Organomet. Chem., 371 (1989) C26.
508 E.G. Bakalbassis, A.J.L. Pombeiro and C.A.Tsipis, J. Organomet. Chem., in press.
509 G. Trinquier, J. Am. Chem. Soc., 104 (1982) 6969.
510 G. Trinquier and G. Bertrand, Inorg. Chem., 24 (1985) 3842.
511 D. Goubeau, G. Pfister-Guilluzo, A. Marinetti and F. Mathey, Inorg. Chem., 24 (1985) 4133.
512 G.Pfister-Guilluzo and D. Goubeau, in A. Veillard (Ed.), Quantum Chemistry: The Challenge of Transition Metals and Coordination Chemistry, NATO ASI Series, Reidel, Dordrecht, 1986, p. 333.
513 A. Marinetti, F. Mathey, J. Fischer and A. Mitschler, J. Am. Chem. Soc., 104 (1982) 4482.
514 C.J. Pickett, M.Y. Mohammed, K.S. Ryder and J. Talarmin, in H. Bothe, F.J. de Brujin and W.E. Newton (Eds.), Nitrogen Fixation: Hundred Years After, Fischer, Stuttgart, 1988, p. 51.
515 A. Ozaki, Acc. Chem. Rev., 14 (1981) 16.
516 R.A. Henderson, G.J. Leigh and C.J. Pickett, Adv. Inorg. Chem. Radiochem., 27 (1983) 197.
517 D.J. Darensburg and R.A. Kudaroski, Adv. Organomet. Chem., 22 (1983) 129.
518 D.A. Palmer and R. Van Eldik, Chem. Rev., 83 (1983) 651.
519 P. Pelikan and R. Bŏca, Coord. Chem. Rev., 55 (1984) 55.
520 K. Hori, Y. Asai and T. Yamade, Inorg. Chem., 22 (1983) 3218.
521 T. Yamade, K. Hori and K. Fukui, Inorg. Chem., 21 (1982) 2046.
522 T. Yamade, K. Hori and K. Fukui, Inorg. Chem., 21 (1982) 2816.
523 M.R.A. Blomberg and P.E.M. Siegbahn, Chem. Phys., 87 (1984) 189.
524 N.M. Kostic and R.F. Fenske, J. Organomet. Chem., 233 (1982) 337.
525 A.K. Rappé, Inorg. Chem., 23 (1984) 995.
526 A.K. Rappé, Inorg. Chem., 25 (1986) 4686.
527 R.A. Wheeler, M-H. Whangbo, T. Hughbanks, R. Hoffmann, J.K. Burdett and T.A. Albright, J. Am. Chem. Soc. 108 (1986) 2222.
528 C. Mealli, R. Hoffmann and A. Stockis, Inorg. Chem., 23 (1984) 56.
529 S. Sakaki and A. Dedieu, J. Organomet. Chem., 314 (1986) C63.
530 S. Sakaki and A. Dedieu, Inorg. Chem., 26 (1987) 3278.
531 S. Sakaki and K. Ohkubo, Inorg. Chem., 27 (1988) 2020.
532 A. Mavridis, K. Kunze, J.F. Harrison and J. Allison, in T. Marks (Ed.), Bond Energies and the Thermodynamics of Organometallic Reactions, ACS Symp. Ser., (1989).
533 A. Mavridis, personal communication, 1990.
534 J.O. Noell and K. Morokuma, Inorg. Chem., 18 (1979) 2774.
535 O.-Z. Shi, T.G. Richmond, W.C. Trogler and F. Basolo, Inorg. Chem., 23 (1984) 957.
536 M. Kersting and R. Hoffmann, Inorg. Chem., 29 (1990) 279.
537 D.F.T. Tuan and R. Hoffmann, Inorg. Chem., 24 (1985) 871.
538 S. Sakaki, M. Nishikawa and A. Ohyoshi, J. Am. Chem. Soc., 102 (1980) 4062.
539 H. Kurosawa, M. Emoto, H. Ohnishi, K. Miki, N. Kasai, K. Tatsumi and A. Nakamura, J. Am. Chem. Soc., 109 (1987) 6333.
540 M.E. Silver, O. Eisenstein and R.C. Fay, Inorg. Chem., 22 (1983) 759.
541 M.P. Sigalas and C.A. Tsipis, Inorg. Chem., 25 (1986) 1875.
542 E.G. Bakalbassis, G.A. Katsoulos and C.A. Tsipis, Inorg. Chem., 26 (1987) 3151.
543 C.C. Hadjikostas, G.A. Katsoulos, M.P. Sigalas and C.A. Tsipis, Can. J. Chem., 67 (1989) 902.
544 W.P. Anderson and D.M. Baird, Inorg. Chem., 27 (1988) 3240.
545 C.A. Tsipis, G.A. Katsoulos, E.G. Bakalbassis and M.P. Sigalas, Struct. Chem., 1 (1990) 523.
546 I. Jano, Theor. Chim. Acta, 66 (1985) 341.